UNIVERSITY OF CALIFORNIA SAN DIEGO

Characterization of Marine Teleost Ionocytes in the Gill, Skin, and Inner Ear Epithelia and their Implications for Ocean Acidification

A dissertation submitted in partial satisfaction of the requirements for the degree Doctor of Philosophy

in

Marine Biology

by

Garfield Tsz Kwan

Committee in charge:

Professor Martin Tresguerres, Chair
Professor Ronald S. Burton
Professor Philip A. Hastings
Professor Frank L. Powell
Professor Gregory W. Rouse

2020

The Dissertation of Garfield Tsz Kwan is approved, and it is acceptable in quality and form for publication on microfilm and electronically:

_____

_____

_____

_____

_____

Chair

University of California San Diego
2020

DEDICATION

This dissertation is dedicated to four women who have had an extraordinary impact on my life:

Polly Leung, my mother, for lovingly raising me in a foreign country and relentlessly supporting me through school.

Helen Richard, my 2nd grade teacher, for patiently teaching me English and encouraging me to read.

Megan Jara, my high school counselor, for gently daring me to dream and fostering a tenacity to apply for academic scholarships.

Cecilia Chow, my partner and wife, for unrelentingly pushing me to pursue my dreams and to take (unwanted but necessary) breaks.

EPIGRAPH

"Time is money, and I have neither."
Me, *My Dissertation*

"There's a million things I haven't done, just you wait."
Lin-Manuel Miranda, *Hamilton*

"Men suffer more from imagining too little than too much."
Phineas Taylor Barnum, *The Greatest Showman*

TABLE OF CONTENTS

LIST OF FIGURES

Chapter 2

Chapter 3

Chapter 4

Chapter 6

Chapter 7

LIST OF TABLES

ACKNOWLEDGMENTS

This dissertation is the cumulation of investments by a vast number of mentors. I am exceedingly grateful for your consistent guidance, counsel, and support.

I would first like to thank my advisor, Martin Tresguerres, for taking a chance on me. I am thankful for your candid criticisms that challenge me to excel, and your genuine desire to generate quality research. Thank you for investing in me so that I may become a better researcher and writer. Whether it be conversations in-person, communication through email, or exchanges via text, you were readily available as a mentor, and most importantly, as a friend. Thank you for guiding me through professional struggles and consoling me through personal hardships. Additionally, thank you for your pragmatic and honest feedback, which has ultimately influenced both my research and my outreach endeavors. Thank you for providing me with the opportunities to travel and engage with the international, scientific community at places I would never have dreamt of visiting. Research has molded me into who I am today, and you were the perfect advisor for this role.

I would also like to thank my committee members: Greg Rouse, Ron Burton, Phil Hastings, and Frank Powell. Thank you for taking the time to meet with me and discuss my research. The unnerving qualifying and defense examinations have made me a better researcher, in part, due to your mentorship.

I would not be here today were it not for the many mentors in my life: Helen Richard, my first teacher in the United States, patiently taught me English when I first arrived and struggled with the language. Megan Jara, my high school counselor, tirelessly supporting me and fostering the tenacity to pursue academic opportunities. I am extremely grateful to Karen Stocks, who advocated on my behalf and connected me with my first laboratory experience with Stuart

Sandin and Jennifer Smith. I am grateful to Stuart, Jen, and their laboratory manager, Currie Dugas for giving me my first taste of research. I am thankful for Gabriele Wienhausen and her enduring support and career advice throughout my early research career. Thank you to Jonathan Shurin for providing teaching and research opportunities, though I was almost arrested during one unforgettable research project (never letting that go!). Ed Parnell and Lena Gerwick for confronting my tendencies to overcommit, then subsequently (yet kindly) kicked me out of their respective labs to dedicate my time to focus on a single research project. Thank you to Lisa Levin and Michael Navarro for preparing me to face the rigor of graduate school and providing me with opportunities to grow as a scientist. I am also grateful to Chris Murphy for his guidance throughout and beyond the UC LEADS program. Thank you to Jonathan Deroba for his mentorship in fisheries science, and to the NOAA Hollings Scholar program for the scholarship and research opportunities. Thank you to Victor Vacquier and Gary Moy for critiquing my writing and research progress during the early days of my graduate program. Finally, I am grateful to Currie Dugas, Levi Lewis, and Noelle Bowlin for their friendship, mentorship, and inspiration to pursue a PhD while I was still an undergraduate.

To Jinae Roa, thank you for teaching me the key biochemical skills I have mastered today. Besides being a stellar researcher, you were always ready to listen when times were rough. To Daniel Yee, thank you for reminding me that you can enjoy life and still excel in research – I am glad you are always around to laugh and commiserate with. I am truly grateful to the lab family I have had the chance to work, laugh, flip cups, and share a drink with, including Megan Barron, Lauren Linsmayer, Katie Barott, Jörn Thomsen, Cristina Salmerón Salvador, Alex Clifford, Till Harter, Sidney Perez, Jenny Tu, Angus Blacklaw, Mikayla Ortega, Jason Ho, Cameron Hasssibi, Bethany Shimasaki, Radha Karra, Lucia Rodriguez, Yuzo Yanagitsuru, Lara

Jansen, Corey Jew, Amalia Serna, Anna Blanchard, Ryan Myers, and Samantha Nöel. Special thanks to Taylor Smith, Shane Finnerty, Gabriel Lopez, and Kaelan Prime for their help with animal husbandry and laboratory work. I have been incredibly lucky to have great undergraduate volunteers; it has been a pleasure to serve as your mentor.

My research projects wouldn't have been feasible without Phil Zerofski and Ashley Palinkas. I am grateful for your assistance in the collection and maintenance of the aquarium. Special thanks to Nick Wegner for providing advice and samples during the critical months prior to candidacy, and to Leonardo Andrade, for his assistance on inner ear fixation the few months leading to my defense. Thank you to Dave Checkley and Sara Shen for setting up the larval white seabass collaboration with Hubbs Sea World Research Institute (HSWRI). I am also thankful for Mark Drawbridge, Erica Bromby-Fanning, Eric McIntire, and the rest of the HSWRI staff that made part of my dissertation work possible. To Trevor Hamilton, Debi Kilb, and Sue Edwards, I am thankful for your gentle reminders about what truly matters in life – something that is easily forgotten in this profession.

The staff at Scripps have made my graduate experience both easier and more vibrant. Josh Reeves, thank you for your undergraduate advising and for the many opportunities to attend SACNAS as part of the Scripps delegation. Thank you to Jane Teranes, who gave me my first official teaching appointment at Scripps. Also, thank you to the many department and division staffs including Gilbert Bretado, Maureen McGreevy, Jessica Gonzales, Denise Darling, Shelley Weisel, Olivia Padilla, James Pollock, Gregory Jackson, Marty Tullar, Jackie Tran, Josh Schmidt, Dejan Ristic, and Yvonne Bohan. Thank you for handling the many behind-the-scenes administrative tasks. Thank you to the Scripps communication team, especially to Rob Monroe and Brittany Hook for giving me the opportunity to attend COP24 and experience the chaos

behind international climate negotiations, and for writing about Squidtoons Comics in the Scripps news outlet.

I want to thank the many funding and research programs that have supported me over the years. Thank you to the UCSD San Diego Fellowship for funding my first two years, and to the NSF Graduate Research Fellowship Program for funding the next three years of my graduate degree. I am thankful for the funding support from NSF grants IOS #1354181 and #1754994 to Martin Tresguerres. I am grateful to the NSF Graduate Internship Fellowship Program for providing funding and the opportunity to work with the team at NOAA Southwest Fisheries Science Center. I am also grateful for the travel grants funded by the Graduate Student Association, Company of Biologist, and the Society for Experimental Biology. Thank you to Mark Bayley, Tobias Wang, and the Elisabeth og Knud Petersens Fond for the incredible opportunity to take the Acid Base and Ion Regulation Course in Can Tho, Vietnam. I am grateful to be awarded the NSF Postdoctoral Research Fellowship Program in Biology, a delightful and encouraging reinforcement as I prepare for my defense and pursue an academic career. Finally, I am sincerely grateful for the many reference letter writers that made these opportunities attainable: Stuart Sandin, Gabriele Wienhausen, Jonathan Shurin, Lisa Levin, Jonathan Deroba, Trevor Hamilton, Nick Wegner, Greg Rouse, and Martin Tresguerres.

My friends have been a consistent source of support and relief throughout graduate school. Renny Ng, Vincent Hui, Pierre Lau, Mark Chang, James Lee, Ray Sheng, Shunpei Kobayashi – thank you for cheering me on throughout the process. You are never far when I need someone to talk to. Special thanks to Kaitlyn Lowder for our office chats and mutual commiseration. Thank you also to Nati Delherbe for the laughs, hugs, and somber reminders of how “your papers won’t hug you at night”. Thank you to Dana Song – Squidtoons was necessary

for my mental health, and it would have been very different without you. Shout out to my graduate school cohort of 2014; thank you for the love and support.

Last but not least, thank you to my family, both near and far, for rooting and cheering me on. Special thanks to Martin Ma for your love and support – especially in the early years. To my partner and wife, Cecilia Chow – words cannot express my gratitude. You have supported me every step of the way; thank you for your encouragement and support manifested in forms I did not even know I needed. Thank you for supporting me before I was even accepted into graduate school, and for continuing to urge me to pursue my dream job within academia. And to my parents, both of whom uprooted their lives in Hong Kong and moved to a foreign country just so I can have opportunities such as this. Polly and Ken Kwan, thank you for your unconditional love and support – I hope you're proud of me.

Chapter II, in full, is a reprint of the material as it appears in Kwan, G.T., Hamilton, T.J., and Tresguerres, M. (2017). CO_2-induced ocean acidification does not affect individual or group behaviour in a temperate damselfish. *Royal Society Open Science*, 4(7), 170283. The dissertation author was the primary investigator and author of this material. The material is used by permission of Royal Society Publishing.

Chapter III, in full, is a reprint of the material as it appears in Kwan, G.T., Finnerty, S.H., Wegner, N.C., and Tresguerres, M., 2019. Quantification of Cutaneous Ionocytes in Small Aquatic Organisms. *Bio-Protocol*, 9(09), e3227. The dissertation author was the primary investigator and author of this material. The material is used by permission of Bio-Protocol.

Chapter IV, in full, is a reprint of the material as it appears in Kwan, G.T., Wexler, J.B., Wegner, N.C., and Tresguerres, M., 2019. Ontogenetic changes in cutaneous and branchial ionocytes and morphology in yellowfin tuna (*Thunnus albacares*) larvae. *Journal of*

Comparative Physiology B, 189(1), 81-95. The dissertation author was the primary investigator and author of this material. The material is used by permission of Springer.

Chapter V, in part, is currently being prepared for submission for publication of the material. Shen, S.G., Kwan, G.T., Tresguerres, M., and Checkley, D.M. (*in prep*). Physiological resilience of white seabass (*Atractoscion nobilis*) larvae to CO_2-induced ocean acidification. The dissertation author was the co-primary investigator and author of this material.

Chapter VI, in part, has been submitted for publication of the material as it may appear in *Journal of Comparative Physiology – B*. Kwan, G.T., Smith, T.R., and Tresguerres, M. (*in review*). Immunological characterization of two types of ionocytes in the inner ear epithelium of Pacific Chub Mackerel (*Scomber japonicus*). The dissertation author was the primary investigator and author of this material.

Chapter VII, in part is currently being prepared for submission for publication of the material. Kwan, G.T., Prime, K., Andrade, L.R., and Tresguerres, M. (*in prep*). Responses of Splitnose Rockfish (*Sebastes diploproa*) gill and inner ear ionocytes to hypercapnia. The dissertation author was the primary investigator and author of this material.

VITA

2013 Bachelor of Science, Marine Biology, Scripps Institution of Oceanography, University of California San Diego

2016 Master of Science, Biological Oceanography, Scripps Institution of Oceanography, University of California San Diego

2020 Doctor of Philosophy, Marine Biology, Scripps Institution of Oceanography, University of California San Diego

FIRST-AUTHOR PUBLICATIONS

Kwan, G.T., Smith, T.R., and Tresguerres, M. *in review*. Immunological characterization of two types of ionocytes in the inner ear epithelium of Pacific Chub Mackerel (*Scomber japonicus*). *Journal of Comparative Physiology B*.

Kwan, G.T., Finnerty, S.H., Wegner, N.C., and Tresguerres, M. 2019. Quantification of Cutaneous Ionocytes in Small Aquatic Organisms. *Bio-Protocol*, 9(09), e3227.

Kwan, G.T., Wexler, J.B., Wegner, N.C., and Tresguerres, M. 2019. Ontogenetic changes in cutaneous and branchial ionocytes and morphology in yellowfin tuna (*Thunnus albacares*) larvae. *Journal of Comparative Physiology B*, 189(1), 81-95.

Kwan, G.T., Hamilton, T.J., and Tresguerres, M. 2017. CO_2-induced ocean acidification does not affect individual or group behaviour in a temperate damselfish. *Royal Society Open Science*, 4(7), 170283.

CO-AUTHOR PUBLICATIONS

Weinrauch, A.M., **Kwan, G.T.**, Tresguerres, M., Goss, G.G. *in review*. Mechanisms of digestive acidification highlight the transitional evolutionary state of the Pacific hagfish. *Proceedings of the Royal Society B*.

Thinh, P.V., Phuong, N.T., Brauner, C.J., Huong, D.T.T., Wood, A.T., **Kwan, G.T.**, Conner, J.L., Bayley, M., and Wang, T. 2018. Acid-base regulation in the air-breathing swamp eel (*Monopterus albus*) at different temperatures. *The Journal of Experimental Biology*, 221(10), jeb172551.

Hill, R.W., Armstrong, E.J., Inaba, K., Morita, M., Tresguerres, M., Stillman, J.H., Roa, J.N., and **Kwan, G.T.** 2018. Acid secretion by the boring organ of the burrowing giant clam, *Tridacna crocea*. *Biology Letters*, 14: 20180047.

Hamilton, T.J., **Kwan, G.T.**, Gallup, J., and Tresguerres, M. 2016. Acute fluoxetine exposure alters crab anxiety-like behaviour, but not aggressiveness. *Scientific Reports*, 6:19850.

Navarro, M., **Kwan, G.T.**, Batalov, O., Choi, C.Y., Pierce, N.T. and Levin, L.A. 2016. Development of embryonic market squid, *Doryteuthis opalescens*, under chronic exposure to low environmental pH and [O_2]. *PLoS ONE*, 11(12):e0167461.

Shurin, J.B., Abbott, R., Deal, M.S., **Kwan, G.T.**, Litchman, E., McBride, R., Mandal, S., and Smith, V.H., 2013. Industrial-strength ecology: trade-offs and opportunities in algal biofuel production. *Ecology Letters*, 16(11), 1393-1404.

BOOK PUBLICATIONS

Kwan, G., Song, D. 2018. Squidtoons: Exploring ocean science with comics. *Andrews McMeel Publishing*.

ABSTRACT OF THE DISSERTATION

Characterization of Marine Teleost Ionocytes in the Gill, Skin, and Inner Ear Epithelia and their Implications for Ocean Acidification

by

Garfield Tsz Kwan

Doctor of Philosophy in Marine Biology

University of California San Diego, 2020

Professor Martin Tresguerres, Chair

Ionocytes are specialized epithelial cells that excrete or absorb ions across an epithelium to regulate ionic, osmotic and acid-base levels in internal fluids. These ionocytes perform a wide range of functions (e.g. osmoregulation, pH regulation, and calcification) across various organs (e.g. gill, skin, inner ear). As atmospheric CO_2 levels rise and oceanic pH levels fall, teleosts may

increase their investment on ionocytes to survive in future ocean conditions. But generally speaking, the gill, skin, and inner ear ionocytes within marine teleost are not well characterized. This dissertation contains research spanning five southern Californian teleosts: the Blacksmith *Chromis punctipinnis*, the Yellowfin Tuna *Thunnus albacares*, the White Seabass *Atractoscion nobilis*, the Pacific Mackerel *Scomber japonicus*, and the Splitnose Rockfish *Sebastes diploproa*. In Chapter II, I investigated the individual and group behavioral responses of the Blacksmith, a temperate damselfish, after exposure to CO_2-induced low-pH conditions. In Chapter III, I describe a novel technique used to quantify skin ionocytes in larval fishes. In Chapter IV, I applied the Chapter III's technique to document developmental patterns in the skin and gill ionocytes of larval Yellowfin Tuna. In Chapter V, I investigated larval White Seabass response to hypercapnia by monitoring oxygen consumption rate and quantifying ionocyte abundance and relative ionocyte area across development. In Chapter VI, I characterized two types of inner ear ionocytes responsible for otolith calcification in the Pacific Mackerel. In Chapter VII, I investigated whether future CO_2 /pH conditions would affect the gill and inner ear ionocytes of Splitnose Rockfish. Altogether, this work across the multiple teleosts demonstrates that ionocytes 1) have the plasticity to respond to external pH stress, 2) are sufficient to maintain internal homeostasis despite significant differences in CO_2/pH levels, and 3) differ greatly in protein, morphology, and function depending on the tissue in question.

CHAPTER I

General Introduction

Background on Dissertation Focus. The original focus of my dissertation was to investigate fish behavioral responses to ocean acidification (OA) and the underlying biochemical and cellular processes. The number studies on the effects of OA on marine organisms surged during the 2010s. Many of those studies found dramatic effects on marine fishes, including improper behavioral reaction to predators (Dixson et al., 2010; Cripps et al., 2011) and habitat cues (Munday et al., 2009), impaired learning (Ferrari et al., 2012; Chivers et al., 2014), and increased anxiety behavior (Hamilton et al., 2013). Although this altered behavior was proposed to be due to malfunction of γ-aminobutyric acid type A ($GABA_A$) receptors in the brain (Nilsson et al., 2012), experimental evidence at the biochemical, cellular, and neurobiological levels was lacking. Thus, I decided to tackle this question.

The first experiments of my PhD examined the effects of OA on the behavior of Blacksmith (*Chromis punctipinnis*) and Splitnose Rockfish (*Sebastes diploproa*). Together with other research that was being conducted in my laboratory at the time, my results indicated that these two species responded differently to OA: while the anxiety-like behavior of rockfish was altered (Hamilton et al., 2013), that of blacksmith was not (Kwan et al., 2017). This was exciting because it suggested species-specific physiological neurophysiological mechanisms that could confer differential resilience or sensitivity to OA, which I could study. However, upon much reading of the literature I was surprised to find that the knowledge on basic neurological function of fishes was very limited, including $GABA_A$ receptor function, composition of the cerebral spinal fluid (CSF), and the characterization of ionocytes within the choroid plexus (which regulates the acid-base and ionic composition of the CSF). Combined with the lack of neurobiological and surgical resources and expertise available at SIO, it became obvious that my original goal of characterizing the effects of OA on fish neurobiology and behavior would take

much longer than the typical duration of a PhD degree. Thus, I switched my focus to understanding other interesting effects of OA on fish, namely the cellular mechanisms involved in maintaining blood acid-base balance and those behind increased otolith calcification.

Ionocytes maintain osmotic and acid-base homeostasis. Ionocytes are specialized epithelial cells that excrete or absorb ions across an epithelium to regulate ionic, osmotic and A/B levels in internal fluids. Importantly, "ionocyte" is a generic name. Multiple types of ionocytes are present in different epithelia. Each type of ionocyte exists to transports specific ion(s) to serve a defined physiological role(s). A typical ionocyte has one or more ATPase enzymes that provide the driving force for ion transport, and a suite of additional ion-transporting proteins (i.e. channels, exchangers, enzymes, and cotransporters) that are differentially located in either their apical ("external facing") or basolateral ("internal facing") membrane. The collective function of the ion-transporting proteins within an ionocyte, combined with the function of all ionocytes subtypes, determines the ultimate physiological role of an epithelium. In this chapter, I will briefly discuss current knowledge on the ionocytes in the gill, skin, and inner ear epithelium – with an emphasis on marine teleost.

The ocean presents several significant physiological challenges to teleost cell and whole-body physiology. For example, seawater (SW) has roughly 3-fold more NaCl than the fish's internal plasma. Because excess salt entering the body can cause ion-imbalance and induce dehydration, marine fishes must actively excrete NaCl into seawater. Moreover, upwelling conditions can increase environmental carbon dioxide (CO_2) by 2.5-fold, which rapidly diffuses into the fish's internal plasma, generating protons (H^+) and inducing blood acidosis. Because increased H^+ can affect protein structure and enzyme function, marine fishes must actively

regulate H^+ concentration to maintain optimal pH. Furthermore, metabolic conditions can also present periodic challenges to the animal's physiology. For example, CO_2, H^+, or bicarbonate (HCO_3^-) generated from processes such as cellular respiration and food digestion can result in acidosis or alkalosis in the blood plasma, respectively. Altogether, marine fishes must regulate ions (e.g. Na^+, Cl^-, H^+, and HCO_3^-) to maintain nominal osmotic and acid-base (A/B) homeostasis.

The majority of ionocyte research has been investigated on freshwater fishes. But due to intrinsic osmotic and ionic differences in the environment, studies on freshwater species are not directly applicable to marine teleosts. Freshwater fishes are hyperosmotic to their environment, so they must actively absorb NaCl and produce dilute urine to maintain fluid homeostasis. In contrast, the marine fishes are hypoosmotic to their environment, thus they must drink seawater and actively excrete NaCl and produce concentrated urine to retain suitable fluid levels. As a result, freshwater and marine fishes must utilize different ion transporters to maintain ionic and osmotic balance. Furthermore, trans-epithelial H^+ and HCO_3^- secretion necessary for A/B regulation is often coupled to Na^+ and Cl^- absorption, respectively. Ultimately, the ionocytes within freshwater and marine teleosts have fundamentally different mechanisms.

Ionocytes in the gill epithelium. Specialized NaCl-secreting ionocytes (formerly known as chloride cells) were first described in the gills of a marine European eel (*Anguilla vulgaris*) (Keys, 1931; Keys and Willmer, 1932). Subsequent studies found the gill ionocytes to be mitochondrion-rich, contain abundant Na^+/K^+-ATPase (NKA) and $Na^+/K^+/Cl^-$ co-transporter (NKCC) in its highly infolded basolateral membrane, and Cl^- channels in its apical membrane (reviewed in Hirose et al., 2003; Evans et al., 2005). NKA is the driving force for marine fish

osmoregulation; its generation of an electrochemical gradient ultimately overcomes the concentration gradient and drives Cl ions into surrounding seawater, with Na^+ following via a transepithelial pathway. Functional evidence of NKA's role in NaCl secretion was demonstrated using drug inhibition: ouabain nearly completely inhibits Na^+ and Cl^- secretion against a large concentration gradient (Silva et al., 1977). Altogether, the accepted model for ionocyte's NaCl secretion is as follows: NKA, powered by ATP hydrolysis, maintains a low intracellular [Na^+] that drives the movement of Cl- into the ionocyte via basolateral NKCC. Next, the inside negative membrane potential drives Cl^- into SW through apical Cl^- channels, which in turn promotes paracellular Na^+ excretion following the transepithelial electrochemical gradient (reviewed in Marshall, 2002; Hirose et al., 2003; Evans et al., 2005).

The fish's osmoregulatory capacity is also known to be plastic. Exposure to increased salinity would result in diffusive NaCl gain and water loss, which if left unchecked could lead to cell shrinkage and mortality. One short-term response to hyper-saline stress includes the widening of the ionocyte's apical membrane and the extension of its microvilli to facilitate increased NaCl secretion (Varsamos et al., 2002a). Additionally, a long-term exposure to hyper-saline conditions led to the synthesis of new ionocytes along the gill lamellae (Varsamos et al., 2002a) and increased abundance of basolateral NKA and NKCC within each ionocyte (Tipsmark et al., 2002).

The same gill NKA-rich ionocytes are also proposed to be responsible for H^+ secretion. The current working hypothesis proposes acid secretion into SW via apical Na^+ H^+ exchanger (NHE) is made possible by 1) the low intracellular [Na^+] gradient generated by NKA, 2) the high [Na^+] in the surrounding SW, and 3) the catalyzing of CO_2 and H_2O into H^+ and HCO_3^- by intracellular carbonic anhydrase (CA) (reviewed in Hirose et al., 2003; Evans et al., 2005). NHE

has been immunolocalized within NKA-rich cells of marine teleosts (Edwards et al., 1999; Catches et al., 2006; Hiroi and McCormick, 2012; Christensen et al., 2012). Additionally, experimental evidence seems to support this model: 1) drug suppression of NHE inhibits acid secretion, and 2) sufficient external NaCl is necessary to maintain pH levels in the Longhorn Sculpin (*Myoxocephalus octodecimspinosus*) (Claiborne et al., 1997).

In contrast, the ionocyte responsible for secreting HCO_3^- within marine teleosts remains uncharacterized. Thus far, only one type of ionocyte has been described within marine teleosts. Given that multiple types of A/B regulating ionocytes were previously reported in freshwater teleosts (Hwang et al., 2011; Hiroi and McCormick, 2012; Hsu et al., 2014), there may be other type of ionocyte that remains undescribed within the marine teleosts. This illustrates the gap that exists between our understanding of freshwater and marine teleosts. Therefore, additional investigation of ionocytes within marine teleosts is necessary to assess whether the currently proposed A/B mechanisms apply to all seawater teleosts, or if species-specific differences exist.

Ionocytes in the skin epithelium. Similar to adult teleosts, larval teleosts hypo-osmoregulate their internal fluids (Alderdice, 1988; Varsamos et al., 2005). But unlike their adult counterparts, marine larval fishes lack developed gills and initially secrete NaCl using ionocytes in their skin (Holliday, 1969; Roberts et al., 1973; Alderdice, 1988; Hiroi et al., 1998; Katoh et al., 2000; Schreiber, 2001; Varsamos et al., 2001; Bodinier et al., 2010). As development progresses, skin ionocyte abundance decreases while gill ionocyte abundance progressively increases (Ayson et al., 1994; Hiroi et al., 1998, 1999; Varsamos et al., 2002b). This shift in ionocyte distribution is intrinsically related to the reduction in surface-area-to-volume ratio that takes place as an organism grows. Smaller larvae have relatively large surface-area-to-volume

ratio, thereby allowing gas exchange and ion transport to take place at adequate diffusion rates across the skin (Rombough, 1999). But as the larvae grows larger, their surface-area-to-volume ratio decreases, thereby increasing the diffusion distance between capillaries and the surrounding water and ultimately hampering both gas exchange and ion transport (Rombough, 1999). However, larger larvae would also have more developed branchial structures (gill and in some cases pseudobranch) – which provide the necessary respiratory surface area and osmoregulation capacity to keep up with their increased total metabolic rate (reviewed in Rombough 2007). As development continues, the bulk of the gas exchange and ion-transport would transition to the gill lamellae and gill ionocytes, respectively.

Because larval skin ionocytes function as the adult gill ionocytes, their characteristics are unsurprisingly similar. Just like gill ionocytes, skin ionocytes are rich in mitochondria, express abundant basolateral NKA and NKCC, and contain apical CFTR (Li et al., 1995; van der Heijden et al., 1999; Katoh et al., 2000; Varsamos et al., 2002b; Hiroi et al., 2005; Lorin-Nebel et al., 2006; Sucré et al., 2012). Both NaCl secretion (in marine larvae) and NaCl absorption (in freshwater larvae) by skin ionocytes have been demonstrated, although osmoregulation in freshwater larvae has been more extensively studied (reviewed in Rombough, 2007). Given the evidence, it is generally accepted that marine larval skin ionocytes 1) are the main site for NaCl secretion and 2) utilize the same mechanism models as proposed in adult fishes.

Larval skin ionocytes have also been proposed to regulate plasma A/B levels. The skin ionocytes of seawater-acclimated medaka (an euryhaline species) have been shown to excrete H^+ (Liu et al., 2016), and subsequent drug inhibitions suggest the involvement of NHE and CA similar to the A/B regulation mechanism proposed for marine teleost. While A/B regulation in skin ionocytes has not been fully characterized, multiple larval teleosts species have been

reported to survive acute levels of extreme hypercapnia – with nearly 100% survival even at 1% CO_2 (10,000 μatm) (Kikkawa et al., 2003, 2004). The larval fishes' survival in this extremely hypercapnic condition implies they have robust A/B regulatory capacity, specifically to remove H^+ from the blood plasma to maintain proper pH levels. Further research is necessary to determine whether A/B regulation is maintained through the NKA-rich ionocytes of larval marine fishes, or whether acid secretion occurs within a different subtype of ionocyte altogether.

Ionocytes in the inner-ear epithelium. Unlike gill and skin ionocytes, inner ear ionocytes are not exposed to the external seawater environment. However, inner-ear ionocytes perform similar roles proposed for gill and skin ionocytes such as transporting ions and maintaining A/B levels to promote otolith calcification. Together with the surrounding inner ear organ, the otoliths play an integral role in maintaining equilibrium and hearing nearby predator and/or prey. The otoliths (sagitta, lapillus, and asteriscus) are calcified within a viscous, acellular fluid called the endolymph secreted by the surrounding epithelial otolithic ionocytes. Otoliths are $CaCO_3$ structures that continuously grow throughout the fish's life (Campana and Neilson, 1985) forming a series of concentric rings that are used to estimate age and growth for stock assessment studies (Pannella, 1971). Trace chemical and isotope analysis on otolith rings can also provide important information about early life history (Swearer et al., 1999), exposure to environmental salinity and temperature (Campana, 1999; Elsdon and Gillanders, 2002), and dietary changes (Radtke et al., 1996; Nelson et al., 2011; von Biela et al., 2015). As a result, the inner ear otoliths are part of an essential sensory organ as well as a vital research asset.

The otolith is composed of a combination of protein matrix and calcium carbonate ($CaCO_3$), a compound that necessitates ample Ca^{2+} and HCO_3^- ions in an alkaline pH, low [H^+]

environment. To maintain a suitable calcification environment, ionocytes in the inner ear epithelium must actively exchange ions with adjacent blood vessels (Mayer-Gostan et al., 1997; Pisam et al., 1998). Previous measurements have found the endolymph fluids have nearly half [Na^+], and triple the [HCO_3^-], 41-fold higher [K^+], and nearly 1 pH unit higher compared to the blood (Payan et al., 1997; Takagi, 1997; Ghanem et al., 2008) – a feat that cannot be achieved without active ion-transport occurs between the blood and the endolymph. Previous immunohistochemical studies have documented two types of ionocytes in the inner-ear epithelium. The first type of ionocyte is rich in mitochondrion and contains abundant basolateral NKA (Takagi, 1997), whereas the second type of ionocyte has abundant carbonic anhydrase (Tohse et al., 2004, 2006). Basolateral NKCC has also been detected in the inner-ear ionocytes (Abbas and Whitfield, 2009), although it remains unconfirmed which type of ionocyte it is expressed within. Other proteins involved in Ca^{2+}, H^+, and HCO_3^- transport have been proposed (Mugiya and Yoshida, 1995; Payan et al., 1997, 2004; Tohse and Mugiya, 2001), but their presence in the inner ear epithelium remains unverified.

Increasing atmospheric CO_2 leads to ocean acidification. As global CO_2 level rises due to the burning of fossil fuels, cement production, and land use changes (Raupach et al., 2007), roughly a third of the atmospheric CO_2 is readily absorbed by the surface ocean (Caldeira and Wickett, 2003; Sabine, 2004) resulting in a decrease in ocean pH (increase in [H^+]) and subsequent decrease in [CO_3^{2-}] (Caldeira and Wickett, 2003; Sabine, 2004; Raupach et al., 2007). This phenomenon is called ocean acidification (OA). Compared to pre-industrial levels, pCO_2 has increased from ~280 to ~400 μatm and average global surface ocean pH has decreased by ~0.1 units (Caldeira and Wickett, 2003; Sabine, 2004). At the current rate of change, projections

predict atmospheric CO_2 to increase to ~1,000 and ~2,000 μatm and an associated global surface ocean pH drop to 7.7 and 7.4 by the year 2100 and 2300, respectively (Caldeira and Wickett, 2005; Meehl et al., 2007). Many OA reviews have already been written (Fabry et al., 2008; Heuer and Grosell, 2014; Clements and Hunt, 2015; Tresguerres and Hamilton, 2017), therefore I will only discuss studies relevant to this dissertation below.

Ocean acidification and adult fishes. Exposure to high CO_2 low pH conditions rapidly acidifies the fish's internal blood plasma. In response, teleost fish actively secretes H^+ into surrounding seawater and accumulates HCO_3^- in their blood plasma. The Japanese Flounder (*Paralichthys olivaceus*) only needed 8 hours to recover from the acidotic pressure induced by 10,000 and 30,000 μatm, but could not recover from exposure to 50,000 μatm of CO_2 (Hayashi et al., 2004). Even so, 10,000 μatm of CO_2 is still 10-fold higher than the future ocean conditions predicted for the year 2100 (Meehl et al., 2007). Thus, it may come as no surprise that the Gulf Toadfish (*Opsanus beta*) also recovers its pH within 4 and 8 hours after acute exposure to 1,000 and 1,900 μatm of CO_2, respectively (Esbaugh et al., 2012). Due to their robust capacity to maintain plasma pH despite extreme high CO_2 low pH levels, researchers initially believed fishes will be resilient to future OA condition (Ishimatsu et al., 2004).

However, subsequent OA studies found an array of sublethal and potentially negative effects. Laboratory studies exposed various coral reef fishes to ~1,000 μatm of CO_2 and found improper reaction to predator, prey, parental and habitat cues (Munday et al., 2009; Dixson et al., 2010; Cripps et al., 2011; Welch et al., 2014). Field-based studies also reported impaired homing ability and habitat preference (Devine et al., 2012; Devine and Munday, 2013). Many of these OA behavioral studies have been compiled (reviewed in Clements and Hunt, 2015), but the

mechanisms that induces these behavioral changes remain inconclusive – and more recently challenged in subsequent replication studies (Clark et al., 2020). The currently proposed mechanism for OA-induced behavioral changes postulates the accumulation of HCO_3^- in blood plasma that buffers pH is associated with a reduction in $[Cl^-]$, and that the altered $[HCO_3^-]$ and $[Cl^-]$ induces malfunction of gamma-aminobutyric acid type A ($GABA_A$) brain receptors (Nilsson et al., 2012). This hypothesis is supported by reports that OA-induced behavioral changes were reversed by gabazine, a $GABA_A$ receptor inhibitor (Nilsson et al., 2012; Hamilton et al., 2013; Heuer and Grosell, 2014). But this model is not without its discrepancies; the only study that analyzed the blood plasma of a teleost exposed to OA reported an increase in $[HCO_3^-]$, but no significant difference in $[Cl^-]$ (Esbaugh et al., 2016; reviewed in Tresguerres and Hamilton, 2017). Furthermore, recent OA studies on coral reef fishes found no differences in response to predator cues within the laboratory (Sundin et al., 2017), nor did they find impaired homing ability and habitat preference in the field (Raby et al., 2018).

Additionally, most of the previous OA studies analyzed individual behavior under stable, laboratory conditions. This environment does not adequately represent the large, natural variability of coastal environments caused by near shore processes such as upwelling and primary production. In the La Jolla kelp forest, *p*CO2 levels at 7 and 17m depths can range from 246 μatm to 820 μatm (pH ~8.18 to ~7.77) and from 353 μatm to 1,016 μatm (pH ~8.06 to ~7.67), respectively (Frieder et al., 2012). Thus, laboratory studies that analyzes animal responses to oscillating pH conditions would yield a better indicator of fish behavior in future ocean conditions.

Ocean acidification and larval fishes. Gill ionocytes are thought to be the main site of pH regulation in adult fishes. However, larval fishes lack developed gill ionocytes, thus researchers initially hypothesized larval fishes were more vulnerable to OA than their adult counterparts (c.f. Ishimatsu et al., 2008; Baumann et al., 2012; Hurst et al., 2013; Crespel et al., 2017). However, this idea was supported by early hypercapnic studies that exposed larval marine fishes to CO_2 levels between 10,000 to 100,000 μatm. Furthermore, these results appears to show the opposite since preflexion larval Red Sea Bream (*Pagrus major*) and Japanese Whiting (*Sillago japonica*) can tolerate ~60,000 μatm of CO_2, whereas their postflexion and juvenile counterparts can tolerate up to ~20,000 μatm of CO_2 (Kikkawa et al., 2003). Nevertheless, more recent research using more realistic CO_2 levels sought to predict larval fish responses to future ocean conditions. In contrast to the more severe CO_2 treatments, recent OA studies (1,000 – 2,500 μatm) often found nuanced, species-specific differences, and at times even conflicting intra-species disparity. For example, exposure to ~1,000 μatm of CO_2 resulted in significantly higher mortality in larval Atlantic Cod (*Gadus morhua*) (Stiasny et al., 2016), no difference in larval Atlantic herring (*Clupea harengus*) (Sswat et al., 2018), but significantly lower mortality in larval European Sea Bass (Pope et al., 2014) compared to their respective counterparts exposed to present day CO_2 levels (~400 μatm). Furthermore, conflicting survivorship results have been reported on larval Atlantic Cod despite similar CO_2 exposure levels (Frommel et al., 2013; Stiasny et al., 2016). Therefore, larval fish response to extreme hypercapnic conditions appears to differ from their response to near-future CO_2 levels.

OA studies on larval skin ionocytes and relevant acid-secreting proteins (e.g. NKA) are relatively unexplored. Previous study reported increased whole body NKA mRNA levels within OA-exposed Japanese Medaka (*Oryzias latipes*) larvae (Tseng et al., 2013), which suggests an

upregulation of H^+ secreting machinery. However, increased gene expression doesn't necessarily translate to increased protein abundance. In a separate study, OA-exposed Atlantic Cod larvae did not show any appreciable differences in NKA-rich ionocyte density compared to control larvae (Dahlke et al., 2017). These differences may be due to species-specific sensitivity, their differing techniques in estimating larval pH regulating capacities prevent direct comparisons. Additionally, both of these studies analyzed larvae within 24 hours of hatching, and differences that may appear at later larval stages cannot be ruled out. Thus, it remains unclear whether larval fishes can tolerate future CO_2 levels.

Ocean acidification and inner ear ion transport. Originally, it was predicted that fish otoliths would calcify at slower rates under OA conditions as decreasing pH reduces CO_3^{2-} availability (Ishimatsu et al., 2008). However, that prediction considered SW pH and CO_3^{2-} instead of the medium that the inner ear and its otoliths "experience" (i.e. fish blood plasma and endolymph, respectively). Indeed, Checkley *et al.* (2009) found a 8% and 16% increase in sagittal otolith area of White Seabass (*Atractoscion nobilis*) larvae reared in ~1,000 and ~2600 μatm of CO_2, respectively. Scientists proposed the enlarged otolith size is due to the increased plasma HCO_3^- accumulated to buffer against OA-induced blood acidosis (Heuer and Grosell, 2014). Many of the subsequent studies on both larval and juvenile fishes have found similar results: OA-like conditions increased otolith sizes in larval Orange Clownfish (*Amphiprion percula*) (~1700 μatm) and juvenile Three-Spined Stickleback (*Gasterosteus aculeatus*) (~1000 μatm) (Munday et al., 2011a; Schade et al., 2014). However, not all of these studies found significant increased otolith sizes: larval Atlantic Herring (*Clupea harengus*) (~1300 – 4600 μatm) and juvenile Spiny Damselfish (*Acanthochromis polyacanthus*) (~850 μatm) (Franke and

Clemmesen, 2011; Maneja et al., 2013). These contradictory results suggest increased plasma HCO_3^- alone is insufficient to explain increased otolith calcification, and that additional underlying processes may be involved.

The inner ear is a critical sensory organ involved in maintaining balance and sensing soundwaves. Therefore, the sudden increase in otolith size has been proposed to negatively affect the inner ear sensory systems. But to my knowledge, no study thus far has linked OA-induced increased otolith calcification to inner ear dysfunction. In contrast, one study exposed larval Cobia (*Rachycentron canadum*) to 2100 μatm of CO_2 and detected a 25% increase in otolith size, which was proposed to increase the larvae's hearing range by 50% (Bignami et al., 2013a). This has the potential to both benefit (e.g. increased capacity to detect prey, predators, mates) and/or harm (e.g. increased background noise may drown out sounds of prey, predator, mates) the organism. But since the study did not test hearing ability on larval fishes, it remains unverified whether hearing range indeed increases under OA conditions. To date, only one study has examined the effects of OA conditions on an otolith-dependent sensory response. The vestibulo-ocular reflex describes the rotation of the eye in the opposite direction of the head to compensate for movement and maintain visual acuity. In the larval White Seabass, their vestibulo-ocular reflex was not disrupted by the 20% and 37% increase in sagittae and lapilli otolith size induced from exposure to 2500 μatm of CO_2 (Shen et al., 2016). While other inner ear sensory system (e.g. hearing, balance) may be affected, it is currently unknown how future ocean conditions will affect the teleost inner-ear sensory system, or the fishery scientist toolkit. Furthermore, the process in which otoliths calcify is not well understood. Therefore, a better mechanistic understanding of the cells responsible for calcifying the otolith under natural conditions may

provide insights on how OA-induced HCO_3^- increase in the blood plasma would affect otolith growth, and potentially affect the inner ear.

In summary, without the basic knowledge on gill, skin, and inner ear ionocytes, our predictions on how marine fishes will respond to future ocean conditions are more correlative than causative. Therefore, this dissertation seeks to broaden our understanding of gill, skin, and inner ear ionocytes and their response to hypercapnic conditions.

Objectives. The goal of this dissertation was to characterize the ionocytes within the gill, skin, and otolithic epithelia of marine fishes and their potential responses to high CO_2 low pH conditions. These studies focused on species local to Southern California, specifically Blacksmith (*Chromis punctipinnis*), Yellowfin Tuna (*Thunnus albacares*), White Seabass (*Atractoscion nobilis*), Pacific Mackerel (*Scomber scombrus*), and Splitnose Rockfish (*Sebastes diploproa*). This body of research contributes fundamental understanding regarding the ionocyte protein expression and morphology as well as whole-animal behavior in response to hypercapnia within both larval and adult marine teleosts. The goal is accomplished in the following dissertation chapters:

1. Chapter II reports on the behavioral responses of the Blacksmith, a temperate damselfish, to CO_2-induced low-pH conditions.
2. Chapter III details a novel technique used to quantify skin ionocytes in larval fishes.
3. Chapter IV applies the technique detailed in Chapter II to document developmental patterns in the skin and gill ionocytes of larval Yellowfin Tuna.
4. Chapter V describes the responses of larval White Seabass to hypercapnic conditions.
5. Chapter VI characterizes two types of inner ear ionocytes responsible for otolith calcification in the Pacific Mackerel.
6. Chapter VII investigates whether end-of-century CO_2/pH conditions would affect the gill and inner ear ionocytes of Splitnose Rockfish.

References

Abbas, L., and Whitfield, T. T. (2009). Nkcc1 (Slc12a2) is required for the regulation of endolymph volume in the otic vesicle and swim bladder volume in the zebrafish larva. Development, 136: 2837–2848. doi:10.1242/dev.034215.

Alderdice, D. F. (1988). Osmotic and ionic regulation in teleost eggs and larvae. *In* Fish Physiology, pp. 163–251. Academic Press, Cambridge, MA.

Ayson, F. G., Kaneko, T., Hasegawa, S., and Hirano, T. (1994). Development of mitochondrion-rich cells in the yolk-sac membrane of embryos and larvae of tilapia, *Oreochromis mossambicus*, in fresh water and seawater. Journal of Experimental Zoology, 270: 129–135.

Baumann, H., Talmage, S. C., and Gobler, C. J. (2012). Reduced early life growth and survival in a fish in direct response to increased carbon dioxide. Nature Climate Change, 2: 38–41. Nature Publishing Group. doi:10.1038/nclimate1291.

Bignami, S., Enochs, I. C., Manzello, D. P., Sponaugle, S., and Cowen, R. K. (2013). Ocean acidification alters the otoliths of a pantropical fish species with implications for sensory function. Proceedings of the National Academy of Sciences, 110: 7366–7370. doi:10.1073/pnas.1301365110.

Bodinier, C., Sucré, E., Lecurieux-Belfond, L., Blondeau-Bidet, E., and Charmantier, G. (2010). Ontogeny of osmoregulation and salinity tolerance in the gilthead sea bream *Sparus aurata*. Comparative biochemistry and physiology. Part A, Molecular & integrative physiology, 157: 220–228. Elsevier B.V. doi:10.1016/j.cbpa.2010.06.185.

Caldeira, K., and Wickett, M. E. (2003). Oceanography: anthropogenic carbon and ocean pH. Nature, 425: 365.

Caldeira, K., and Wickett, M. E. (2005). Ocean model predictions of chemistry changes from carbon dioxide emissions to the atmosphere and ocean. Journal of Geophysical Research-Part C-Oceans, 110: 12 pp.-12 pp.

Campana, S. E., and Neilson, J. D. (1985). Microstructure of Fish Otoliths. Canadian Journal of Fisheries and Aquatic Sciences, 42: 1014–1032.

Campana, S. (1999). Chemistry and composition of fish otoliths: pathways, mechanisms and applications. Marine Ecology Progress Series, 188: 263–297. doi:10.3354/meps188263.

Catches, J. S., Burns, J. M., Edwards, S. L., and Claiborne, J. B. (2006). Na+/H+ antiporter, V-H+-ATPase and Na+/K+-ATPase immunolocalization in a marine teleost (*Myoxocephalus octodecemspinosus*). Journal of Experimental Biology, 209: 3440–3447.

Checkley, D. M., Dickson, A. G., Takahashi, M., Radich, J. A., Eisenkolb, N., and Asch, R. (2009). Elevated CO2 enhances otolith growth in young fish. Science (New York, N.Y.), 324: 1683.

Chivers, D. P., McCormick, M. I., Nilsson, G. E., Munday, P. L., Watson, S. A., Meekan, M. G., Mitchell, M. D., Corkill, K. C., and Ferrari, M. C. O. (2014). Impaired learning of predators and lower prey survival under elevated CO2: a consequence of neurotransmitter interference. Global Change Biology, 20: 515–522. doi:10.1111/gcb.12291.

Christensen, A. K., Hiroi, J., Schultz, E. T., and McCormick, S. D. (2012). Branchial ionocyte organization and ion-transport protein expression in juvenile alewives acclimated to freshwater or seawater. Journal of Experimental Biology, 215: 642–652. doi:10.1242/jeb.063057.

Claiborne, J. B., Perry, E., Bellows, S., and Campbell, J. (1997). Mechanisms of acid-base excretion across the gills of a marine fish. The Journal of Experimental Zoology, 279: 509–520.

Clark, T. D., Raby, G. D., Roche, D. G., Binning, S. A., Speers-Roesch, B., Jutfelt, F., and Sundin, J. (2020). Ocean acidification does not impair the behaviour of coral reef fishes. Nature, 577: 370–375. Springer US. doi:10.1038/s41586-019-1903-y.

Clements, J., and Hunt, H. (2015). Marine animal behaviour in a high CO2 ocean. Marine Ecology Progress Series, 536: 259–279. doi:10.3354/meps11426.

Crespel, A., Zambonino-Infante, J.-L., Mazurais, D., Koumoundouros, G., Fragkoulis, S., Quazuguel, P., Huelvan, C., Madec, L., Servili, A., and Claireaux, G. (2017). The development of contemporary European sea bass larvae (*Dicentrarchus labrax*) is not affected by projected ocean acidification scenarios. Marine Biology, 164: 155. Springer Berlin Heidelberg. doi:10.1007/s00227-017-3178-x.

Cripps, I. L., Munday, P. L., and McCormick, M. I. (2011). Ocean acidification affects prey detection by a predatory reef fish. PloS one, 6: e22736. doi:10.1371/journal.pone.0022736.

Dahlke, F. T., Leo, E., Mark, F. C., Pörtner, H. O., Bickmeyer, U., Frickenhaus, S., and Storch, D. (2017). Effects of ocean acidification increase embryonic sensitivity to thermal extremes in Atlantic cod, *Gadus morhua*. Global Change Biology, 23: 1499–1510.

Devine, B. M., Munday, P. L., and Jones, G. P. (2012). Rising CO2 concentrations affect settlement behaviour of larval damselfishes. Coral Reefs, 31: 229–238. doi:10.1007/s00338-011-0837-0.

Devine, B. M., and Munday, P. L. (2013). Habitat preferences of coral-associated fishes are altered by short-term exposure to elevated CO2. Marine Biology, 160: 1955–1962. doi:10.1007/s00227-012-2051-1.

Dixson, D. L., Munday, P. L., and Jones, G. P. (2010). Ocean acidification disrupts the innate ability of fish to detect predator olfactory cues. Ecology Letters, 13: 68–75. doi:10.1111/j.1461-0248.2009.01400.x.

Edwards, S. L., Tse, C. M., and Toop, T. (1999). Immunolocalisation of NHE3-like immunoreactivity in the gills of the rainbow trout (*Oncorhynchus mykiss*) and the blue-throated wrasse (*Pseudolabrus tetrious*). Journal of anatomy, 195 (Pt 3: 465–469.

Elsdon, T. S., and Gillanders, B. M. (2002). Interactive effects of temperature and salinity on otolith chemistry: challenges for determining environmental histories of fish. Canadian Journal of Fisheries and Aquatic Sciences, 59: 1796–1808. doi:10.1139/f02-154.

Esbaugh, A. J., Heuer, R., and Grosell, M. (2012). Impacts of ocean acidification on respiratory gas exchange and acid-base balance in a marine teleost, *Opsanus beta*. Journal of Comparative Physiology B: Biochemical, Systemic, and Environmental Physiology, 182: 921–934.

Esbaugh, A. J., Ern, R., Nordi, W. M., and Johnson, A. S. (2016). Respiratory plasticity is insufficient to alleviate blood acid–base disturbances after acclimation to ocean acidification in the estuarine red drum, *Sciaenops ocellatus*. Journal of Comparative Physiology B: Biochemical, Systemic, and Environmental Physiology, 186: 97–109. Springer Berlin Heidelberg.

Evans, D. H., Piermarini, P. M., and Choe, K. P. (2005). The Multifunctional Fish Gill: Dominant Site of Gas Exchange, Osmoregulation, Acid-Base Regulation, and Excretion of Nitrogenous Waste. Physiological Reviews, 85: 97–177. doi:10.1152/physrev.00050.2003.

Fabry, V. J., Seibel, B. A., Feely, R. A., and Orr, J. C. (2008). Impacts of ocean acidification on marine fauna and ecosystem processes. ICES Journal of Marine Science, 65: 414–432. doi:10.1093/icesjms/fsn048.

Ferrari, M. C. O., Manassa, R. P., Dixson, D. L., Munday, P. L., McCormick, M. I., Meekan, M. G., Sih, A., and Chivers, D. P. (2012). Effects of ocean acidification on learning in coral reef fishes. PLoS ONE, 7: e31478. doi:10.1371/journal.pone.0031478.

Franke, A., and Clemmesen, C. (2011). Effect of ocean acidification on early life stages of Atlantic herring (*Clupea harengus L.*). Biogeosciences, 8: 3697–3707. doi:10.5194/bg-8-3697-2011.

Frieder, C. A., Nam, S. H., Martz, T. R., and Levin, L. A. (2012). High temporal and spatial variability of dissolved oxygen and pH in a nearshore California kelp forest. Biogeosciences, 9: 3917–3930. doi:10.5194/bg-9-3917-2012.

Frommel, A. Y., Schubert, A., Piatkowski, U., and Clemmesen, C. (2013). Egg and early larval stages of Baltic cod, *Gadus morhua*, are robust to high levels of ocean acidification. Marine Biology, 160: 1825–1834.

Ghanem, T. A., Breneman, K. D., Rabbitt, R. D., and Brown, H. M. (2008). Ionic composition of endolymph and perilymph in the inner ear of the oyster toadfish, *Opsanus tau*. Biological Bulletin, 214: 83–90.

Hamilton, T. J., Holcombe, A., and Tresguerres, M. (2013). CO2-induced ocean acidification increases anxiety in rockfish via alteration of GABAA receptor functioning. Proceedings of the Royal Society B: Biological Sciences, 281: 20132509. doi:10.1098/rspb.2013.2509.

Hayashi, M., Kita, J., and Ishimatsu, A. (2004). Acid-base responses to lethal aquatic hypercapnia in three marine fishes. Marine Biology, 144: 153–160.

Heuer, R. M., and Grosell, M. (2014). Physiological impacts of elevated carbon dioxide and ocean acidification on fish. AJP: Regulatory, Integrative and Comparative Physiology, 307: R1061–R1084. doi:10.1152/ajpregu.00064.2014.

Hiroi, J., Kaneko, T., Seikai, T., and Tanaka, M. (1998). Developmental sequence of chloride cells in the body skin and gills of Japanese Flounder (*Paralichthys olivaceus*) larvae. Zoological science, 15: 455–60. doi:10.2108/0289-0003(1998)15[455:DSOCCI]2.0.CO;2.

Hiroi, J., Kaneko, T., and Tanaka, M. (1999). In vivo sequential changes in chloride cell morphology in the yolk-sac membrane of Mozambique tilapia (*Oreochromis mossambicus*) embyros and larvae during seawater adaptation. Journal of Experimental Biology, 202: 3485–3495.

Hiroi, J., McCormick, S. D., Ohtani-Kaneko, R., and Kaneko, T. (2005). Functional classification of mitochondrion-rich cells in euryhaline Mozambique tilapia (*Oreochromis mossambicus*) embryos, by means of triple immunofluorescence staining for Na+/K+-ATPase, Na +/K+/2Cl- cotransporter and CFTR anion channel. Journal of Experimental Biology, 208: 2023–2036.

Hiroi, J., and McCormick, S. D. (2012). New insights into gill ionocyte and ion transporter function in euryhaline and diadromous fish. Respiratory Physiology and Neurobiology, 184: 257–268. Elsevier B.V. doi:10.1016/j.resp.2012.07.019.

Hirose, S., Kaneko, T., Naito, N., and Takei, Y. (2003). Molecular biology of major components of chloride cells. Comparative Biochemistry and Physiology - B Biochemistry and Molecular Biology, 136: 593–620.

Holliday, F. G. T. (1969). The effects of salinity on the eggs and larvae of teleosts. *In* Fish physiology, pp. 293–311. Academic Press, Cambridge, MA.

Hsu, H. H., Lin, L. Y., Tseng, Y. C., Horng, J. L., and Hwang, P. P. (2014). A new model for fish ion regulation: Identification of ionocytes in freshwater- and seawater-acclimated medaka (*Oryzias latipes*). Cell and Tissue Research, 357: 225–243.

Hurst, T. P., Fernandez, E. R., and Mathis, J. T. (2013). Effects of ocean acidification on hatch size and larval growth of walleye pollock (*Theragra chalcogramma*). ICES Journal of Marine Science, 70: 812–822. doi:10.1093/icesjms/fst053.

Hwang, P.-P., Lee, T.-H., and Lin, L.-Y. (2011). Ion regulation in fish gills: recent progress in the cellular and molecular mechanisms. AJP: Regulatory, Integrative and Comparative Physiology, 301: R28–R47. doi:10.1152/ajpregu.00047.2011.

Ishimatsu, A., Kikkawa, T., Hayashi, M., Lee, K.-S., and Kita, J. (2004). Effects of CO2 on Marine Fish: Larvae and Adults. Journal of Oceanography, 60: 731–741.

Ishimatsu, A., Hayashi, M., and Kikkawa, T. (2008). Fishes in high-CO2, acidified oceans. Marine Ecology Progress Series, 373: 295–302. doi:10.3354/meps07823.

Katoh, F., Shimizu, A., Uchida, K., and Kaneko, T. (2000). Shift of chloride cell distribution during early life stages in seawater-adapted killifish, *Fundulus heteroclitus*. Zoological Science, 17: 11–18.

Keys, A. B. (1931). Chloride and water secretion and absorption by the gills of the eel. Zeitschrift für vergleichende Physiologie, 15: 364–388. doi:10.1007/BF00339115.

Keys, A., and Willmer, E. N. (1932). 'Chloride secreting cells' in the gills of fishes, with special reference to the common eel. The Journal of Physiology, 76: 368–378. doi:10.1113/jphysiol.1932.sp002932.

Kikkawa, T., Ishimatsu, A., and Kita, J. (2003). Acute CO2 tolerance during the early developmental stages of four marine teleosts. Environmental Toxicology, 18: 375–382.

Kikkawa, T., Kita, J., and Ishimatsu, A. (2004). Comparison of the lethal effect of CO2and acidification on red sea bream (*Pagrus major*) during the early developmental stages. Marine Pollution Bulletin, 48: 108–110.

Kwan, G. T., Hamilton, T. J., and Tresguerres, M. (2017). CO 2 -induced ocean acidification does not affect individual or group behaviour in a temperate damselfish. Royal Society Open Science, 4: 170283. doi:10.1098/rsos.170283.

Li, J., Eygensteyn, J., Lock, R., Verbost, P., Heijden, A., Bonga, S., and Flik, G. (1995). Branchial chloride cells in larvae and juveniles of freshwater tilapia *Oreochromis mossambicus*. Journal of Experimental Biology, 198: 2177–2184.

Liu, S.-T., Horng, J.-L., Chen, P.-Y., Hwang, P.-P., and Lin, L.-Y. (2016). Salt secretion is linked to acid-base regulation of ionocytes in seawater-acclimated medaka: new insights into the salt-secreting mechanism. Scientific Reports, 6: 31433. Nature Publishing Group. doi:10.1038/srep31433.

Lorin-Nebel, C., Boulo, V., Bodinier, C., and Charmantier, G. (2006). The Na+/K+/2Cl- cotransporter in the sea bass *Dicentrarchus labrax* during ontogeny: involvement in osmoregulation. The Journal of experimental biology, 209: 4908–4922.

Maneja, R. H., Frommel, a. Y., Geffen, a. J., Folkvord, a., Piatkowski, U., Chang, M. Y., and Clemmesen, C. (2013). Effects of ocean acidification on the calcification of otoliths of larval Atlantic cod *Gadus morhua*. Marine Ecology Progress Series, 477: 251–258.

Marshall, W. S. (2002). Na+, Cl-, Ca2+ and Zn2+ transport by fish gills: Retrospective review and prospective synthesis. Journal of Experimental Zoology, 293: 264–283.

Mayer-Gostan, N., Kossmann, H., Watrin, A., Payan, P., and Boeuf, G. (1997). Distribution of ionocytes in the saccular epithelium of the inner ear of two teleosts (*Oncorhynchus mykiss* and *Scophthalmus maximus*). Cell and Tissue Research, 289: 53–61.

Meehl, G. A., Stocker, T. F., Collins, W. D., Friedlingstein, P., Gaye, A. T., Gregory, J. M., Kitoh, A., Knutti, R., Murphy, J. M., Noda, A., Raper, S. C. B., Watterson, I. G., Weaver, A. J., and Zhao, Z.-C. (2007). 2007: Global climate projections. *In* Climate Change 2007: Contribution of Working Group I to the Fourth Assessment Report of the Intergovernmental Panel on Climate Change, pp. 747–846. Cambridge University Press, Cambridge, UK.

Mugiya, Y., and Yoshida, M. (1995). Effects of Calcium Antagonists and Other Metabolic on in Vitro Calcium Deposition on Otoliths Rainbow Trout *Oncorhynchus mykiss*. Fisheries (Bethesda), 61: 1026–1030.

Munday, P. L., Dixson, D. L., Donelson, J. M., Jones, G. P., Pratchett, M. S., Devitsina, G. V, and Døving, K. B. (2009). Ocean acidification impairs olfactory discrimination and homing ability of a marine fish. Proceedings of the National Academy of Sciences, 106: 1848–1852. doi:10.1073/pnas.0809996106.

Munday, P. L., Gagliano, M., Donelson, J. M., Dixson, D. L., and Thorrold, S. R. (2011). Ocean acidification does not affect the early life history development of a tropical marine fish. Marine Ecology Progress Series, 423: 211–221.

Nelson, J., Hanson, C. W., Koenig, C., and Chanton, J. (2011). Influence of diet on stable carbon isotope composition in otoliths of juvenile red drum *Sciaenops ocellatus*. Aquatic Biology, 13: 89–95.

Nilsson, G. E., Dixson, D. L., Domenici, P., McCormick, M. I., Sørensen, C., Watson, S.-A., and Munday, P. L. (2012). Near-future carbon dioxide levels alter fish behaviour by interfering with neurotransmitter function. Nature Climate Change, 2: 201–204. Nature Publishing Group. doi:10.1038/nclimate1352.

Pannella, G. (1971). Fish Otoliths : Daily Growth Layers and Periodical Patterns. Science, 173: 1124–1127.

Payan, P., Kossmann, H., Watrin, a, Mayer-Gostan, N., and Boeuf, G. (1997). Ionic composition of endolymph in teleosts: origin and importance of endolymph alkalinity. The Journal of Experimental Biology, 200: 1905–1912.

Payan, P., De Pontual, H., Bœuf, G., and Mayer-Gostan, N. (2004). Endolymph chemistry and otolith growth in fish. Comptes Rendus Palevol, 3: 535–547. doi:10.1016/j.crpv.2004.07.013.

Pisam, M., Payan, P., LeMoal, C., Edeyer, A., Boeuf, G., and Mayer-Gostan, N. (1998). Ultrastructural study of the saccular epithelium of the inner ear of two teleosts, *Oncorhynchus mykiss* and *Psetta maxima*. Cell and Tissue Research, 294: 261–270.

Pope, E. C., Ellis, R. P., Scolamacchia, M., Scolding, J. W. S., Keay, A., Chingombe, P., Shields, R. J., Wilcox, R., Speirs, D. C., Wilson, R. W., Lewis, C., and Flynn, K. J. (2014). European sea bass, *Dicentrarchus labrax*, in a changing ocean. Biogeosciences, 11: 2519–2530.

Raby, G. D., Sundin, J., Jutfelt, F., Cooke, S. J., and Clark, T. D. (2018). Exposure to elevated carbon dioxide does not impair short-term swimming behaviour or shelter-seeking in a predatory coral-reef fish. Journal of Fish Biology, 93: 138–142. doi:10.1111/jfb.13728.

Radtke, R. L., Lenz, P., Showers, W., and Moksness, E. (1996). Environmental information stored in otoliths: insights from stable isotopes. Marine Biology, 127: 161–170. doi:10.1007/BF00993656.

Raupach, M. R., Marland, G., Ciais, P., Le Quere, C., Canadell, J. G., Klepper, G., and Field, C. B. (2007). Global and regional drivers of accelerating CO2 emissions. Proceedings of the National Academy of Sciences, 104: 10288–10293. doi:10.1073/pnas.0700609104.

Roberts, R. J., Bell, M., and Young, H. (1973). Studies on the skin of plaice (*Pleuronectes platessa L.*). II. The development of larval plaice skin. Journal of Fish Biology, 5: 103–108. doi:10.1111/j.1095-8649.1973.tb04435.x.

Rombough, P. J. (1999). The gill of fish larvae. Is it primarily a respiratory or an ionoregulatory structure? Journal of Fish Biology, 55: 186–204. doi:10.1111/j.1095-8649.1999.tb01055.x.

Rombough, P. (2007). The functional ontogeny of the teleost gill: which comes first, gas or ion exchange? Comparative Biochemistry and Physiology - A Molecular and Integrative Physiology, 148: 732–742.

Sabine, C. L. (2004). The oceanic sink for anthropogenic CO2. Science, 305: 367–371. doi:10.1126/science.1097403.

Schade, F. M., Clemmesen, C., and Mathias Wegner, K. (2014). Within- and transgenerational effects of ocean acidification on life history of marine three-spined stickleback (*Gasterosteus aculeatus*). Marine Biology, 161: 1667–1676.

Schreiber, A. M. (2001). Metamorphosis and early larval development of the flatfishes (Pleuronectiformes): An osmoregulatory perspective. Comparative Biochemistry and Physiology - B Biochemistry and Molecular Biology, 129: 587–595.

Shen, S. G., Chen, F., Schoppik, D. E., and Checkley, D. M. (2016). Otolith size and the vestibulo-ocular reflex of larvae of white seabass *Atractoscion nobilis* at high pCO2. Marine Ecology Progress Series, 553: 173–182.

Silva, P., Solomon, R., Spokes, K., and Epstein, F. H. (1977). Ouabain inhibition of gill Na-K-ATPase: Relationship to active chloride transport. Journal of Experimental Zoology, 199: 419–426.

Sswat, M., Stiasny, M. H., Jutfelt, F., Riebesell, U., and Clemmesen, C. (2018). Growth performance and survival of larval Atlantic herring , under the combined effects of elevated temperatures and CO 2. PLoS ONE: 1–19.

Stiasny, M. H., Mittermayer, F. H., Sswat, M., Voss, R., Jutfelt, F., Chierici, M., Puvanendran, V., Mortensen, A., Reusch, T. B. H., and Clemmesen, C. (2016). Ocean acidification effects on Atlantic cod larval survival and recruitment to the fished population. PLoS ONE, 11: 1–11.

Sucré, E., Vidussi, F., Mostajir, B., Charmantier, G., and Lorin-Nebel, C. (2012). Impact of ultraviolet-B radiation on planktonic fish larvae: alteration of the osmoregulatory function. Aquatic Toxicology, 109: 194–201. Elsevier B.V. doi:10.1016/j.aquatox.2011.09.020.

Sundin, J., Amcoff, M., Mateos-González, F., Raby, G. D., Jutfelt, F., and Clark, T. D. (2017). Long-term exposure to elevated carbon dioxide does not alter activity levels of a coral reef fish in response to predator chemical cues. Behavioral Ecology and Sociobiology, 71: 108. Behavioral Ecology and Sociobiology. doi:10.1007/s00265-017-2337-x.

Swearer, S. E., Caselle, J. E., Lea, D. W., and Warner, R. R. (1999). Larval retention and recruitment in an island population of a coral-reef fish. Nature, 402: 799–802.

Takagi, Y. (1997). Meshwork arrangement of mitochondria-rich, Na+,K+-ATPase-rich cells in the saccular epithelium of rainbow trout (*Oncorhynchus mykiss*) inner ear. Anatomical Record, 248: 483–489.

Tipsmark, C. K., Madsen, S. S., Seidelin, M., Christensen, A. S., Cutler, C. P., and Cramb, G. (2002). Dynamics of Na+,K+,2Cl- cotransporter and Na+,K+-ATPase expression in the branchial epithelium of brown trout (*Salmo trutta*) and Atlantic salmon (*Salmo salar*). Journal of Experimental Zoology, 293: 106–118.

Tohse, H., and Mugiya, Y. (2001). Effects of enzyme and anion transport inhibitor on in vitro incorporation of inorganic carbon and calcium into endolymph and otoliths in salmon *Oncorhynchus masou*. Comparative Biochemistry and Physiology - A Molecular and Integrative Physiology, 128: 177–184.

Tohse, H., Ando, H., and Mugiya, Y. (2004). Biochemical properties and immunohistochemical localization of carbonic anhydrase in the sacculus of the inner ear in the salmon *Oncorhynchus masou*. Comparative Biochemistry and Physiology - A Molecular and Integrative Physiology, 137: 87–94.

Tohse, H., Murayama, E., Ohira, T., Takagi, Y., and Nagasawa, H. (2006). Localization and diurnal variations of carbonic anhydrase mRNA expression in the inner ear of the rainbow trout *Oncorhynchus mykiss*. Comparative biochemistry and physiology. Part B, Biochemistry & molecular biology, 145: 257–64. doi:10.1016/j.cbpb.2006.06.011.

Tresguerres, M., and Hamilton, T. J. (2017). Acid-base physiology, neurobiology and behaviour in relation to CO2 -induced ocean acidification. The Journal of Experimental Biology, 220: 2136–2148. doi:10.1242/jeb.144113.

Tseng, Y. C., Hu, M. Y., Stumpp, M., Lin, L. Y., Melzner, F., and Hwang, P. P. (2013). CO2-driven seawater acidification differentially affects development and molecular plasticity along life history of fish (*Oryzias latipes*). Comparative Biochemistry and Physiology - A Molecular and Integrative Physiology, 165: 1190–130. Elsevier Inc. doi:10.1016/j.cbpa.2013.02.005.

van der Heijden, A. J. H., van der Meij, J. C. A., Flik, G., and Wendelaar Bonga, S. E. (1999). Ultrastructure and distribution dynamics of chloride cells in tilapia larvae in fresh water and sea water. Cell and Tissue Research, 297: 119–130.

Varsamos, S., Connes, R., Diaz, J. P., Charmantier, G., and Dicentrarchus, L. (2001). Ontogeny of osmoregulation in the European sea bass. Marine Biology, 138: 909–915.

Varsamos, S., Diaz, J. P., Charmantier, G. U. Y., Flik, G., Blasco, C., and Connes, R. (2002a). Branchial chloride cells in sea bass (*Dicentrarchus labrax*) adapted to fresh water, seawater, and doubly concentrated seawater. Journal of Experimental Zoology, 293: 12–26.

Varsamos, S., Diaz, J., Charmantier, G., Blasco, C., Connes, R., and Flik, G. (2002b). Location and morphology of chloride cells during the post-embryonic development of the European sea bass, *Dicentrarchus labrax*. Anatomy and Embryology, 205: 203–213.

Varsamos, S., Nebel, C., and Charmantier, G. (2005). Ontogeny of osmoregulation in postembryonic fish: A review. Comparative Biochemistry and Physiology - A Molecular and Integrative Physiology, 141: 401–429.

von Biela, V., Newsome, S., and Zimmerman, C. (2015). Examining the utility of bulk otolith δ13C to describe diet in wild-caught black rockfish *Sebastes melanops*. Aquatic Biology, 23: 201–208. doi:10.3354/ab00621.

Welch, M. J., Watson, S.-A., Welsh, J. Q., McCormick, M. I., and Munday, P. L. (2014). Effects of elevated CO2 on fish behaviour undiminished by transgenerational acclimation. Nature Climate Change, 2: 2–5. doi:10.1038/nclimate2400.

CHAPTER II

CO_2-induced ocean acidification does not affect individual or group behaviour in a temperate damselfish

ROYAL SOCIETY OPEN SCIENCE

rsos.royalsocietypublishing.org

Research

Cite this article: Kwan GT, Hamilton TJ, Tresguerres M. 2017 CO_2-induced ocean acidification does not affect individual or group behaviour in a temperate damselfish. *R. Soc. open sci.* **4**: 170283. http://dx.doi.org/10.1098/rsos.170283

Received: 28 March 2017
Accepted: 7 June 2017

Subject Category:
Biology (whole organism)

Subject Areas:
physiology/behaviour/environmental science

Keywords:
climate change, upwelling, GABA, blacksmith, anxiety, shoaling

Authors for correspondence:
Trevor James Hamilton
e-mail: trevorjameshamilton@gmail.com
Martin Tresguerres
e-mail: mtresguerres@ucsd.edu

†These authors contributed equally to this study.

Electronic supplementary material is available online at https://dx.doi.org/10.6084/m9.figshare.c.3808141.

THE ROYAL SOCIETY PUBLISHING

CO_2-induced ocean acidification does not affect individual or group behaviour in a temperate damselfish

Garfield Tsz Kwan[1], Trevor James Hamilton[2,3,†] and Martin Tresguerres[1,†]

[1]Marine Biology Research Division, Scripps Institution of Oceanography, University of California San Diego, 9500 Gilman Drive, La Jolla, CA 92093, USA
[2]Department of Psychology, MacEwan University, Edmonton, Alberta, Canada T5 J 4S2
[3]Neuroscience and Mental Health Institute, University of Alberta, Edmonton, Alberta, Canada T6G 2H7

TJH, 0000-0002-8990-8247; MT, 0000-0002-7090-9266

Open ocean surface CO_2 levels are projected to reach approximately 800 μatm, and ocean pH to decrease by approximately 0.3 units by the year 2100 due to anthropogenic CO_2 emissions and the subsequent process of ocean acidification (OA). When exposed to these CO_2/pH values, several fish species display abnormal behaviour in laboratory tests, an effect proposed to be linked to altered neuronal $GABA_A$ receptor function. Juvenile blacksmith (*Chromis punctipinnis*) are social fish that regularly experience CO_2/pH fluctuations through kelp forest diurnal primary production and upwelling events, so we hypothesized that they might be resilient to OA. Blacksmiths were exposed to control conditions (pH 7.92; pCO_2 540 μatm), constant acidification (pH 7.71; pCO_2 921 μatm) and oscillating acidification (pH 7.91, pCO_2 560 μatm (day), pH 7.70, pCO_2 955 μatm (night)), and caught and tested in two seasons of the year when the ocean temperature was different: winter (16.5 ± 0.1°C) and summer (23.1 ± 0.1°C). Neither constant nor oscillating CO_2-induced acidification affected blacksmith individual light/dark preference, inter-individual distance in a shoal or the shoal's response to a novel object, suggesting that blacksmiths are tolerant to projected future OA conditions. However, blacksmiths tested during the winter demonstrated significantly higher dark preference in the individual light/dark preference test, thus confirming season and/or water temperature as relevant factors to consider in behavioural tests.

1. Introduction

Atmospheric carbon dioxide (CO_2) is rapidly increasing due to burning of fossil fuels, cement production and land use changes [1]. Since the industrial revolution, the ocean has absorbed approximately 30% of atmospheric CO_2, which has raised CO_2 levels in the surface ocean from approximately 280 to approximately 400 µatm [2,3]. This has resulted in a reduction in ocean pH and a shift in carbonate chemistry, a process called ocean acidification (OA) [2–4]. The current global surface ocean pH is already 0.1 units lower than the pre-industrial level, and the Intergovernmental Panel on Climate Change's IS92a 'business as usual' projection predicts a further CO_2 increase to approximately 800 µatm and an associated pH drop of 0.3–0.4 units by the year 2100 [4,5].

Numerous laboratory studies have found behavioural changes in response to future OA conditions including improper reaction to predator, prey, parental and habitat cues [6–8]. Studies have also reported decreases [9,10] and increases [11] in behavioural lateralization, impaired learning [12,13], increased anxiety-like behaviour [14] and increased boldness [15] (reviewed in [16]). Field-based OA experiments have additionally documented impaired predatory cue detection [7,17,18], homing ability [19] and habitat preference [20]. Many of those effects seem to be at least partially due to altered movement of Cl^- ions through γ-aminobutyric acid type A ($GABA_A$) receptors, because administration of the $GABA_A$ antagonist gabazine restored the discrimination of olfactory cues [21], behavioural lateralization [9,10] and learning [12] (reviewed in [22]). Additionally, the application of gabazine induced anxiety-like behaviour in control fish to levels similar to fish exposed to OA conditions [14]. However, some other studies have reported a lack of effect of OA-like conditions on fish subjected to tests on behavioural lateralization, emergence from shelter, predator odour avoidance, foraging and anxiety-like behaviour [23–26], suggesting fish species-specific responses to OA.

$GABA_A$ receptors are the major inhibitory mechanism in the central nervous system of vertebrate animals, including marine fish [27,28]. A widespread approach to examining whether $GABA_A$ receptors are functioning abnormally is through the testing of anxiety-like behaviour. These tests are based on evidence that activation of $GABA_A$ receptors inhibits neural excitability, thus causing a reduction in anxiety; conversely, anxiety is potentiated by $GABA_A$ receptor antagonist drugs [29,30]. The light/dark preference test is a common test for anxiety-like behaviour in mice [31,32] and zebrafish [33], and has recently been used also in other fish species [14,25,34,35]. In the light/dark preference test, an organism is placed in a rectangular arena containing walls that are white on one-half of the arena and dark on the other half. An anxious organism will have a tendency to seek the dark side of the arena to hide from aversive stimuli, while a less anxious organism typically explores the light side of the arena. The administration of pharmacological compounds can have a significant impact on the behaviour of the organism in the light/dark preference test. For example, the $GABA_A$ agonists diazepam, clonazepam, bromazepam and chlordiazepoxide decreased the time spent in the dark zone in zebrafish [36,37]. Conversely, $GABA_A$ antagonists such as picrotoxin and gabazine increased the time spent in the dark zone, and therefore anxiety, in mice [38], zebrafish [39] and splitnose rockfish (*Sebastes diploproa*) [14]. As OA is proposed to alter $GABA_A$ receptor functioning [21,40,41], tests of anxiety-like behaviour like the light/dark preference test are well suited to investigate this potential mechanism of physiological change [14].

To date, most OA studies have investigated the effects of elevated CO_2-induced acidification based on global-scale surface ocean predictions, and have acclimated fish to constantly elevated CO_2 (and thereby reduced pH) levels. However, this situation does not adequately represent the large, natural variability of coastal environments caused by near shore processes such as upwelling, water advection and primary production [42–45]. Furthermore, in some instances, coastal CO_2/pH changes can exceed the predicted pH changes of the global surface ocean [45]. For example, in the La Jolla kelp forest (San Diego, USA), pH at 7 and 17 m depths can range from 8.07 ($pCO_2 \sim 246$ µatm) to 7.87 ($pCO_2 \sim 820$ µatm) and from 7.80 ($pCO_2 \sim 353$ µatm) to 7.67 ($pCO_2 \sim 1016$ µatm), respectively [44]. Time-series data in the La Jolla kelp forest have also shown diurnal pH fluctuation ranging from 8.2 to 7.8 [44]. However, to date there are no reports of fish behavioural or physiological responses to current environmentally relevant CO_2/pH variability (although [15] tested the effects of fluctuating CO_2 from 450 to 2000 µatm in freshwater).

Similarly, most studies on the effects of OA on fish have so far focused on individual behaviour, yet roughly half of the world's fish species live in shoals for part of their life and about one-quarter of the world's fish species live in shoals for their entire life [46]. Shoaling is defined as any group of fish that remain together for social reasons [47,48]. Unlike schooling, shoaling fish do not necessarily display coordinated swimming [48]. Nonetheless, shoaling fish still benefit from enhanced predator detection [49], foraging [50] and social learning [51,52]. In the laboratory, shoaling behaviour has also

been proposed as an index of anxiety (reviewed in [36]). These studies, and others in banded killifish (*Fundulus diaphanus*) [53], demonstrate that, in response to predatory cues or invasive stimuli, the shoal will become tighter (i.e. nearest neighbour distance (NND) and inter-individual distance (IID) will decrease). Conversely, pharmacological administration of anxiety-reducing (anxiolytic) drugs, some of which alter $GABA_A$ receptors, results in shoal dispersion (i.e. increased NND and IID) [54,55]. To the best of our knowledge, there have only been two studies on the effects of OA on shoaling behaviour: one reported a decreased tendency to associate with familiar shoal-mates in blue-green puller damselfish (*Chromis viridis*) [56], and the other described lower shoal cohesion in sand smelt (*Atherina presbyter*) [57].

Another understudied aspect of OA is the potential induction of differential effects on aquatic organisms during different seasons. If the effects of OA on fish behaviour were indeed caused by malfunction of neuronal functions as current models propose, such differential effects could exist due to differences in temperature, hormonal or nutritional status among other factors.

To answer some of these questions, we used blacksmith (*Chromis punctipinnis*), a damselfish found year-round in southern California waters [58,59]. Both juvenile and adult blacksmiths form loosely oriented shoals when unthreatened, and tighten into well-oriented shoals when threatened [58,59]. Juvenile blacksmiths typically live within 15 m of the surface, hiding in the kelp while feeding on the abundant plankton in the current [58]. Adult blacksmiths are found deeper in the water column, typically among rocky reefs and kelp forests [58,59].

Thus, the current study has the following objectives: (i) examine the impacts of future pH/CO_2 levels on blacksmith individual behaviour; (ii) investigate the impacts of future pH/CO_2 levels on blacksmith shoaling behaviour; (iii) compare the effects of oscillating acidification versus constant acidification on blacksmith individual and shoaling behaviour; and (iv) compare behavioural responses of blacksmiths collected and tested in different seasons of the year.

2. Material and methods

Juvenile blacksmiths were caught from drifting kelp paddies off the shores of La Jolla, adjacent to the Scripps Coastal Reserve (La Jolla, USA) in December 2014 and August 2015. Fish were collected and tested in two experimental sets to determine whether seasonal variability and/or water temperature may also affect blacksmith responses to CO_2/pH. Blacksmiths from the same kelp paddies were habituated together within the Scripps Institution of Oceanography (SIO) flowing seawater aquarium for at least 30 days prior to experimentation. Blacksmiths were fed daily with live brine shrimp nauplii and frozen copepods. The initial behavioural measurements were performed in January 2015 (16.5 ± 0.1°C) on blacksmiths caught in December 2014. A subsequent set of individual behavioural measurements and a set of group behavioural measurements were performed in September 2015 (23.1 ± 0.1°C) on blacksmiths caught in August 2015. Blacksmiths were randomly selected from the holding tanks (January: $n = 47$; 3.2 ± 0.58 cm; 0.48 ± 0.02 g; September: $n = 105$; 3.3 ± 0.21 cm; 0.39 ± 0.01 g). There were no significant differences in length (January: $F_{2,44} = 0.399$; $p = 0.674$; September: $F_{2,44} = 1.166$; $p = 0.321$) or weight (January: $F_{2,48} = 0.838$; $p = 0.439$; September: $F_{2,48} = 0.987$; $p = 0.380$) within treatments. Blacksmiths were randomly assigned to control CO_2/pH (January: $pCO_2 = 549 \pm 5$ µatm, 7.91 ± 0.00 pH units; September: $pCO_2 = 530 \pm 3$ µatm, 7.93 ± 0.00 pH units), constant acidification (January: $pCO_2 = 983 \pm 19$ µatm, 7.68 ± 0.01 pH units; September: $pCO_2 = 859 \pm 9$ µatm, 7.74 ± 0.01 pH units) and oscillating acidification (January: day: $pCO_2 = 587 \pm 4$ µatm, 7.89 ± 0.00 pH units; night: $pCO_2 = 1066 \pm 66$ µatm, 7.65 ± 0.03 pH units; September: day: $pCO_2 = 532 \pm 4$ µatm, 7.93 ± 0.00 pH units; night: $pCO_2 = 845 \pm 2$ µatm, 7.75 ± 0.00 pH units) treatments (table 1, electronic supplementary material, figure S1). Testing took place after 7 (individual behaviour) or 11 days (group behaviour) of exposure to control, constant or oscillating CO_2 acidification. This time frame was chosen because it is consistent and comparable with our previous study on rockfish [14].

Seawater was continuously pumped from the Scripps Coastal Reserve into the header tanks, where the IKS Aquastar system (Karlsbad, Germany) monitored and recorded the temperature and pH values as well as manipulated the pH by bubbling CO_2 gas into the three header tanks (electronic supplementary material, figure S1). The control header tank was not manipulated, and therefore reflected current local water conditions normally experienced by juvenile blacksmiths. Each header tank supplied water to three 20 l experimental tanks ($0.3\,l\,min^{-1}$) housing six blacksmiths each, and was covered with a transparent fibreglass lid to limit atmospheric exposure and slow CO_2 degassing. Experimental tanks were randomly arranged and located on a shelf directly below the header tanks (see more details in 'Data analysis').

Table 1. Water chemistry during January 2015 and September 2015 experiments. pH_{nbs}, alkalinity, salinity and temperature were measured as described in Material and methods. pCO_2, $\Omega_{aragonite}$ and $\Omega_{calcite}$ were calculated using CO_2SYS. Data presented as mean ± s.e.m.)

			oscillating acidification	
	control	constant acidification	day	night
January 2015				
pH_{nbs}	7.91 ± 0.00	7.68 ± 0.01	7.89 ± 0.00	7.65 ± 0.03
alkalinity (µmol $kgSW^{-1}$)	2234.04 ± 0.27	2232.81 ± 2.30	2233.99 ± 0.78	2233.70 ± 0.00
salinity (PSU)	33.4 ± 0.1	33.4 ± 0.1	33.4 ± 0.1	33.4 ± 0.1
pCO_2 (µatm)	549 ± 5	983 ± 19	587 ± 4	1066 ± 66
$\Omega_{aragonite}$	1.90 ± 0.01	1.19 ± 0.02	1.80 ± 0.02	1.10 ± 0.06
$\Omega_{calcite}$	2.95 ± 0.02	1.85 ± 0.03	2.80 ± 0.02	1.70 ± 0.09
Temp (°C)		16.5 ± 0.1		
September 2015				
pH_{nbs}	7.93 ± 0.00	7.74 ± 0.01	7.93 ± 0.00	7.75 ± 0.00
alkalinity (µmol $kgSW^{-1}$)	2235.40 ± 2.02	2234.60 ± 1.33	2234.40 ± 1.85	2245.00 ± 0.00
salinity (PSU)	33.5 ± 0.3	33.5 ± 0.3	33.5 ± 0.3	33.5 ± 0.2
pCO_2 (µatm)	530 ± 3	859 ± 9	532 ± 4	845 ± 2
$\Omega_{aragonite}$	2.48 ± 0.02	1.73 ± 0.02	2.50 ± 0.03	1.80 ± 0.01
$\Omega_{calcite}$	3.79 ± 0.04	2.64 ± 0.03	3.80 ± 0.04	2.70 ± 0.01
Temp (°C)		23.1 ± 0.1		

Additional pH measurements on header and experimental tanks were performed daily using a HACH portable pH probe (HQ40d with pH probe PHC101) to confirm proper electrode function and ensure that pH levels in the header tanks matched those in the animal tanks. Furthermore, discrete water samples were taken on the first, middle and last day of exposure and analysed for total alkalinity, salinity and pH in the Dickson laboratory (SIO; table 1). These discrete water samples were used to validate the IKS pH electrode measurements and calculate pCO_2, $\Omega_{aragonite}$ and $\Omega_{calcite}$ using CO2SYS (v.2.1), with dissociation constants from Mehrbach *et al*. [60] as refitted by Dickson & Millero [61] (see also [62]) (table 1) [60–62]. Lighting was maintained in a 12 L : 12 D cycle using an automatic timer. In the oscillating acidification treatment, the IKS system triggered the CO_2/pH switch two hours before the light/dark switch (electronic supplementary material, figure S1).

2.1. General behavioural testing protocol

All testing took place between the hours of 6.00 and 18.00. Recordings were captured by a FireWire 400 Color Industrial Camera with a Tamron CCTV lens (2.8–12 mm, f/1.4), and the videos were analysed with Ethovision XT motion tracking software system (v.10, Noldus, Leesburg, VA, USA). The arenas were placed in an enclosed testing chamber with even lighting. The arena was rotated 180° every four trials throughout the testing to compensate for any unintentional visual or auditory stimuli. All subjects were gently coaxed into a 500 ml container with their respective treatment water and transferred into a 30.5 × 15.3 cm area surrounded by white walls to allow the fish to acclimate to the conditions inside the testing chamber and arena. After 15 min, each blacksmith (or shoal of blacksmiths) was released into the centre of the testing arena. Testing began immediately afterwards and was recorded by an overhead camera. All blacksmiths were tested in their respective water treatment, and blacksmiths in the oscillating CO_2/pH treatment were tested in control CO_2/pH seawater as this was the condition experienced during the day, which was when behavioural testing took place. Blacksmiths were not fed for 24 h prior to behavioural testing [14]. Four blacksmiths from control, three from constant acidification and three from oscillating acidification treatments (all from different holding tanks) died during the exposure period from undetermined causes. Therefore, group behavioural testing was conducted with five blacksmiths in all cases.

2.2. Individual behaviour: light/dark preference test

The light/dark preference test was similar to earlier studies on zebrafish [63], splitnose rockfish [14] and black perch (*Embiotoca jacksoni*) [34]. The testing arena (30.5 cm × 15.3 cm × 19.0 cm) had black or white plastic walls (electronic supplementary material, figure S2), and was filled to a height of 7 cm with the respective treatment water. The bottom of the arena was white in both the light and dark zones to allow for motion tracking throughout the arena. The colour of the floor, white or black, has been previously shown to have no effect on light or dark zone preference in the light/dark preference test [63]. After seven days of treatment exposure, individual blacksmiths were placed into the arena for 15 min and the duration spent in the dark zone was quantified. Blacksmiths in the September experiment were returned to their experimental tanks for subsequent group behaviour testing.

2.3. Group behaviour: shoaling test

The shoaling test was based on previous studies on zebrafish [64,65]. The testing arena was a white, plastic, circular arena filled with 6 cm of the respective treatment water (electronic supplementary material, figure S2). After 11 days of treatment exposure, a shoal of five blacksmiths from the September experiment were simultaneously placed into the arena and recorded for 15 min. IID (the average distance of an individual fish to all other shoal mates) and time near the wall (thigmotaxis, 3.3 cm from the arena wall) were quantified. Each shoal of five blacksmiths constituted one sample, and a total of six shoals per treatment were analysed. The size of the thigmotaxic zone was based on the average body length of blacksmith (3.3 cm).

2.4. Group behaviour: novel object test

After 15 min of recording in the shoaling test (described above), a novel object was placed in the centre of the arena and fish behaviour was further recorded for another 15 min (electronic supplementary material, figure S2). The novel object was a multicoloured Lego figurine (5 cm tall) to avoid innate colour preference [14,15]. IID and time spent close to the novel object (both 3.3 and 6 cm radius) were analysed. These distances were chosen based on the average length of fish in this study and the radius used in previous novel object studies [14]. To the best of our knowledge, this was the first time the novel object test has been combined with a shoaling test. The rationale was that the novel object may be perceived as either predatory [66] or shelter-like stimuli [14], and this response may be altered by OA-like conditions.

2.5. Data analysis

Experimental tank effect was considered a random factor and nested in each treatment, which satisfies the experimental design guidelines proposed by Cornwall & Hurd [67]. Data were pooled when tank effect was determined to be conservatively not significant at $p \geq 0.250$ (electronic supplementary material, table S1) [68]. The Shapiro–Wilk and Levene tests were used to evaluate the assumptions of normality and homogeneity (electronic supplementary material, table S1). Individual light/dark preference test behaviour was analysed using two-way analysis of variance (ANOVA) with month of the year (January, September) and pH treatments (control, constant acidification, oscillating acidification) as variables. One-sample *t*-tests were also used in the light/dark preference test parameters to compare time spent in a particular zone to 450 s (half of the duration of the test), as commonly used in these types of study [6,14,35]. Shoaling and novel object test behaviours were analysed with one-way ANOVA. All statistical analyses were completed using R (v. 0.98.1103) [69] and the R-package 'car' [70]. Unless otherwise noted, all values are given as mean ± s.e.m.

3. Results

3.1. Individual behaviour: light/dark preference test

We first examined whether constant or oscillating acidification affected individual blacksmith light/dark preference (January: $n = 15$, 16, 16 and September: $n = 17$, 17, 17; control, constant acidification, oscillating acidification, respectively). Two-way ANOVA detected significant seasonal effect (January versus September experiments) on dark preference ($F_{1,92} = 7.9540$, $p = 0.0059$), but no significant effect of CO_2/pH (control, constant acidification, oscillating acidification) ($F_{2,92} = 0.3557$, $p = 0.7017$) or

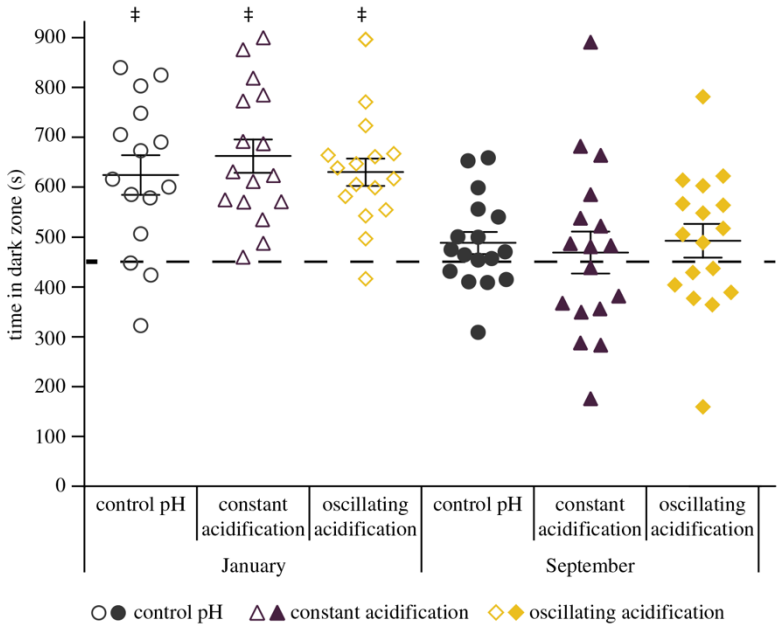

Figure 1. Control, constant acidification and oscillating acidification-exposed *Chromis punctipinnis* were individually placed in the light/dark preference test arena and their location recorded for 900 s. In January ($n = 15$–16), fish from all three treatments spent significantly more time in the dark zone than 450 s ($^{\ddagger}p < 0.0001$ in all cases), while in September ($n = 17$) they did not. Time spent in the dark zone was significantly affected by season (January versus September; $F_{1,92} = 7.9540$, $p = 0.0059$), but it was not significantly affected by CO_2/pH treatments ($F_{2,92} = 0.3557$, $p = 0.7017$). There were no significant interaction effects ($F_{2,92} = 0.4629$, $p = 0.6309$). Data presented as mean ± s.e.m.

interaction effect ($F_{2,92} = 0.4629$, $p = 0.6309$; figure 1). Similarly, one-sample *t*-test indicated that all three pH treatment groups in the January experiments spent significantly more than 450 s in the dark zone ($p < 0.0001$ for all three pH treatments), whereas none of the CO_2/pH treatment groups in the September experiments had a significant preference for either the light or the dark zone ($p = 0.1018$, $p = 0.6549$, $p = 0.2309$ for control, constant acidification and oscillating acidification, respectively).

3.2. Group behaviour: shoaling test

We next examined whether constant or oscillating acidification affected blacksmith's shoaling behaviour ($n = 6$ shoals per treatment), with each data point representing a shoal of five fish. One-way ANOVA indicated no significant effect of constant or oscillating acidification on either thigmotaxis ($F_{2,15} = 0.621$, $p = 0.551$) or IID ($F_{2,15} = 0.502$, $p = 0.615$; figure 2).

3.3. Group behaviour: novel object test

Finally, we analysed the behaviour of a group of five blacksmiths after the introduction of a novel object ($n = 6$ shoals per treatment). One-way ANOVA found no significant differences in constant or oscillating acidification in either time near the object (6 cm radius; $F_{2,15} = 0.159$, $p = 0.855$) or IID ($F_{2,15} = 0.312$, $p = 0.737$; figure 3). There were also no significant differences ($F_{2,15} = 0.283$, $p = 0.758$) when a 3.3 cm radius was used to analyse time near the object.

4. Discussion

A common limitation of laboratory studies is that the experimental conditions do not mimic the conditions experienced by fishes in the wild. With this in mind, we added two variables not commonly implemented in OA studies; oscillating acidification to replicate the natural variability encountered in

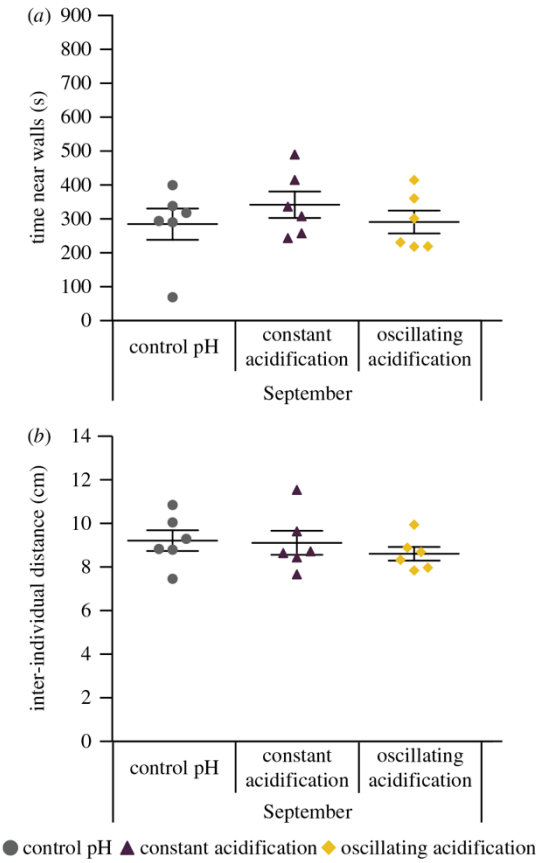

Figure 2. Control, constant acidification and oscillating acidification-exposed *Chromis punctipinnis* were placed into a shoaling test arena in groups of five and their locations recorded for 900 s ($n = 6$ shoals per treatment). (*a*) Time near walls was not affected by CO_2/pH treatments ($F_{2,15} = 0.621$, $p = 0.551$). (*b*) Inter-individual distance was also not affected by CO_2 treatments ($F_{2,15} = 0.502$, $p = 0.615$). Data presented as mean ± s.e.m. This test was only performed on the September groups.

kelp forests and seagrass beds, and testing of group behaviour to examine the natural social behaviour that is observed in most fish species. However, neither individual nor group behaviour were affected by either constant or oscillating acidification, suggesting that blacksmiths are resilient to environmental CO_2/pH variability and to near-future OA scenarios, at least in relation to the parameters tested. On the contrary, the season in which blacksmiths were caught and tested did affect individual blacksmith behaviour, which warrants further investigation.

The lack of effect of OA conditions on blacksmith light/dark preference is in contrast with our earlier study on splitnose rockfish, in which exposure to constant acidification induced a significant dark preference [14]. The aforementioned rockfish study and the current blacksmith study are comparable, because both collected fish from drifting kelp paddies offshore of La Jolla, California, exposed them to similar CO_2/pH conditions and quantified fish behaviour using the same light/dark preference test. Constant and oscillating acidification also did not affect the group behaviour parameters tested on blacksmith in this study. These results have important caveats. Firstly, although the means of IID and thigmotaxis from control and treatments were not statistically different from each other and there were no obvious trends, the low number of replicates ($n = 6$) affects the statistical power. However, because each replicate was a shoal of five fish, and because there were three experimental conditions, our sample size of $n = 6$ for each condition involved the use of 90 fish. Thus, increasing the number of replicates represents a challenge both in terms of infrastructure and testing logistics. Additionally, the lack of information about blacksmith group behaviour and relevant experimental tests makes it difficult to

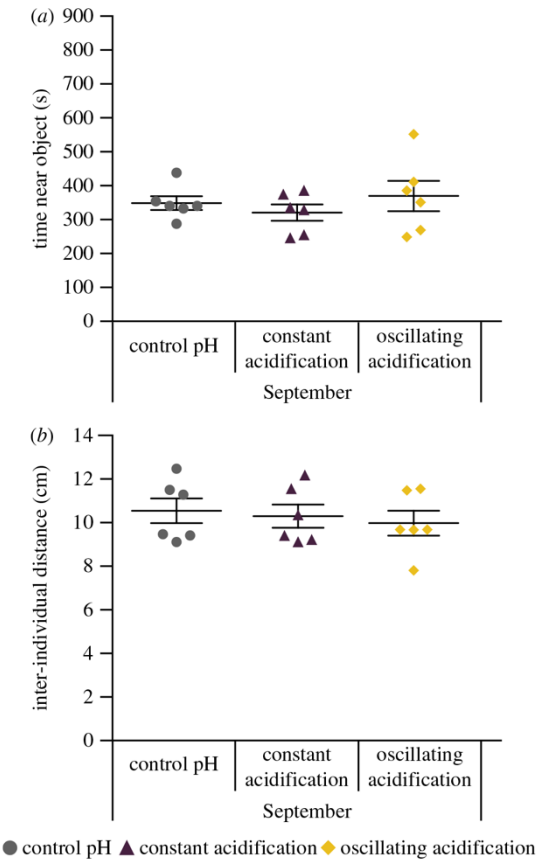

Figure 3. Immediately after the shoaling test, a novel object was placed into the arena and shoal behaviour was recorded for 900 s ($n = 6$ shoals per treatment). (*a*) Time near novel object was not affected by CO_2/pH treatments ($F_{2,15} = 0.159$, $p = 0.855$). (*b*) Inter-individual distance to conspecifics was also not affected by CO_2/pH treatments ($F_{2,15} = 0.312$, $p = 0.737$). Data presented as mean ± s.e.m. This test was only performed on the September groups.

assess the relevance of the results for real-world conditions. These limitations clearly indicate that there is a need for more research and resources dedicated to OA studies.

One mainstream hypothesis behind OA-induced behavioural changes in fish is altered intracellular/extracellular bicarbonate and chloride gradients which change $GABA_A$ receptor function as a side effect of blood acid–base regulation [21,40,41] (reviewed in [22]). As fish accumulate HCO_3^- to buffer blood pH, Cl^- concentration is proposed to be reduced in an equimolar amount, and reverse the flux of Cl^- across $GABA_A$ receptors [21]. Thus, GABA-induced $GABA_A$ receptor opening could result in neuronal depolarization instead of hyperpolarization, which could explain the alteration in behaviours.

Multiple studies have reported alterations in fish anxiety-like behaviour in response to elevated CO_2 levels. In addition to the above-mentioned increased anxiety in rockfish [14], OA-exposed marine three-spined stickleback (*Gasterosteus aculeatus*) spent significantly less time near the novel object, similarly suggesting increased anxiety [10]. CO_2 acidification also induced an alteration in anxiety-like behaviour in pink salmon in freshwater; however, in this case, anxiety was decreased in the novel-approach test [15]. However, exposure to elevated CO_2 levels did not affect the behaviour of several other fish species subjected to similar tests. For example, OA-like conditions did not significantly affect predator avoidance [23], behavioural lateralization or boldness [24] in juvenile Atlantic cod (*Gadus morhua*), and it also did not affect anxiety-like behaviour in red drum (*Sciaenops ocellatus*) [25].

These species-specific differences have been attributed to a variety of potential causes, from different iono-regulatory mechanisms and capacity, to different life-history traits [15], such as living in a marine, estuarine or freshwater environment, living in the open ocean, kelp forest, mangrove or reef, or being

a migratory species (reviewed in [41]). The lack of effect of OA on blacksmith behaviour in the current study could be due to a variety of not mutually exclusive reasons. For example, blacksmiths may be able to regulate the acid/base status of their internal fluids, so OA-relevant elevations in CO_2 levels do not affect neuronal function, or they may be able to regulate neuronal membrane potential to offset potential effects of OA on the chemistry of their internal fluids (reviewed in [41]). Exploring these mechanisms in fish species whose behaviour is altered by OA-like conditions, and comparing them to species that are resilient could provide valuable insights on the potential effects of OA on fish in the wild. However, this is not a trivial task, as it requires measuring the concentrations of HCO_3^- and Cl^- inside neurons and in cerebrospinal fluid. This has never been done in any fish, and is extremely challenging because the putative changes in ion concentrations are small and likely to be affected by the sampling procedures (reviewed in [41]).

Another interesting and unexpected finding from our study was the significantly different anxiety-like behaviour measured in both control and OA conditions in experiments in January (winter) compared to the experiments in September (late summer). Both sets of experiments were conducted under identical illumination and diet conditions; however, seawater temperature was approximately 6.50°C higher in the summer. Thus, the difference in dark preference between winter and summer could have been due to temperature. However, several other potentially relevant parameters were not measured, such as hormonal levels, and cannot be ruled out. Regardless, the observed differences in control behaviours between the two seasons strengthens the finding that the OA-like conditions tested here have no effect on blacksmith because there was no effect of OA on anxiety-like behaviour in either season. However, effects of OA on other aspects of blacksmith behaviour, most notably olfactory discrimination, have not been investigated here and will constitute the basis for future research.

Blacksmith responses in the current study also differed from studies on tropical damselfish that have found a variety of behavioural impairments in response to OA-like conditions, including altered behavioural lateralization (yellowtail demoiselle, *Neopomacentrus azysron*) [21], altered olfactory abilities (*Pomacentrus wardi* [18]; *Dascyllus aruanus* and *P. moluccensis* [71]) and impaired learning of olfactory cues (*P. amboinensis* [12,13]). Interestingly, the ability to sense anti-predator cues after OA-like treatments was considerably different in four congeneric species of damselfish (*P. moluccensis, P. amboinensis, P. nagasakiensis and P. chrysurus*) [72]. Because these fish shared similar ecology and life history, the authors concluded that their differential resilience to OA-like conditions may be due to unidentified physiological differences [72]. The differential response to OA-like conditions between blacksmith (a temperate damselfish) and tropical damselfishes may be explained by the same rationale. However, variability in life stages and ecological habitats make a direct comparison to our study difficult. Furthermore, performing light/dark and shoaling tests on tropical damselfish species, or olfactory discrimination tests on blacksmith, is necessary for direct comparisons between species.

In summary, the behaviour of juvenile blacksmith was not affected by CO_2-acidified conditions previously demonstrated to affect juveniles of a sympatric rockfish species. These results suggest these two fish species are not equally susceptible to the predicted future OA, and identify blacksmith and splitnose rockfish as a potential 'winner' and 'loser' species, respectively. However, this possibility should be experimentally confirmed by other behavioural and physiological tests, which would ideally combine laboratory and field studies.

Ethics. All experiments were approved by the SIO-UCSD animal care committee under protocol no. S10320 in compliance with the IACUC guidelines for the care and use of experimental animals. All animals were collected under permit (#SCP13227) issued by the California Department of Fish and Wildlife.

Data accessibility. The datasets supporting this article are presented in the text, table, figures and electronic supplementary material.

Authors' contributions. T.J.H. and M.T. conceived the study. All authors designed the experiments, analysed results and wrote the manuscript. G.T.K. performed the experiments. All authors gave their final approval for the publication.

Competing interests. The authors declare no competing interests.

Funding. G.T.K. is supported by the San Diego Fellowship and the National Science Foundation Graduate Research Fellowship Program (NSF-GRFP). This study was funded by UCSD Academic Senate Award, NSF (EF #1220641) and an Alfred P. Sloan research Fellowship Grant (BR2013-103) to M.T., and Natural Sciences and Engineering Research Council (NSERC) Discovery grant to T.J.H. (04843).

Acknowledgements. We thank Phil Zerofski (SIO) for collecting the fish and helping with aquarium matters, and Radha Karra, Mikayla Ortega, Yuzo Yanagitsuru and Dr Cristina Salmerón Salvador (Tresguerres laboratory, SIO) for their help with fish care and data collection. Dr Stuart Sandin (SIO), Lynn Waterhouse (SIO) and Dr Carlos Luquet (CONICET-Argentina) provided valuable assistance with statistical analyses. We are grateful to Carlsbad Aquafarm (Carlsbad, CA) for donating aquarium supplies.

References

1. Raupach MR, Marland G, Ciais P, Le Quere C, Canadell JG, Klepper G. 2007 Global and regional drivers of accelerating CO_2 emissions. *Proc. Natl Acad. Sci. USA* **104**, 10 288–10 293. (doi:10.1073/pnas.0700609104)
2. Caldeira K, Wickett ME. 2003 Oceanography: anthropogenic carbon and ocean pH. *Nature* **425**, 365. (doi:10.1038/425365a)
3. Sabine CL. 2004 The oceanic sink for anthropogenic CO_2. *Science* **305**, 367–371. (doi:10.1126/science.1097403)
4. Orr JC *et al.* 2005 Anthropogenic ocean acidification over the twenty-first century and its impact on calcifying organisms. *Nature* **437**, 681–686. (doi:10.1038/nature04095)
5. Meehl GA *et al.* 2007 Global climate projections. In *Climate Change 2007: Contribution of Working Group I to the Fourth Assessment Report of the Intergovernmental Panel on Climate Change*, pp. 747–846. Cambridge, UK: Cambridge University Press.
6. Cripps IL, Munday PL, McCormick MI. 2011 Ocean acidification affects prey detection by a predatory reef fish. *PLoS ONE* **6**, e22736. (doi:10.1371/journal.pone.0022736)
7. Dixson DL, Munday PL, Jones GP. 2010 Ocean acidification disrupts the innate ability of fish to detect predator olfactory cues. *Ecol. Lett.* **13**, 68–75. (doi:10.1111/j.1461-0248.2009.01400.x)
8. Munday PL, Dixson DL, Donelson JM, Jones GP, Pratchett MS, Devitsina GV. 2009 Ocean acidification impairs olfactory discrimination and homing ability of a marine fish. *Proc. Natl Acad. Sci. USA* **106**, 1848–1852. (doi:10.1073/pnas.0809996106)
9. Domenici P, Allan B, McCormick MI, Munday PL. 2012 Elevated carbon dioxide affects behavioural lateralization in a coral reef fish. *Biol. Lett.* **8**, 78–81. (doi:10.1098/rsbl.2011.0591)
10. Jutfelt F, de Souza KB, Vuylsteke A, Sturve J. 2013 Behavioural disturbances in a temperate fish exposed to sustained high-CO_2 levels. *PLoS ONE* **8**, e65825. (doi:10.1371/journal.pone.0065825)
11. Green L, Jutfelt F. 2014 Elevated carbon dioxide alters the plasma composition and behaviour of a shark. *Biol. Lett.* **10**, 20140538. (doi:10.1098/rsbl.2014.0538)
12. Chivers DP *et al.* 2014 Impaired learning of predators and lower prey survival under elevated CO_2: a consequence of neurotransmitter interference. *Glob. Change Biol.* **20**, 515–522. (doi:10.1111/gcb.12291)
13. Ferrari MCO, Manassa RP, Dixson DL, Munday PL, McCormick MI, Meekan MG. 2012 Effects of ocean acidification on learning in coral reef fishes. *PLoS ONE* **7**, e31478. (doi:10.1371/journal.pone.0031478)
14. Hamilton TJ, Holcombe A, Tresguerres M. 2014 CO_2-induced ocean acidification increases anxiety in rockfish via alteration of GABAA receptor functioning. *Proc. R. Soc. B* **281**, 20132509. (doi:10.1098/rspb.2013.2509)
15. Ou M Hamilton TJ, Eom J, Lyall EM, Gallup J, Jiang A. 2015 Responses of pink salmon to CO_2-induced aquatic acidification. *Nat. Clim. Change* **5**, 950–955. (doi:10.1038/nclimate2694)
16. Clements J, Hunt H. 2015 Marine animal behaviour in a high CO_2 ocean. *Mar. Ecol. Prog. Ser.* **536**, 259–279. (doi:10.3354/meps11426)
17. Ferrari MCO, Dixson DL, Munday PL, McCormick MI, Meekan MG, Sih A. 2011 Intrageneric variation in antipredator responses of coral reef fishes affected by ocean acidification: implications for climate change projections on marine communities. *Glob. Change Biol.* **17**, 2980–2986. (doi:10.1111/j.1365-2486.2011.02439.x)
18. Munday PL, Dixson DL, McCormick MI, Meekan M, Ferrari MCO, Chivers DP. 2010 Replenishment of fish populations is threatened by ocean acidification. *Proc. Natl Acad. Sci. USA* **107**, 12 930–12 934. (doi:10.1073/pnas.1004519107)
19. Devine BM, Munday PL, Jones GP. 2012 Homing ability of adult cardinalfish is affected by elevated carbon dioxide. *Oecologia* **168**, 269–276. (doi:10.1007/s00442-011-2081-2)
20. Devine BM, Munday PL. 2013 Habitat preferences of coral-associated fishes are altered by short-term exposure to elevated CO_2. *Mar. Biol.* **160**, 1955–1962. (doi:10.1007/s00227-012-2051-1)
21. Nilsson GE, Dixson DL, Domenici P, McCormick MI, Sørensen C, Watson S-A. 2012 Near-future carbon dioxide levels alter fish behaviour by interfering with neurotransmitter function. *Nat. Clim. Change* **2**, 201–204. (doi:10.1038/nclimate1352)
22. Heuer RM, Grosell M. 2014 Physiological impacts of elevated carbon dioxide and ocean acidification on fish. *AJP Regul. Integr. Comp. Physiol.* **307**, R1061–R1084. (doi:10.1152/ajpregu.00064.2014)
23. Jutfelt F, Hedgärde M. 2013 Atlantic cod actively avoid CO_2 and predator odour, even after long-term CO_2 exposure. *Front. Zool.* **10**, 81. (doi:10.1186/1742-9994-10-81)
24. Jutfelt F, Hedgärde M. 2015 Juvenile Atlantic cod behavior appears robust to near-future CO_2 levels. *Front. Zool.* **12**, 1–7. (doi:10.1186/s12983-015-0104-2)
25. Lonthair J, Ern R, Esbaugh AJ. 2017 The early life stages of an estuarine fish, the red drum (*Sciaenops ocellatus*), are tolerant to high pCO_2. *ICES J. Mar. Sci.* **74**, 1042–1050. (doi:10.1093/icesjms/fsw225)
26. Heinrich DDU, Watson S-A, Rummer JL, Brandl SJ, Simpfendorfer CA, Heupel MR. 2016 Foraging behaviour of the epaulette shark *Hemiscyllium ocellatum* is not affected by elevated CO_2. *ICES J. Mar. Sci.* **73**, 633–640. (doi:10.1093/icesjms/fsv085)
27. Shin LM, Liberzon I. 2010 The neurocircuitry of fear, stress, and anxiety disorders. *Neuropsychopharmacology* **35**, 169–191. (doi:10.1038/npp.2009.83)
28. Stewart A *et al.* 2011 Pharmacological modulation of anxiety-like phenotypes in adult zebrafish behavioral models. *Prog. Neuro-Psychopharmacol. Biol. Psychiatry* **35**, 1421–1431. (doi:10.1016/j.pnpbp.2010.11.035)
29. Enna SJ. 1984 Role of γ-aminobutyric acid in anxiety. *Psychopathology* **17**, 15–24. (doi:10.1159/000284073)
30. Nestoros JN. 1984 GABAergic mechanisms and anxiety: an overview and a new neurophysiological model. *Can. J. Psychiatry* **29**, 520–529. (doi:10.1177/070674378402900614)
31. Bourin M, Hascoët M. 2003 The mouse light/dark box test. *Eur. J. Pharmacol.* **463**, 55–65. (doi:10.1016/S0014-2999(03)01274-3)
32. Kalueff AV, Keisala T, Minasyan A, Kumar SR, LaPorte JL, Murphy DL. 2008 The regular and light-dark Suok tests of anxiety and sensorimotor integration: utility for behavioral characterization in laboratory rodents. *Nat. Protoc.* **3**, 129–136. (doi:10.1038/nprot.2007.516)
33. Maximino C, de Brito TM, da Silva Batista AW, Herculano AM, Morato S, Gouveia A. 2010 Measuring anxiety in zebrafish: a critical review. *Behav. Brain Res.* **214**, 157–171. (doi:10.1016/j.bbr.2010.05.031)
34. Hamilton TJ, Morrison RA, Palenik B, Tresguerres M. 2014 Exposure to bloom-like concentrations of two marine *Synechococcus* cyanobacteria (strains CC9311 and CC9902) differentially alters fish behaviour. *Conserv. Physiol.* **2**, 1–9. (doi:10.1093/conphys/cou020.)
35. Maximino C, Marques de Brito T, Dias CAGDM, Gouveia A, Morato S. 2010 Scototaxis as anxiety-like behavior in fish. *Nat. Protoc.* **5**, 209–16. (doi:10.1038/nprot.2009.225)
36. Maximino C *et al.* 2012 A comparison of the light/dark and novel tank tests in zebrafish. *Behaviour* **149**, 1099–1123. (doi:10.1163/1568539X-00003029)
37. Sackerman J *et al.* 2010 Zebrafish behavior in novel environments: effects of acute exposure to anxiolytic compounds and choice of *Danio rerio* line. *Int. J. Comp. Psychol.* **23**, 43–61. (doi:10.2964/jsik.kuni0223)
38. Heredia L, Torrente M, Colomina MT, Domingo JL. 2014 Assessing anxiety in C57BL/6 J mice: a pharmacological characterization of the open-field and light/dark tests. *J. Pharmacol. Toxicol. Methods* **69**, 108–114. (doi:10.1016/j.vascn.2013.12.005)
39. Wong K *et al.* 2010 Analyzing habituation responses to novelty in zebrafish (*Danio rerio*). *Behav. Brain Res.* **208**, 450–457. (doi:10.1016/j.bbr.2009.12.023)
40. Nilsson GE, Lefevre S. 2016 Physiological challenges to fishes in a warmer and acidified future. *Physiology* **31**, 409–417. (doi:10.1152/physiol.00055.2015)
41. Tresguerres M, Hamilton TJ. 2017 Acid–base physiology, neurobiology and behaviour in relation to CO_2-induced ocean acidification. *J. Exp. Biol.* **220**, 2136–2148. (doi:10.1242/jeb.144113)
42. Delille B, Borges A, Delille D. 2009 Influence of giant kelp beds (*Macrocystis pyrifera*) on diel cycles of pCO_2 and DIC in the sub-Antarctic coastal area. *Estuar. Coast. Shelf Sci.* **81**, 114–122. (doi:10.1016/j.ecss.2008.10.004)
43. Fabry VJ, Seibel BA, Feely RA, Orr JC. 2008 Impacts of ocean acidification on marine fauna and ecosystem processes. *ICES J. Mar. Sci.* **65**, 414–432. (doi:10.1093/icesjms/fsn048)
44. Frieder CA, Nam SH, Martz TR, Levin LA. 2012 High temporal and spatial variability of dissolved oxygen and pH in a nearshore California kelp forest. *Biogeosciences* **9**, 3917–3930. (doi:10.5194/bg-9-3917-2012)
45. Hofmann GE *et al.* 2011 High-frequency dynamics of ocean pH: a multi-ecosystem comparison. *PLoS ONE* **6**, e28983. (doi:10.1371/journal.pone.0028983)
46. Shaw E. 1978 Schooling fishes: the school, a truly egalitarian form of organization. *Am. Sci.* **66**, 166–175.
47. Kennedy GJA, Pitcher TJ. 1975 Experiments on homing in shoals of the European minnow, *Phoxinus phoxinus* (L). *Trans. Am. Fish Soc.* **104**, 454–457.

(doi:10.1577/1548-8659(1975)104< 454:EOHISO> 2.0.CO;2)

48. Pitcher TJ. 1983 Heuristic definitions of fish shoaling behaviour. *Anim. Behav.* **31**, 611–613. (doi:10.1016/S0003-3472(83)80087-6)
49. Pitcher T. 1979 Sensory information and the organization of behaviour in a shoaling cyprind fish. *Anim. Behav.* **27**, 126–149. (doi:10.1016/0003-3472(79)90133-7)
50. Baird TA, Ryer CH, Olla BL. 1991 Social enhancement offoraging on an ephemeral food source in juvenile walleye pollock, *Theragra chalcogramma*. *Environ. Biol. Fishes* **31**, 307–311. (doi:10.1007/BF00000697)
51. Ryer CH, Olla BL. 1991 Information transfer and the facilitation and inhibition offeeding in a schooling fish. *Environ. Biol. Fishes* **30**, 317–323. (doi:10.1007/BF02028847)
52. Brown C, Laland KN. 2003 Social learning in fishes: a review. *Fish Fish.* **4**, 280–288. (doi:10.1046/j.1467-2979.2003.00122.x)
53. Hoare DJ, Couzin ID, Godin JGJ, Krause J. 2004 Context-dependent group size choice in fish. *Anim. Behav.* **67**, 155–164. (doi:10.1016/j.anbehav.2003.04.004)
54. Tsubokawa T, Saito K, Kawano H, Kawamura K, Shinozuka K, Watanabe S. 2009 Pharmacological effects on mirror approaching behavior and neurochemical aspects of the telencephalon in the fish, medaka (*Oryzias latipes*). *Soc. Neurosci.* **4**, 276–286. (doi:10.1080/17470910802625215)
55. Gebauer DL, Pagnussat N, Piato ÂL, Schaefer IC, Bonan CD, Lara DR. 2011 Effects of anxiolytics in zebrafish: similarities and differences between benzodiazepines, buspirone and ethanol. *Pharmacol. Biochem. Behav.* **99**, 480–486. (doi:10.1016/j.pbb.2011.04.021)
56. Nadler LE, Killen SS, McCormick MI, Watson S, Munday PL. 2016 Effect of elevated carbon dioxide on shoal familiarity and metabolism in a coral reef fish. *Conserv. Physiol.* **4**, cow052. (doi:10.1093/conphys/cow052)
57. Lopes AF, Morais P, Pimentel M, Rosa R, Munday PL, Goncalves EJ. 2016 Behavioural lateralization and shoaling cohesion of fish larvae altered under ocean acidification. *Mar. Biol.* **163**, 243. (doi:10.1007/s00227-016-3026-4)
58. Limbaugh C. 1964 Notes on the life history of two Californian omacentrids: Garibaldis, *Hypsypops rubicunda* (Girard), and Blacksmiths, *Chromis punctipinnis* (Cooper). *Pacific Sci.* **18**, 41–50.
59. Love M. 2011 *Certainly more than you want to know about the fishes of the Pacific coast*. Santa Barbara, CA: Really Big Press.
60. Mehrbach C, Culberson CH, Hawley JE, Pytkowicz RM. 1973 Measurement of the apparent dissociation constants of carbonic acid in seawater at atmospheric pressure. *Limnol. Oceanogr.* **18**, 897–907. (doi:10.4319/lo.1973.18.6.0897)
61. Dickson AG, Millero FJ. 1987 A comparison of the equilibrium constants for the dissociation of carbonic acid in seawater media. *Deep Sea Res. Part A Oceanogr. Res. Pap.* **34**, 1733–1743. (doi:10.1016/0198-0149(87)90021-5)
62. Lewis E, Wallace DWR. 1998 *CO2SYS DOS program developed for CO_2 system calculations*. Oak Ridge, TN: Carbon Dioxide Information Analysis Center, Oak Ridge National Laboratory, US Department of Energy.
63. Holcombe A, Howorko A, Powell RA, Schalomon M, Hamilton TJ. 2013 Reversed scototaxis during withdrawal after daily-moderate, but not weekly-binge, administration of ethanol in zebrafish. *PLoS ONE* **8**, e63319. (doi:10.1371/journal.pone.0063319)
64. Wright D, Krause J. 2006 Repeated measures of shoaling tendency in zebrafish (*Danio rerio*) and other small teleost fishes. *Nat. Protoc.* **1**, 1828–1831. (doi:10.1038/nprot.2006.287)
65. Miller N, Gerlai R. 2007 Quantification of shoaling behaviour in zebrafish (*Danio rerio*). *Behav. Brain Res.* **184**, 157–166. (doi:10.1016/j.bbr.2007.07.007)
66. Johnson A, Hamilton TJ. 2017 Modafinil decreases anxiety-like behaviour in zebrafish. *PeerJ* **5**, e2994. (doi:10.7717/peerj.2994)
67. Cornwall CE, Hurd CL. 2015 Experimental design in ocean acidification research: problems and solutions. *ICES J. Mar. Sci.* **73**, 572–81. (doi:10.1093/icesjms/fsv118)
68. Quinn GP, Keough MJ. 2002 *Experimental design and data analysis for biologists*, vol. 277. Cambridge, UK: Cambridge University Press.
69. R Development Core Team. 2013 *R: a language and environment for statistical computing*. Vienna, Austria: R foundation for statistical computing.
70. Fox J, Weisberg S. 2011 *An {R} companion to applied regression*, 2nd edn. Thousand Oaks, CA: Sage.
71. Munday PL, Cheal AJ, Dixson DL, Rummer JL, Fabricius KE. 2014 Behavioural impairment in reef fishes caused by ocean acidification at CO_2 seeps. *Nat. Clim. Change* **4**, 487–492. (doi:10.1038/nclimate2195)
72. Ferrari MCO, McCormick MI, Munday PL, Meekan MG, Dixson DL, Lonnstedt Ö. 2011 Putting prey and predator into the CO_2 equation—qualitative and quantitative effects of ocean acidification on predator-prey interactions. *Ecol. Lett.* **14**, 1143–1148. (doi:10.1111/j.1461-0248.2011.01683.x)

Chapter II, in full, is a reprint of the material as it appears in Kwan, G.T., Hamilton, T.J., and Tresguerres, M. (2017). CO_2-induced ocean acidification does not affect individual or group behaviour in a temperate damselfish. *Royal Society Open Science*, 4(7), 170283. The dissertation author was the primary investigator and author of this material. The material is used by permission of Royal Society Publishing.

CHAPTER III

Quantification of cutaneous ionocytes in small aquatic organisms

bio-protocol www.bio-protocol.org/e3227 Bio-protocol 9(09): e3227. DOI:10.21769/BioProtoc.3227

Quantification of Cutaneous Ionocytes in Small Aquatic Organisms

Garfield T. Kwan[1, *], Shane H. Finnerty[1], Nicholas C. Wegner[2] and Martin Tresguerres[1, *]

[1]Marine Biology Research Division, Scripps Institution of Oceanography, University of California, San Diego, La Jolla, USA; [2]Fisheries Resources Division, Southwest Fisheries Science Center, NOAA Fisheries, La Jolla, USA

*For correspondence: tfkwan@ucsd.edu; mtresguerres@ucsd.edu

[Abstract] Aquatic organisms have specialized cells called ionocytes that regulate the ionic composition, osmolarity, and acid/base status of internal fluids. In small aquatic organisms such as fishes in their early life stages, ionocytes are typically found on the cutaneous surface and their abundance can change to help cope with various metabolic and environmental factors. Ionocytes profusely express ATPase enzymes, most notably Na^+/K^+ ATPase, which can be identified by immunohistochemistry. However, quantification of cutaneous ionocytes is not trivial due to the limited camera's focal plane and the microscope's field-of-view. This protocol describes a technique to consistently and reliably identify, image, and measure the relative surface area covered by cutaneous ionocytes through software-mediated focus-stacking and photo-stitching–thereby allowing the quantification of cutaneous ionocyte area as a proxy for ion transporting capacity across the skin. Because ionocytes are essential for regulating ionic composition, osmolarity, and acid/base status of internal fluids, this technique is useful for studying physiological mechanisms used by fish larvae and other small aquatic organisms during development and in response to environmental stress.

Keywords: Chloride cell, Mitochondrion-rich cell, Skin, Larvae, Osmoregulation, pH regulation, ATPase, Ocean acidification

[Background] Ionocytes (formerly called chloride cells and mitochondrion-rich cells) are specialized cells that transport ions to regulate the ionic composition, osmolarity, and acid/base status of internal fluids (reviewed in Evans *et al.*, 2005). Ionocytes typically express high levels of the enzyme Na^+/K^+ ATPase, which can be used to visualize them using immunohistochemical techniques. In larval and juvenile fishes, ionocytes are present throughout the skin (reviewed in Varsamos *et al.*, 2005). The abundance, distribution, and size of ionocytes can change during development, as well as in response to environmental stressors such as temperature, acidification, salinity, hypoxia, UV light, and pollutants. However, accurate and consistent quantification of cutaneous ionocytes can be difficult due to their presence in large numbers (tens of thousands), non-homogenous distribution, and being masked by pigmented cells. In addition, ionocyte quantification throughout the entire skin of an organism is often limited by the microscope's field-of-view (Fridman *et al.*, 2011) and both the camera's field-of-view and focal plane (Hiroi *et al.*, 1999; Varsamos *et al.*, 2002). Because ionocyte distribution is often quite variable across the larval skin, estimations of ionocyte abundance based on a single photograph and focal plane may not be representative of the organism as a whole, and therefore not reliable or

Bio-protocol 9(09): e3227.
DOI:10.21769/BioProtoc.3227

repeatable. As such, previous studies that utilized immunohistochemistry to identify and quantify ionocytes have been descriptive in nature (Hwang, 1989; Hiroi *et al.*, 1998; Katoh *et al.*, 2000), which precludes replication and comparison across species and treatments.

Here, we describe a protocol involving immunohistochemistry, photo-microscopy, and photo-editing software that allows estimating ionocyte number, size, density, and relative coverage of cutaneous ionocytes with high accuracy. Unlike previous studies, our method resolves both frame-of-view and focal plane limitations through focus-stacking and photo-stitching software, effectively digitizing a 3-D fish larva into a 2-D image. Additionally, the resulting digital image retains its high-resolution–thereby allowing the accurate quantification of all ionocytes on one side of the larva along with their average size and the larva's surface area. These parameters can then be inputted into a simple equation to estimate the cutaneous ionocyte ion-transporting capacity in relation to the total skin surface area of the specimen. For larger specimens in which counting all cutaneous ionocytes is cumbersome and time-consuming, we developed a random sampling protocol that allows highly accurate cutaneous ionocyte estimations after counting ionocytes within 10% of the skin surface area. For example, the estimated number of cutaneous ionocytes in a 13.7 mm long Yellowfin Tuna (*Thunnus albacares*) specimen was 15,342, which was only 3.6% higher than the actual 14,795 cutaneous ionocytes counted in the entire fish skin (Kwan *et al.*, 2019). We believe this method will be valuable for future studies quantifying cutaneous ionocytes in larval and juvenile fish as well as other small aquatic organisms during development and in response to various environmental stress (*e.g.*, ocean warming, hypoxia, and acidification).

Materials and Reagents

1. PCR Reaction Strips (8 x 0.2 ml) attached flat cap (Simport, catalog number: T320-2N)
2. 1.7 ml microcentrifuge tubes (Corning, catalog number: MCT-175-C)
3. 15 ml plastic tubes (Corning Brand, catalog number: 352196)
4. Microscope slides (Thermo Fisher Scientific, catalog number: 12-550-15) or concave microscope slides (United Scientific Supplies, catalog number: CS3X11)
5. Microscope coverslips (*e.g.*, VWR, catalog number: 48366 045)
6. Microscope small Petri dish trays (MatTek Corp, catalog number: P35GC-1.5-10-C)
7. Petri dish (Corning Brand, catalog number: 351029) or any other container
8. Specimen of interest
   Note: This protocol is optimized for small (< 30 mm) samples with relatively low natural pigmentation and. high transparency. This protocol could be used for other specimens, but additional optimization of immunostaining and image acquisition might be required.
9. Deionized (DI) water
10. 10x Phosphate buffer saline (PBS) (Corning Incorporated, catalog number: 46-013-CM)
11. 20% paraformaldehyde (PFA) (Electron Microscopy Sciences, catalog number: 15713)
12. 200-proof (100%) Ethyl alcohol (Decon Laboratories, catalog number: 2701)

Bio-protocol 9(09): e3227.
DOI:10.21769/BioProtoc.3227

13. 30% (w/v) hydrogen peroxide (Sigma-Aldrich, catalog number: H3410)
14. α5 Na^+/K^+ ATPase (NKA) antibody (Developmental Studies Hybridoma Bank, catalog number: a5–supernatant)
    Notes:
    a. *This monoclonal antibody has specifically recognized NKA from multiple classes of aquatic organisms including: bony fishes (Wilson et al., 2000 and 2002; Yang et al., 2013; Tang et al., 2014; Kwan et al., 2019), elasmobranch fishes (Piermarini and Evans, 2001; Roa et al., 2014; Roa and Tresguerres, 2017), and hagfish (Clifford et al., 2015).*
    b. *This protocol may be adapted for other proteins following validation of primary antibodies in the species of interest. However, successful localization using different primary antibodies may require optimizing the fixation and immunohistochemical procedures described here.*
15. Vectastain® Elite® ABC HRP ready-to-use kit (Vector Laboratories, catalog number: PK-7200), includes:
    a. Normal horse serum blocking solution
    b. Pan-specific secondary antibody solution
    c. Streptavidin peroxidase solution
16. 3,3-diaminobenzidine (DAB) Peroxidase Substrate stored at 4 °C (Vector Laboratories, catalog number: SK-4100)
17. Sodium azide (Thermo Fisher Scientific, catalog number: S227I-25)
18. 1.2x phosphate buffer saline (PBS) solution (see Recipes)
19. 4% paraformaldehyde (PFA) fixative solution (see Recipes)
20. 3% hydrogen peroxide solution (see Recipes)
21. 1.0x PBS solution (see Recipes)
22. DAB substrate working solution (see Recipes)
23. 10% sodium azide stock solution (see Recipes)
24. 0.02% sodium azide working solution (see Recipes)

Equipment

1. Fridge (4 °C) and freezer (-80 °C)
2. Chemical fume hood
3. Borosilicate glass vial (Thermo Fisher Scientific, catalog number: 033374)
4. Shake table (*e.g.*, VWR, Standard Orbital Shaker, Model 1000) or rotator (*e.g.*, Thermo Fisher Scientific, Tube Revolver/Rotator, catalog number: 88881001)
5. Transfer pipette (Thermo Fisher Scientific, catalog number: 1368050) or any other pipette suitable for your specimen of interest
6. Fine forceps (Fine Science Tools, catalog number: 26029-10) or any forceps that does not damage your specimen of interest
7. Camera-mounted microscope(s) Leica DMR compound microscope for smaller samples

Bio-protocol 9(09): e3227.
DOI:10.21769/BioProtoc.3227

(< 5 mm SL), Leica MZ9.5 stereomicroscope for larger samples (> 5 mm)
8. Microscope light source (Ludl Electronic Products [LEP] [12 V, 100 W], catalog number: 99019)
9. Microscope mounted camera (Canon, Rebel T3i single lens reflex camera)
10. Compatible camera with SD card
11. Anti-vibration table for microscopy imaging
12. Microscope stage micrometer standard
13. Monitor for microscope camera's live-feed imaging
14. Camera remote for wireless shutter release (Canon RC-6)

Software

1. Helicon Focus (HeliconSoft, Version 6.7.2 or later, www.heliconsoft.com)
2. Adobe Photoshop (Adobe Systems, version CS3 or higher, www.adobe.com)
3. Fiji (https://imagej.net/Fiji), or ImageJ (https://imagej.nih.gov/ij/download.html) with cell counter plugin (https://imagej.nih.gov/ij/plugins/cell-counter.html)
4. Adobe Illustrator (Adobe Systems, Version 19.2.0 or later, www.adobe.com)
5. R (https://www.r-project.org)

Procedure

An overview of this protocol is shown below (Figure 1). The time necessary to finish this procedure varies with the size of each sample. At the minimum, this procedure will take at least 3 days.

Bio-protocol 9(09): e3227.
DOI:10.21769/BioProtoc.3227

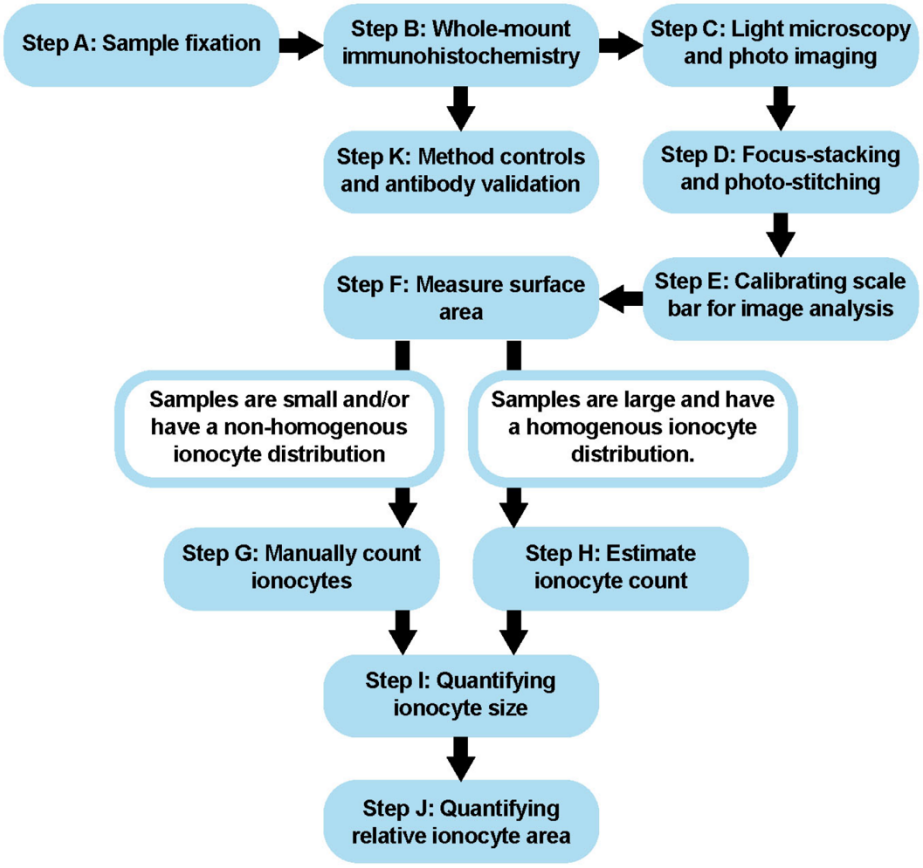

Figure 1. Procedural Overview. Schematic showing the major steps of this protocol.

A. Sample fixation

1. Euthanize specimen in accordance with an approved animal care protocol.
2. Incubate samples in fixative solution (see Recipes 1 and 2) in any water-tight container (*e.g.*, borosilicate glass vial) on a rotator/shake table overnight (8-12 h) at 4 °C.

   Notes:

   a. *All samples should be fully immersed in the fixative. Multiple samples can be fixed together. In Kwan et al., 2019, 6-10 fish larvae (ranging from 3-25 mm in length) were fixed in 10 ml of fixative within a 20 ml borosilicate glass vial. Adjust container, volume, and fixative according to your specimen of interest. Rinsing the samples prior to fixation is not required.*

   b. *The ethanol washes (Steps A3 and A4) can be replaced with three 10 min PBS washes if the samples are to be immediately processed for immunohistochemistry.*
3. Remove fixative, then incubate samples in 50% ethanol on a shake table overnight (8-12 h) at 4 °C.
4. Remove 50% ethanol, then incubate samples in 70% ethanol for long-term storage at 4 °C.

Bio-protocol 9(09): e3227.
DOI:10.21769/BioProtoc.3227

B. Whole-mount immunohistochemistry

1. Begin rehydrating samples by transferring onto a Petri dish with tap water for 1 min.
2. After initial rinse, transfer samples into a plastic tube (*e.g.*, 0.2 ml PCR tube or 1.7 ml microcentrifuge tube depending on larval size) with tap water (filled to max volume) and further incubate for 10 min at room temperature on a rotator/shake table.
   Notes:
   a. *All samples should be fully immersed in solution. In Kwan et al., 2019, fish larva (< 20 mm in length) were incubated in a 1.7 ml microcentrifuge tube and immersed in ~1 ml of solution. Larger samples will require a larger container and more solution (and vice versa). Adjust container and solution volume accordingly.*
   b. *During solution changes, it is preferable to remove the solution from the container–as opposed to moving the sample to containers with different solutions. This minimizes damage to the sample. This applies to all solution changes.*
   c. *If changing solution with a plastic transfer pipette becomes problematic, consider using a more appropriately sized pipette (P200 pipette with a 200 µl tip for 0.2 ml PCR tube and P1000 pipette with a 1,000 µl tip) for changing solutions. Adjust according to your sample and/or container.*
3. Remove water, then incubate samples in freshly prepared 3% hydrogen peroxide (see Recipe 3) for 10 min at room temperature on a rotator/shake table.
   Notes:
   a. *During solution changes, it is preferable to remove the solution from the container–as opposed to moving the sample to containers with different solutions. This minimizes damage to the sample. This applies to all solution changes.*
   b. *This step may be extended to 1 h if there is intense pigmentation and/or non-specific background staining.*
4. Remove 3% hydrogen peroxide solution, then incubate samples in normal horse serum (NHS) blocking solution for 15 min at room temperature on a rotator/shake table.
5. Prepare primary antibody solution (*e.g.*, α5 NKA antibody: 20 ng/ml in NHS blocking solution).
6. Remove NHS, then incubate samples in primary antibody solution and leave on a rotator/shake table overnight (≥ 8 h) at room temperature or (preferably) at 4 °C.
   Note: This step may be modified for various antibody validation controls. See Procedure K for details.
7. Remove primary antibody solution, then rinse samples in 1x PBS (see Recipe 4) for 5 min at room temperature on a rotator/shake table. Repeat two more times for a total of three rinses.
8. Remove 1x PBS wash, then incubate samples in pan-specific secondary antibody solution for 30 min at room temperature on a rotator/shake table.
9. Remove pan-specific secondary antibody solution, then rinse samples in 1x PBS for 5 min at room temperature on a rotator/shake table. Repeat two more times for a total of three rinses.
10. Remove 1x PBS wash, then incubate samples in streptavidin peroxidase solution for 15 min at

Bio-protocol 9(09): e3227.
DOI:10.21769/BioProtoc.3227

room temperature on a rotator/shake table.

11. Remove streptavidin peroxidase solution, then rinse samples in 1x PBS for 5 min at room temperature on a rotator/shake table. Repeat two more times for a total of three rinses.
12. Prepare the DAB substrate working solution (see Recipe 5) according to the manufacturer's instruction in a separate container (*e.g.*, 15 ml centrifuge tube).
13. Remove 1x PBS wash, then incubate samples in DAB substrate working solution for 20 s at room temperature.

    Notes:

    a. *The sensitivity of this portion is highly dependent on the tissue sample and antibody of interest. Because DAB staining is irreversible, start with 20 s and increase incubation time if darker staining is necessary. Optimal incubation time should be determined by the investigator(s).*
    b. *Incubating samples for a longer duration may result in darker background staining. If this becomes an issue, consider diluting the DAB substrate working solution with DI water.*
14. Remove DAB substrate working solution, then rinse samples in DI water for 10 min at room temperature on a rotator/shake table. Repeat two more times for a total of three rinses.
15. Store in DI water at 4 °C until imaging.
16. For long-term storage (1 week or longer), store in PBS + 0.02% sodium azide (see Recipes 6 and 7).

    Note: Sodium azide is very toxic. Samples incubated within sodium azide should be given multiple DI water washes before handling and imaging.

C. Light microscopy and imaging

1. Carefully transfer sample onto a microscope slide, concave microscope slide, or a glass bottom dish for examination under a light microscope.
2. Add DI water to keep sample from drying out, and secure sample with a coverslip to prevent unintentional movement.
3. Switch on the live feed option on the DSLR camera.
4. Switch off the autofocus option on the DSLR camera.
5. Set camera to manual or aperture priority mode. Adjust the following parameters until image is optimal: camera ISO, camera aperture, microscope aperture, light source brightness.
6. For optimal imaging, use a wireless remote controller to trigger shutter release.

   Note: Avoid bumping into the entire camera apparatus. Because the exposure time of each photograph will likely require ~1 s per image, any movement of the microscope, sample, camera, and surrounding can cause blurriness.
7. Starting at one end (*e.g.*, head of fish specimen), photograph sample at each focal plane (Z-stack) within the field of view. Manually adjust the focus until the entire Z-stack is finished (Figures 2A-2E). Be careful to not move the image in the X or Y-dimension.

   Notes:

Bio-protocol 9(09): e3227.
DOI:10.21769/BioProtoc.3227

a. *The image may differ between the microscope lens and camera (shown on the live feed monitor). Always use the camera's focal plane and image accordingly.*
b. *Shooting the Z-stack in consecutive order (front to back or vice versa) is preferable as it may help during post-processing.*
c. *Ensure that your sample does not drift in the x or y plane between images for proper post-processing.*
d. *An exact Z-step (distance between each image) ranges greatly amongst samples. After each image, turn the fine focus until the next plane is in focus. In Kwan et al., 2019, most images took around 6-8 images per Z-stack.*

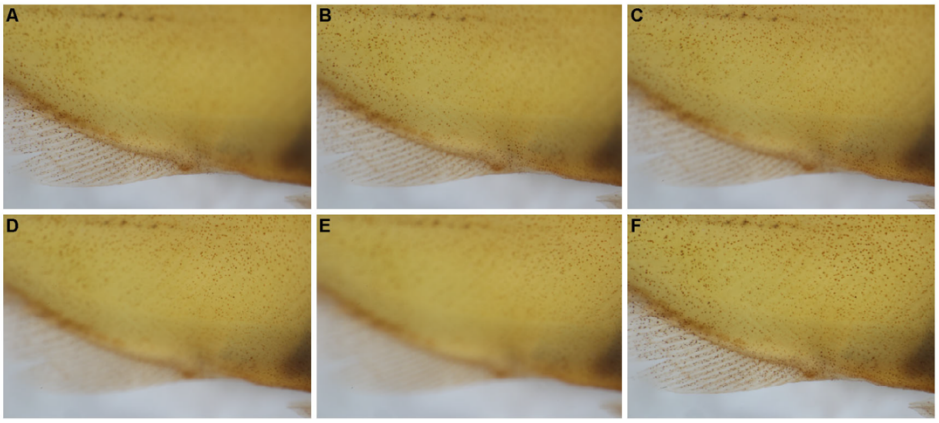

Figure 2. Example of Z-stacks and focus stacking. After photographing a Z-stack on the ventral body (A-E), the focused portions of each image were stacked together via focus stacking (F).

8. Move to the next unphotographed area, taking care to overlap consecutive Z-stacks by at least ~20% to ensure photo stitching accuracy (Figure 3).

Bio-protocol 9(09): e3227.
DOI:10.21769/BioProtoc.3227

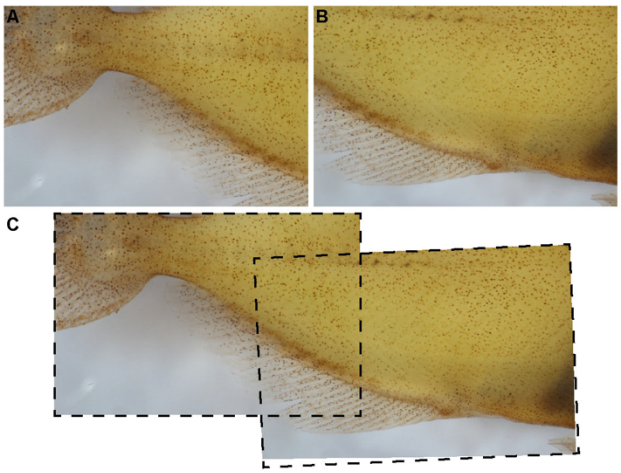

Figure 3. Overlap of Z-stacks are necessary for proper photo-stitching. Each Z-stack (A, B) should have ~20% of overlapping area for optimal photo-stitching (C).

9. Continue imaging Z-stacks until the entire sample has been photographed.
10. Photograph the microscope standard at a height equal to approximately half of the sample's thickness.
    Note: The same scale bar can be applied across multiple samples as long as the magnification of the microscope has not changed and the sample thickness is relatively similar.

D. Focus-stacking and photo-stitching

Notes:

a. A video tutorial explaining the focus-stacking process can be found at youtube–Quick Start with Helicon Focus (published by HeliconSoft).

b. A video tutorial explaining the photo-stitching process can be found at youtube–How to Stitch Multiple Photos Together Automatically with Photomerge in Photoshop (published by Photoshop Video Academy).

1. Import each stack of images into Helicon Soft and render focus-stacking.
   Notes:
   a. Begin with Method C (pyramid).
   b. If the edge of the image becomes distorted (halo effect), troubleshoot with Method A (weighted average) or Method B (depth map)–and increase the "radius" value. Read more about the different methods here: https://www.heliconsoft.com/helicon-focus-main-parameters/.
   c. Other focus-stacking software (e.g., Adobe Photoshop) may be used, though the processing speed and quality of results may vary.
2. Repeat for each stack of images. Save images.
3. Open all focus-stacked images in Adobe Photoshop and check for processing artifacts (Figure

Bio-protocol 9(09): e3227.
DOI:10.21769/BioProtoc.3227

4). If artifacts exist, use the “Crop” tool (hotkey: C) to discard the artifact. Save all changes before proceeding.

Figure 4. Example of artifacts created during focal stacking. Artifacts such as blurred areas along the edge of the Z-stack may appear (black arrow) and should be cropped out of the image.

4. With all focus-stacked images opened in Adobe Photoshop and vetted for artifacts, use the photo-stitching tool (File > Automate > Photomerge …).
5. Select “Add Open Files” (all files must be already saved), select “Auto”, then “OK”.
   Note: If there are many stacks to stitch together, this step may take a while. If computer crashes, try using a computer with more RAM and stronger processor.
6. Check for artifacts or unphotographed areas. Save image.
7. Open the image containing microscope standard taken back in Step C10. Using the “Rectangle Marquee” tool (hotkey: M) to measure a known width (*e.g.*, 1 mm).
8. Use the “Brush” tool (hotkey: B) to fill in the rectangle with a color that contrasts well with the background.
9. With the colored rectangle still in selection, copy (Windows hotkey: Ctrl + C; Mac hotkey: Cmd + C) the scale bar and paste (Windows hotkey: Ctrl + V; Mac hotkey: Cmd + V) onto the photo-stitched image of the sample. Save image.

E. Calibrating measurement tools for image analysis/ionocyte quantification
   Note: A video tutorial explaining this process can be found at Youtube–Set calibration in ImageJ (published by remotelab PloyU).
   1. Open the photo-stitched image in FIJI/ImageJ.
   2. Using the “magnifying glass” tool or by pushing the “+” key, zoom in on the scale bar.
      Note: Hover the mouse cursor over the area you want to zoom in before pushing “+”. You can also push “-” to zoom out.
   3. Using the “straight line” tool, draw a line across the scale bar–holding shift to lock the line at a

Bio-protocol 9(09): e3227.
DOI:10.21769/BioProtoc.3227

90° angle.

4. At the top of the window (screen for Mac), click on Analyze > Set Scale. The distance in pixels should already be filled in as that is the line you just drew. Fill in the "Known Distance" and "Unit of Length" (*e.g.*, 1 mm), then click "OK".
   Note: If the same scale bar is being used across multiple samples, then select the box next to "Global". In doing so, the pixel to mm ratio will be remembered across windows (samples).
5. To ensure accuracy, open up the microscope standard image previously taken during "Step C10". Using the "straight line" tool, draw a line across the imaged scale bar and measure (hotkey: M). If done properly, the difference between the imaged scale bar and the "measured" distance should be negligible.

Note: From this point forward, this protocol will regard the sample as a fish specimen. Other samples could be similarly quantified, though some modifications to this protocol may be necessary.

F. Surface area estimation

1. Using FIJI/ImageJ's "straight line" tool, measure (hotkey: M) the standard length of the fish larva. Record this value.
   Note: The "segmented line" tool (right click (Mac: command + click) on the "straight line" tool) can be used if the fish larva was fixed or placed in a curved position.
2. With the "Freehand Selection" tool, trace the fish larva to measure (hotkey: M) its surface area. Record this value.
   Note: If freehand drawing using a mouse proves difficult, try using a tablet and stylus.
3. Using the "Freehand Selection" tool, trace regions of interest where ionocyte distribution may differ (in this example we use head, body, and fins) and measure (hotkey: M). Record these values.

G. Counting cutaneous ionocytes

Notes:

a. This technique is suitable for smaller fish specimens (< 5 mm standard length) and samples with a non-homogenous distribution of ionocytes.
b. A video tutorial explaining this process can be found at Youtube–Count Items in ImageJ (published by Timothy Spier).

1. Open FIJI/ImageJ.
2. If using ImageJ, be sure the "Cell Counter" plugin has been installed (see Software).
3. Open the photo-stitched image in FIJI/ImageJ.
4. Go to Plugin > Analyze > Cell Counter > Cell Counter.
5. In the Cell Counter window, click "Initialize", select "Type 1", and zoom ("+") in on the area of interest.
6. Using your mouse, left click to denote a cell at that location. The count will be updated next to "Type 1" in the Cell Counter window. Record this value.

Bio-protocol 9(09): e3227.
DOI:10.21769/BioProtoc.3227

7. To remove an erroneous count, check the box next to “Delete Mode”. Next, click on the point you would like to remove. Uncheck the box to proceed with counting.
8. Use the “Save Markers” option in the Cell Counter window to save your work.

H. Estimating number of cutaneous ionocytes

Note: This technique is suitable for larger fish specimens with a homogenous ionocyte distribution. Because there is likely species-specific variation in ionocyte distribution, this estimation technique needs to be ground truthed with manual cell counts (Procedure G) before utilizing.

1. Open the photo-stitched image with scale bar in Adobe Illustrator.

   Notes:

   a. To zoom in, use the zoom tool (hotkey: Z) and click.

   b. To zoom out, use the zoom tool (hotkey: Z), hold ctrl (Mac: hold Cmd) and click.
2. Adjust the artboard (hotkey: Shift + O) to fit the photo-stitched image. If the photo-stitched image is larger than the maximum artboard size, scale down the image size by 1) clicking on the image, 2) hovering over a corner anchor point, 3) holding “shift”, and 4) dragging to reduce image size.
3. Change the name of this layer to “image”, and lock it. Create four additional layers and arrange them in this order: fin count, body count, head count, grid, image (from top to bottom) (Figure 5).

   Notes:

   a. You may have other areas of interest requiring additional layers

   b. A layer is only editable when it is 1) visible, 2) unlocked, and 3) selected.

   c. Layer(s) at the top will cover the layer(s) at the bottom.

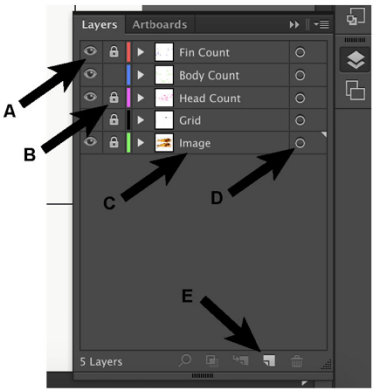

Figure 5. Key buttons within the layers window. The eye symbol (A) controls the visibility of that layer, whereas the lock symbol (B) controls whether that layer is editable. To change the name of the layer, double click on the name (C). To select everything in that layer, click on the circle in the layer of interest (D). To add another layer, click “create new layer” (E).

4. Toggle the “Ruler” option (Window: Ctrl + R; Mac: Cmd + R). Right click on the ruler and change

Bio-protocol 9(09): e3227.
DOI:10.21769/BioProtoc.3227

to “pixels”.

5. Using the rectangle tool (hotkey: M), drag a rectangle across the scale bar (Figure 6A).
6. On the second row from the top towards the right side of the window, find and click the orange “Transform”.
7. Record the value listed next to “W” (Figure 6B). This value will assist you in converting between pixels and the measured metric unit.

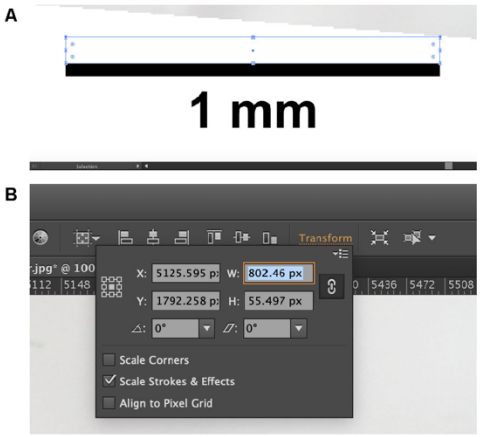

Figure 6. Finding the conversion between digital pixels and measured metric units. Draw a rectangle across the scale bar (A). The width of the rectangle should then appear in the “Transform” window (B). Use this value to convert between the computer pixels and the metric system.

8. Using the standard length that was calculated back in Step F1, calculate the value equal to 2% of the fish specimen’s standard length.
9. Using the rectangle tool, click (not drag) to create a shape with custom width and height dimensions. Input the 2% standard length value into both the “Width” and “Height” dimension (make a square).
   Note: For example, if the standard length of specimen = 8.80 mm, then 2% of the standard length is 0.176 mm.
10. Copy and paste the squares until a grid overlays the entire fish (Figure 7).
    Note: To expedite this process, below are some helpful shortcuts:
    a. *Select All: “Windows: Ctrl + A, Mac: Cmd + A”*
    b. *Copy: “Windows: Ctrl + C; Mac: Cmd + C”*
    c. *Paste in place: “Windows: Ctrl + Shift + V; Mac: Cmd + Shift + V”*
    d. *While dragging newly pasted cells, hold “Shift” to lock the squares in the X or Y plane.*
    e. *By default, illustrator should “auto-snap” your selection to place. If this is turned off, go to Preferences > Selection and Anchor Display and check the box “Snap to Point”.*

Bio-protocol 9(09): e3227.
DOI:10.21769/BioProtoc.3227

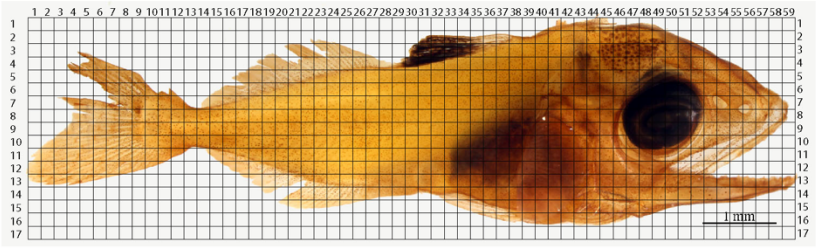

Figure 7. Example of an overlying grid over a photo-stitched yellowfin tuna specimen. Each square's length is equal to 2% of the larva's standard length.

11. Number the grid's x and y axes.
12. Calculate the area of an individual square. Record this value.
    Note: For example, if the standard length of specimen = 8.80 mm, then the area of each square is 0.031 mm^2.
13. Using the measurements from Steps F2 and F3, calculate how many squares will require counting to cover 10% of each region of interest (*e.g.*, head, body, fins). Record the number of squares necessary to cover at least 10% of each region.
    Notes:
    a. *If the area of the head region = 4.9 mm^2 and each square is 0.031 mm^2, then:* $10\%\ of\ the\ head\ region = \frac{(4.9\ mm^2 * 0.10)}{0.031\ mm^2\ square^{-1}} = 15.806\ squares.$ *Round up and count 16 squares to adequately cover at least 10% of the head region.*
    b. *Separation of different body regions is necessary as variation in regional ionocyte density may occur due to species-specific or developmental stage-specific differences.*
14. Open R. Copy and paste in the provided codes (see `Note #1` below). Adjust the number for the X and Y coordinates accordingly before using.
    Note: Step-by-step instruction for using this R below:

```
### Note #1
### Beginning of code
# Generating random coordinates
# Step-by-step instruction
#
# Objective: this will randomly generate 500 (x,y) coordinates
# Step 1) In line 15, replace "59" with the number of squares on the
x-axis
# Step 2) In line 16, replace "17" with the number of squares on the
y-axis
# Step 3) highlight everything (Windows: ctrl + A; Mac: cmd + A)
# Step 4) hold "Shift" and hit "enter"
# Step 5) see output in the R Console window.
```

Bio-protocol 9(09): e3227.
DOI:10.21769/BioProtoc.3227

```
# Note 1: Some coordinates may be repeated; skip if repeated.
# Note 2: If 500 (x,y) coordinates is not enough, repeat until the
quota for each region is reached.

x.coord = sample(1:59, replace=T, 500)
y.coord = sample(1:17, replace=T, 500)
rand.coords <- data.frame(x.coord,y.coord)
rand.coords

### End of code
```

15. For each randomly generated coordinate, disqualify for counting if the square contains any of the following:
    a. Background space, glare, or other photography artifacts (Figure 8A).
    b. Folding, invaginations, pigments, which prevent accurate counts (Figure 8B).
    c. More than one region of interest: head, body, fins (Figure 8C).

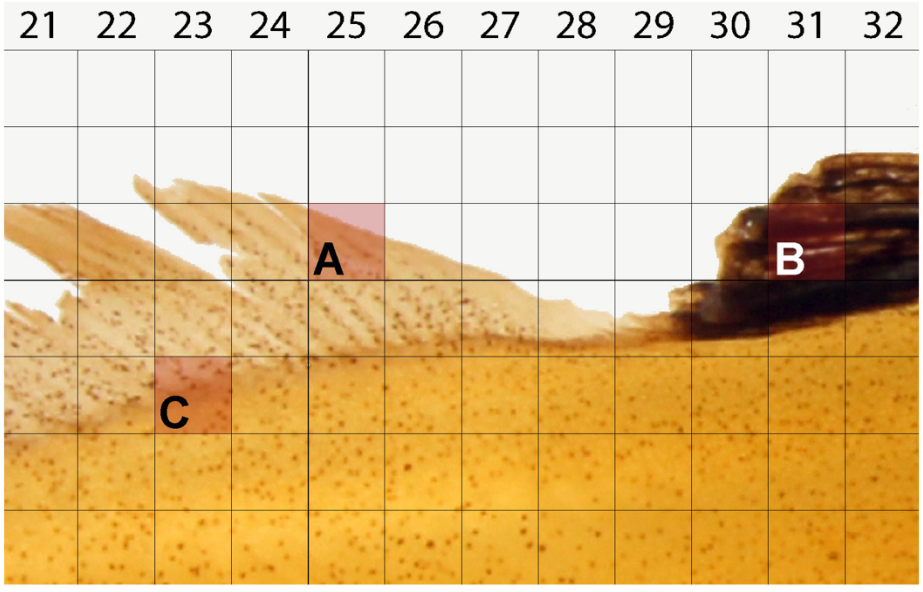

Figure 8. Example of squares unsuitable for cell counting. Randomly generated coordinates must not contain the following features: background space (A), foldings, invaginations, pigments, or other dark space (B), and space inclusive of more than one region *e.g.*, box containing both body and fin (C).

16. If the square meets the above criteria, then mark for counting.
    Notes:

Bio-protocol 9(09): e3227.
DOI:10.21769/BioProtoc.3227

a. *To quickly designate the square for counting, use the "Pencil tool" (hotkey: N) to scribble a marking.*
b. *To avoid accidently moving the grid or the underlying image, be sure to lock both the grid and image layer (see Figure 5B).*

17. Count the cells within Adobe illustrator. For each region, record the number of ionocytes present in the randomly-chosen grid squares.
    Note: To quickly record the number of cells in the square, use the "Type tool" (hotkey: T) and click within the square, then type the number of counted cells. Hit "Esc" to exit this mode.
18. If the grid lines happen to overlap the immunostained cells, count only the cells intersecting with the top and right sides of the square. This will ensure no double-counting of the cells if two squares were randomly chosen next to each other.
    Note: If the grid lines are too thick or the cells are located directly underneath the lines, try selecting the grid layer (hit the rightmost circle in the grid layer; Figure 5D) and reducing the "stroke" value to "0.5", or reducing the opacity to 50% for better viewing.
19. Continue until at least 10% of each region (head, body, fins) have been counted (Figure 9).

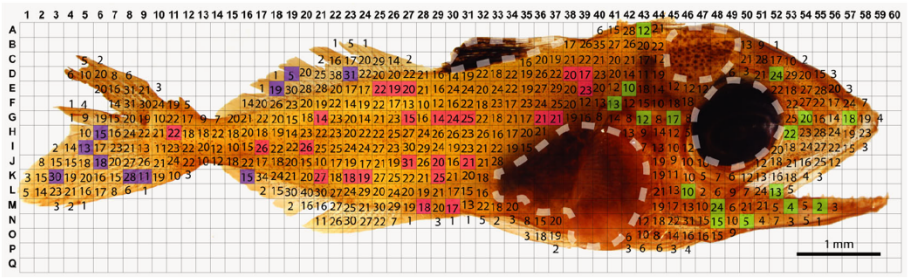

Figure 9. Method for quantification of cutaneous ionocytes in yellowfin tuna specimen and early stage juveniles (>5 mm standard length). Ionocytes were identified by their intense NA^+/K^+-ATPase immunostaining and counted within randomly sampled boxes of the overlaid grid within the head (green), body (pink), and fin (blue) regions. Dashed white lines outline regions that were not sampled due to heavy pigmentation preventing accurate ionocyte counts. The estimated ionocyte count (15,342 cells) was ground truthed with manual ionocyte count (colorless regions; 14,795 cells). The estimated relative ionocyte area for this larva is 3.75%. Figure from Kwan *et al.*, 2019.

20. Calculate the estimation using the following equation:

$$\text{Estimated total ionocytes} = \left(Area_{head} * \left(\frac{Ionocyte_{head}}{(Square_{head} * Area_{Square})}\right)\right) + \left(Area_{body} * \left(\frac{Ionocyte_{body}}{(Square_{body} * Area_{Square})}\right)\right) + \left(Area_{fin} * \left(\frac{Ionocyte_{fin}}{(Square_{fins} * Area_{Square})}\right)\right)$$

Notes:

a. *$Area_{head,\ body,\ or\ fins}$ = measured area of head, body, or fins region (Step F3).*

Bio-protocol 9(09): e3227.
DOI:10.21769/BioProtoc.3227

b. *Ionocyte$_{head, body, or fins}$ = sum of ionocytes counted per region (Step H17).*
c. *Square$_{head, body, or fins}$ = number of squares counted per region (Step H13).*
d. *Area$_{square}$ = size of each square = (standard length*0.02)^2 (Step H12).*

I. Quantifying ionocyte size

1. Open up ImageJ and set scale bar as discussed in Procedure E.
2. With the "Freehand Selection" tool, zoom in (hotkey: +) and trace individual cutaneous ionocytes to estimate their relative surface areas.
   Note: If freehand drawing proves difficult, try using a tablet and stylus.
3. Repeat Step I2 until you have measured 20 cells from different regions of interest (*e.g.*, head, body, and fins).
4. Calculate the average ionocyte size using the following equation:

$$Average\ Ionocyte\ Size = \left(Average\ Ionocyte\ Size_{Head} * \left(\frac{Area_{Head}}{Area_{Total}}\right)\right) + \left(Average\ Ionocyte\ Size_{Body} * \left(\frac{Area_{Body}}{Area_{Total}}\right)\right) + \left(Average\ Ionocyte\ Size_{Fins} * \left(\frac{Area_{Fins}}{Area_{Total}}\right)\right)$$

Area$_{head, body, or fins}$ were calculated in Step F3.
Area$_{total}$ was calculated in Step F2.

J. Quantifying relative ionocyte area

$$\text{Relative ionocyte area} = \frac{(Estimated\ total\ ionocytes * Average\ ionocyte\ size)}{Total\ surface\ area}$$

Estimated total ionocytes were calculated in Step H20.
Average ionocyte size were calculated in Step I4.
Total surface area were calculated in Step F2.

K. Method controls and antibody validation

1. **Non-specific secondary and tertiary antibody binding control:** designate several fish specimens as negative controls by omitting the primary antibody during Step B6 (leave in NHS blocking solution overnight at 4 °C). Fish specimens incubated with the primary NKA antibody should result in positive staining (Figure 10A). In contrast, fish specimens without the primary antibody should result in the absence of staining (Figure 10B).
   Notes:
   a. *Performing this negative control step is a great way to identify and avoid the natural pigments present on the organism of interest (Step H15).*
   b. *If necessary, the negative-control fish specimens can be re-incubated and utilized. Simply*

Bio-protocol 9(09): e3227.
DOI:10.21769/BioProtoc.3227

repeat all of Procedure B to re-immunostain said sample(s).

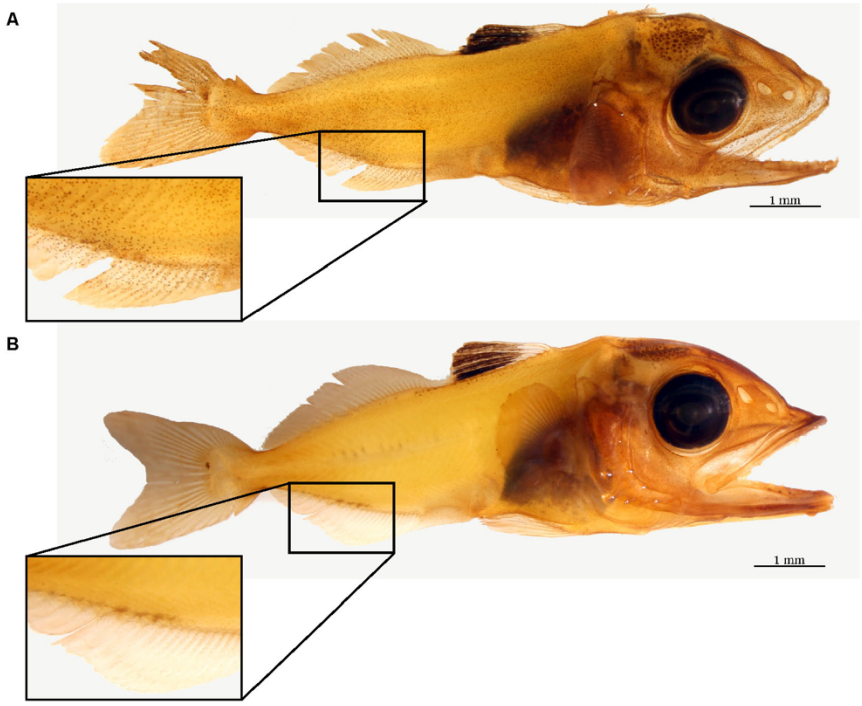

Figure 10. Negative control for immunohistochemistry. The difference between a yellowfin tuna specimen incubated with (A) and without (B) Na^+/K^+-ATPase (NKA) antibodies. The brown precipitate seen in the top larva denotes NKA presence on the cutaneous surface, whereas the absence of brown staining on the bottom larva serves a successful negative control. Note the areas containing naturally occurring pigment in both specimens should be avoided during estimation.

2. Primary antibody specificity via western blotting: flash frozen tissue (-80 °C) should be sampled along with the fixed tissue for western blotting, which should yield a single band close the predicted size of your protein of interest (Figure 11). See supplementary material 2 in Kwan *et al.* (2019) for protocol and additional details.

Bio-protocol 9(09): e3227.
DOI:10.21769/BioProtoc.3227

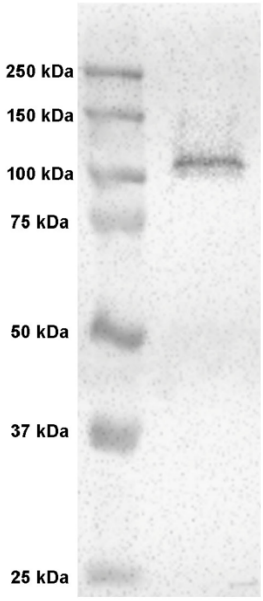

Figure 11. Western blot of Na^+/K^+-ATPase (NKA) in yellowfin tuna tissue. Western blot with anti-NKA monoclonal antibodies on yellowfin tuna tissue yielded a single ~108 kDa band, which matched the predicted size of the protein. Figure adapted from Kwan *et al.*, 2019.

Data analysis

Ionocyte count (Step H20), average ionocyte size (Step I4), and relative ionocyte area (Step J1) data across development is best depicted in a scatterplot and explained using regression models. In Kwan *et al.*, 2019, we examined the relationships of relative ionocyte area across standard length and days post hatching using linear regressions. The slope of the linear regression explains the steepness of the line, with the null hypothesis being zero, whereas R^2 describes the regression's goodness-of-fit. Other developmental metrics that may be applicable include accumulated thermal units and total length of the sample. Development may not always be linear; therefore, researchers should choose their own regressions according to your field of study. If the experiment includes multiple treatments or species, the comparison of the regression's slope should be examined with *t*-test (2 treatments total) or Analysis of Covariance (3 or more treatments). See Zar (2014) for additional details.

Recipes

1. 1.2x phosphate buffer saline (PBS) solution (1 L)
   120 ml of 10x PBS stock solution
   880 ml of deionized water

Bio-protocol 9(09): e3227.
DOI:10.21769/BioProtoc.3227

2. 4% paraformaldehyde (PFA) fixative solution (10 ml)
   a. Break open a PFA ampule (20% stock solution) within the fume hood
   b. Add 2 ml of PFA stock solution into 8 ml of 1.2x PBS solution (Recipe 1), for a final concentration of 4% PFA in 1 M PBS. Invert to mix
   c. Remaining PFA stock solution can be stored at 4 °C for up to six months
   d. 4% PFA fixative solution can be stored at 4 °C for up to one week
3. 3% hydrogen peroxide solution (10 ml)
   1 ml of 30% hydrogen peroxide
   9 ml of tap water
4. 1.0x PBS solution (1 L)
   100 ml of 10x PBS stock solution
   900 ml of deionized water
5. DAB substrate working solution (same as manufacturer instruction) (~5 ml)
   5 ml of DI water
   2 drops of buffer stock solution (DAB substrate kit)
   4 drops of DAB stock solution (DAB substrate kit)
   2 drops of hydrogen peroxide solution (DAB substrate kit)
6. 10% sodium azide stock solution (10 ml)
   10 ml of 1.0x PBS
   1 g of sodium azide
7. 0.02% sodium azide working solution (10 ml)
   10 ml 1.0x PBS
   20 µl of 10% sodium azide stock solution (Recipe 6)

Acknowledgments

This protocol corresponds to the methods and experiments presented in Kwan *et al.* (2019). The larval yellowfin tuna and white seabass samples (*Atractoscion nobilis*) used to create and optimize this protocol were provided by the Inter-American Tropical Tuna Commission (IATTC) and the Hubbs Sea World Research Institute (HSWRI). We are grateful to Jeanne Wexler (IATTC) for her contributions to the original project, and for rearing and sampling the yellowfin tuna larvae. We thank Diomedes Ballesteros, Lina Castillo, Susana Cusatti, Danisin Dominguez, Agustin Ortega, Daniel Perez, Dario Ramires, Daniel Solis, Luis Tejada, and Carlos Vergara for assisting with the production and rearing of yellowfin tuna larvae at the Achotines Laboratory in Panama. We thank Daniel Margulies (IATTC) and Vernon Scholey (IATTC) for developing the yellowfin tuna rearing methods and supervising the spawning and larval rearing at the Achotines Laboratory. We are grateful to Erica Brombay-Fanning (HSWRI), Eric McIntire (HSWRI), Sabrina Sobel (HSWRI), and Christy Varga (HSWRI) for the rearing and sampling the white seabass larvae of larval white seabass. We thank Mark Drawbridge (HSWRI) for supervising the spawning and larval rearing at the Leon R.

Raymond Marine Fish Hatchery in Carlsbad, USA. The authors would like to thank Dr. Greg Rouse for the use of microscope and camera equipment, Sabine Faulhaber for technical assistance with the scanning electron microscope, and Taylor Smith for her assistance in dissection and imaging. G.T.K. was supported by the San Diego Fellowship and the National Science Foundation Graduate Research Fellowship Program.

Competing interests

The authors declare no competing interests.

Ethics

All experiments were approved by the Scripps Institution of Oceanography/University of California, San Diego animal care committee under protocol no. S10320 in compliance with the Institutional Animal Care and Use Committee (IACUC) guidelines for the care and use of experimental animals.

References

1. Clifford, A. M., Goss, G. G., Roa, J. N. and Tresguerres, M. (2015). Acid/base and ionic regulation in hagfish. In: *Hagfish Biology*. Science Publishers, Boca Raton, pp. 277-292.
2. Evans, D. H., Piermarini, P. M. and Choe, K. P. (2005). The multifunctional fish gill: dominant site of gas exchange, osmoregulation, acid-base regulation, and excretion of nitrogenous waste. *Physiol Rev* 85(1): 97-177.
3. Fridman, S., Bron, J. E. and Rana, K. J. (2011). Ontogenetic changes in location and morphology of chloride cells during early life stages of the Nile tilapia Oreochromis niloticus adapted to fresh and brackish water. *J Fish Biol* 79(3): 597-614.
4. Hiroi, J., Kaneko, T., Seikai, T. and Tanaka, M. (1998). Developmental sequence of chloride cells in the body skin and gills of Japanese flounder (*Paralichthys olivaceus*) larvae. *Zoolog Sci* 15(4): 455-460.
5. Hiroi, J., Kaneko, T. and Tanaka, M. (1999). *In vivo* sequential changes in chloride cell morphology in the yolk-sac membrane of mozambique tilapia (*Oreochromis mossambicus*) embryos and larvae during seawater adaptation. *J Exp Biol* 202 Pt 24: 3485-3495.
6. Hwang, P. P. (1989). Distribution of chloride cells in teleost larvae. *J Morphol* 200(1): 1-8.
7. Katoh, F., Shimizu, A., Uchida, K. and Kaneko, T. (2000). Shift of chloride cell distribution during early life stages in seawater-adapted Killifish, *Fundulus heteroclitus*. *Zoolog Sci* 17(1): 11-18.
8. Kwan, G. T., Wexler, J. B., Wegner, N. C. and Tresguerres, M. (2019). Ontogenetic changes in cutaneous and branchial ionocytes and morphology in yellowfin tuna (*Thunnus albacares*) larvae. *J Comp Physiol B* 189(1): 81-95.
9. Piermarini, P. M. and Evans, D. H. (2001). Immunochemical analysis of the vacuolar proton-

ATPase B-subunit in the gills of a euryhaline stingray (*Dasyatis sabina*): effects of salinity and relation to Na^+/K^+-ATPase. *J Exp Biol 204*(Pt 19): 3251-3259.

10. Roa, J. N., Munevar, C. L. and Tresguerres, M. (2014). Feeding induces translocation of vacuolar proton ATPase and pendrin to the membrane of leopard shark (*Triakis semifasciata*) mitochondrion-rich gill cells. *Comp Biochem Physiol A Mol Integr Physiol* 174: 29-37.
11. Roa, J. N. and Tresguerres, M. (2017). Bicarbonate-sensing soluble adenylyl cyclase is present in the cell cytoplasm and nucleus of multiple shark tissues. *Physiol Rep* 5(2). pii: e13090.
12. Tang, C. H., Leu, M. Y., Yang, W. K. and Tsai, S. C. (2014). Exploration of the mechanisms of protein quality control and osmoregulation in gills of *Chromis viridis* in response to reduced salinity. *Fish Physiol Biochem* 40(5): 1533-1546.
13. Varsamos, S., Diaz, J. P., Charmantier, G., Blasco, C., Connes, R. and Flik, G. (2002). Location and morphology of chloride cells during the post-embryonic development of the european sea bass, *Dicentrarchus labrax*. *Anat Embryol (Berl)* 205(3): 203-213.
14. Varsamos, S., Nebel, C. and Charmantier, G. (2005). Ontogeny of osmoregulation in postembryonic fish: a review. *Comp Biochem Physiol A Mol Integr Physiol* 141(4): 401-429.
15. Wilson, J. M., Randall, D. J., Donowitz, M., Vogl, A. W. and Ip, A. K. (2000). Immunolocalization of ion-transport proteins to branchial epithelium mitochondria-rich cells in the mudskipper (*Periophthalmodon schlosseri*). *J Exp Biol* 203(Pt 15): 2297-2310.
16. Wilson, J. M., Whiteley, N. M. and Randall, D. J. (2002). Ionoregulatory changes in the gill epithelia of coho salmon during seawater acclimation. *Physiol Biochem Zool* 75(3): 237-249.
17. Yang, W. K., Kang, C. K., Chang, C. H., Hsu, A. D., Lee, T. H. and Hwang, P. P. (2013). Expression profiles of branchial FXYD proteins in the brackish medaka *Oryzias dancena*: a potential saltwater fish model for studies of osmoregulation. *PLoS One* 8(1): e55470.
18. Zar, J.H. (2014). Comparing simple linear regression. In: *Biostatistical Analysis*. In: Pearson, H. (Ed.). pp: 387-404.

Chapter III, in full, is a reprint of the material as it appears in Kwan, G.T., Finnerty, S.H., Wegner, N.C., and Tresguerres, M., 2019. Quantification of Cutaneous Ionocytes in Small Aquatic Organisms. *Bio-Protocol*, 9(09), e3227. The dissertation author was the primary investigator and author of this material. The material is used by permission of Bio-Protocol.

CHAPTER IV

Ontogenetic changes in cutaneous and branchial ionocytes and morphology in yellowfin tuna (*Thunnus albacares*) larvae

Journal of Comparative Physiology B
https://doi.org/10.1007/s00360-018-1187-9

ORIGINAL PAPER

Ontogenetic changes in cutaneous and branchial ionocytes and morphology in yellowfin tuna (*Thunnus albacares*) larvae

Garfield T. Kwan[1] · Jeanne B. Wexler[2] · Nicholas C. Wegner[3] · Martin Tresguerres[1]

Received: 9 March 2018 / Revised: 1 October 2018 / Accepted: 16 October 2018

Abstract
The development of osmoregulatory and gas exchange organs was studied in larval yellowfin tuna (*Thunnus albacares*) from 2 to 25 days post-hatching (2.9–24.5 mm standard length, SL). Cutaneous and branchial ionocytes were identified using Na^+/K^+-ATPase immunostaining and scanning electron microscopy. Cutaneous ionocyte abundance significantly increased with SL, but a reduction in ionocyte size and density resulted in a significant decrease in relative ionocyte area. Cutaneous ionocytes in preflexion larvae had a wide apical opening with extended microvilli; however, microvilli retracted into an apical pit from flexion onward. Lamellae in the gill and pseudobranch were first detected ~ 3.3 mm SL. Ionocytes were always present on the gill arch, first appeared in the filaments and lamellae of the pseudobranch at 3.4 mm SL, and later in gill filaments at 4.2 mm SL, but were never observed in the gill lamellae. Unlike the cutaneous ionocytes, gill and pseudobranch ionocytes had a wide apical opening with extended microvilli throughout larval development. The interlamellar fusion, a specialized gill structure binding the lamellae of ram-ventilating fish, began forming by ~ 24.5 mm SL and contained ionocytes, a localization never before reported. Ionocytes were retained on the lamellar fusions and also found on the filament fusions of larger sub-adult yellowfin tuna; however, sub-adult gill ionocytes had apical pits. These results indicate a shift in gas exchange and NaCl secretion from the skin to branchial organs around the flexion stage, and reveal novel aspects of ionocyte localization and morphology in ram-ventilating fishes.

Keywords Chloride cell · Osmoregulation · Fish larvae · Mitochondrion-rich cell · Ionocyte · Gill morphology

Introduction

Marine teleost fish are hypoosmotic and hypoionic compared to seawater, and actively maintain the NaCl concentration in their blood plasma and extracellular fluids ~ 60% lower than seawater (reviewed in Evans et al. 2005). In adult fish, the resulting diffusive NaCl gain and water loss are counteracted by water absorption in the intestine and active NaCl excretion by specialized gill cells called ionocytes (formerly known as chloride cells or mitochondrion-rich cells) (Marshall and Nishioka 1980; Zadunaisky 1996; reviewed in; Evans et al. 2005). NaCl excretion against the electrochemical gradient is powered by highly abundant Na^+/K^+-ATPases (NKA) located in the highly infolded basolateral membrane of ionocytes, working in concert with basolateral $Na^+/K^+/Cl^-$ co-transporters and apical Cl^- channels (reviewed in Hirose et al. 2003; Evans et al. 2005). Osmoregulation in adult marine teleosts has been thoroughly studied from the whole animal to the molecular level (Evans et al. 1999, 2005; Evans 2002, 2008). It is clear that larval marine

Communicated by G. Heldmaier.

Electronic supplementary material The online version of this article (https://doi.org/10.1007/s00360-018-1187-9) contains supplementary material, which is available to authorized users.

✉ Jeanne B. Wexler
jwexler@iattc.org

✉ Nicholas C. Wegner
nick.wegner@noaa.gov

✉ Martin Tresguerres
mtresguerres@ucsd.edu

[1] Marine Biology Research Division, Scripps Institution of Oceanography, University of California San Diego, 9500 Gilman Drive, La Jolla, CA 92093, USA

[2] Inter-American Tropical Tuna Commission, 8901 La Jolla Shores Drive, La Jolla, CA 92037, USA

[3] Fisheries Resources Division, Southwest Fisheries Science Center, NOAA Fisheries, 8901 La Jolla Shores Drive, La Jolla, CA 92037, USA

Published online: 24 October 2018

teleosts also hypo-osmoregulate their internal fluids (Alderdice 1988; Varsamos et al. 2005), and that NaCl excretion initially takes place across the skin and shifts to the gills when these develop (e.g., Roberts et al. 1973; Hiroi et al. 1998; Katoh et al. 2000; Varsamos et al. 2001; Bodinier et al. 2010). However, many unknowns remain including potential species-specific timing of the shift from skin to gill osmoregulation, the role of the pseudobranch, and the relationship between osmoregulation and gas exchange.

Cutaneous ionocytes in fish larvae were first detected in marine European plaice (*Pleuronectes platessa*) by silver nitrate staining (Shelbourne 1957). Currently, cutaneous ionocytes in fish larvae are usually identified based on their high NKA abundance using immunohistochemical techniques (van der Heijden et al. 1999; Katoh et al. 2000; Varsamos et al. 2002a). At hatching, ionocytes are present throughout the yolk sac and the skin (Holliday 1969; Alderdice 1988; Schreiber 2001; reviewed in; Varsamos et al. 2005). As the fish develops, ionocyte density decreases in the skin and progressively increases at the interlamellar space on the gill filaments (Ayson et al. 1994; Hiroi et al. 1998, 1999; Varsamos et al. 2002a). By the time fish become juveniles, the bulk of NaCl excretion takes place across the gills, with cutaneous ionocytes altogether disappearing in some species as adults (Whitear 1970). This shift in ionocyte distribution is intrinsically related to the reduction in surface to volume ratio that takes place as an organism grows. In smaller larvae with a relatively large surface area to volume ratio, gas exchange and ion transport can take place at adequate rates across the skin (c.f. Goss et al. 1994; Perry and Goss 1994; Varsamos et al. 2002a; Katoh et al. 2003). As larvae grow larger, their surface area to volume ratio decreases, the diffusion distance between capillaries and the surrounding water increases, and developing skin scales and mucus further obstruct diffusion. However, branchial structures (gills and in some cases the pseudobranch) develop and increase the total surface area—providing additional respiratory and osmoregulation capacity to keep up with increased total metabolic rate (reviewed in Rombough 2007).

Several studies have thus examined the transition of osmoregulatory function from the skin to the gills during larval development (Ayson et al. 1994; Hiroi et al. 1998, 1999; Varsamos et al. 2002a). However, little is known about this transition in highly active fishes, such as tunas (family Scombridae) and billfishes (families Istiophoridae and Xiphiidae), which support multibillion dollar fisheries worldwide and differ from most other fishes in their exceptionally high energetic demands and adaptations for ram ventilation. Specifically, tunas, billfishes, and their relatives have significantly larger gill surface areas (Muir and Hughes 1969; Palzenberger and Pohla 1992; Wegner et al. 2010) and thinner lamellae (Muir 1970; Muir and Brown 1971; Olson et al. 2003; Wegner et al. 2006) than most other fishes to optimize respiratory gas exchange and meet their high metabolic rates. While advantageous for enhancing O_2 uptake, additional gill surface area and decreased diffusion distances should increase NaCl diffusive gain, potentially requiring additional NaCl-excreting ionocytes to maintain ionic balance. In addition, while the majority of fish species utilize muscular pumping of the buccal and opercular chambers to ventilate the gills, tunas and other active fish species utilize ram ventilation to drive water into their branchial chambers through fast forward swimming (Brown and Muir 1970; Stevens 1972; Roberts 1975; Stevens and Lightfoot 1986; Wegner et al. 2012, 2013). To prevent gill filaments and lamellae from collapsing under high water flow, some ram ventilators including tunas, bonitos, and billfishes have developed specialized structures that bind together adjacent lamellae (interlamellar and lamellar fusions) and or adjacent filaments (filament fusions) to provide added gill rigidity (Muir and Kendall 1968; Wegner et al. 2006, 2013).

This study thus examines the larval development of osmorespiratory functional morphology in the yellowfin tuna (*Thunnus albacares*, Bonnaterre, 1788), a highly active and ram-ventilating species. The yellowfin tuna spawns in tropical and subtropical oceans worldwide (Schaefer 2001), and supports multinational sport and commercial fishery activities worth $15 billion USD in 2014 (Galland et al. 2016). Yellowfin tuna larvae are usually found within the upper mixed layer of warm waters predominantly between 20 and 30 m and as deep as 50 m (Leis et al. 1991; Boehlert et al. 1992; Boehlert and Mundy 1994), where they are exposed to variable ocean conditions that can affect survival. Several research facilities and aquaculture programs worldwide have supported studies on the early developmental stages of yellowfin tuna, including larval morphology, food selection, age validation, and growth rates (Ambrose 1996; Kaji et al. 1999; Margulies et al. 2001, 2007, 2016; Wexler et al. 2001, 2003, 2007). The objectives of the present study were to investigate the appearance of gas exchange and osmoregulatory structures during larval yellowfin tuna development.

Methods

Larval rearing conditions

A developmental series of yellowfin tuna larvae from 2.9 to 24.5 mm standard length (SL), corresponding to 2–25 days post-hatching (dph), were raised from fertilized eggs collected from a broodstock population of yellowfin tuna that spawn naturally and nearly daily in a land-based tank at the Inter-American Tropical Tuna Commission's Achotines Laboratory in Panama (Wexler et al. 2003; Margulies et al. 2007). Yellowfin tuna eggs and larvae were raised in a flow-through, filtered

seawater system with pH = 8.08 ± 0.03 (mean ± standard error of the mean), temperature = 28.30 ± 0.07 °C, dissolved O_2 = 6.08 ± 0.05 mg/L, and salinity = 33.24 ± 0.06 ppt (Supplementary material 1). Dissolved O_2 levels declined slightly as larval metabolic activity and development increased but were always above 5.5 mg/L, which is within the optimum range for normal survival and growth (Wexler et al. 2011). The eggs hatched approximately 24 h after spawning and the yolk sac larvae were stocked at a density of 13 larvae L^{-1} (11,000 larvae) in each of three 828 L circular tanks. The seawater flow rate into each tank was maintained at 1.8 L min^{-1}, which resulted in three complete water exchanges per day. Four diffusers in each tank provided aeration according to standard protocols for each developmental stage (Margulies et al. 2016). Lights were set to a 12:12 light/dark cycle with stepped lighting during the first and last hours of the light cycle. Larvae from the three tanks were transferred at 13 dph to a larger, 1260-L-volume tank and water flow rates were increased to maintain approximately three complete water exchanges per day. Beginning at 2 dph, larvae were fed mean daily food levels of 2700–3600 enriched rotifers L^{-1} during the first 17 days of feeding: 1–22 copepods L^{-1} between 8 and 10 and between 21 and 23 dph, 50–208 enriched *Artemia* nauplii (Instar II stage) L^{-1} between 9 and 14 dph, and 7–28 yolk sac larvae L^{-1} between 14 and 25 dph. During feeding, a combination of *Nannochloropsis* sp. and *Thalassiosira* sp. algae was maintained in each tank at densities of approximately 1 million cells L^{-1}, which helped maintain prey quality and improve prey contrast to facilitate feeding.

Growth and development

Weighted exponential growth models were fitted to the SL and dry weight at age (x) data using Minitab® Inc. 2018 Statistical Software. Because the variances were not homogeneous, the inverse of the variance for SL and dry weight at age were used to calculate the weights in the models. Specific growth rates (SGR) as a percentage per day [$SGR = (e^b - 1) \times 100$] (Ricker 1975) were estimated for SL and dry weight using the weight- and length-specific growth coefficients (b) of the weighted exponential models. For larval SL, a total of 255 fishes were sampled: dph 2 = 25, dph 3 = 15, dph 4 = 15, dph 5 = 10, dph 6 = 10, dph 7 = 15, dph 8 = 15, dph 9 = 15, dph 10 = 10, dph 11 = 10, dph 12 = 15, dph 13 = 15, dph 14 = 15, dph 15 = 6, dph 16 = 5, dph 18 = 10, dph 22 = 10, dph 25 = 39. For larval weight, a total of 86 fishes were sampled: dph 2 = 14, dph 4 = 12, dph 9 = 15, dph 14 = 15, dph 18 = 10, dph 22 = 10, dph 25 = 10. Stages of morphological and physiological development of yellowfin tuna larvae were determined based on descriptions by Ambrose (1996) and Kaji et al. (1999).

Anti-NKA antibody

The α5 mouse monoclonal antibody used in this study was raised against the α-subunit of chicken NKA (Lebovitz et al. 1989, Developmental Studies Hybridoma Bank, Iowa City, IA, USA). This antibody specifically recognizes NKA α-subunits from multiple elasmobranch and teleost fishes including leopard shark (*Triakis semifasciata*; Roa et al. 2014; Roa and Tresguerres 2017), coho salmon (*Oncorhynchus kitsutch*; Wilson et al. 2002), blue-green damselfish (*Chromis viridis*; Tang et al. 2014), and giant mudskipper (*Periophthalmondon schlosseri*; Wilson et al. 2000), among others. We confirmed that the α5 antibody also recognizes the α-subunit of NKA in the yellowfin tuna (Supplementary material 2).

Immunohistochemistry

Beginning at the time of first feeding (2.2 dph), daily samples of 5–10 yellowfin larvae were collected, anesthetized with MS-222, and fixed in 3% paraformaldehyde, 0.35% glutaraldehyde, 0.1 M, pH 7.4 cacodylate buffer (cat# 15949 Electron Microscopy Sciences, Hatfield, PA, USA) for 6 h at 4 °C, 50% ethanol for 6 h at 4 °C, and then stored in 70% ethanol at 4 °C. For comparison with larval samples, gill samples from three sub-adult yellowfin tuna (54.9, 63.3, and 91.0 cm fork length) were collected by hook and line off the coast of San Diego, and fixed in 4% paraformaldehyde or 10% formalin buffered in seawater. Whole-mount immunohistochemical staining followed the protocol in Vectastain Ready-to-Use Kit (Vector Laboratories, Burlingame, USA) with some minor modifications. Fixed samples were treated with 3% hydrogen peroxide and tap water for 10 min, incubated in blocking buffer (normal horse serum) for 15 min, and incubated overnight with the anti-NKA antibody (1:1000 dilution in blocking buffer). The following day, samples were rinsed in phosphate buffered saline (3 × 10 min each) and incubated in pre-diluted biotinylated pan-specific secondary antibodies (Vector Laboratories) for 30 min. The samples were then rinsed and incubated in streptavidin/peroxidase reagent for 15 min. After rinsing, samples were stained with diaminobenzidine (DAB Peroxidase Substrate Kit; Vector Laboratories) according to the manufacturer's recommendations. A subset of samples was treated in an identical manner except that they were incubated in blocking buffer instead of primary antibody; these served as negative controls and had no specific staining.

Fluorescence immunohistochemistry followed protocols previously reported in Roa et al. (2014). The gills of fixed yellowfin tuna larvae were excised and consecutively

immersed in 95% ethanol (10 min), 100% ethanol (3 × 10 min), safeclear (3 × 10 min), and paraffin (55 °C) (3 × 30 min). Paraffin blocks solidified overnight and were cut into 10 µm sections using a rotary microtome. Three consecutive sections of each sample were placed on a slide and left in an incubator overnight (32 °C). Paraffin was removed in safeclear (10 min × 3), and rehydrated in 100%, 95%, 70% ethanol, and phosphate buffer saline (PBS; 10 min each). Slides were incubated in blocking buffer (PBS-Tx, 0.02% normal goat serum, 0.0002% keyhole limpet hemocyanin; 1 h), then incubated in the primary antibody (1:2000 in blocking buffer) overnight at RT. Slides were washed in PBS (10 min × 3), then incubated in goat anti-mouse Alexa Fluor™ 546 (ThermoFisher, Waltham, USA) secondary antibody (1:500, 1 h) and Hoechst 33342 (1:1000, 10 min) at RT. After they were washed again in PBS (10 min × 3), slides were mounted in Fluorogel with tris buffer (Electron Microscopy Sciences).

Light microscopy and imaging

Under the microscope, ionocytes were identified by their solid dark color resulting from intense NKA immunostaining. Yellowfin tuna larvae < 5 mm SL were examined using a Leica DMR compound microscope (Leica Microsystems, Inc., Buffalo Grove, IL, USA). Yellowfin tuna larvae > 5 mm SL were viewed with a Leica S8APO stereomicroscope. Images were captured with a Canon Rebel T3i SLR camera, z-stacked with Helicon Focus software (HeliconSoft, Kharkov, Ukraine), and stitched with Adobe Photoshop CS6 (Adobe Systems, San Jose, USA). All imaging on the skin was performed on the larva's right side. The gills and pseudobranch of yellowfin tuna larvae were also stained and studied. In this study, the term 'branchial' refers to both the pseudobranch and the gill. Branchial ionocytes were identified as explained above for the skin. All imaging of the branchial structures was performed on the larva's left side with its operculum pulled back.

Quantification of ionocyte number, size, density, and relative ionocyte area

After the images were processed as described above and counted by a researcher, ionocyte size and the larval surface area were traced with a stylus and measured through the freehand tool from the image analysis software Fiji (version 1.0; Schindelin et al. 2012).

Because NKA is present in the ionocyte basolateral membrane, the immunostained region is not on the skin surface. Therefore, the reporting of the percentage of "body surface occupied" by ionocytes (e.g., Varsamos et al. 2002a, b) based on NKA immunostaining is not technically correct. Instead, "relative ionocyte area" was calculated as the number of cutaneous ionocytes multiplied by their average area, then divided by the skin surface area. This parameter is a proxy for cutaneous ionocyte ion transporting capacity in relation to diffusional ion movement across the skin.

In larvae < 5 mm SL, all cutaneous ionocytes were counted and the skin surface area was measured using Fiji. In larger fish, the total number of cutaneous ionocytes was estimated by extrapolating counts from 10% of the total skin surface area by overlaying the sample's surface area with square coordinates, with each square's side corresponding to 2% of the larva SL (Supplementary Material 3). To account for potential differences in cell densities in the head, trunk, and fins, the number of squares sampled from each region was proportional to the surface area of each region. The squares were chosen by coding a random coordinate generator in R (ver. 0.98.1103), but discarded if (1) a square contained skin area from more than one region; (2) it contained glare, blank space (background beyond edge of fish), or pigment cells (which made it difficult to accurately identify all nearby ionocytes); (3) it contained area from the eye. The pectoral fin was removed and separately imaged and measured because it partially overlaps with the larvae's body. The first dorsal fin was excluded in the analysis because it is retractable and heavily pigmented, which prevented accurate measurements. To validate this sampling technique, the estimated number of cutaneous ionocytes was compared to the actual number counted throughout the entire skin for four larvae of different sizes (5.2, 8.8, 11.4, and 13.7 mm SL). The difference between the estimated and actual number of cutaneous ionocytes was $5.1 \pm 0.5\%$.

Scanning electron microscopy

Yellowfin tuna samples were imaged using scanning electron microscopy (SEM) following protocols described in Wegner et al. (2013). Briefly, fixed samples were dehydrated to 100% tert-butyl alcohol in 25% increments over 24 h, frozen in 100% tert-butyl alcohol at 4 °C, and freeze dried using a VirTis benchtop freeze dryer (SP Industries, Gardiner, New York). Samples were then sputter-coated with gold and viewed using a FEI Quanta 600 SEM (FEI, Hillsboro, OR) under high-vacuum mode.

Statistics

Normalized ionocyte density across regions was analyzed with a one-way ANOVA ($\alpha = 0.05$), while ionocyte count and relative ionocyte area across development were fitted

with linear regressions using Graphpad Prism 6 (Graphpad, La Jolla, CA, USA).

Results

Growth and development

SL ($n = 255$) and dry weight ($n = 86$) increased exponentially between 2 and 25 dph (Fig. 1). The SGRs and 95% confidence intervals for SL and dry weight were $8.7 \pm 0.20\%$ d^{-1} and $37.0 \pm 1.0\%$ d^{-1}, respectively. Yellowfin tuna larvae in this study were in preflexion stage at ≤ 5 mm SL, notochord flexion stage between 5 and 7 mm SL, postflexion stage between 7 and 14 mm SL, and transformation stage between 14 and 24.5 mm SL (Fig. 1).

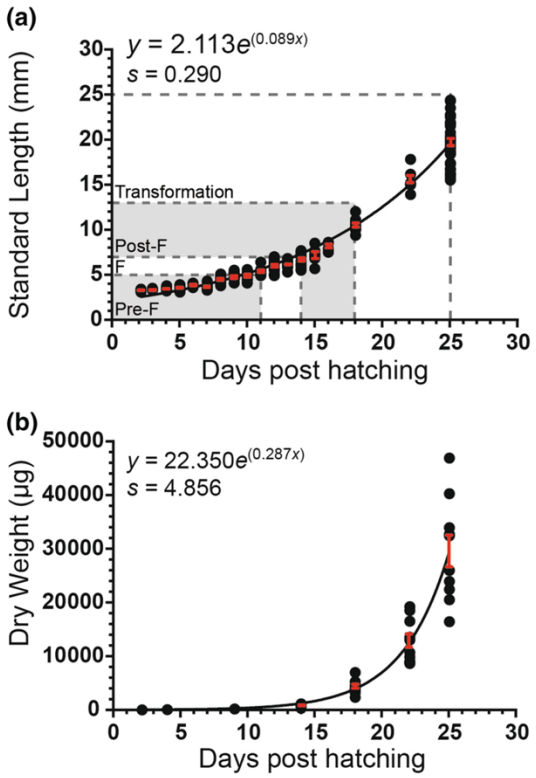

Fig. 1 Growth and development of yellowfin tuna larvae between 2 and 25 days post-hatching plotted against **a** standard length ($n = 255$) and **b** dry weight ($n = 86$), with their respective standard error bars (red error bars), non-linear regression equation, and standard error of the weighted exponential regression (s) fitted to the data. Dry weights were always > 0, but are below detection limits of scale for younger fish. *Pre-F* preflexion, *F* flexion, *Post-F* postflexion. (Color figure online)

Cutaneous ionocyte distribution throughout larval development

Yellowfin tuna larvae ($n = 18$) were selected to cover a range of SL between 2.9 and 24.5 mm throughout larval development. In the smallest larva (2.9 mm SL, 3 dph), ionocytes were predominately distributed along the head, pectoral fin, and anterior end of the trunk (Fig. 2a). Larvae in the flexion stage (~ 5–7 mm SL, 11–14 dph) additionally had ionocytes towards the end of the trunk, especially along the lateral midline and caudal fin rays (Fig. 2b). During the postflexion stage (7–14 mm SL, 14–18 dph), ionocytes were present throughout the body and concentrated on the head and along the lateral midline (Fig. 2c). Ionocytes were still present throughout the skin in the largest fish (24.5 mm SL, 25 dph) (Fig. 2d). There were no significant differences in normalized ionocyte densities between the head, trunk, and fins across development (ANOVA: $F_{2,42} = 0.8742$, $p = 0.4246$).

Cutaneous ionocyte number, size, density, and relative ionocyte area throughout larval development

The number of cutaneous ionocytes linearly increased with SL ($F_{1,16} = 146.8$, $p < 0.0001$; $r^2 = 0.9017$; Fig. 3a). Average cutaneous ionocyte size was ~ 300 µm^2 in 2.9 mm SL larvae, but it sharply decreased and plateaued at ~ 100 µm^2 in larvae 5 mm SL and larger (Figs. 2 insets and 3b). Cutaneous ionocyte density (number of cells per mm^2) had a biphasic pattern: it initially increased sharply, peaked at 5–7 mm SL, and then gradually decreased throughout the remainder of the development period examined (Fig. 3c). Relative ionocyte area decreased linearly with SL (linear regression: $F_{1,16} = 87.78$; $p < 0.001$; $r^2 = 0.8458$; Fig. 4a), with age (linear regression: $F_{1,16} = 38.85$; $p < 0.0001$; $r^2 = 0.7080$; Fig. 4b), and with accumulated thermal units (ATUs) (linear regression: $F_{1,16} = 42.54$; $p < 0.0001$; $r^2 = 0.7267$; Supplementary Material 4).

Branchial lamellae and ionocytes throughout larval development

Ionocytes were present in the gill arches in all examined larvae within the developmental time series examined (2.9–24.5 mm SL). Very small gill filaments and developing lamellae were detected as early as ~ 3.3 mm SL (4 dph); both were devoid of ionocytes (Fig. 5a, b). Ionocytes were first observed on the gill filament at 4.2 mm SL (7 dph; Fig. 5c, d). In post-flexion larvae (> 7 mm SL; > 14 dph), the gill filaments and lamellae continued to elongate and ionocytes remained present on the gill arch and filament (Fig. 5e, f). In the largest larva sampled (24.5 mm SL; 25 dph), the distal edges of adjacent gill lamellae began fusing together

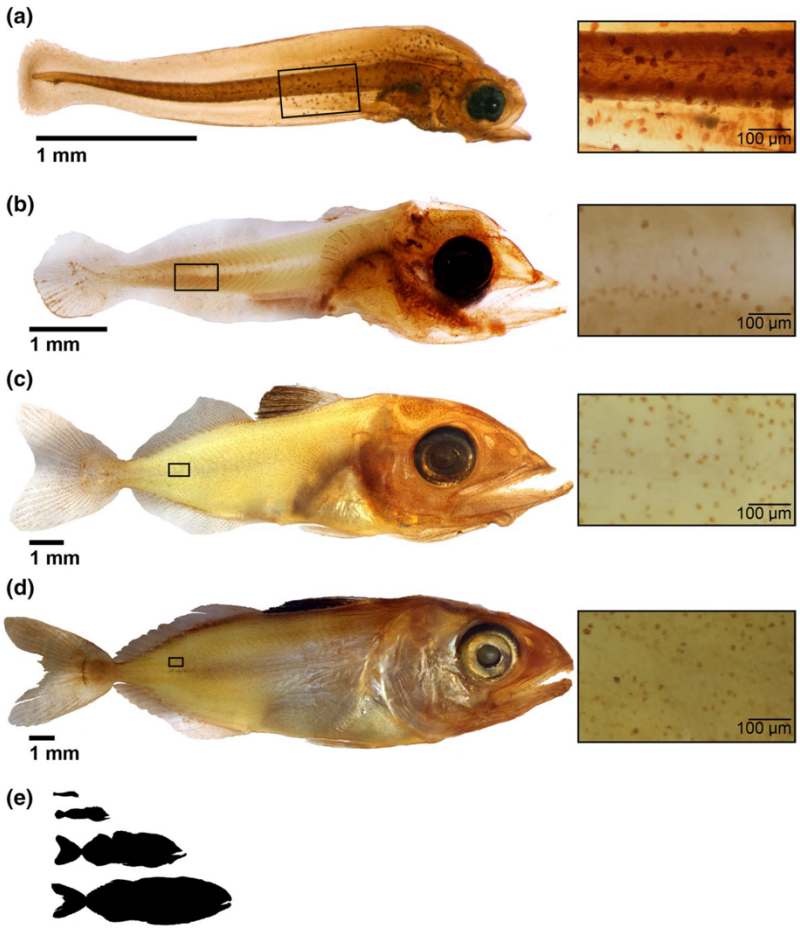

Fig. 2 Cutaneous ionocyte distribution across larval development in yellowfin tuna, with insets showing a magnified view of the ionocytes from each individual. **a** A 3.0 mm standard length (SL) larva showing ionocytes predominately on the head and the anterior region of the trunk. **b** Flexion larva (6.2 mm SL) showing cutaneous ionocytes beginning to appear on fin rays and throughout the trunk. **c** A 13.8 mm SL postflexion larva showing abundant cutaneous ionocytes still present throughout the body, particularly in the head and mid-lateral regions. **d** Cutaneous ionocytes in a 19.1 mm SL transformation-stage yellowfin. **e** Relative size comparison of the specimens shown in **a**–**d**

to form interlamellar fusions (Fig. 5g, h)—the precursor to complete lamellar fusions which develop later. Ionocytes were present along the interlamellar fusion (Fig. 5g, h), but were not observed on the actual gill lamellae of the larvae.

Pseudobranch lamellae were detected as early as ~3.3 mm SL (4 dph). In the pseudobranch, ionocytes were first observed in the filament and lamellae at ~3.4 mm SL (4 dph). Unlike the gills, pseudobranch ionocytes were present on both the filament and the lamellae throughout larval development, and adjacent pseudobranch lamellae did not fuse together in the size range examined (Fig. 6).

Ionocyte morphology throughout larval development

SEM imaging of larval yellowfin tuna skin and branchial structures ($n = 19$) identified three main epithelial cell types: pavement cells, mucous cells, and ionocytes. Pavement cells were characterized by their polygonal shape and array of microridges, while mucous cells had a smoothly-lined deep cavity from which mucus was often observed emerging. In the skin, there was a shift in ionocyte apical morphology around the flexion stage (~5–7 mm SL; 11–14 dph) from a wide area with extended microvilli (Fig. 7a) to pits (Fig. 7b). However, branchial ionocytes in both the pseudobranch (Fig. 6a, c) and the gills (Fig. 7c, d) had widened apical membranes with extended microvilli in all larval samples observed. Ionocytes on the fins had a wide and shallow apical membrane morphology (Fig. 7e, f).

Differential interference contrast (DIC) microscopy (also known as Nomarski interference contrast) overlaid with NKA immunofluorescence confirmed that the gill cells with wide apical membrane and extended microvilli were indeed ionocytes (Fig. 8).

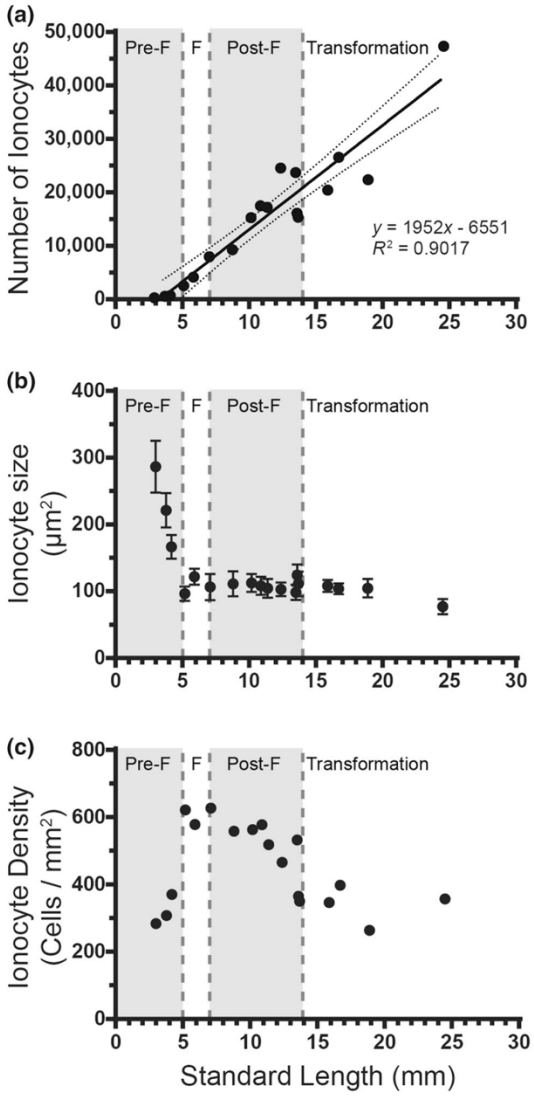

Fig. 3 Cutaneous ionocyte number (**a**), size (**b**), and density (**c**) in larval yellowfin tuna ($n = 18$) ranging from 2.9 to 24.5 mm in standard length. Dotted lines in **a** denote 95% confidence levels. Error bars in **b** (gray) denote standard error of the mean. *Pre-F* preflexion, *F* flexion, *Post-F* postflexion

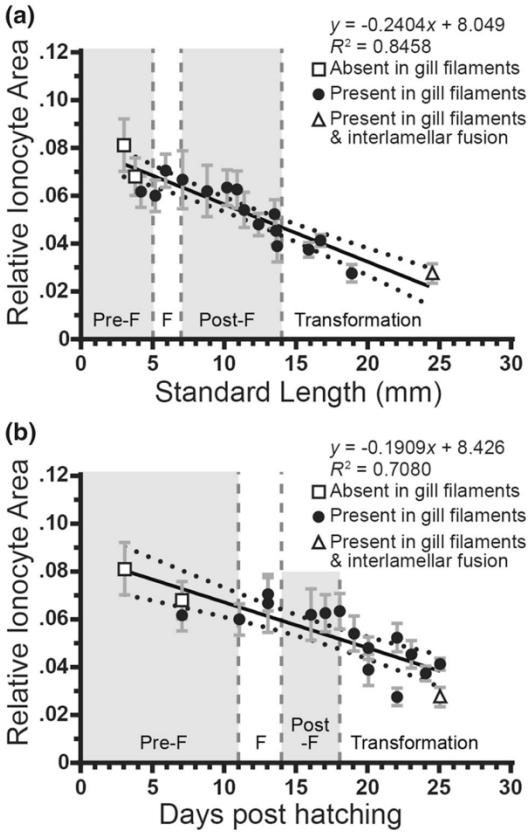

Fig. 4 Cutaneous ionocyte area relative to total skin surface area through larval yellowfin tuna development ($n = 18$) in relation to **a** standard length (linear regression: $F_{1,16} = 87.78$; $p < 0.001$; $r^2 = 0.8458$) and **b** days post-hatching (linear regression: $F_{1,16} = 38.80$; $p < 0.0001$; $r^2 = 0.7080$). The black line shows the linear regression curve and dotted lines denote 95% confidence levels. Error bars (gray) denote standard error of the mean. Ionocyte absence in gills, presence in the gill filaments, and presence in interlamellar fusions and in the gill filaments is noted as a square, circle, and triangle, respectively. *Pre-F* preflexion, *F* flexion, *Post-F* postflexion

Gill ionocytes in sub-adult fish

The gills from sub-adult yellowfin tuna had ionocytes in the filaments and filament fusions (Fig. 9a), lamellar fusions (Fig. 9b), and also at the base of some lamellae. Ionocytes typically appeared retracted within apical pits (Fig. 9c, d).

Discussion

The survival pattern of the larvae reared for this study was typical of other yellowfin tuna cohorts raised in the laboratory from fertilized eggs where the majority of the mortality occurs during the first 10 days after hatching (Margulies et al. 2016). Larval metamorphosis was rapid and similar to previous studies (Ambrose 1996; Kaji et al. 1999; Margulies et al. 2016), and the variation and range in lengths increased with increasing dph (Fig. 1). This was likely due to different consumption, prey encounter, and metabolic rates. The gill morphology of the larger larvae within the same age group

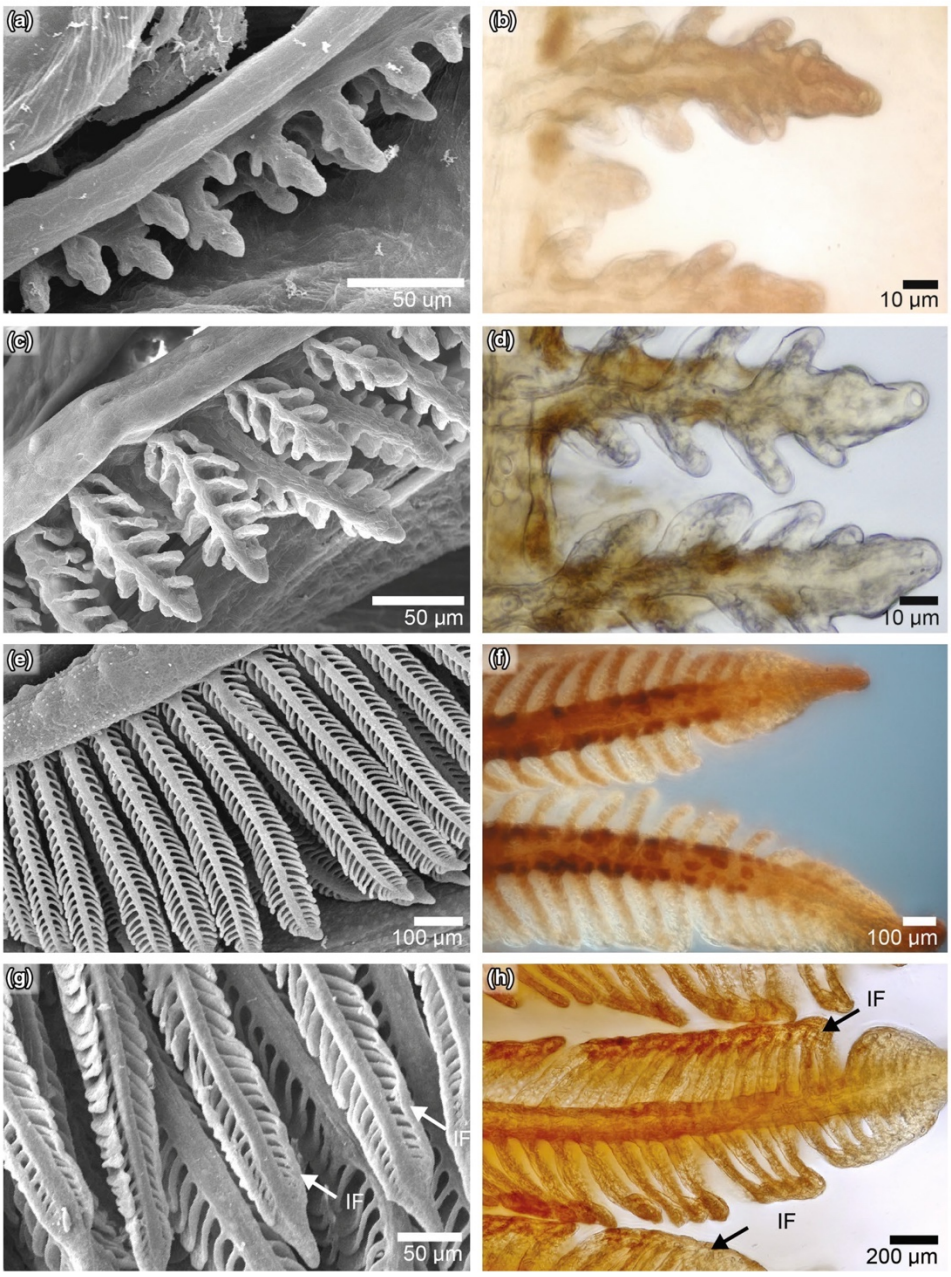

Fig. 5 Paired scanning electron micrographs **(a, c, e, g)** and Na^+/K^+ ATPase immunostained light microscopy images **(b, d, f, h)** showing the gill development and presence of ionocytes in a developmental time series of yellowfin tuna larvae. **a** Newly budding gills from a 3.3 mm standard length (SL) (4 dph) larva. **b** Absence of ionocytes in the gills of a 3.8 mm SL (6 dph) larva. **c** Further developed and defined filaments and lamellae in a 6.5 mm SL (15 dph) larva. **d** Strongly stained ionocytes in the gill filaments of a 4.2 mm SL (7 dph) larva. **e** The gill filaments and lamellae of a 15.4 mm SL (18 dph) larva. **f** Ionocytes in the gill filaments of a 16.7 mm SL (24 dph) larva. **g** Gills of a 20.5 mm SL (24 dph) transformation-stage larva showing the initial formation of interlamellar fusions binding adjacent lamellae near the filament tip. **h** Ionocytes on the gill filament and in the interlamellar fusions of a 24.5 mm SL (25 dph) yellowfin. Interlamellar fusions (IF) are indicated by arrows

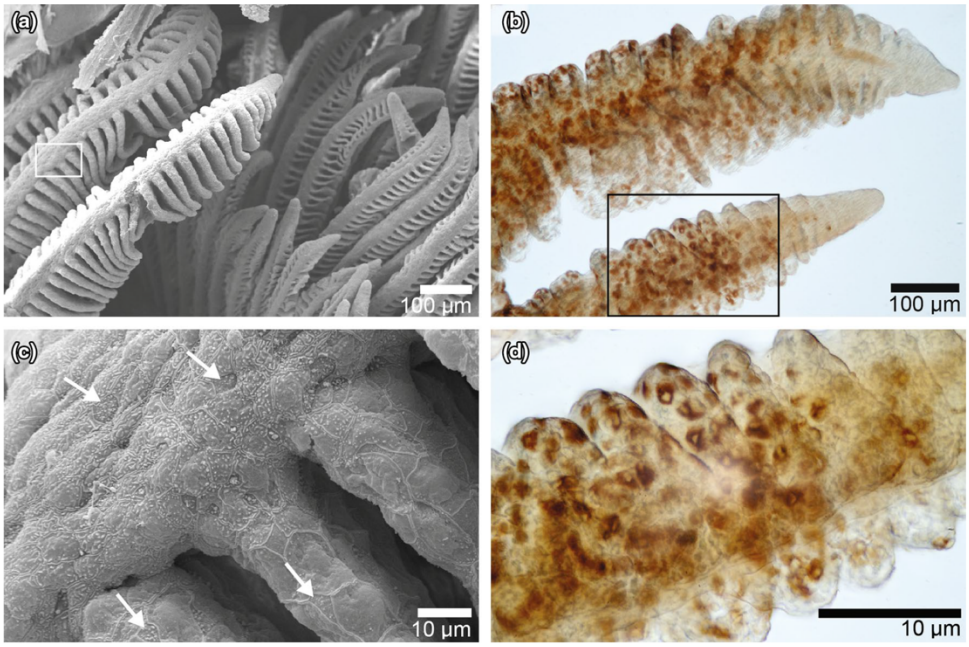

Fig. 6 Scanning electron **(a, c)** and light microscopy images **(b, d)** showing the presence of ionocytes on the filaments and lamellae of the pseudobranch of 18 mm standard length (SL) (25 dph) (**a, c**) and 19.6 mm SL (25 dph) transformation-stage yellowfin larvae (**b, d**). In **a** pseudobranch filaments are shown in the left foreground with gill filaments shown in the background (right). **c, d** are magnified views of the boxes shown in **a, b**, respectively. White arrows in **c** show the exposed apical surface of ionocytes on both the filament and lamellae of the pseudobranch

was more developed and indicated a more advanced stage in the transition from cutaneous to branchial gas exchange. This was especially evident at 25 dph larvae (672.38 ATU), where we did not observe interlamellar fusions in the smaller larvae (16.7 mm SL), but did so in the larger larvae (24.5 mm SL). These factors should be considered in future comparative studies of physiological and morphological development of yellowfin tuna larvae.

During the flexion stage, yellowfin tuna larvae have increased metabolic demands due to increasing ossification and chondrification and the rapid development of the digestive, neurological, and sensory systems (Richards and Dove 1971; Tanaka et al. 1996; Margulies 1997; Kaji et al. 1999). The increased development of the pseudobranch and gills as well as the transition from cutaneous to branchial gas exchange and osmoregulation also appear to take place around the flexion stage. In young larvae (< ~ 3.3 ml SL), the majority of gas exchange and osmoregulatory ion transport takes place across the skin. This is possible due to the large surface area to volume ratio of the larvae and the presence of abundant skin ionocytes (c.f. Goss et al. 1994; Perry and Goss 1994; Varsamos et al. 2002a; Katoh et al. 2003). As larvae grow larger (> ~ 3.3 ml SL), the pseudobranch and gills provide additional respiratory and osmoregulatory surface area to compensate for the decreased surface area to volume ratio and to keep up with increased metabolic rate. Although the total number of cutaneous ionocytes linearly increased throughout development, ionocyte size became smaller around the flexion stage—resulting in a linear decrease in relative ionocyte area and therefore active ion exchange capacity on the skin. This shift in ionocyte localization closely parallels previous studies in other marine teleosts, including larval Japanese flounder (*Paralichthys olivaceus*), killifish (*Fundulus heteroclitus*), European seabass (*Dicentrarchus labrax*), and gilthead sea bream (*Sparus aurata*) (Hiroi et al. 1998; Katoh et al. 2000; Varsamos et al. 2002a; Bodinier et al. 2010). Altogether, this indicates a shift in cutaneous to branchial osmoregulation around the flexion stage.

The apical morphology of cutaneous ionocytes also changed dramatically around the flexion stage, switching from a wide opening with extended microvilli in preflexion larvae to a pit in post-flexion larvae. During this transition, the number of branchial ionocytes progressively increased, and these ionocytes always had a wide apical opening with extended microvilli. The most extensively studied and

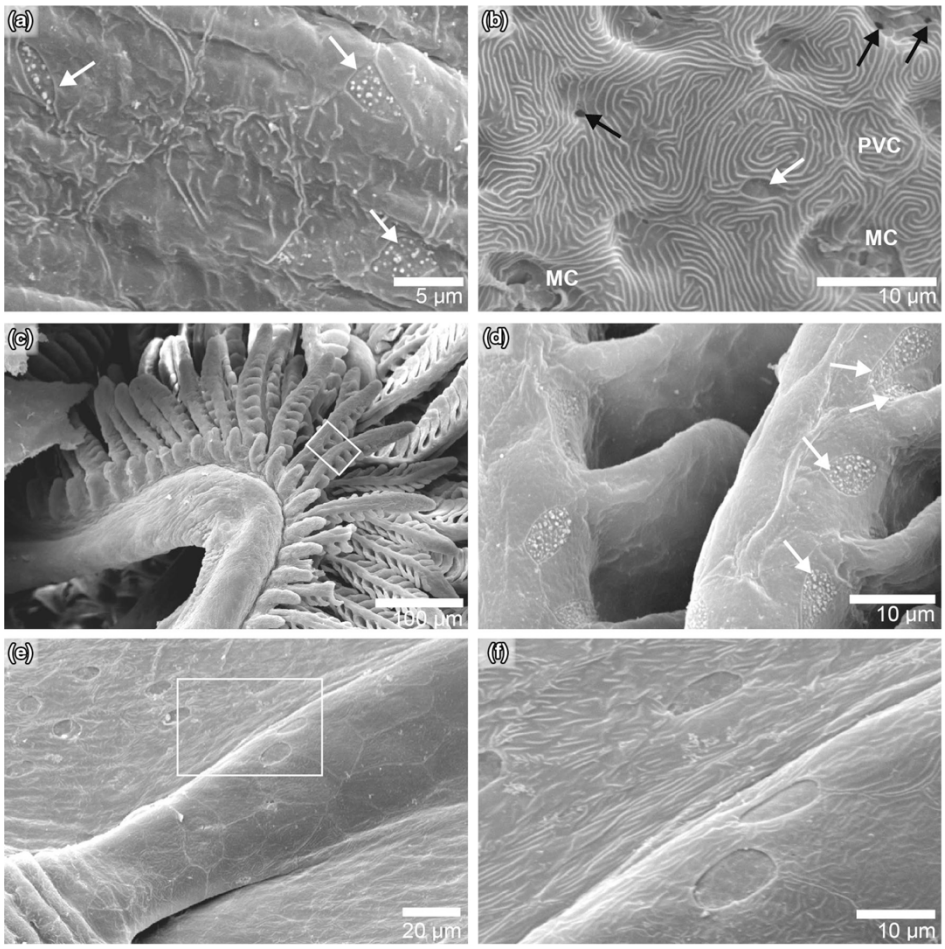

Fig. 7 Scanning electron micrographs of yellowfin tuna skin, gills, and dorsal fin. **a** Cutaneous ionocytes in a 3.8 mm standard length (SL), (10 dph) larva showing their exposed apical surfaces and protruding micovilli prior to the appearance of ionocytes in the gills. **b** Cutaneous ionocytes in a 6.5 mm SL (16 dph) larva, after the appearance of branchial ionocytes. **c** Gill arches, filaments, and lamellae from a 9.9 mm (20 dph) larva. **d** Higher magnification image of the white box shown in **c** showing gill filament ionocytes with exposed apical microvilli. **e** Second dorsal fin of a 9.9 mm SL (20 dph) larva showing the presence of ionocytes. **f** Higher magnification image of the white box in **e** showing dorsal fin ionocytes having a large exposed apical area that lacks extended microvilli. *PVC* pavement cell, *MC* mucous cells, black arrow ionocyte in apical pit; white arrow ionocyte with extended apical microvilli

reported ionocyte apical morphology is in the form of an apical pit (reviewed in Evans et al. 2005). However, a variety of ionocyte apical morphologies have been reported in gills from marine fish, including different degrees of exposure of the apical surface and microvilli (Laurent and Hebibi 1989; Franklin 1990; King and Hossler 1991; Brown 1992; Varsamos et al. 2002b). The exposure of gill ionocytes from European sea bass to doubly concentrated seawater showed that they undergo significant morphofunctional changes that include increased exposed apical surface area and NKA abundance (Varsamos et al. 2002b). Because survival in doubly concentrated seawater requires more active hypo-osmotic regulation, this ionocyte apical morphology has been linked to increased rates of NaCl excretion (Varsamos et al. 2002b). Based on that model, the change in apical morphology of cutaneous ionocytes of yellowfin tuna larvae during the flexion stage suggests downregulation, although not necessarily cessation, of NaCl excretion across the skin. Conversely, the exposed apical membrane and extended microvilli in branchial ionocytes of all larvae

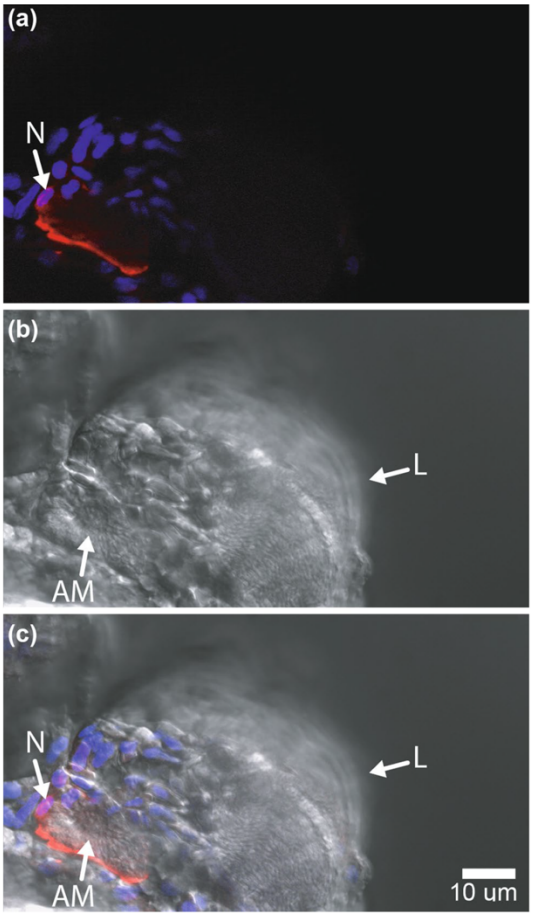

Fig. 8 Cross-section of an ionocyte on the gill filament of a post-flexion larval yellowfin tuna (12.2 mm SL; 24 dph). **a** Intense Na^+/K^+ ATPase signal was detected in the basolateral membrane of the ionocyte and **b** extended microvilli was observed in the widened apical pit of the ionocyte. The two images were merged in **c**. *N* nucleus of the ionocyte, *AM* apical membrane, *L* lamellae

that were examined suggest they were excreting NaCl at a high rate. However, only apical pits were observed in gills of the larger sub-adult yellowfin tuna examined which may reflect a decrease in mass-specific ionoregulation with growth as the fish surface area to volume ratio continues to decline. Altogether, our observations suggest covering and uncovering of the apical surface is a regulatory mechanism for ion transport in yellowfin tuna, similar to NaCl excretion in gills from European sea bass (Varsamos et al. 2002b) and to NaCl absorption in gills from freshwater teleosts (Goss et al. 1992a, b).

By the end of the transformation stage (~25 mm SL), branchial ionocytes also appeared along the gill interlamellar fusions, specialized gill structures found in some scombrids and billfishes that help the gills withstand the high-pressure ventilatory steam created by ram ventilation (Muir and Kendall 1968; Wegner et al. 2006, 2013). In yellowfin tuna, interlamellar fusions from adjacent filaments begin to merge together to form complete lamellar fusions starting about 3.2 cm FL (Wegner et al. 2013), and these are followed later by the development of filament fusions (Muir and Kendall 1968; Wegner et al. 2013). Examination of two larger yellowfin showed that ionocytes persist in these gill fusions as they grow. We hypothesize this novel ionocyte localization on the gill fusions is related to the need of yellowfin tuna (and presumably other scombrids and billfishes) for additional sites for ion regulation to maintain their large gill surface areas and a thin respiratory epithelial thickness (0.5–1.0 µm) required to meet their high metabolic demands (Hughes 1970; Wegner et al. 2006, 2010).

The physiological role(s) of the pseudobranch remains unclear (reviewed in Laurent and Dunel-Erb1984). In all larvae examined, the pseudobranch was extended within the buccal cavity and therefore exposed to environmental seawater. Furthermore, ionocytes developed on the pseudobranch filament and lamellae in high densities earlier than in the gill filaments, and remained abundant and with their apical surface exposed in the largest larvae (24.5 mm SL; 25 dph). These observations indicate the pseudobranch plays an important role in gas exchange and osmoregulation in developing yellowfin tuna larvae.

The yellowfin tuna larvae in the current study were raised in a land-based facility with optimal and near-constant salinity (~33 ppt), temperature (~28 °C), dissolved O_2 (~6 mg/L), and pH (~8.1) levels (Supplementary Material 1), which are representative of nearshore coastal conditions. However, the oceanic environment can be more variable. For example, yellowfin tuna spawn year-round off the coast of Costa Rica and Panama (Orange 1961; Schaefer 2001) where larvae are present at depths down to 50 m and may be exposed to seasonal changes in seawater salinity (28–35 ppt) and temperature (16–30 °C) (Lauth and Olson 1996; Owen 1997; Alory et al. 2012), and to changes in dissolved O_2 (2.0–7.3 mg/L) and pH (7.86–8.01) during upwelling events (Lauth and Olson 1996; Owen 1997; Rixen et al. 2012). In other teleosts, ionocytes have been shown to appear on the gill lamellae during hypo- (Uchida and Kaneko 1996; Sasai et al. 1998; Hirai et al. 1999; Zydlewski and McCormick 2001) and hyper-osmotic stress (Varsamos et al. 2002b), and upon experimentally induced decrease in temperature (Masroor et al. 2018), O_2 (Mitrovic et al. 2009), and pH levels (Leino and McCormick 1984). In addition, ionocyte distribution in marine teleost larvae may be affected by solar ultraviolet-B radiation (Sucré et al. 2012). If similar changes in ionocyte abundance and distribution occur in

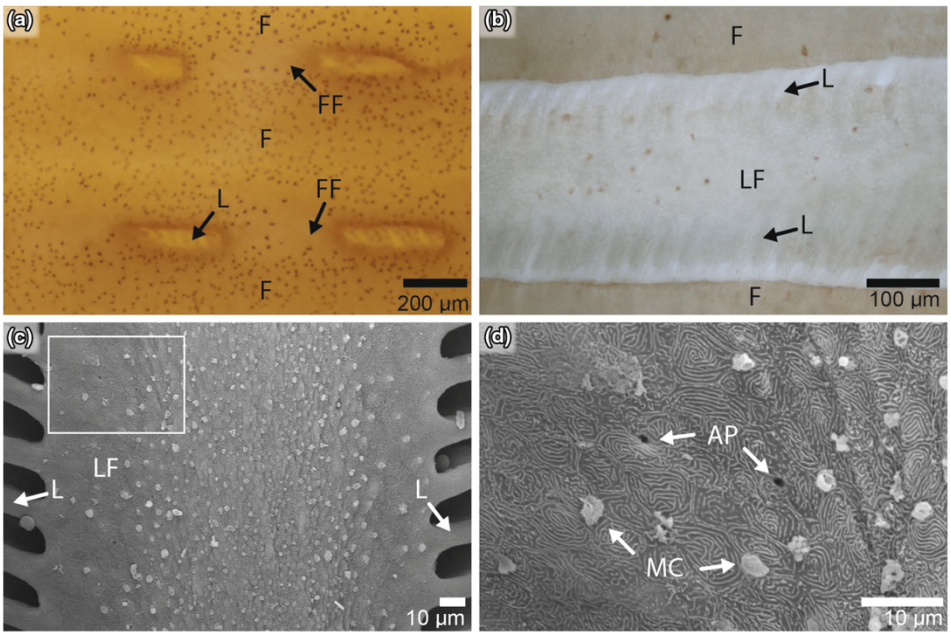

Fig. 9 Na^+/K^+ ATPase immunostained light microscopy images revealing ionocytes on the **a** filament, filament fusion, and **b** lamellar fusion of a sub-adult yellowfin tuna (54.9 cm fork length). **c** Scanning electron micrographs of ionocytes within the lamellar fusion of a sub-adult yellowfin tuna (91.0 cm fork length). **d** Higher magnification image of the white box in **c** showing lamellar fusion ionocytes in an apical pit. *FF* filament fusion, *F* filament, *L* lamella, *LF* lamellar fusion, *AP* apical pit, *MC* mucous cell

yellowfin tuna larvae exposed to changing environmental conditions, they would necessarily increase the thickness of the lamellar epithelium potentially affecting O_2 uptake. Such changes could compromise larval metabolic capacity, especially during the flexion stage.

In closing, this study provides a detailed description of the early development of gas exchange and osmoregulatory morphology of yellowfin tuna under optimum and constant rearing conditions. This information can be used as a baseline reference for studies of potential effects of environmental stressors on yellowfin tuna during early development in both aquaculture and the wild. Our study identified the flexion stage as a key transition point from cutaneous to branchial gas exchange and osmoregulation, the pseudobranch as a potentially important organ for gas exchange and osmoregulation during early development, and an unexpectedly complex apical ionocyte morphology. Finally, ionocytes were identified for the first time in interlamellar fusions of larval yellowfin tuna, and in the lamellar and filament fusions of larger individuals. Future in-depth studies should investigate whether morphological changes in ionocyte apical morphology is a regulatory mechanism for ion transport in marine fish, and its relevance for the physiology of fish living in a changing environment.

Acknowledgements This study was supported by the Inter-American Tropical Tuna Commission. We are grateful to the technical staff of the Achotines Laboratory in Panama for their assistance with measurements and larval rearing of yellowfin tuna. We thank Daniel Margulies and Vernon Scholey of the IATTC for development of yellowfin rearing methods and supervision of the spawning and larval rearing at the Achotines Laboratory. The authors would like to thank Dr. Greg Rouse for the use of microscope and camera equipment, Sabine Faulhaber for technical assistance with the scanning electron microscope, Taylor Smith for her assistance in dissection and imaging, and Johnathan Evanilla and Dan Fuller for providing sub-adult yellowfin tuna samples. We also thank William Watson (Southwest Fisheries Science Center) and Alex Da-Silva (Inter-American Tropical Tuna Commission) for helpful review comments. Lastly, we thank the editor and two anonymous reviewers for their helpful comments on an earlier draft. G.T.K. was supported by the San Diego Fellowship and the National Science Foundation Graduate Research Fellowship Program.

Compliance with ethical standards

Conflict of interest This study followed all applicable institutional guidelines for the care and use of animals. The authors declare they have no conflict of interest.

References

Alderdice DF (1988) Osmotic and ionic regulation in teleost eggs and larvae. In: Fish physiology. Academic Press, Cambridge, pp 163–251

Alory G, Maes C, Delcroix T, Reul N, Illig S (2012) Seasonal dynamics of sea surface salinity off Panama: the far eastern Pacific fresh pool. J Geophys Res Ocean 117:1–13. https://doi.org/10.1029/2011JC007802

Ambrose DA (1996) Scombridae: mackerels and tunas. In: Moser H (ed) The stages of fishes in the California current region, Calif. Coop. Ocean. Fish. Inves. Lawrence, Kansas, pp 1270–1285

Ayson FG, Kaneko T, Hasegawa S, Hirano T (1994) Development of mitochondrion-rich cells in the yolk-sac membrane of embryos and larvae of tilapia, *Oreochromis mossambicus*, in fresh water and seawater. J Exp Zool 270:129–135. https://doi.org/10.1002/jez.1402700202

Bodinier C, Sucré E, Lecurieux-Belfond L, Blondeau-Bidet E, Charmantier G (2010) Ontogeny of osmoregulation and salinity tolerance in the gilthead sea bream *Sparus aurata*. Comp Biochem Physiol A Mol Integr Physiol 157:220–228. https://doi.org/10.1016/j.cbpa.2010.06.185

Boehlert GW, Mundy BC (1994) Vertical and onshore-offshore distributional patterns of tuna larvae in relation to physical habitat features. Mar Ecol Prog Ser 107:1–13

Boehlert GW, Watson W, Sun LC (1992) Horizontal and vertical distributions of larval fishes around an isolated oceanic island in the tropical Pacific. Deep Res 39:439–466. https://doi.org/10.1016/0198-0149(92)90082-5

Brown P (1992) Gill chloride cell surface-area is greater in freshwater-adapted adult sea trout (*Salmo trutta*, L.) than those adapted to sea water. J Fish Biol 40:481–484. https://doi.org/10.1111/j.1095-8649.1992.tb02596.x

Brown CE, Muir BS (1970) Analysis of ram ventilation of fish gills with application to skipjack tuna (*Katsuwonus pelamis*). J Fish Res Board Can 27:1637–1652. https://doi.org/10.1139/f70-184

Evans DH (2002) Cell signaling and ion transport across the fish gill epithelium. J Exp Zool 293:336–347. https://doi.org/10.1002/jez.10128

Evans DH, Keys A (2008) Teleost fish osmoregulation: what have we learned since August Krogh, Homer Smith. AJP Regul Integr Comp Physiol 295:R704–R713. https://doi.org/10.1152/ajpregu.90337.2008

Evans D, Piermarini P, Potts W (1999) Ionic transport in the fish gill epithelium. J Exp Zool 283, 641–652. https://doi.org/10.1002/(SICI)1097-010X(19990601)283:7%3C641::AID-JEZ3%3E3.0.CO;2-W.

Evans DH, Piermarini PM, Choe KP (2005) The multifunctional fish gill: dominant site of gas exchange, osmoregulation, acid-base regulation, and excretion of nitrogenous waste. Physiol Rev 85:97–177. https://doi.org/10.1152/physrev.00050.2003

Franklin CE (1990) Surface ultrastructural changes in the gills of sockeye salmon (teleostei: *Oncorhynchus nerka*) during seawater transfer: comparison of successful and unsuccessful seawater adaptation. J Morphol 206:13–23. https://doi.org/10.1002/jmor.1052060103

Galland G, Rogers A, Nickson A (2016) Netting billions: a global valuation of tuna. Pew Charitible Trust, pp 1–22

Goss GG, Laurent P, Perry SF (1992a) Evidence for a morphological component in acid-base regulation during environmental hypercapnia in the brown bullhead (*Ictalurus nebulosus*). Cell Tissue Res 268:539–552. https://doi.org/10.1007/BF00319161

Goss GG, Perry SF, Wood CM, Laurent P (1992b) Mechanisms of ion and acid-base regulation at the gills of freshwater fish. J Exp Zool 263:143–159. https://doi.org/10.1002/jez.1402630205

Goss GG, Laurent P, Perry SF (1994) Gill morphology during hypercapnia in brown bullhead (*Ictalurus nebulosus*): role of chloride cells and pavement cells in acid-base regulation. J Fish Biol 45:705–718. https://doi.org/10.1111/j.1095-8649.1994.tb00938.x

Hirai N, Tagawa M, Kaneko T, Seikai T, Tanaka M (1999) Distributional changes in branchial chloride cells during freshwater adaptation in Japanese sea bass *Lateolabrax japonicus*. Zool Sci 16:43–49. https://doi.org/10.2108/zsj.16.43

Hiroi J, Kaneko T, Seikai T, Tanaka M (1998) Developmental sequence of chloride cells in the body skin and gills of Japanese flounder (*Paralichthys olivaceus*) larvae. Zool Sci 15:455–460

Hiroi J, Kaneko T, Tanaka M (1999) In vivo sequential changes in chloride cell morphology in the yolk-sac membrane of Mozambique tilapia (*Oreochromis mossambicus*) embyros and larvae during seawater adaptation. J Exp Biol 202:3485–3495

Hirose S, Kaneko T, Naito N, Takei Y (2003) Molecular biology of major components of chloride cells. Comp Biochem Physiol B Biochem Mol Biol 136:593–620. https://doi.org/10.1016/S1096-4959(03)00287-2

Holliday FGT (1969) The effects of salinity on the eggs and larvae of teleosts. In: Fish physiology. Academic Press, Cambridge, pp 293–311

Hughes GM (1970) Morphological measurements on the gills of fishes in relation to their respiratory function. Folia Morph 18:78–95

Kaji T, Tanaka M, Oka M, Takeuchi H, Ohsumi S, Teruya K, Hirokawa J (1999) Growth and morphological development of laboratory-reared Yellowfin Tuna *Thunnus albacares* and early juveniles, with special emphasis on the digestive system. Fish Sci 65, 700–707. https://doi.org/10.2331/fishsci.65.700

Katoh F, Shimizu A, Uchida K, Kaneko T (2000) Shift of chloride cell distribution during early life stages in seawater-adapted killifish, *Fundulus heteroclitus*. Zool Sci 17:11–18. https://doi.org/10.2108/zsj.17.11

Katoh F, Hyodo S, Kaneko T (2003) Vacuolar-type proton pump in the basolateral plasma membrane energizes ion uptake in branchial mitochondria-rich cells of killifish *Fundulus heteroclitus*, adapted to a low ion environment. J Exp Biol 206:793–803. https://doi.org/10.1242/jeb.00159

King JAC, Hossler FE (1991) The gill arch of the striped bass (*Morone saxatilis*). IV. Alterations in the ultrastructure of chloride cell apical crypts and chloride efflux following exposure to seawater. J Morphol 209:165–176. https://doi.org/10.1002/jmor.1052090204

Laurent P, Dunel-Erb S (1984) The pseudobranch: morphology and function. In: Hoar WS, Randall DJ (ed) Gills. Academic Press, Cambridge, pp 285–323

Laurent P, Hebibi N (1989) Gill morphometry and fish osmoregulation. Can J Zool 67:3055–3063. https://doi.org/10.1139/z89-429

Lauth RR, Olson RJ (1996) Distribution and abundance of larval Scombridae in relation to the physical environment in the northwestern Panama Bight. InterAm Trop TunaComm Bull 21:127–167

Lebovitz RM, Takeyasu K, Fambrough DM (1989) Molecular characterization and expression of the (Na++ K+)-ATPase alpha-subunit in *Drosophila melanogaster*. EMBO J 8:193–202

Leino RL, McCormick JH (1984) Morphological and morphometrical changes in chloride cells of the gills of *Pimephales promelas* after chronic exposure to acid water. Cell Tissue Res 236:121–128. https://doi.org/10.1007/bf00216521

Leis JM, Trnski T, Vivien MH-, Renon J, Dufour V, Moudni KE, Galzin R (1991) High concentrations of tuna larvae (Pisces: Scombridae) in near-reef waters of French Polynesia (Society and Tuamotu Islands). Bull Mar Sci 48:150–158

Margulies D (1997) Development of the visual system and inferred performance capabilities of larval and early juvenile scombrids. Mar Freshw Behav Physiol 30:75–98. https://doi.org/10.1080/10236249709379018

Margulies D, Wexler JB, Bentler KT, Suter JM, Masuma S, Tezuka N, Teruya K, Oka M, Kanematsu M, Nikaido H (2001) Early life history studies of Yellowfin tuna, *Thunnus albacares*. InterAm Trop Tuna Comm Bull 22:9–20

Margulies D, Suter JM, Hunt SL, Olson RJ, Scholey VP, Wexler JB, Nakazawa A (2007) Spawning and early development of captive Yellowfin Tuna (*Thunnus albacares*). Fish Bull 105:249–265

Margulies D, Scholey VP, Wexler JB, Stein MS (2016) Research on the reproductive biology and early life history of Yellowfin Tuna *Thunnus albacares* in Panama. In: Advances in Tuna Aquaculture: From Hatchery to Market. Elsevier, Amsterdam, pp 77–114

Marshall WS, Nishioka RS (1980) Relation of mitochondria-rich chloride cells to active chloride transport in the skin of a marine teleost. J Exp Zool 214:147–156. https://doi.org/10.1002/jez.1402140204

Masroor W, Farcy E, Gros R, Lorin-Nebel C (2018) Effect of combined stress (salinity and temperature) in European sea bass *Dicentrarchus labrax* osmoregulatory processes. Comp Biochem Physiol Part A 215:45–54. https://doi.org/10.1016/j.cbpa.2017.10.019

Mitrovic D, Dymowska A, Nilsson GE, Perry SF (2009) Physiological consequences of gill remodeling in goldfish (*Carassius auratus*) during exposure to long-term hypoxia. AJP Regul Integr Comp Physiol 297:R224–R234. https://doi.org/10.1152/ajpregu.00189.2009

Muir BS (1970) Contribution to the study of blood pathways in teleost gills. Copeia 1970:19 https://doi.org/10.2307/1441971

Muir BS, Brown CE (1971) Effects of blood pathway on the blood-pressure drop in fish gills, with special reference to tunas. J Fish Res Board Can 28:947–955. https://doi.org/10.1139/f71-140

Muir BS, Hughes GM (1969) Gill dimensions for three species of tunny. J Exp Biol 51:271–285

Muir BS, Kendall JI (1968) Structural modifications in the gills of tunas and some other oceanic fishes. Copeia 1968:388 https://doi.org/10.2307/1441767

Olson KR, Dewar H, Graham JB, Brill RW (2003) Vascular anatomy of the gills in a high energy demand teleost, the skipjack tuna (*Katsuwonus pelamis*). J Exp Zool 297A:17–31. https://doi.org/10.1002/jez.a.10262

Orange CJ (1961) Spawning of yellowfin tuna and skipjack in the eastern tropical Pacific, as inferred from studies of gonad development. InterAm Trop Tuna Comm Bull 5:459–526

Owen RW (1997) Oceanographic atlas of habitats of larval tunas in the Pacific Ocean off the Azuero Peninsula, Panama. InterAm Trop Tuna Comm Data Rep 9:1–32

Palzenberger M, Pohla H (1992) Gill surface area of water-breathing freshwater fish. Rev Fish Biol Fish 2:187–216. https://doi.org/10.1007/BF00045037

Perry SF, Goss GG (1994) The effects of experimentally altered gill chloride cell-surface area on acid-base regulation in rainbow trout during metabolic alkalosis. J Comp Physiol B Biochem Syst Environ Physiol 327–336 https://doi.org/10.1007/BF00346451

Richards WJ, Dove GR (1971) Internal development of young tunas of the genera Katsuwonus, Euthynnus, Auxis, and Thunnus (Pisces, Scombridae). Copeia 1971:72 https://doi.org/10.2307/1441600

Ricker W (1975) Computation and interpretation of biological statistics of fish populations. Bull Fish Res Board Can 191:382

Rixen T, Jiménez C, Cortés J (2012) Impact of upwelling events on the sea water carbonate chemistry and dissolved oxygen concentration in the Gulf of Papagayo (Culebra Bay), Costa Rica: implications for coral reefs. Rev Biol Trop 60:187–195

Roa JN, Munévar CL, Tresguerres M (2014) Feeding induces translocation of vacuolar proton ATPase and pendrin to the membrane of leopard shark (*Triakis semifasciata*) mitochondrion-rich gill cells. Comp Biochem Physiol Part A Mol Integr Physiol 174:29–37. https://doi.org/10.1016/j.cbpa.2014.04.003

Roberts J (1975) Active branchial and ram gill ventilation in fishes. Biol Bull 148:85–105

Roberts RJ, Bell M, Young H (1973) Studies on the skin of plaice (*Pleuronectes platessa* L.). II. The development of larval plaice skin. J Fish Biol 5:103–108. https://doi.org/10.1111/j.1095-8649.1973.tb04435.x

Rombough P (2007) The functional ontogeny of the teleost gill: which comes first, gas or ion exchange? Comp Biochem Physiol A Mol Integr Physiol 148:732–742. https://doi.org/10.1016/j.cbpa.2007.03.007

Sasai S, Kaneko T, Hasegawa S, Tsukamoto K (1998) Morphological alteration in two types of gill chloride cells in Japanese eels (*Anguilla japonica*) during catadromous migration. Can J Zool 76:1480–1487. https://doi.org/10.1139/z98-072

Schaefer KM (2001) Reproductive biology of tunas. In: Block BA, Stevens ED (eds) Tuna: physiology, ecology, and evolution. Academic Press, San Diego, pp 225–270

Schindelin J, Arganda-Carreras I, Frise E, Kaynig V, Longair M, Pietzsch T, Preibisch S, Rueden C, Saalfeld S, Schmid B et al (2012) Fiji: an open-source platform for biological-image analysis. Nature Methods 9:676 https://doi.org/10.1038/nmeth.2019

Schreiber AM (2001) Metamorphosis and early larval development of the flatfishes (Pleuronectiformes): an osmoregulatory perspective. Comp Biochem Physiol B Biochem Mol Biol 129:587–595. https://doi.org/10.1016/S1096-4959(01)00346-3

Shelbourne JE (1957) Site of chloride regulation in marine fish larvæ. Nature 180:920–922. https://doi.org/10.1038/180920a0

Stevens E (1972) Some aspects of gas exchange in tuna. J Exp Biol 56:809–823

Stevens ED, Lightfoot EN (1986) Hydrodynamics of water flow in front of and through the gills of skipjack tuna. Comp Biochem Physiol Part A Physiol 83:255–259. https://doi.org/10.1016/0300-9629(86)90571-2

Sucré E, Vidussi F, Mostajir B, Charmantier G, Lorin-Nebel C (2012) Impact of ultraviolet-B radiation on planktonic fish larvae: alteration of the osmoregulatory function. Aquat Toxicol 109:194–201. https://doi.org/10.1016/j.aquatox.2011.09.020

Tanaka M, Kaji T, Nakamura Y, Takahashi Y (1996) Developmental strategy of scombrid larvae: high growth potential related to food habits and precocious digestive system development. In: Watanabe Y, Yamashita Y, Oozeki Y (eds) Survival strategies in early life stages of marine resources. A A. Balkema, Rotterdam, pp 125–139

Tang CH, Leu MY, Yang WK, Tsai SC (2014) Exploration of the mechanisms of protein quality control and osmoregulation in gills of *Chromis viridis* in response to reduced salinity. Fish Physiol Biochem 40:1533–1546. https://doi.org/10.1007/s10695-014-9946-3

Uchida K, Kaneko T (1996) Enhanced chloride cell turnover in the gills of Chum Salmon fry in seawater. Zool Sci 13:655–660. https://doi.org/10.2108/zsj.13.655

van der Heijden AJH, van der Meij JCA, Flik G, Wendelaar Bonga SE (1999) Ultrastructure and distribution dynamics of chloride cells in tilapia larvae in fresh water and sea water. Cell Tissue Res 297:119–130. https://doi.org/10.1007/s004410051339

Varsamos S, Connes R, Diaz JP, Charmantier G, Dicentrarchus L (2001) Ontogeny of osmoregulation in the European sea bass. Mar Biol 138:909–915. https://doi.org/10.1007/s002270000522

Varsamos S, Diaz J, Charmantier G, Blasco C, Connes R, Flik G (2002a) Location and morphology of chloride cells during the post-embryonic development of the European sea bass, *Dicentrarchus labrax*. Anat Embryol (Berl) 205:203–213. https://doi.org/10.1007/s00429-002-0231-3

Varsamos S, Diaz JP, Charmantier GUY, Flik G, Blasco C, Connes R (2002b) Branchial chloride cells in sea bass (*Dicentrarchus labrax*) adapted to fresh water, seawater, and doubly concentrated

seawater. J Exp Zool 293:12–26. https://doi.org/10.1002/jez.10099

Varsamos S, Nebel C, Charmantier G (2005) Ontogeny of osmoregulation in postembryonic fish: a review. Comp Biochem Physiol A Mol Integr Physiol 141:401–429. https://doi.org/10.1016/j.cbpb.2005.01.013

Wegner NC, Sepulveda CA, Graham JB (2006) Gill specializations in high-performance pelagic teleosts, with reference to striped marlin (*Tetrapturus audax*) and wahoo (*Acanthocybium solandri*). Bull Mar Sci 79:747–759

Wegner NC, Sepulveda CA, Bull KB, Graham JB (2010) Gill morphometrics in relation to gas transfer and ram ventilation in high-energy demand teleosts: Scombrids and billfishes. J Morphol 271:36–49. https://doi.org/10.1002/jmor.10777

Wegner NC, Lai NC, Bull KB, Graham JB (2012) Oxygen utilization and the branchial pressure gradient during ram ventilation of the shortfin mako, *Isurus oxyrinchus*: is lamnid shark-tuna convergence constrained by elasmobranch gill morphology? J Exp Biol 215:22–28. https://doi.org/10.1242/jeb.060095

Wegner NC, Sepulveda CA, Aalbers SA, Graham JB (2013) Structural adaptations for ram ventilation: gill fusions in scombrids and billfishes. J Morphol 274:108–120. https://doi.org/10.1002/jmor.20082

Wexler JB, Margulies D, Masuma S, Tezuka N, Teruya K, Oka M, Kanematsu M, Nikaido H (2001) Age validation and growth of yellowfin tuna, *Thunnus albacares*, larvae reared in the laboratory. InterAm Trop Tuna Comm Bull 22:52–71

Wexler JB, Scholey VP, Olson RJ, Margulies D, Nakazawa A, Suter JM (2003) Tank culture of Yellowfin Tuna, *Thunnus albacares*: developing a spawning population for research purposes. Aquaculture 220:327–353. https://doi.org/10.1016/S0044-8486(02)00429-5

Wexler JB, Chow S, Wakabayashi T, Nohara K, Margulies D (2007) Temporal variation in growth of Yellowfin Tuna (*Thunnus albacares*) larvae in the Panama Bight, 1990–97. Fish Bull 105:1–18

Wexler JB, Margulies D, Scholey VP (2011) Temperature and dissolved oxygen requirements for survival of Yellowfin Tuna, *Thunnus albacares*, larvae. J Exp Mar Biol Ecol 404:63–72. https://doi.org/10.1016/j.jembe.2011.05.002

Whitear M (1970) The skin surface of bony fishes. J Zool 160:437–454

Wilson JM, Randall DJ, Donowitz M, Vogl AW, Ip AK (2000) Immunolocalization of ion-transport proteins to branchial epithelium mitochondria-rich cells in the mudskipper (*Periophthalmodon schlosseri*). J Exp Biol 203:2297–2310

Wilson JM, Whiteley NM, Randall DJ (2002) Ionoregulatory changes in the gill epithelia of coho salmon during seawater acclimation. Physiol Biochem Zool 75:237–249. https://doi.org/10.1086/341817

Zadunaisky JA (1996) Chloride cells and osmoregulation. Kidney Int 49:1563–1567. https://doi.org/10.1038/ki.1996.225

Zydlewski J, McCormick SD (2001) Developmental and environmental regulation of chloride cells in young American shad, *Alosa sapidissima*. J Exp Zool 290:73–87

Journal of Comparative Physiology B
https://doi.org/10.1007/s00360-018-1187-9

Supplementary Material

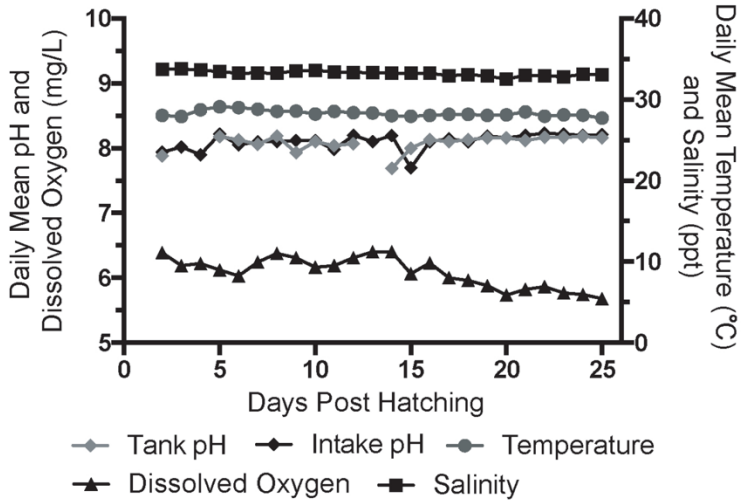

Supplementary material 1: Daily mean tank pH, intake pH, temperature (°C), dissolved O2 (mg/L), and salinity (ppt) throughout the yellowfin tuna larvae sampling period.

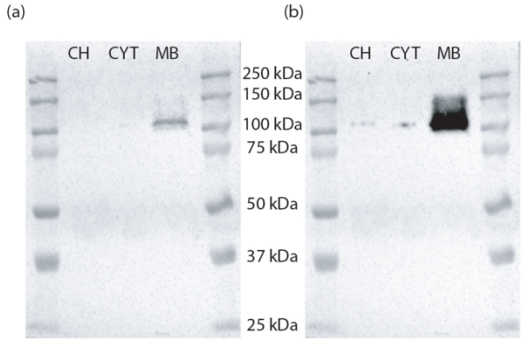

Supplementary material 2: Western blot with anti-Na+/K+-ATPase (NKA) monoclonal antibodies on sub-adult yellowfin tuna gill tissue yielded a single ~ 108 kDa band, which matches the predicted size of the protein. a NKA signal in the membrane fraction (MB) was significantly stronger (exposure time: 4 s) than b the crude homogenate (CH) and cytoplasm (CYT) fraction (exposure time: 304 s). This indicates NKA is present in the basolateral membrane as expected. Western blot method: gill samples were dissected from yellowfin tuna, immediately flash frozen in liquid N2, and kept at − 80 °C until processed. Frozen gill tissue was pulverized with porcelain mortar and pestle and mixed in an ice-cold protease inhibiting buffer (250 mmol L−1 sucrose, 1 mmol L−1 EDTA, 30 mmol L−1 Tris, 10 mmol L−1 benzamidine hydrochloride hydrate, 200 mmol L−1 phenylmethanesulfonyl fluoride, 1 mol L−1 dithiothreitol, pH 7.5). Debris was removed by low-speed centrifugation (3000×g for 10 min, 4 °C), and the resulting solution was saved as the crude homogenate fraction. A subset of the crude homogenate fraction was further subjected to a medium speed centrifugation (21130×g for 30 min, 4 °C), and the supernatant and membrane pellet was saved as the cytoplasmic fraction and the plasma membrane fraction, respectively. The total protein concentration of the three fractions was determined by Bradford protein assay, and 5 µg protein was combined with 2× Laemmli buffer (90%) and 2-mercapaethanol (10%). After heating at 70°C for 5 min, proteins were separated in 7.5% polyacrylamide mini gel (60 V 15 min, 200 V 45 min). Proteins were then transferred to a polyvinylidene difluoride (PVDF) membrane using a wet transfer cell (90 mA 8 h) (Bio-Rad, Hercules, CA, USA). After transfer, the PVDF membrane was incubated in blocking buffer (Tris-buffered saline, 1% tween, 10% skim milk) at room temperature (RT) for 1 h and incubated with the anti-NKA antibody (1.5 µg/mL) at 4 °C overnight. On the following day, the PVDF membrane was washed three times (10 min each) in Tris-buffered saline + 1% tween (TBS-T), incubated in goat anti-mouse HRP-linked secondary antibodies (1:10,000, Bio-Rad) at RT for 1 h and washed three times (10 min each) in TBS-T. Protein bands were made visible using ClarityTM Western ECL Substrate (Bio-Rad), and imaged and analyzed in a Bio-Rad Universal III Hood using ImageQuant software (Bio-Rad).

Published online: 24 October 2018

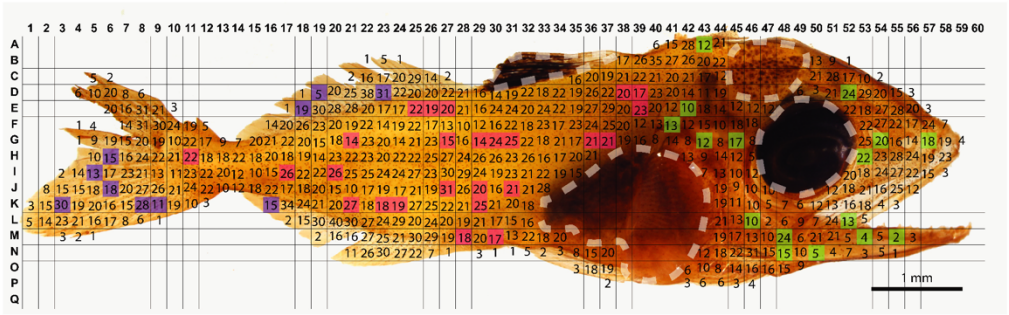

Supplementary material 3: Method for quantification of cutaneous ionocytes in yellowfin tuna larvae and early-stage juveniles >5 m SL. Ionocytes were identified by their intense Na+/K+-ATPase immunostaining and counted within randomly sampled boxes of the overlaid grid within the head (green), trunk (pink), and fin (blue) regions. Dashed white lines outline regions that were not sampled due to heavy pigmentation preventing accurate ionocyte counts .

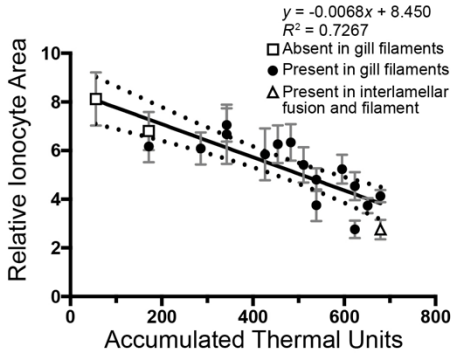

Supplementary material 4: Cutaneous ionocyte area relative to total skin surface area through larval yellowfin tuna development (n = 18) in relation to accumulated thermal units (linear regression: $F_{1,16} = 42.54$; $p < 0.001$; $r2 = 0.7267$). The black line shows the linear regression curve and dotted lines denote 95% confidence levels. Error bars (gray) denote standard error of the mean. Ionocyte absence in gills, presence in the gill filaments, and presence in interlamellar fusions and in the gill filaments is noted as a square, circle, and triangle, respectively.

Published online: 24 October 2018

Chapter IV, in full, is a reprint of the material as it appears in Kwan, G.T., Wexler, J.B., Wegner, N.C., and Tresguerres, M., 2019. Ontogenetic changes in cutaneous and branchial ionocytes and morphology in yellowfin tuna (*Thunnus albacares*) larvae. *Journal of Comparative Physiology B*, 189(1), 81-95. The dissertation author was the primary investigator and author of this material. The material is used by permission of Springer.

CHAPTER V

Physiological resilience of white seabass (*Atractoscion nobilis*) larvae to CO_2-induced ocean acidification

Abstract

CO_2-induced ocean acidification (OA) has been proposed to increase the energy demand for acid-base regulation in fish larvae at the expense of growth. However, most studies have used extremely high pCO_2 levels, and/or acutely exposed fish larvae to elevated pCO_2. Here, we collected white seabass (*Atractoscion nobilis*) fertilized eggs from an aquaculture facility where fish stocks are routinely exposed to extremely acidified conditions (pH as low as 7.16; and pCO_2 as high as 2,428 μatm), and exposed them to current (542 ± 28 μatm) and pCO_2 levels predicted for the year 2100 (1831 ± 105 μatm) between fertilization and five days post-hatching (dph). Because the enzyme Na+-K+-ATPase (NKA) in fish larvae skin ionocytes provides the driving force for acid secretion, we measured NKA protein abundance and skin ionocyte size and density, and calculated relative ionocyte skin area as a proxy for total ionoregulatory surface. Although 5 dph larvae exposed to elevated pCO_2 had increased skin ionocyte density, average ionocyte size was reduced compared to control larvae resulting in unchanged relative ionocyte skin area. The lack of effect of elevated pCO_2 on NKA was further supported by unchanged NKA protein abundance in whole larvae. Furthermore, elevated pCO_2 did not affect OCR or length, suggesting OA does not significantly affect aerobic energy consumption or energy allocation. Overall, our results suggest that early (up to 5 dph) white seabass larvae exposed to OA can maintain acid/base homeostasis without significantly upregulating NKA abundance, aerobic energy consumption, or compromising growth.

Introduction

The survival of life early life stages depends on a combination of oceanographic, hydrographic, climatic, biological, and trophodynamic factors (reviewed in Houde, 2009). Because pelagic fish eggs and larvae lack mobility, they are highly vulnerable to environmental stressors, which thus exert strong control over recruitment dynamics and mortality (reviewed in Houde, 2009). Ocean acidification (OA) caused by increased absorption of atmospheric CO_2 resulting from anthropogenic sources is a growing concern for fish early life stages. By the year 2100, atmospheric CO_2 is projected to reach ~1,000 ppm, with surface ocean pCO_2 predicted to closely follow and pH to decline from 8.1 to 7.7 (Caldeira and Wickett, 2005; Meehl et al., 2007). In addition, recirculating aquaculture systems (RAS) are often used for commercial purposes to raise fish in high stocking densities, resulting in CO_2 buildup to levels that can be several folds higher than those predicted to occur under the most extreme future OA scenarios (reviewed in Ellis et al 2017). Thus, understanding the physiological responses of fish larvae to elevated CO_2 levels may help predict ecological impacts, manage fisheries, and improve aquaculture practices.

White seabass (*Atractoscion nobilis*) is an important sport and commercial croaker species found along the Western North American coast from Alaska to the Gulf of California; adults live over rocky bottoms, in the surf zone, and in kelp beds near which they usually spawn (Eschmeyer et al 1983). The experiments that originally reported enlarged otoliths in fish larvae exposed to OA-like conditions were conducted on white seabass (Checkley et al 2009), an effect that was repeatedly obtained in this (Shen et al., 2016) and other fish species (Munday et al., 2011b; Bignami et al., 2013a). In addition, it has been hypothesized that ongoing OA could increase energetic demand and alter the growth and development of larval fish in the wild

(reviewed in Ishimatsu et al., 2004, 2008). However, experimental outcomes have varied greatly possibly as a result of different conditions such as fish species, age, and magnitude and duration of the elevated CO_2 exposure. Since exposure to elevated CO_2 levels induces an immediate acidification of internal fluids measured within adult fishes (Esbaugh et al., 2012; Hvas et al., 2016), the larval fishes' resilience and vulnerability to OA are often attributed to the ability to maintain acid/base homeostasis, or lack thereof.

Adult fish have an excellent capacity to maintain blood acid/base homeostasis, which they achieve by excreting excess acid and base across the gill epithelium using specialized cells called ionocytes (reviewed in Evans et al., 2005). Larval fish lack developed ionocytes on their gills, which is often interpreted as another factor that contributes to a presumed increased vulnerability of fish early life stages to OA (c.f. Ishimatsu et al., 2008; Baumann et al., 2012; Hurst et al., 2013; Crespel et al., 2017). Unfortunately, the small size of fish larvae and the relatively small magnitude of the putative OA-induced acid/base disturbances prevent direct measurements of plasma pH and CO_2. However, marine larval teleost fishes are strong hypo osmo- and iono-regulators just like adult fishes are, indicating a great capacity for ion transport despite the lacking gills (reviewed in Alderdice, 1988). Indeed, larval fishes possess abundant ionocytes in their skin, which are functionally similar to the gill ionocytes of adult fishes (reviewed in Varsamos et al., 2005; Rombough, 2007; Glover et al., 2013; Zimmer et al., 2017).

Most of the energy that is required for acid/base and ionic regulation is used by enzyme Na^+/K^+ ATPase (NKA), which is abundantly present in the basolateral membrane of ionocytes and provides the driving force for H^+ secretion into seawater *via* apical Na^+/H^+ exchangers (reviewed in Evans et al., 2005; Perry and Gilmour, 2006; Hwang et al., 2011; Hiroi and McCormick, 2012). Surprisingly, few studies have examined the effects of OA on NKA in fish

larval stages that lack gills. In Japanese medaka (*Oryzias latipes*), OA-exposed larvae demonstrated increased whole body NKA mRNA levels (Tseng et al., 2013) suggesting upregulation of the machinery involved in H^+ secretion. However, OA-exposed Atlantic cod (*Gadus morhua*) larvae did not show any appreciable differences in NKA protein expression in yolk sac ionocytes compared to controls (Dahlke et al., 2017). While the discrepancy between these two studies may be due to species-specific sensitivity to OA, the different techniques that were used to quantify NKA prevent any definitive conclusions. Importantly, both studies focused on larvae within 24h of hatching, so other responses at later (but still gill-lacking) larval stages cannot be ruled out.

The main goal of the current study was to investigate the effects of elevated CO_2 levels on skin NKA expression in developing, gill-lacking, white seabass larvae using the same experimental conditions as in the previous studies that reported enlarged otoliths (Checkley et al 2009, Shen et al, 2016). To avoid confounding effects from feeding, we studied larvae up to 5 dph, which still rely on their yolk sac for nutrition and do not eat. NKA was chosen because this enzyme utilizes all the ATP involved in driving H^+ secretion into seawater. In addition to looking at NKA abundance in whole larvae, we calculated "relative ionocyte area", a metric that takes into account the number and size of cutaneous NKA-rich cells in relation to the body surface area and serves as a proxy for cutaneous ion transporting capacity (Kwan et al., 2019a, b). To evaluate potential effects on energy demand as a result of exposure to OA, we also measured the resting oxygen consumption rate (OCR) of 5 dph larvae, as well as their weight to determine potential effects on growth. In an effort to capture variability of responses, the experiments were repeated on three occasions, each time with a different batch of larvae.

Contrary to our predictions, none of the measured parameters were affected by exposure to ~2,000 μatm (pH ~7.40) from the time of fertilization to 5 dph. An effort to identify potential factors that explain this apparent acid-base resilience of white seabass larvae to OA led to the realization that the aquaculture tank where the broodstock fish were housed and fertilization occurred also experienced OA-like conditions. The implications for the effects of ongoing OA on wild fish are discussed.

Materials and Methods

Parental Conditions within the Recirculating Aquaculture System

Wild-caught adult white seabass (>61 cm, >9.1 kg; n = 24) were housed in broodstock tanks at the HSWRI hatchery in Carlsbad, USA between 2009 and 2012. Water parameters was monitored daily, and soda ash (Na_2CO_3) was added when necessary to maintain a pH level of 7.6 ± 0.01 and an alkalinity level of 2289 ± 23 μmol kg^{-1} SW^{-1} (Figure 4.1A). As a result, the parents of white seabass larvae have been exposed to an elevated pCO_2 level of 1247 ± 28 μatm (Figure 4.1A) for nearly 5 years. Dissolved oxygen and salinity levels were maintained at 9.10 ± 0.05 mg/L and 33.6 ± 0.03 ppt, respectively (Figure 4.1B). Spawning was induced through photothermal manipulation, raising the seawater temperature from 14°C to 18°C to mimic the warmer spawning season (Figure 4.1B). Floating fertilized and viable white seabass eggs were caught in a mesh at the outflow. Experiments were repeated three times (EX 1, EX 2, and EX 3), each time with eggs collected on a different day. On the morning following the spawning of larvae used in EX 1, EX 2, and EX 3, the pH of the outflowing water was recorded at 7.39, 7.39, and 7.53, respectively. Following collection, the eggs were sorted and transferred into our experimental system within 12 hours post-fertilization.

Experimental System

The experimental system consists of six (3 replicate tanks per treatment) water-jacketed, 5-L glass vessels with jacket water maintained at 18.0°C. Vessels were continuously bubbled with a certified air-CO_2 gas mixture of 400 μatm (control) and 2500 μatm (elevated) pCO_2. The average pCO_2 of control and elevated pCO_2 vessels was 542 ± 28 μatm and 1831 ± 105 μatm, respectively (Table 1). Control and elevated pCO_2 vessels had an average pH of 7.93 ± 0.02 and 7.46 ± 0.03, respectively (Table 1).

In the laboratory, 400 eggs were transferred into each of the experimental vessels containing filtered seawater that were fully equilibrated at control or elevated pCO_2 levels. Larvae were reared until 5 dph. Animal care and experimental procedures were approved by the University of California San Diego Institutional Animal Care and Use Committee under protocol S12161.

In all three experiments, length measurements were performed on live 5 dph larvae, euthanized, and fixed in 3% paraformaldehyde, 0.35% glutaraldehyde, 0.1 M cacodylate buffer (cat# 15949 Electron Microscopy Sciences, Hatfield, PA, USA) for immunohistochemistry. Furthermore, larvae aged 2 – 4 dph from EX 3 were also fixed for comparison across developmental period. Additionally, larvae were flash frozen in liquid nitrogen for western blot analysis. Finally, larvae from EX 1 and EX 2 were placed into microrespiration chambers for oxygen consumption measurements. High mortality was detected in one control and one elevated pCO_2 treatment within EX 3, and were subsequently excluded from all analyses.

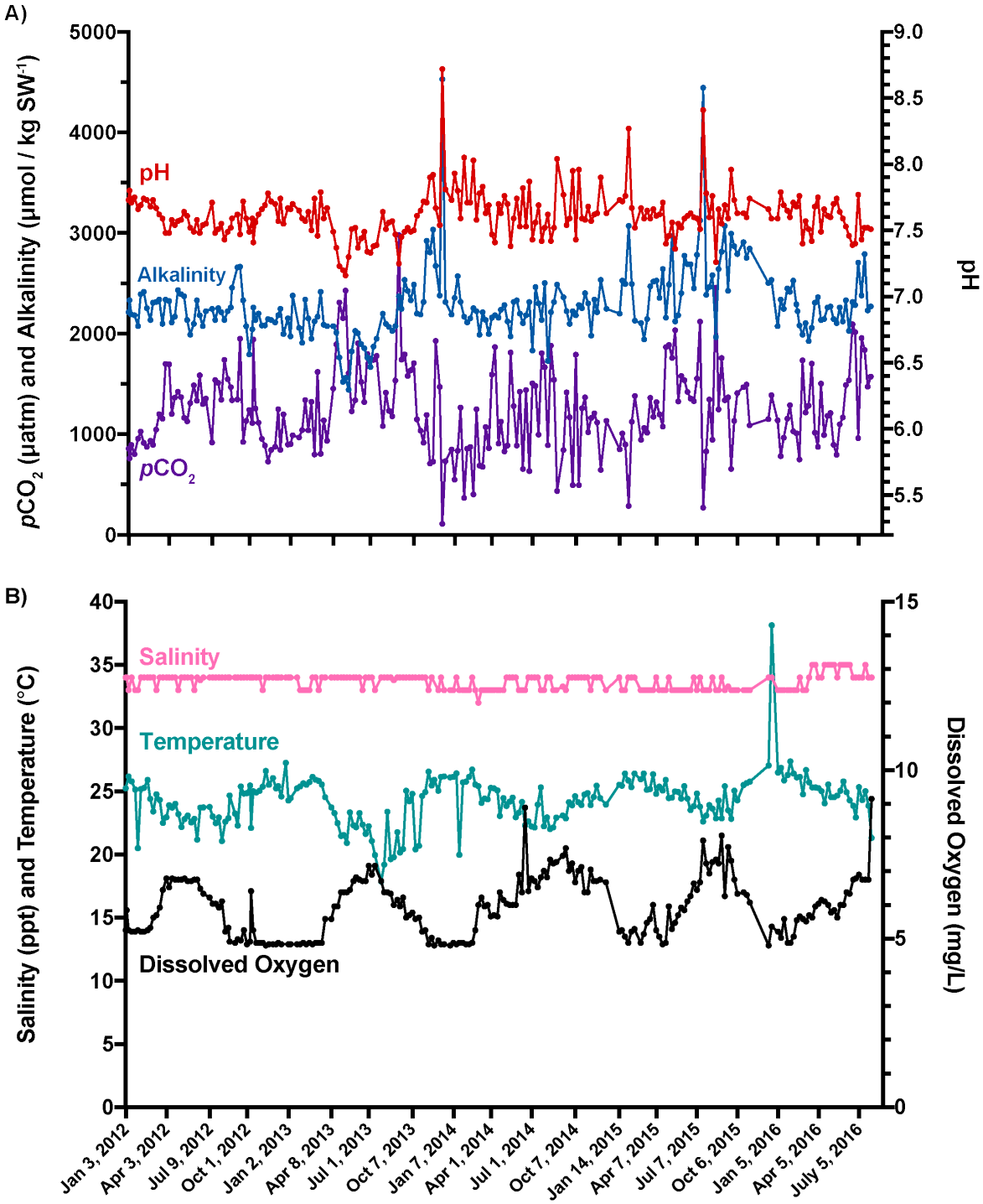

Figure 5.1: Water chemistry of broodstock fish tank. Adult white seabass was collected between 2009 – 2012, and housed within a recirculating aquaculture system at the Hubbs SeaWorld Research Institute. pH (A), alkalinity (B), pCO_2 (C), salinity, temperature, and dissolved oxygen (D) are reported from January 2012 to August 2016 (date of our last collection).

Table 5.1: Seawater carbonate chemistry measurements. Values are measured salinity (Sal), temperature (Temp), total alkalinity (A_T) and dissolved inorganic carbon (DIC) for each of the control and elevated pCO_2 vessels for all experiments. Partial pressure of CO_2 (pCO_2) and pH were estimated using the software CO2Calc.

Date	EX	Vessel	Sal	Temp (°C)	A_T (µmol kg^{-1})	DIC (µmol kg^{-1})	pCO_2 (µatm)	pH
06/20/16	1	1	33.64	18.0	2262.0	2102.3	601	7.89
06/20/16	1	2	33.62	18.0	2270.2	2095.7	552	7.93
06/20/16	1	3	33.65	18.0	2269.9	2092.5	543	7.93
06/20/16	1	1	33.61	18.1	2262.5	2271.6	2097	7.39
06/20/16	1	2	33.64	18.0	2259.4	2268.9	2094	7.39
06/20/16	1	3	33.64	18.0	2264.3	2276.6	2145	7.38
07/04/16	2	1	33.61	18.0	2269.2	2061.7	454	7.99
07/04/16	2	2	33.61	18.0	2263.5	2094.9	569	7.91
07/04/16	2	3	33.64	18.0	2268.0	2078.3	503	7.96
07/04/16	2	1	33.60	18.0	2263.1	2253.0	1799	7.45
07/04/16	2	2	33.61	18.1	2269.5	2258.2	1792	7.46
07/04/16	2	3	33.62	18.0	2263.5	2251.9	1777	7.46
08/02/16	3	2	33.63	18.0	2257.9	2070.3	506	7.96
08/02/16	3	3	33.62	18.1	2247.7	2123.3	754	7.80
08/02/16	3	1	33.63	18.0	2262.6	2266.3	2005	7.41
08/02/16	3	3	33.62	18.1	2244.5	2252.2	2061	7.40

At the end of the experiment, 250-mL seawater samples were collected from each vessel and poisoned with 100 µL of mercuric chloride for inorganic carbon chemistry measurements. A_T and dissolved inorganic carbon chemistry (DIC) were measured using open-cell potentiometric titration and coulometry, respectively. The software CO_2Calc (Robbins et al., 2010) was used to estimate pH and pCO_2 from the measured A_T and DIC.

Anti-NKA Antibody

The anti-NKA antibody used in our experiment is a monoclonal antibody raised against the α-subunit of chicken NKA (Lebovitz et al., 1989) was purchased from Developmental Studies Hybridoma Bank (α5; Iowa University). This antibody is routinely used for detecting

NKA α-subunits in teleosts (Melzner et al., 2009b; Yang et al., 2013; Tang et al., 2014; Kwan et al., 2019b) and elasmobranchs (Roa et al., 2014; Roa and Tresguerres, 2017).

Whole-mount immunohistochemistry

To immunostain our samples, we utilized the Vectastain® Universal HRP R.T.U. kit (Vector Laboratories, Inc., Burlingame, CA, USA) and the 3,3-diaminobenzidine (DAB) tetrahydrochloride kit with only a few deviations from the manufacturer's instructions. After 4 hours of fixation, samples were transferred to 50% ethanol overnight, and stored in 70% ethanol for later analysis. To immunolocalize ionocytes, larvae were rehydrated in phosphate buffered saline (PBS), incubated in 3% hydrogen peroxide for 10 min to devitalize endogenous peroxidases, and immersed in blocking buffer (Vector Laboratories; 2.5% normal goat serum diluted in 10 mmol l^{-1} phosphate buffered saline) for 30 min to block non-specific antibody binding sites. Anti-NKA antibody (1.5 μg/mL) was mixed into blocking buffer and incubated with the samples overnight at room temperature. Additionally, a subset of larvae was incubated without the primary antibody to serve as our methodology control (not shown). The following day, larvae were rinsed with PBS (5 min per wash, 3 washes total), incubated with a universal pan-specific secondary antibody linked to horseradish peroxidase (Vector Laboratories) for 30 min, and followed by another three PBS washes. Afterwards, samples were immersed in peroxidase-streptavidin complex for 15 min, stained with 3,3-diaminobenzidine (DAB) tetrahydrochloride (Vector Laboratories) for 15 min, and then rinsed in deionized water before imaging and photo processing.

Quantifying relative ionocyte area

The details regarding photo-microscopy imaging, focal-stacking, photo-stitching, and quantifying relative ionocyte area can be found in our methodology paper (Kwan et al., 2019a). Briefly, ionocytes were identified based on their dark brown color resulting from DAB precipitation. Ionocytes were manually counted using the "cell counter" tool in Image J, and ionocyte size and larva surface area were traced and measured using the "free hand" tool. Relative ionocyte area was calculated as the number of cutaneous ionocytes multiplied by their average area, then divided by the larva's surface area.

Western Blot analysis

Frozen larvae were pulverized in liquid nitrogen by mortar and pestle, mixed in ice-cold homogenization buffer (250 mmol l^{-1} sucrose, 1 mmol l^{-1} EDTA, 30 mmol l^{-1} Tris, 10 mmol l^{-1} BHH, 200 mmol l^{-1} PMSF, 1 mol l^{-1} DTT, pH 7.5), and centrifuged at 500 g for 10 min at 4°C to remove debris. The total protein concentration of the crude homogenate was determined by Bradford Protein Assay.

To prepare for western blot analysis, homogenized samples were denatured in sample buffer (90% 2x Laemmli buffer and 10% β-Mercaptoethanol) and heated for 5 min at 70°C. Five μg of total protein from each treatment and experiment were separated in a Mini-PROTEAN® TGX Stain-Free™ Precast Gel (Bio-Rad Laboratories, Inc., Hercules, CA, USA) at 200V for 45 min. An additional sample of control larvae was homogenized to serve as a reference standard across all gels and used to normalize results from different gels. Proteins were transferred to

Polyvinylidene difluoride (PVDF) membranes using the Trans-Blot® Turbo™ System (Bio-Rad Laboratories, Inc., Hercules, CA, USA) semi-dry transfer cell for 30 min at 25V.

After transfer, PVDF membranes were blocked in tris-saline buffer with 0.1% Tween (TBS-T) and 10% nonfat dry milk for 1 hour at room temperature, then incubated overnight with the anti-NKA antibody (1.5 μg/mL) at 4°C on a shake table. After 3 washes in TBS-T for 20 min each, PVDF membranes were blocked for 1 hour and incubated with a secondary goat anti-mouse NKA antibody (1:10,000) at room temperature on a shake table. Following 3 washes in TBS-T for 20 min each, PVDF membranes were analyzed using chemiluminescence on a ChemiDoc™ MP system (Bio-Rad Laboratories, Inc., Hercules, CA, USA), and NKA protein abundance was quantified using Image Lab™ software (Bio-Rad Laboratories, Inc., Hercules, CA, USA).

Oxygen consumption rate

OCR was measured using a Unisense MicroRespiration System and accompanying software, SensorTrace Rate (Unisense A/S, Aarhus, Denmark). Five larvae were removed from an individual vessel and placed into a 4-mL glass microrespiration chamber containing seawater from their respective vessel. OCR measurements of groups of larvae are common given their small size (Cattano et al., 2016; Peck and Moyano, 2016). The chamber was placed onto a magnetic stir rack and the seawater was stirred at 600 rpm by a glass-embedded micromagnet. The magnetic stir rack holding the chamber was submerged in a water bath at 18.0°C. Larvae were allowed to acclimate for 10 min before oxygen measurements were recorded.

An oxygen microsensor was inserted into the chamber through a capillary in the lid and the resulting signal was measured by a picoammeter (Microsensor Multimeter). Oxygen

concentration was measured for 50 min, during which the larvae were visually inspected for 1 min every 15 min to observe behavior. OCR measurements were performed in duplicate for each vessel using two chambers simultaneously. Oxygen measurements were also recorded in EX 3 for blanks that contained only seawater from each vessel to obtain the background microbial respiration rate, and the average blank OCR was subtracted from the OCR measurements in all experiments. While experiments by other researchers have used UV-sterilized seawater mixed with antibiotics to reduce bacterial respiration (Pimentel et al., 2014b), we used the source water from the vessels to limit changes to pH and pCO_2. Following oxygen measurements, the length of larvae was measured to the nearest 0.1 mm using a dissecting microscope.

On the morning of each experiment, oxygen microelectrodes were polarized to remove oxygen that had accumulated within the electrolyte during storage and calibrated. A two-point calibration was performed by measuring the signals of the microsensors in anoxic seawater in the 0-calibration chamber and in seawater saturated with oxygen by rigorous air bubbling for 5 min, both at 18.0°C.

A linear regression of oxygen concentration over time was performed and the slope of the line was taken as the OCR for each group of five larvae. Duplicate measurements for each vessel were averaged and the contribution of bacterial respiration was removed. The OCR of an individual larva was estimated by dividing the group OCR by five. Statistical analyses were performed on these individual-based OCR ($\mu L\ O_2\ ind^{-1}\ h^{-1}$) estimates.

Data analysis

Length, relative ionocyte area, total NKA protein abundance, and individual-based OCR were analyzed using two-tailed, two-way Analysis of Variance (2-way ANOVA) with

interaction, with pCO_2 and EX as predictor variables. Linear regression was used to assess changes in relative ionocyte area as a function of pCO_2 for larvae at 2 to 5 dph. Tukey HSD post-hoc tests assessed differences between experiments and treatment groups. Model residuals for all response variables were normally distributed, as determined by Shapiro-Wilks. Homoscedasticity was tested using the Bartlett test and satisfied for all response variables except length. An alpha level of 0.05 was used for significance in all statistical tests. Unless otherwise stated, values are mean and standard error. Statistical analyses were performed in R version 3.1.2 (R Development Core Team, 2013).

Results

In both control and elevated pCO_2 treatments, ionocytes were concentrated on the yolk sac (2 dph larva) and on the anterior end of larva (Figure 4.2). From 2 to 5 dph, the relative ionocyte area (n = 24; 12 per treatment, 3 per dph) significantly decreased in both control and elevated pCO_2 treatment throughout development (2-way ANOVA: $F_{3, 16} = 7.391$, $p = 0.003$; Table S1). While both control and elevated pCO_2 larvae experienced a linear decline in relative ionocyte area during development (control = $F_{1, 10} = 8.053$, $p = 0.018$; elevated = $F_{1, 10} = 16.500$, $p = 0.002$; Figure 4.3A), the rate of change was not significantly different between control and elevated pCO_2 larvae ($F_{1, 20} = 0.169$; $p = 0.686$). Subsequent comparisons between day 2 (p = 0.725), 3 ($p = 0.630$), 4 ($p = 0.580$), and 5 ($p = 0.993$) were also not significantly different (Figure 4.3B; Table S1).

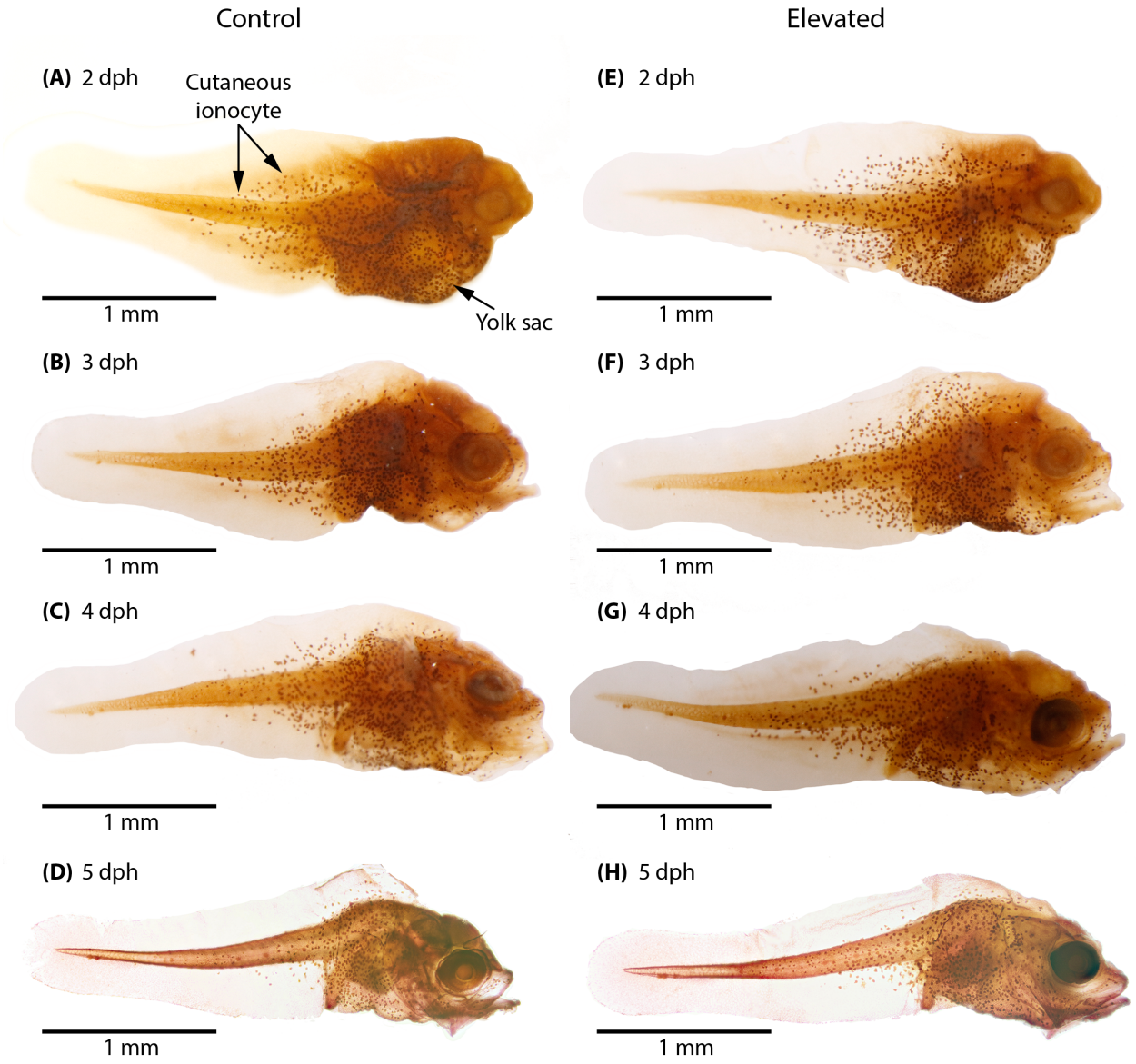

Figure 5.2: Cutaneous ionocytes in 2-5 days post hatching white seabass larvae exposed to control or elevated pCO_2 conditions. Representative images showing Na^+-K^+-ATPase immunostained cutaneous ionocytes in larvae. (A-D) control treatment; (E-H) elevated pCO_2 treatment; dph = days post hatching.

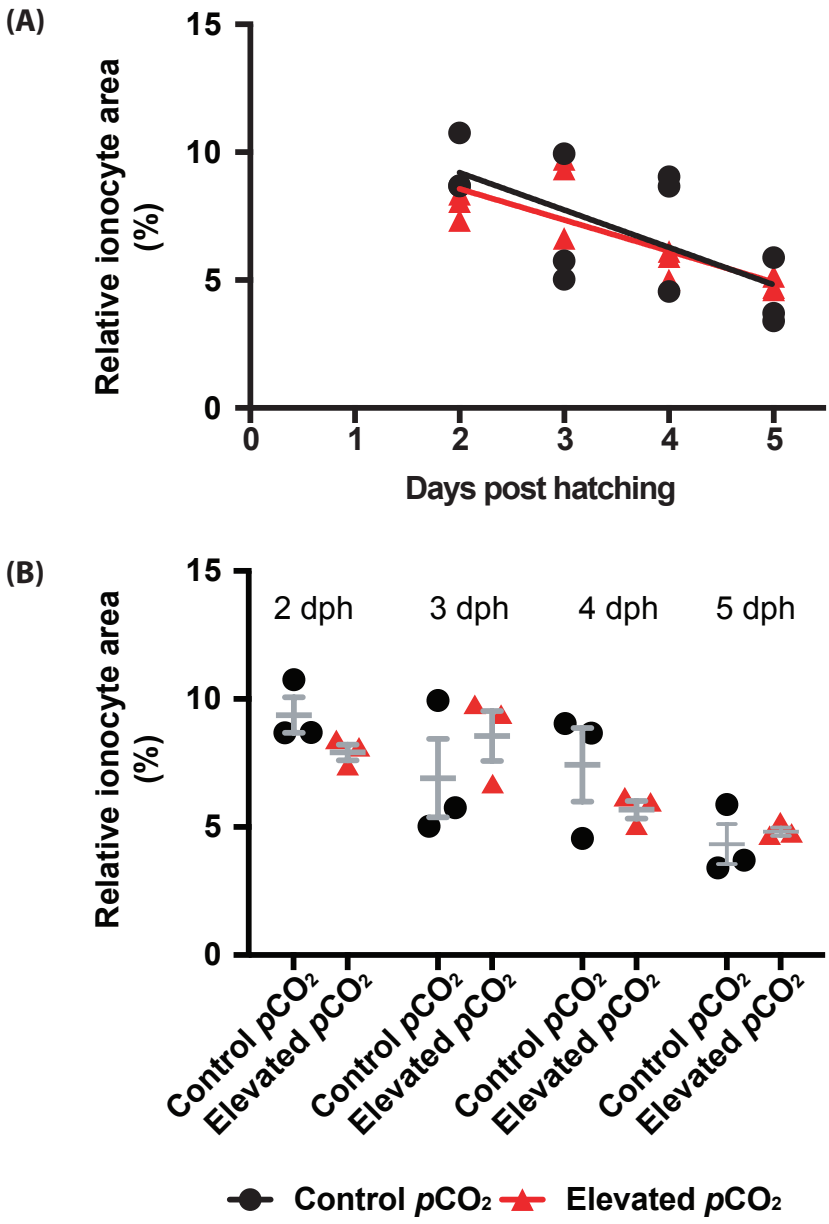

Figure 5.3: Relative ionocyte area of white seabass larvae from 2 to 5 days post hatching in control and elevated pCO_2 conditions. The relative ionocyte area of control (black) and elevated (red) pCO_2 larvae at 2 to 5 days post hatching displayed as a linear regression (A) and as a separated scatterplot (B). Comparison of the regression and the within days post hatching found no significant differences between larvae incubated in control and elevated pCO_2 conditions. Data are means ± S.E.M.

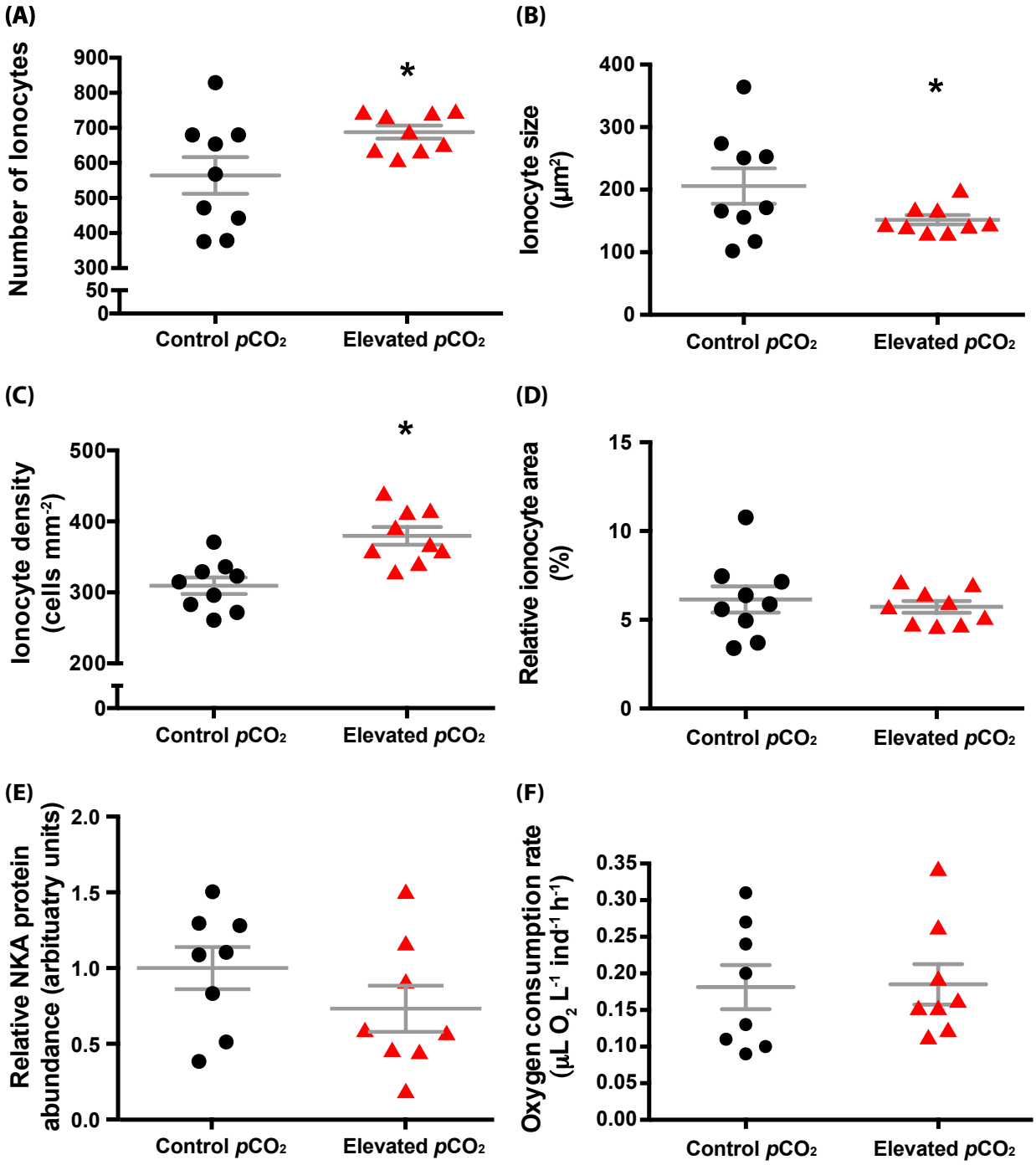

Figure 5.4: Ionocyte number, size, and density in white seabass larvae in control and elevated pCO_2 conditions. The number of ionocytes, ionocyte size, and ionocyte density of 5 dph larvae at control (black) and elevated (red) pCO_2 compared together (A, C, E) and within experimental trials (B, D, F). Asterisks indicate significance at an alpha level of 0.05. Data are means ± S.E.M.

Additional 5 dph larvae from each EX were immunostained to localize their ionocytes (Supplementary Figure 4.1). The number of ionocytes in 5 dph larvae (n = 18; 9 per treatment) reared at control pCO_2 (309.56 ± 11.62 cells mm^{-2}) was significantly lower than larvae reared at elevated pCO_2 (379.67 ± 12.51 cells mm^{-2}) (2-way ANOVA: $F_{1, 12} = 13.75$, $p = 0.003$; Figure 4.4A). However, both EX (2-way ANOVA: $F_{2, 12} = 4.956$, $p = 0.02$) and their interaction of pCO_2 and EX (2-way ANOVA: $F_{2, 12} = 5.510$, $p = 0.020$) were also significant (Supplementary Figure 4.2A). In contrast, the average ionocyte size in 5 dph larvae reared at control pCO_2 (205.94 ± 28.32 μm^2) was significantly larger than larvae reared at elevated pCO_2 (152.09 ± 7.49 μm^2) (2-way ANOVA: $F_{1, 12} = 9.984$, $p = 0.008$; Figure 4.4B). Similarly, both EX (2-way ANOVA: $F_{2, 12} = 12.128$, $p = 0.001$) and the interaction of pCO_2 and EX (2-way ANOVA: $F_{2, 12} = 5.510$, $p = 0.020$) were also significant (Supplementary Figure 4.2B). Lastly, larvae reared at control pCO_2 had lower ionocyte density than larvae reared at elevated pCO_2 (2-way ANOVA: $F_{1, 12} = 33.244$; $p < 0.001$; Figure 4.4C), though interaction was also significant (2-way ANOVA: $F_{2, 12} = 6.861$, $p = 0.0103$; Supplementary Figure 4.2C). This trend of increased ionocyte density in elevated pCO_2 larvae was evident across all experiments and significant in EX 1 and EX 2 (Tukey HSD: $p < 0.05$; Supplementary Table 2).

However, when the ionocyte number, size, and density are analyzed together as relative ionocyte area, larvae reared at control pCO_2 (6.14 ± 0.74%) were not significantly different from larvae reared at elevated pCO_2 (5.73 ± 0.33%) (2-way ANOVA: $F_{1, 12} = 0.561$, $p = 0.468$; Figure 4.4D), though there was an experiment effect in EX 1 (2-way ANOVA: $F_{2, 12} = 7.892$, $p = 0.006$; Supplementary Figure 4.2D; Supplementary Table 4.2).

Western blots revealed a single band at ~100 kDA in the whole-body crude homogenates of larvae (Supplementary Figure 4.3). Total NKA protein abundance was not significantly

affected by pCO_2 (2-way ANOVA: $F_{1, 10} = 1.844$, $p = 0.204$; Figure 3E). Average total NKA protein abundance was 1.00 ± 0.14 for control larvae and 0.73 ± 0.15 for treatment larvae (Figure 4.4E; Supplementary Figure 4.2E, Supplementary Table 4.3).

During the microrespiration trials, larvae from both control and elevated pCO_2 treatments were observed to be mostly inactive, engaging in swimming bursts only to re-orient themselves. Elevated pCO_2 did not affect larva OCR (2-way ANOVA: $F_{1, 10} = 0.046$, $p = 0.834$; Figure 4.4F). Average OCR was 0.18 ± 0.03 μL O_2 ind^{-1} h^{-1} for control larvae ($n = 16$) and 0.19 ± 0.03 μL O_2 ind^{-1} h^{-1} for elevated pCO_2 larvae ($n = 16$; Supplementary Table 4.4). Across experiments, OCR ranged from 0.09 to 0.34 μL O_2 ind^{-1} h^{-1} (Table S4). Mean baseline OCR, which is the average OCR of control and elevated pCO_2 larvae combined, differed among experiments (Tukey HSD: $p < 0.001$; Supplementary Figure 4.2F), with a value of 0.17 ± 0.02, 0.11 ± 0.02, and 0.30 ± 0.02 μL O_2 ind^{-1} h^{-1}, in EX 1, EX 2 and EX 3, respectively (Supplementary Table 4.4).

Larva total length was measured in 5 dph larvae from EX 1 and EX 2. Although larvae in EX 2 were significantly smaller (3.53 ± 0.01 mm; $n = 59$) than larvae in EX 1 (3.63 ± 0.02 mm; $n = 60$; $p < 0.001$, Tukey HSD: $p < 0.05$), total length was not affected by pCO_2 (2-way ANOVA: $F_{1, 115} = 1.040$, $p = 0.310$).

Discussion

The current study utilized larval white seabass (*Atractoscion nobilis*) spawned from adult fish kept at Hubbs Sea World Research Institute (HSWRI). Through the Ocean Resources Enhancement and Hatchery Program, HSWRI has been breeding, raising, and releasing white seabass throughout the Southern California Bight since 1986 in an effort to replenish natural populations (Vojkovich and Crooke, 2001; Hervas et al., 2010). The adult white seabass within

HSWRI's RAS broodstock tank have been chronically exposed to elevated pCO_2 (~1,200 µatm) and low pH levels (~7.6), both of which exceed OA predictions for the year 2100 (Caldeira and Wickett, 2005).

Two previous OA studies have also utilized larvae spawned from white seabass adults kept at HWSRI. Larval mass did not differ between control and OA treatments (Checkley et al., 2009a). However, larval white seabass exposed to CO_2-induced low-pH conditions had significantly larger otolith area and otolith mass (Checkley et al., 2009a; Shen et al., 2016), but no difference in vestibulo-ocular reflex – an otolith-stimulated eye rotation behavior used to maintain visual acuity (Shen et al., 2016). These two previous studies suggest larval white seabass are affected by, but can tolerate, elevated pCO_2 conditions.

Our data indicates white seabass larvae are able to use extant NKA-powered ion-transporting ionocytes without compromising total energy consumption to tolerate pCO_2 levels projected by 2250 (IPCC, 2013). There was no effect of pCO_2 on any of the physiological variables we measured: relative ionocyte area for 2 to 5 dph larvae, relative NKA protein abundance for 5 dph larvae, OCR, and length. These results suggest that exposure to elevated pCO_2 levels previously documented to increase otolith calcification did not induce a respiratory acidosis within larval white seabass, which therefore did not undergo major physiological changes to restore acid-base balance.

Our results may not be surprising given the unique physiological challenges to acid-base balance that the larvae encounter daily. At 5 dph, larvae do not possess fully functional gills and rely on cutaneous ionocytes to perform gas and ion exchange (Wales, 1997; reviewed in Varsamos et al., 2005; Pelster, 2008). Although the total surface area to volume ratio for gas exchange is 2.5 to 6 times larger for larvae than adults (Pelster, 2008), the skin epithelium lacks

the countercurrent exchange system present in the gills (Evans et al., 2005) and is therefore less effective at gas exchange. Additionally, the limited mobility of larvae and absence of ventilatory mechanisms creates a thick diffusional boundary layer that constrains the outward diffusion of CO_2 (Rombough, 1992). Due to the rapid growth of metabolizing tissue during early development, larva resting OCRs are 50-80% higher than that of juveniles and adults (Post and Lee, 1996), which implies proportionally higher CO_2 production (Melzner et al., 2009b). Furthermore, OCR and thus CO_2 production, can increase four-fold during activity (Lasker and Threadgold, 1968). These challenges require larvae to possess robust, active mechanisms for H^+ secretion and HCO_3^- uptake in order to sustain acid-base homeostasis and meet metabolic requirements (i.e., OCR and somatic growth) when faced with an exceedingly high internal pCO_2 environment.

The apparent physiological resilience of larvae could also be influenced by the preconditioning of the spawning broodstock to elevated pCO_2 and low pH conditions, specifically the quality of their eggs (yolk sac abundance) due to an abundance of nutrients, and genetic or epigenetic selection. The measured pH of the broodstock tanks on the morning of egg collection for EX 1-3 ranged from 7.39 to 7.53, with estimates of pCO_2 up to 2320 μatm. Multi-generational and transplant experiments have demonstrated that adverse effects of elevated pCO_2 on the growth, metabolism, and survival of larvae and juveniles are absent when offspring are spawned from parents residing in elevated pCO_2 conditions (Miller et al., 2012; Allan et al., 2014; Murray et al., 2014; Cattano et al., 2016; Schunter et al., 2016, 2018). Coupled with HSWRI's restocking program (which includes the release of white seabass into the wild), natural population could potentially become resilient to future pCO_2 levels. Future studies examining the effects of broodstock conditions on their larval offspring's yolk sac abundance and genetic

makeup may help clarify whether white seabass is innately tolerant, or preconditioned by aquaculture conditions, to future OA conditions.

An alternative hypothesis is that larvae did experience a physiological response to elevated pCO_2, but high variability within and among experiments, coupled with a low sample size, limited our power to detect a pCO_2 effect. Furthermore, the fraction of NKA protein or activity that is specifically used for acid-base regulation, or the potential existence of specific acid-base regulatory cells, is currently unknown. Therefore, it is possible that acid-base regulation activity may have increased for larvae reared at elevated pCO_2 despite the maintenance of relative ionocyte area. The larger saggital (7-20%) and utricular (37-39%) otoliths in white seabass larvae reared at 2500 μatm (Checkley et al., 2009a; Shen et al., 2016) provide support for the occurrence of acid-base regulation activity as increased ion transport results in higher [HCO_3^-] in the bloodstream, which may diffuse into the otocyst endolymph to facilitate faster otolith growth (Maneja et al., 2013; Heuer and Grosell, 2014).

This study contributes to the growing literature database of metabolic responses of larval fish to OA conditions. Here, we highlight some OA studies on marine larvae with similar response variables: relative ionocyte area, OCR, and length (NKA abundance is excluded as no prior study on larval fish exists). Note that caution must be taken as this may be due to differences in species, developmental stage, and/or treatment condition). Similar to our results, the relative ionocyte area of hatchling cod (*Gadus morhua*) exposed to ~1000 μatm pCO_2 were not significantly different from their control (Dahlke et al., 2017). Previous reports larval OCR in response to elevated pCO_2 ranges from a significant increase in hatchling cod exposed to ~1000 μatm pCO_2 (Dahlke et al., 2017), no effect in 7, 14, and 21 dph Antarctic dragonfish (*Gymodraco acuticeps*) exposed to ~1000 μatm pCO_2 (Flynn et al., 2015), and to a significant

decrease in 0 and 30 dph Senegalese sole (*Solea senegalensis*) exposed to (Pimentel et al., 2014a) as well as in 2 dph dolphinfish (*Coryphaena hippurus*) exposed to ~1600 μatm pCO_2 (Pimentel et al., 2014b). Similarly, the effect of elevated pCO_2 levels on the length of fish larvae is also very variable – with significant increase in 11 dph larval orange clownfish (*Amphiprion percula*) exposed to ~1000 μatm pCO_2 (Munday et al. 2009) and 19 – 28 dph barramundi (*Lates calcarifer*) exposed to ~1600 μatm pCO_2 (Rossi et al., 2015), no effect in 0 dph cinnamon anemonefish (*Amphiprion melanopus*) exposed to ~1000 μatm pCO_2 (Miller et al., 2012) and in 2 – 22 dph cobia (*Rachycentron canadum*) exposed to ~800 and ~2100 μatm pCO_2 (Bignami et al., 2013b), and significant decrease in 7 dph silverside (*Menidia beryllina*) exposed to ~1000 μatm pCO_2 (Baumann et al., 2012) and in 6 dph yellowtail kingfish (*Seriola lalandi*) when exposed to ~900 and ~1700 μatm pCO_2 (Munday et al., 2016). Evidently, there remains no straightforward answer as to how larval fish will respond to future OA conditions.

The varied responses to future elevated pCO_2 conditions in current larval fish studies showcases the need for basic research on larval fish physiology, including the mechanisms of acid-base regulation, chemical composition of the blood and intracellular fluids, and energetic costs of homeostatic processes. A better understanding of larval fish physiology will lead to more informed inferences of results and more accurate predictions about the impacts of OA on fish over their entire life cycle.

Author contributions

S.G.S., M.T., and D.M.C. designed research; S.G.S. and G.T.K. performed research; S.G.S., G.T.K., and M.T. performed statistical analyses; S.G.S., G.T.K., and M.T. wrote the manuscript. All authors gave final approval for publication.

Acknowledgements

We are grateful to Mark Drawbridge, Erica Bromby-Fanning, Eric McIntire, Sabrina Sobel, and Christy Varga, and other staffs at HSWRI for collecting and providing fertilized white seabass eggs and water parameter data. We thank Dr. Lauren Linsmayer and Dr. Greg Rouse (SIO) for their assistance with experiments. Funding was provided by the National Science Foundation Graduate Research Fellowship Program to SGS and GTK, and the San Diego Fellowship to GTK.

Chapter V, in part, is currently being prepared for submission for publication of the material. Shen, S.G., Kwan, G.T., Tresguerres, M., and Checkley, D.M. (*in prep*). Physiological resilience of white seabass (*Atractoscion nobilis*) larvae to CO_2-induced ocean acidification. The dissertation author was the co-primary investigator and author of this material.

Appendix

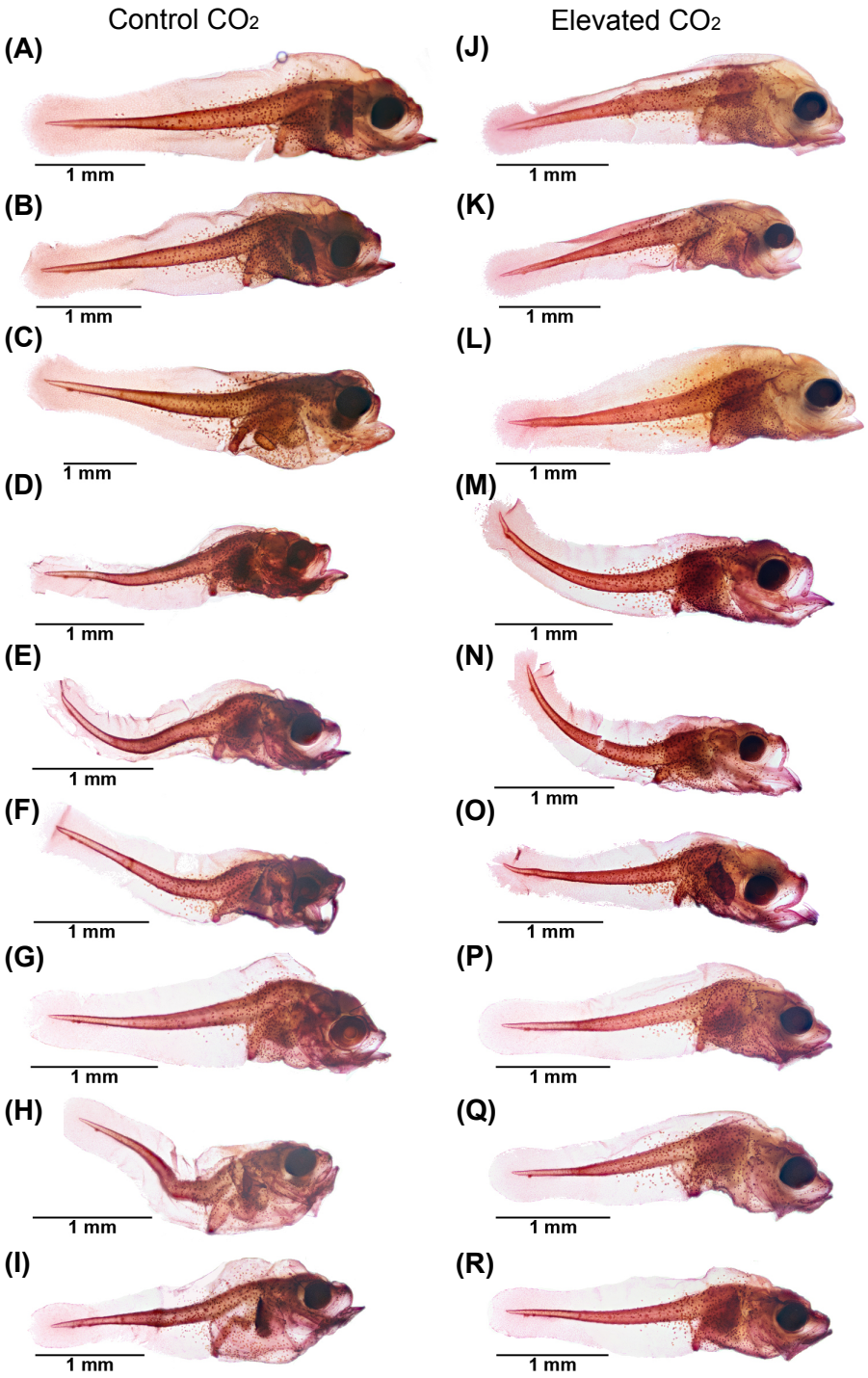

Supplementary Figure 5.1: Images of 5 dph white seabass larvae with immunostained cells labeled with a Na^+-K^+-ATPase antibody. Images show the distribution of cutaneous ionocytes for larvae at control (n = 9) (A-I) and elevated (n = 9) (J-R) pCO_2 for all experiments. Relative ionocyte area dataset is available in Supplementary Information (Table S1).

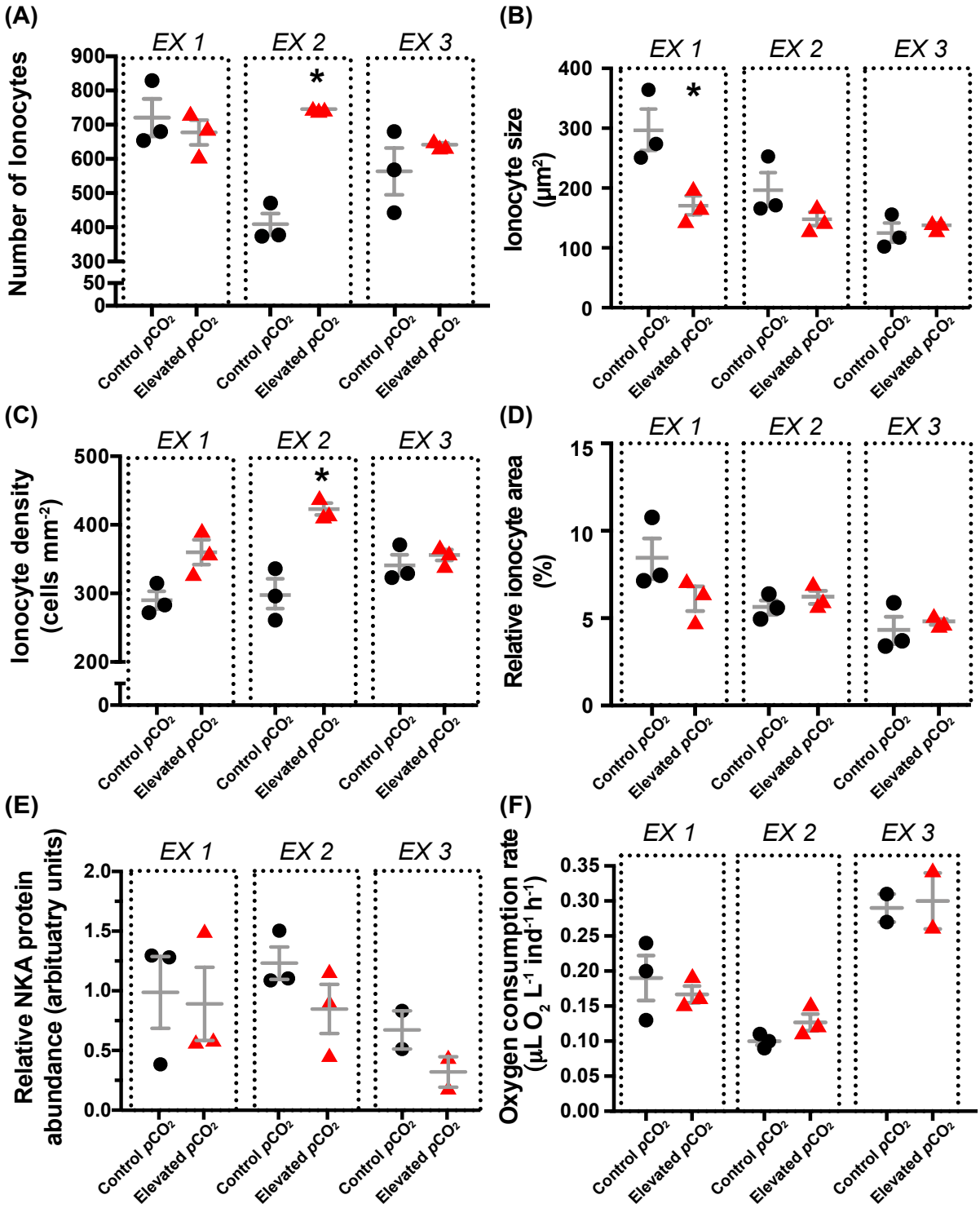

Supplementary Figure 5.2: Ionocyte number, size, and density in white seabass larvae in control and elevated pCO_2 conditions. The number of ionocytes, ionocyte size, and ionocyte density of 5 dph larvae at control (black) and elevated (red) pCO_2 compared together (A, C, E) and within experimental trials (B, D, F). Asterisks indicate significance at an alpha level of 0.05. Data are means ± S.E.M.

Supplementary Table 5.1: Relative ionocyte area for 2 to 5 dph larvae as determined by whole-body immunohistochemistry. Measurements were made for three larvae from one control and elevated pCO_2 vessel each in EX 3 from 2 dph to 5 dph. Data are presented in Figure 4.2. Data for 5 dph larvae in EX 3 are also shown in Table S2. Immunohistochemistry images are shown in Figure S1.

Date	*EX*	*Vessel*	*Age (dph)*	*pCO_2*	*pH*	*Relative ionocyte area (%)*
08/02/16	*3*	*2*	*2*	*506*	*7.96*	*8.70*
08/02/16	*3*	*2*	*2*	*506*	*7.96*	*10.75*
08/02/16	*3*	*2*	*2*	*506*	*7.96*	*8.68*
08/02/16	*3*	*1*	*2*	*2005*	*7.41*	*7.33*
08/02/16	*3*	*1*	*2*	*2005*	*7.41*	*8.35*
08/02/16	*3*	*1*	*2*	*2005*	*7.41*	*8.07*
08/02/16	*3*	*2*	*3*	*506*	*7.96*	*5.03*
08/02/16	*3*	*2*	*3*	*506*	*7.96*	*9.95*
08/02/16	*3*	*2*	*3*	*506*	*7.96*	*5.76*
08/02/16	*3*	*1*	*3*	*2005*	*7.41*	*9.34*
08/02/16	*3*	*1*	*3*	*2005*	*7.41*	*9.72*
08/02/16	*3*	*1*	*3*	*2005*	*7.41*	*6.63*
08/02/16	*3*	*2*	*4*	*506*	*7.96*	*9.05*
08/02/16	*3*	*2*	*4*	*506*	*7.96*	*4.56*
08/02/16	*3*	*2*	*4*	*506*	*7.96*	*8.67*
08/02/16	*3*	*1*	*4*	*2005*	*7.41*	*5.00*
08/02/16	*3*	*1*	*4*	*2005*	*7.41*	*5.92*
08/02/16	*3*	*1*	*4*	*2005*	*7.41*	*6.12*
08/02/16	*3*	*2*	*5*	*506*	*7.96*	*3.41*
08/02/16	*3*	*2*	*5*	*506*	*7.96*	*3.71*
08/02/16	*3*	*2*	*5*	*506*	*7.96*	*5.88*
08/02/16	*3*	*1*	*5*	*2005*	*7.41*	*4.71*
08/02/16	*3*	*1*	*5*	*2005*	*7.41*	*4.62*
08/02/16	*3*	*1*	*5*	*2005*	*7.41*	*5.14*

Supplementary Table 5.2: Ionocyte density, ionocyte size, and relative ionocyte area for 5 dph larvae as determined by whole-body immunohistochemistry.

EX	*Vessel*	*Image*	pCO_2	*pH*	*Ionocyte count*	*Ionocyte size (μm^2)*	*Ionocyte density (cells mm^{-2})*	*Relative ionocyte area (%)*
1	*2*	*A*	*552*	*7.93*	*680*	*274.00*	*272*	*7.45*
1	*2*	*B*	*552*	*7.93*	*654*	*251.02*	*283*	*7.14*
1	*2*	*C*	*552*	*7.93*	*829*	*363.72*	*315*	*10.77*
1	*2*	*D*	*2094*	*7.39*	*733*	*167.32*	*392*	*6.45*
1	*2*	*E*	*2094*	*7.39*	*609*	*199.48*	*359*	*7.15*
1	*2*	*F*	*2094*	*7.39*	*690*	*145.27*	*329*	*4.77*
2	*1*	*G*	*454*	*7.99*	*472*	*165.83*	*336*	*5.59*
2	*1*	*H*	*454*	*7.99*	*376*	*171.31*	*296*	*4.95*
2	*1*	*I*	*454*	*7.99*	*379*	*252.67*	*261*	*6.38*
2	*1*	*J*	*1799*	*7.45*	*748*	*130.37*	*440*	*5.74*
2	*1*	*K*	*1799*	*7.45*	*746*	*144.28*	*416*	*5.98*
2	*1*	*L*	*1799*	*7.45*	*743*	*168.98*	*413*	*6.98*
3	*2*	*M*	*506*	*7.96*	*568*	*102.06*	*329*	*3.41*
3	*2*	*N*	*506*	*7.96*	*443*	*117.14*	*323*	*3.71*
3	*2*	*O*	*506*	*7.96*	*680*	*155.72*	*371*	*5.88*
3	*1*	*P*	*2005*	*7.41*	*635*	*140.93*	*341*	*4.71*
3	*1*	*Q*	*2005*	*7.41*	*637*	*130.51*	*359*	*4.62*
3	*1*	*R*	*2005*	*7.41*	*653*	*141.69*	*368*	*5.14*

Supplementary Table 5.3: Relative NKA protein abundance from whole-body crude homogenates of larvae from western blots. A random fish larva sample was used as a reference standard, loaded in all gels and used to normalize results from different gels. Measurements were made for larvae from each of the control and elevated pCO_2 vessels for all experiments.

Date	*EX*	*Vessel*	*pCO_2 (µatm)*	*pH*	*Relative NKA protein abundance*
06/20/16	*1*	*1*	*601*	*7.89*	*8.0*
06/20/16	*1*	*2*	*552*	*7.93*	*2.4*
06/20/16	*1*	*3*	*543*	*7.93*	*8.1*
06/20/16	*1*	*1*	*2097*	*7.39*	*3.7*
06/20/16	*1*	*2*	*2094*	*7.39*	*3.6*
06/20/16	*1*	*3*	*2145*	*7.38*	*9.4*
07/04/16	*2*	*1*	*454*	*7.99*	*6.8*
07/04/16	*2*	*2*	*569*	*7.91*	*6.9*
07/04/16	*2*	*3*	*503*	*7.96*	*9.4*
07/04/16	*2*	*1*	*1799*	*7.45*	*7.3*
07/04/16	*2*	*2*	*1792*	*7.46*	*2.9*
07/04/16	*2*	*3*	*1777*	*7.46*	*5.7*
08/02/16	*3*	*2*	*506*	*7.96*	*5.2*
08/02/16	*3*	*3*	*754*	*7.80*	*3.2*
08/02/16	*3*	*1*	*2005*	*7.41*	*2.8*
08/02/16	*3*	*3*	*2061*	*7.40*	*1.2*

Supplementary Table 5.4: Oxygen consumption rates (OCR) of larvae. Individual-based OCRs were calculated for larvae at control and elevated pCO_2 for all experiments.

Date	*EX*	*Vessel*	*pCO_2 (µatm)*	*pH*	*OCR (µL O_2 ind^{-1} h^{-1})*
06/20/16	*1*	*1*	*601*	*7.89*	*0.24*
06/20/16	*1*	*2*	*552*	*7.93*	*0.13*
06/20/16	*1*	*3*	*543*	*7.93*	*0.20*
06/20/16	*1*	*1*	*2097*	*7.39*	*0.16*
06/20/16	*1*	*2*	*2094*	*7.39*	*0.19*
06/20/16	*1*	*3*	*2145*	*7.38*	*0.15*
07/04/16	*2*	*1*	*454*	*7.99*	*0.11*
07/04/16	*2*	*2*	*569*	*7.91*	*0.09*
07/04/16	*2*	*3*	*503*	*7.96*	*0.10*
07/04/16	*2*	*1*	*1799*	*7.45*	*0.15*
07/04/16	*2*	*2*	*1792*	*7.46*	*0.12*
07/04/16	*2*	*3*	*1777*	*7.46*	*0.11*
08/02/16	*3*	*2*	*506*	*7.96*	*0.31*
08/02/16	*3*	*3*	*754*	*7.80*	*0.27*
08/02/16	*3*	*1*	*2005*	*7.41*	*0.34*
08/02/16	*3*	*3*	*2061*	*7.40*	*0.26*

References

Allan, B. J. M., Miller, G. M., McCormick, M. I., Domenici, P., and Munday, P. L. (2014). Parental effects improve escape performance of juvenile reef fish in a high-CO2 world. Proceedings of the Royal Society - B-Biological Sciences, 281: 20132179. doi:10.1098/rspb.2013.2179.

Baumann, H., Talmage, S. C., and Gobler, C. J. (2012). Reduced early life growth and survival in a fish in direct response to increased carbon dioxide. Nature Climate Change, 2: 38–41. Nature Publishing Group. doi:10.1038/nclimate1291.

Bignami, S., Enochs, I. C., Manzello, D. P., Sponaugle, S., and Cowen, R. K. (2013a). Ocean acidification alters the otoliths of a pantropical fish species with implications for sensory function. Proceedings of the National Academy of Sciences, 110: 7366–7370. doi:10.1073/pnas.1301365110.

Bignami, S., Sponaugle, S., and Cowen, R. K. (2013b). Response to ocean acidification in larvae of a large tropical marine fish, *Rachycentron canadum*. Global Change Biology, 19: 996–1006.

Caldeira, K., and Wickett, M. E. (2005). Ocean model predictions of chemistry changes from carbon dioxide emissions to the atmosphere and ocean. Journal of Geophsical Research-Part C-Oceans, 110: 12 pp.-12 pp.

Cattano, C., Giomi, F., and Milazzo, M. (2016). Effects of ocean acidification on embryonic respiration and development of a temperate wrasse living along a natural CO2 gradient. Conservation Physiology, 4: 1–10.

Checkley, D. M., Dickson, A. G., Takahashi, M., Radich, J. A., Eisenkolb, N., and Asch, R. (2009). Elevated CO2 enhances otolith growth in young fish. Science (New York, N.Y.), 324: 1683.

Crespel, A., Zambonino-Infante, J.-L., Mazurais, D., Koumoundouros, G., Fragkoulis, S., Quazuguel, P., Huelvan, C., Madec, L., Servili, A., and Claireaux, G. (2017). The development of contemporary European sea bass larvae (*Dicentrarchus labrax*) is not affected by projected ocean acidification scenarios. Marine Biology, 164: 155. Springer Berlin Heidelberg. doi:10.1007/s00227-017-3178-x.

Dahlke, F. T., Leo, E., Mark, F. C., Pörtner, H. O., Bickmeyer, U., Frickenhaus, S., and Storch, D. (2017). Effects of ocean acidification increase embryonic sensitivity to thermal extremes in Atlantic cod, *Gadus morhua*. Global Change Biology, 23: 1499–1510.

Esbaugh, A. J., Heuer, R., and Grosell, M. (2012). Impacts of ocean acidification on respiratory gas exchange and acid-base balance in a marine teleost, *Opsanus beta*. Journal of Comparative Physiology B: Biochemical, Systemic, and Environmental Physiology, 182: 921–934.

Evans, D. H., Piermarini, P. M., and Choe, K. P. (2005). The Multifunctional Fish Gill: Dominant Site of Gas Exchange, Osmoregulation, Acid-Base Regulation, and Excretion of Nitrogenous Waste. Physiological Reviews, 85: 97–177. doi:10.1152/physrev.00050.2003.

Flynn, E. E., Bjelde, B. E., Miller, N. A., and Todgham, A. E. (2015). Ocean acidification exerts negative effects during warming conditions in a developing Antarctic fish. Conservation Physiology, 3: 1–16.

Glover, C. N., Bucking, C., and Wood, C. M. (2013). The skin of fish as a transport epithelium: A review. Journal of Comparative Physiology B: Biochemical, Systemic, and Environmental Physiology, 183: 877–891.

Hervas, S., Lorenzen, K., Shane, M. A., and Drawbridge, M. A. (2010). Quantitative assessment of a white seabass (*Atractoscion nobilis*) stock enhancement program in California: Post-release dispersal, growth and survival. Fisheries Research, 105: 237–243.

Heuer, R. M., and Grosell, M. (2014). Physiological impacts of elevated carbon dioxide and ocean acidification on fish. AJP: Regulatory, Integrative and Comparative Physiology, 307: R1061–R1084. doi:10.1152/ajpregu.00064.2014.

Hiroi, J., and McCormick, S. D. (2012). New insights into gill ionocyte and ion transporter function in euryhaline and diadromous fish. Respiratory Physiology and Neurobiology, 184: 257–268. Elsevier B.V. doi:10.1016/j.resp.2012.07.019.

Houde, E. D. (2009). Recruitment variability. *In* Fish Reproductive Biology: Implications for Assessment and Management, pp. 91–171. Wiley-Blackwell, West Sussex.

Hurst, T. P., Fernandez, E. R., and Mathis, J. T. (2013). Effects of ocean acidification on hatch size and larval growth of walleye pollock (*Theragra chalcogramma*). ICES Journal of Marine Science, 70: 812–822. doi:10.1093/icesjms/fst053.

Hvas, M., Damsgaard, C., Gam, L. T. H., Huong, D. T. T., Jensen, F. B., and Bayley, M. (2016). The effect of environmental hypercapnia and size on nitrite toxicity in the striped catfish (*Pangasianodon hypophthalmus*). Aquatic Toxicology, 176: 151–160. Elsevier B.V. doi:10.1016/j.aquatox.2016.04.020.

Hwang, P.-P., Lee, T.-H., and Lin, L.-Y. (2011). Ion regulation in fish gills: recent progress in the cellular and molecular mechanisms. AJP: Regulatory, Integrative and Comparative Physiology, 301: R28–R47. doi:10.1152/ajpregu.00047.2011.

IPCC. (2013). Climate change 2013: the physical science basis. *In* Contribution of working group 1 to the fifth assessment report of the Intergovernmental Panel on Climate Change, pp. 465–544. Cambridge University Press, Cambridge.

Ishimatsu, A., Kikkawa, T., Hayashi, M., Lee, K.-S., and Kita, J. (2004). Effects of CO2 on Marine Fish: Larvae and Adults. Journal of Oceanography, 60: 731–741.

Ishimatsu, A., Hayashi, M., and Kikkawa, T. (2008). Fishes in high-CO2, acidified oceans. Marine Ecology Progress Series, 373: 295–302. doi:10.3354/meps07823.

Kwan, G. T., Finnerty, S. H., Wegner, N. C., and Tresguerres, M. (2019a). Quantification of Cutaneous Ionocytes in Small Aquatic Organisms. Bio-protocol, 9: e3227.

Kwan, G. T., Wexler, J. B., Wegner, N. C., and Tresguerres, M. (2019b). Ontogenetic changes in cutaneous and branchial ionocytes and morphology in yellowfin tuna (*Thunnus albacares*) larvae. Journal of Comparative Physiology B: Biochemical, Systemic, and Environmental Physiology, 189: 81–95. Springer Berlin Heidelberg. doi:10.1007/s00360-018-1187-9.

Lasker, R., and Threadgold, L. T. (1968). 'Chloride cells' in the skin of the larval sardine. Experimental Cell Research, 52: 582–590.

Lebovitz, R. M., Takeyasu, K., and Fambrough, D. M. (1989). Molecular characterization and expression of the (Na+ + K+)-ATPase alpha-subunit in *Drosophila melanogaster*. The EMBO Journal, 8: 193–202.

Maneja, R. H., Frommel, a. Y., Geffen, a. J., Folkvord, a., Piatkowski, U., Chang, M. Y., and Clemmesen, C. (2013). Effects of ocean acidification on the calcification of otoliths of larval Atlantic cod *Gadus morhua*. Marine Ecology Progress Series, 477: 251–258.

Meehl, G. A., Stocker, T. F., Collins, W. D., Friedlingstein, P., Gaye, A. T., Gregory, J. M., Kitoh, A., Knutti, R., Murphy, J. M., Noda, A., Raper, S. C. B., Watterson, I. G., Weaver, A. J., and Zhao, Z.-C. (2007). 2007: Global climate projections. *In* Climate Change 2007: Contribution of Working Group I to the Fourth Assessment Report of the Intergovernmental Panel on Climate Change, pp. 747–846. Cambridge University Press, Cambridge, UK.

Melzner, F., Gutowska, M. a., Langenbuch, M., Dupont, S., Lucassen, M., Thorndyke, M. C., Bleich, M., and Pörtner, H.-O. (2009). Physiological basis for high CO2 tolerance in marine ectothermic animals: pre-adaptation through lifestyle and ontogeny? Biogeosciences Discussions, 6: 4693–4738.

Miller, G. M., Watson, S. A., Donelson, J. M., McCormick, M. I., and Munday, P. L. (2012). Parental environment mediates impacts of increased carbon dioxide on a coral reef fish. Nature Climate Change, 2: 858–861. Nature Publishing Group. doi:10.1038/nclimate1599.

Munday, P. L., Hernaman, V., Dixson, D. L., and Thorrold, S. R. (2011). Effect of ocean acidification on otolith development in larvae of a tropical marine fish. Biogeosciences, 8: 1631–1641. doi:10.5194/bg-8-1631-2011.

Munday, P. L., Watson, S.-A., Parsons, D. M., King, A., Barr, N. G., Mcleod, I. M., Allan, B. J. M., and Pether, S. M. J. (2016). Effects of elevated CO 2 on early life history development of

the yellowtail kingfish, *Seriola lalandi* , a large pelagic fish. ICES Journal of Marine Science: Journal du Conseil, 73: 641–649. doi:10.1093/icesjms/fsv210.

Murray, C., Malvezzi, A., Gobler, C., and Baumann, H. (2014). Offspring sensitivity to ocean acidification changes seasonally in a coastal marine fish. Marine Ecology Progress Series, 504: 1–11. doi:10.3354/meps10791.

Peck, M. A., and Moyano, M. (2016). Measuring respiration rates in marine fish larvae: Challenges and advances. Journal of Fish Biology, 88: 173–205.

Pelster, B. (2008). Gas exchange. In Fish larval physiology, pp. 91–117. Ed. by R. Finn and B. Kapoor. Science Publishers.

Perry, S. F., and Gilmour, K. M. (2006). Acid-base balance and CO2 excretion in fish: Unanswered questions and emerging models. Respiratory Physiology and Neurobiology, 154: 199–215.

Pimentel, M., Pegado, M., Repolho, T., and Rosa, R. (2014a). Impact of ocean acidification in the metabolism and swimming behavior of the dolphinfish (*Coryphaena hippurus*) early larvae. Marine Biology, 161: 725–729.

Pimentel, M. S., Faleiro, F., Dionisio, G., Repolho, T., Pousao-Ferreira, P., Machado, J., and Rosa, R. (2014b). Defective skeletogenesis and oversized otoliths in fish early stages in a changing ocean. J Exp Biol, 217: 2062–2070. doi:10.1242/jeb.092635.

Post, J., and Lee, J. (1996). Metabolic ontogeny of teleost fishes. Canadian Journal of Fisheries and Aquatic Sciences, 53: 910–923. doi:10.1139/f95-278.

R Development Core Team. (2013). R: A language and environment for statistical computing. R foundation for statistical computing. Vienna, Austria.

Roa, J. N., Munévar, C. L., and Tresguerres, M. (2014). Feeding induces translocation of vacuolar proton ATPase and pendrin to the membrane of leopard shark (*Triakis semifasciata*) mitochondrion-rich gill cells. Comparative Biochemistry and Physiology -Part A : Molecular and Integrative Physiology, 174: 29–37. Elsevier Inc. doi:10.1016/j.cbpa.2014.04.003.

Roa, J. N., and Tresguerres, M. (2017). Bicarbonate-sensing soluble adenylyl cyclase is present in the cell cytoplasm and nucleus of multiple shark tissues. Physiological Reports, 5: e13090. doi:10.14814/phy2.13090.

Robbins, L., Hansen, M., Kleypas, J., and Meylan, S. (2010). CO2Calc - A user-friendly seawater carbon calculator for Windows, Max OS X, and iOS (iPhone). U.S. Geological Survey Open-File Report.

Rombough, P. J. (1992). Oxygen Tensions in Respiring Rainbow (*Oncorhynchus Mykiss*) Larvae. Zoology, I: 23–27.

Rombough, P. (2007). The functional ontogeny of the teleost gill: which comes first, gas or ion exchange? Comparative Biochemistry and Physiology - A Molecular and Integrative Physiology, 148: 732–742.

Rossi, T., Nagelkerken, I., Simpson, S. D., Pistevos, J. C. A., Watson, S., Merillet, L., Fraser, P., Munday, P. L., and Connell, S. D. (2015). Ocean acidification boosts larval fish development but reduces the window of opportunity for successful settlement. Proceedings of the Royal Society B: Biological Sciences, 282: 20151954. doi:10.1098/rspb.2015.1954.

Schunter, C., Welch, M. J., Ryu, T., Zhang, H., Berumen, M. L., Nilsson, G. E., Munday, P. L., and Ravasi, T. (2016). Molecular signatures of transgenerational response to ocean acidification in a species of reef fish. Nature Climate Change, 6: 1014–1018.

Schunter, C., Welch, M. J., Nilsson, G. E., Rummer, J. L., Munday, P. L., and Ravasi, T. (2018). An interplay between plasticity and parental phenotype determines impacts of ocean acidification on a reef fish. Nature Ecology and Evolution, 2: 334–342. Springer US. doi:10.1038/s41559-017-0428-8.

Shen, S. G., Chen, F., Schoppik, D. E., and Checkley, D. M. (2016). Otolith size and the vestibulo-ocular reflex of larvae of white seabass *Atractoscion nobilis* at high pCO2. Marine Ecology Progress Series, 553: 173–182.

Tang, C. H., Leu, M. Y., Yang, W. K., and Tsai, S. C. (2014). Exploration of the mechanisms of protein quality control and osmoregulation in gills of *Chromis viridis* in response to reduced salinity. Fish Physiology and Biochemistry, 40: 1533–1546.

Tseng, Y. C., Hu, M. Y., Stumpp, M., Lin, L. Y., Melzner, F., and Hwang, P. P. (2013). CO2-driven seawater acidification differentially affects development and molecular plasticity along life history of fish (*Oryzias latipes*). Comparative Biochemistry and Physiology - A Molecular and Integrative Physiology, 165: 1190–130. Elsevier Inc. doi:10.1016/j.cbpa.2013.02.005.

Varsamos, S., Nebel, C., and Charmantier, G. (2005). Ontogeny of osmoregulation in postembryonic fish: A review. Comparative Biochemistry and Physiology - A Molecular and Integrative Physiology, 141: 401–429.

Vojkovich, M., and Crooke, S. (2001). White Seabass. In California's living resources: a status report, pp. 206–208. Cal Fish Game, Sacramento.

Wales, B. (1997). Ultrastructural study of chloride cells in the trunk epithelium of larval herring, *Clupea harengus*. Tissue and Cell, 29: 439–447.

Yang, W., Kang, C., Chang, C., Hsu, A., Lee, T., and Hwang, P. (2013). Expression Profiles of Branchial FXYD Proteins in the Brackish Medaka *Oryzias dancena* : A Potential Saltwater Fish Model for Studies of Osmoregulation, 8.

Zimmer, A. M., Wright, P. A., and Wood, C. M. (2017). Ammonia and urea handling by early life stages of fishes. J Exp Biol, 220: 3843–3855.

CHAPTER VI

Immunological characterization of two types of ionocytes in the inner ear epithelium of Pacific Chub Mackerel (*Scomber japonicus*)

Abstract

The inner ear is essential for maintaining balance and hearing predator and prey in the environment. Each inner ear contains three $CaCO_3$ otolith polycrystals, which are calcified within an alkaline, K^+-rich endolymph secreted by the surrounding epithelium. However, the underlying cellular mechanisms are poorly understood, especially in marine fish. Here, we investigated the presence and cellular localization of several ion-transporting proteins within the saccular epithelium of the Pacific Chub Mackerel (*Scomber japonicus*). Western blotting revealed the presence of Na^+/K^+-ATPase (NKA), carbonic anhydrase (CA), Na^+-K^+-$2Cl^-$-co-transporter (NKCC), vacuolar-type H^+-ATPase (VHA), plasma membrane Ca^{2+} ATPase (PMCA), and soluble adenylyl cyclase (sAC). Immunohistochemistry analysis identified two distinct ionocytes types in the saccular epithelium: Type-I ionocytes were mitochondrion-rich and abundantly expressed NKA and NKCC in their basolateral membrane, indicating a role in secreting K^+ into the endolymph. On the other hand, Type-II ionocytes were enriched in cytoplasmic CA and VHA, suggesting they help transport HCO_3^- into the endolymph and remove H^+. Additionally, both types of ionocytes expressed cytoplasmic PMCA, which is likely involved in Ca^{2+} transport and homeostasis, as well as sAC, an evolutionary conserved acid-base sensing enzyme that regulates epithelial ion transport. Furthermore, CA, VHA, and sAC were also expressed within the capillaries that supply blood to the meshwork area, suggesting additional mechanisms that contribute to otolith calcification. This information improves our knowledge about the cellular mechanisms responsible for endolymph ion regulation and otolith formation, and can help understand responses to environmental stressors such as ocean acidification.

Introduction

The inner ear senses gravity and sound waves, which is essential for maintaining balance and hearing predator and prey in the environment (Dijkgraaf, 1960; Furukawa and Ishii, 1967; reviewed in Ladich and Schulz-Mirbach, 2016). Enclosed within each inner ear are the sagittal, lapilli, and asterisci otoliths, which are composed of a protein matrix and calcium carbonate ($CaCO_3$). The higher density of the otolith compared to the inner ear fluid ("endolymph") results in differential inertia that stimulates the adjacent sensory hair cells, which the brain interprets as soundwaves or movement.

Being the largest of the three otoliths, the sagitta and its surrounding saccular epithelium have been most extensively studied. The saccular epithelium has been previously characterized as the macula, meshwork, patches, and intermediate areas (Mayer-Gostan et al., 1997; Pisam et al., 1998). The macula contains the sensory hair cells that detect otolith vibration and movement. This area is flanked by the meshwork area, which contains large ion-transporting cells ("ionocytes"). The patches area is positioned directly across from the macula and contains patches of smaller ionocytes. The intermediate area is largely devoid of ionocytes, but does contain some ionocytes in the area bordering the meshwork area and smaller ionocytes bordering the patches area. Each otolith is calcified within an alkaline, K^+-rich endolymph secreted by its respective saccule, utricle and lagena inner ear epithelium.

In the Rainbow Trout (*Oncorhynchus mykiss*), the endolymph has a pH of ~8, ~30 mmol of HCO_3^-, ~124 mmol of K^+, ~90 mmol of Na^+, and ~1.1 mmol of Ca^{2+} (Payan et al., 1997). When compared to its blood plasma, the endolymph is roughly 0.8 pH unit higher, has twice as much HCO_3^-, ~40-fold higher K^+, half as much Na^+, and twice as much Ca^{2+} (Payan et al., 1997). This dramatic differences between the endolymph and blood plasma are thought to be attributed

to the surrounding ionocytes' activity. To date, two different types of ionocytes have been characterized: one is mitochondrion-rich (MR), has well-developed basolateral membrane infoldings (Mayer-Gostan et al., 1997), and abundantly expresses Na^+/K^+-ATPase (NKA) (Takagi, 1997), whereas the other one has abundant cytoplasmic carbonic anhydrase (CA) (Tohse et al., 2004, 2006). The NKA-rich ionocytes are proposed to be responsible for transporting K^+ (Payan et al., 1999), Ca^{2+} (Mugiya and Yoshida, 1995) and removing H^+ (Payan et al., 1997) from the endolymph, whereas the CA-rich ionocytes are thought to transport HCO_3^- into the endolymph (Tohse and Mugiya, 2001; reviewed in Payan et al., 2004). These models would imply the NKA-rich ionocytes should have different ion-transporting proteins than the CA-rich ionocytes.

Moreover, the endolymph's composition is not homogeneous (Payan et al., 1999; Borelli et al., 2003). The proximal endolymph, which is located between the otolith and the macula and meshwork area, has lower $[K^+]$ and total CO_2 compared to the distal endolymph, which is located between the other side of the otolith and the intermediate and patches area (Payan et al., 1999). Though $[Ca^{2+}]$ does not differ between the proximal and distal endolymph (Payan et al., 1999; Borelli et al., 2003), the proximal endolymph has a 3-fold higher concentration of glycoprotein (Payan et al., 1999), which may chelate Ca^{2+} and catalyze aragonite crystallization (Murayama et al., 2002; Ibsch et al., 2004). Correspondingly, the otolith's proximal surface calcifies faster than the distal surface (Payan et al., 1999; Borelli et al., 2003; Beier et al., 2006). And although it was not directly measured, it was further hypothesized that the pH in the proximal endolymph is lower than the distal endolymph as increased otolith calcification would locally increase $[H^+]$ (Payan et al., 1999). This heterogeneity of the proximal and distal endolymph was proposed to be the result of differential ion transporting activity of meshwork

and patches ionocytes. Under this model, the larger NKA-rich ionocytes in the meshwork area remove K^+ from the proximal endolymph, whereas the smaller NKA-rich ionocytes in the patches area secrete K^+ and absorb H^+ at the distal endolymph (Payan et al., 1999; Allemand et al., 2008). Similarly, other studies speculated that the larger meshwork CA-rich ionocytes remove H^+ from the proximal endolymph (Tohse et al., 2006). These models imply that NKA-rich and CA-rich ionocytes in the meshwork area should express different proteins than their counterparts in the patches area.

Although many other proteins are known to be expressed in the fish inner ear, to our knowledge NKA and CA are the only two ion-transporting proteins established to be specifically present in ionocytes. Basolateral Na^+-K^+-$2Cl^-$-co-transporter (NKCC1; *slc12a2*), NKCC1) is expressed in their developing inner ear of Zebrafish (*Danio renio*) larvae (Abbas and Whitfield, 2009). Although the lack of endolymph accumulation upon NKCC1 genetic disruption indicated a role in K^+ and fluid secretion, the specific cell type where this protein is expressed was not established. Another study detected abundant intracellular acidic compartments in a subset of trout inner ear epithelial cells and hypothesized it indicated removal of H^+ from the endolymph by V-type H^+-ATPase (VHA) (Mayer-Gostan et al., 1997). However, a subsequent study did not find VHA in Zebrafish inner ear ionocytes, and instead reported VHA expression within inner ear sensory hair cells and proposed it acidified the proximal endolymph to retard otolith calcification and maintain distance with the hair cells (Shiao et al., 2005). The plasma membrane Ca^{2+}-ATPase (PMCA; *atp2b1a*) was proposed to be expressed in MR-ionocytes and to transport Ca^{2+} for otolith calcification (Mugiya and Yoshida, 1995; Payan et al., 2002). *In situ* hybridization showed the presence of PMCA mRNA in some epithelial cells surrounding the sensory macula of the developing inner ear of Zebrafish larvae; however, attempts to

immunolocalize the protein were unsuccessful in both larval and adult tissues and thus remain unknown whether PMCA is expressed in ionocytes (Cruz et al., 2009). More recently, a comprehensive transcriptomic and proteomic study concluded NKA, CA, VHA, and PMCA are expressed in the inner ear of black bream (*Acanthopagrus butcheri*) (Thomas et al., 2019). However, those analyses were conducted on samples that contained both inner ear and brain tissue, and thus did not provide insights about protein expression in specific cells. In summary, there are many excellent studies about the ion-transporting proteins involved in otolith calcification, but their use of different fish species, life stages, and techniques greatly complicates attempts to synthesize the available information into a single model describing the ion transporting mechanisms that maintain the distinctive endolymph composition necessary for proper inner ear function.

Although the cellular mechanisms underlying otolith calcification are not completely understood, it is clear that they activities are sensitive to acid-base conditions (reviewed in Allemand et al., 2008). Indeed, diurnal fluctuations in plasma [HCO_3^-] is one of the underlying causes of the otolith's characteristic concentric rings (Tohse and Mugiya, 2008) used to estimate age and growth in stock assessment studies (Pannella, 1971; Campana and Neilson, 1985). And more recently, exposure to ocean acidification conditions has been reported to induce increased otolith size and density in multiple fish species (Checkley et al., 2009; Bignami et al., 2013; Maneja et al., 2013; Munday et al., 2011; Pimentel et al., 2014; Schade et al., 2014; Shen et al., 2016), which has been linked to plasma [HCO_3^-] accumulation resulting from blood acid-base regulation [c.f. (Esbaugh et al., 2012, 2016)]. One possibility is that otolith overgrowth is the direct result of increased transport of plasma [HCO_3^-] into the endolymph. However, increased otolith calcification rate also requires increased secretion of Ca^{2+} and glycoprotein into the

endolymph, and increased H^+ removal. With this in mind, we explored whether the soluble adenylyl cyclase (sAC, adcy10) is expressed within inner ear epithelial ionocytes. This evolutionary conserved acid-base sensing enzyme is stimulated by HCO_3^- to produce cyclic adenosine monophosphate (cAMP), a messenger molecule that can regulate multiple cellular processes *via* protein kinase A mediated phosphorylation on target proteins (reviewed in Tresguerres et al., 2010a; Tresguerres, 2014).

The goal of the current study was to determine how many types of ionocytes are present in the inner ear epithelium of a single species, the Pacific Chub Mackerel (*Scomber japonicus*, Houttuyn, 1782). To this end, we performed thorough immunohistochemical analyses using specific antibodies against NKA, CA, NKCC, VHA, PMCA, and sAC. Unexpectedly, we also detected high abundance of some of these proteins in the cells that form the arterioles that supply blood to the meshwork area. The resulting model about the ion-transporting and regulatory mechanisms underlying endolymph's unique composition improves our understanding about how otoliths are calcified, and will inform subsequent experimental studies to determine if and how they might be affected during environmental stress.

Methods

Tissue Sampling and Preparation

Pacific Chub Mackerel were caught by hook and line off the Scripps pier in San Diego, United States (standard length = 15.3 ± 0.3 cm; weight = 26.9 ± 2.2 g; n = 19). In accordance to protocol S10320 of the University of California, San Diego Institutional of Animal Care and Use Committee, fish were euthanized by spinal pithing and its inner ear tissue dissected. Tissue was either flash frozen in liquid nitrogen and stored in -80°C, or fixed in 4% paraformaldehyde in

phosphate buffer saline (PBS) at 4°C for 8 hours, incubated in 50% ethanol for 8 hours, and stored in 70% ethanol for immunohistochemistry. Protein integrity was prioritized; therefore, the length and weight of the fish were recorded after dissection.

Antibodies

Mitochondria were labeled using a mouse monoclonal antibody against human cytochrome *c* oxidase complex IV (MTC02, catalog #: MA5-12017, Invitrogen, Grand Island, New York, USA); this antibody demonstrates specificity against a broad range of species including coral (Barott et al., 2015a) and shark (Roa et al., 2014). The mouse monoclonal anti-NKA antibody α5 (Lebovitz et al., 1989) was purchased from the Developmental Studies Hybridoma Bank (DSHB, The University of Iowa, Iowa City, IA, USA). This antibody has been extensively validated in fish and is routinely used to detect NKA in multiple fish tissues (Wilson et al., 2000, 2002; Roa et al., 2014; Roa and Tresguerres, 2017; Kwan et al., 2019b). Additionally, NKA was immunodetected using rabbit polyclonal antibodies against the mammalian NKA α-subunit (H300, catalog # SC-28800, Santa Cruz Biotechnology, Dallas, USA), which recognize NKA in gills from multiple fish (Roa et al., 2014; Michael et al., 2016; Allmon and Esbaugh, 2017). Rabbit polyclonal antibodies against human CA II were purchased from Rockland Inc., Gilbertsville, USA (catalog #: 100-401-136); these antibodies are routinely used to immunodetect CA from teleost fishes [e.g. (Georgalis et al., 2006; Qin et al., 2010)], including in the saccular epithelium of Masu Salmon (*Oncorhynchus masou*) (Tohse et al., 2004). The mouse monoclonal anti-NKCC antibody T4 (Lytle et al., 1995) was obtained from DSHB; and has been widely used to detect NKCC in fish tissues (Tresguerres et al., 2010b; Esbaugh and Cutler, 2016), including Zebrafish saccular epithelium (Abbas and Whitfield,

2009). VHA was immunodetected using custom-made rabbit polyclonal antibodies against a peptide in the B subunit (epitope: AREEVPGRRGFPGY; GenScript, Piscataway, USA); this peptide is conserved from cnidarians to mammals (Barott et al., 2015), and has been successfully used to immunodetect VHA in elasmobranch tissues (Roa et al., 2014; Roa and Tresguerres, 2017). The mouse monoclonal anti-PMCA antibody 5F10 against human erythrocyte PMCA was purchased from ThermoFisher Scientific, Waltham, USA (catalog #: MA3-914). sAC was immunodetected using custom-made rabbit polyclonal antibodies against a peptide in the first catalytic domain of Rainbow Trout sAC (epitope: LSSKKGYGADELTR; GenScript). The secondary antibodies were goat anti-mouse IgG-HRP and goat anti-rabbit IgG-HRP conjugate (Bio-Rad, Hercules, CA, USA) for western blot, and goat anti-mouse Alexa Fluor 546, goat anti-rabbit Alexa Fluor 488, and/or goat anti-rabbit Alexa Fluor 555 (Invitrogen, Grand Island, USA) for immunohistochemistry. Each antibody was tested in inner ear samples from at least three different fishes.

Western Blotting

Inner ear tissue was immersed in liquid nitrogen, pulverized in a porcelain grinder, and submerged in an ice-cold, protease inhibiting buffer (250 mmol l^{-1} sucrose, 1 mmol l^{-1} EDTA, 30 mmol l^{-1} Tris, 10 mmol l^{-1} benzamidine hydrochloride hydrate, 200 mmol l^{-1} phenylmethanesulfonyl fluoride, 1 mol l^{-1} dithiothreitol, pH 7.5). Next, debris was removed by low speed centrifugation (3000xg, 10 minutes, 4°C). Total protein concentration in the crude homogenate was determined by the Bradford assay (Bradford, 1976). Samples were mixed with an equal volume of 90% 2x Laemmli buffer and 10% β-mercaptoethanol, and heated at 70°C for 5 minutes. Protein (10 µg per lane) were loaded onto a 7.5% polyacrylamide mini gel (Bio-Rad,

Hercules, CA, USA) and ran at 200 volts for 40 minutes, then transferred to a polyvinylidene difluoride (PVDF) membrane using a Trans-Blot SD Semi-Dry Transfer Cell (Bio-Rad). PVDF membranes were then incubated in tris-buffered saline with 1% tween (TBS-T) with milk powder (0.1 g/mL) at room temperature (RT) for 1 hour, then incubated with primary antibody (a5: 10.5 ng/ml; H300: 100 ng/ml; CA II antibody: 8 µg/ml; T4: 10.4 ng/ml; VHA *b*-subunit: 1.5 µg/ml; Rainbow Trout sAC: 3 µg/ml; 5F10: diluted 1:10,000 from commercial stock) in blocking buffer at 4°C overnight. On the following day, PVDF membranes were washed in TBS-T (three times; 10 minutes each), incubated in the appropriate anti-rabbit or anti-mouse secondary antibodies (1:10,000) at RT for 1 hour, and washed again in TBS-T (three times; 10 minutes each). Bands were made visible through addition of ECL Prime Western Blotting Detection Reagent (GE Healthcare, Waukesha, WI) and imaged and analyzed in a BioRad Universal III Hood using Image Lab software (version 6.0.1; BioRad). Peptide preabsorption with excess peptide (1:5 antibody to peptide ratio; preabsorbed overnight at 4°C on shaker) was performed to verify antibody specificity.

Immunostaining

After fixation, samples were immersed in decalcifying solution (NaCl 450 mM, KCL 10 mM, MgCl 58 mM, Hepes 100 mM, EDTA 0.5 M, pH 7.5, changed daily) for three days at 4°C on a shake table to dissolve the otolith. Once the otolith dissolved, samples were incubated overnight in 70% ethanol and dehydrated through a series of increasing ethanol steps (70%, 95%, 100%, 10 minutes each), SafeClear (3 times; 10 minutes each), warm paraffin (65°C; 3 times; 10 minutes each), before embedding tissue in a paraffin block on an ice pack overnight. The next day, samples were sectioned using a microtome (~10 µm thickness) and mounted onto glass

slides. After drying overnight, paraffin was removed by incubation in SafeClear (3 times; 10 minutes each), and rehydrated in a series of decreasing ethanol steps (100%, 95%, 70%, 10 minutes each). To counter native autofluorescence, samples were immersed with sodium borohydride (1 mg/mL) in ice cold PBS (6 times; 10 minutes each). Samples were then washed in PBS + 0.1% tween (PBS-T) at RT for 5 minutes, incubated in blocking buffer (PBS-T, 0.02% normal goat serum, 0.0002% keyhole limpet hemocyanin) at RT for one hour, and with the primary antibodies (MTC02: 2 µg/ml; a5: 42 ng/ml; H300: 4 µg/ml; CA II antibody: 160 µg/ml; T4: 104 ng/ml; VHA *b*-subunit: 6 µg/ml; Rainbow Trout sAC: 6 µg/ml; 5F10: diluted 1:500 from commercial stock) in blocking buffer and kept in a humid chamber at RT overnight. On the following day, samples were washed in PBS-T (3 times; 10 minutes each) and incubated with the appropriate anti-rabbit or anti-mouse fluorescent secondary antibodies (1:1,000) and nuclear stain Hoechst 33342 (5 µg/mL; Invitrogen) at RT for 1 hour. Samples were washed in PBS-T (three times; 10 minutes each), then mounted in Fluoro-gel with Tris (Electron Microscopy Sciences). Samples were examined and imaged on an epifluorescence microscope (Zeiss AxioObserver Z1). Digital images were adjusted, for brightness and contrast, using Zeiss Axiovision software. Some low magnification images were stitched together to provide pictures of the entire saccular epithelium using Helicon Focus 6 (Helicon Soft Ltd., Kharkov, Ukraine). Peptide preabsorption with excess peptide (1:10 antibody to peptide ratio; preabsorbed overnight at 4°C on shaker) was performed to verify antibody specificity against VHA and sAC.

Results

Western blotting revealed high abundance of NKA, CA, NKCC, VHA, sAC, and PMCA protein in Pacific Chub Mackerel inner ears (Figure 1). The immunoreactive bands matched the

predicted size of each target protein (NKA-α subunit: ~100 kDa with both mono- and polyclonal antibodies; CA: ~30 kDa; NKCC: ~200 kDa; VHA-b subunit: ~55 kDa; PMCA: ~140 kDa; sAC: ~180, 110, and 50 kDa), were sharp and distinct, and were absent in control blots in which the primary antibody was omitted. No bands were detected in anti-VHA and anti-sAC antibodies' pre-immune and peptide pre-absorption controls.

Next, we examined the expression of these proteins within specific saccular epithelial cells using immunohistochemistry. NKA was abundantly expressed within cells adjacent to the endolymph (Figure 2a). Higher magnification images revealed NKA immunostaining produced a dense intracellular speckled pattern (Figure 2b), which indicates NKA is present in the highly infolded basolateral membrane. Double immunolabeling with anti-complex IV antibodies revealed the NKA-rich ionocytes are MR (Figure 2c) and contain abundant NKCC (Figure 2d). Furthermore, the resulting "yellow" signal from dual NKA and NKCC immunolabeling indicated a strong overlap in the basolateral membrane. CA was also highly expressed in specific saccular epithelial cells; however, double immunolabeling revealed CA was present in cells that were not labeled for NKA (Figure 3a) or NKCC1 (Figure 3b). Similarly, double immunolabeling of NKA and VHA (Figure 4a, b, c) revealed that these two proteins were expressed in different cells. By default, this indicates the CA and VHA were expressed in the same cell type. Overall, these results indicate the presence of two types of ionocytes in the saccular epithelium. "Type-I" ionocytes abundantly express NKA and NKCC1 and are MR, and "Type-I" ionocytes abundantly express CA and VHA.

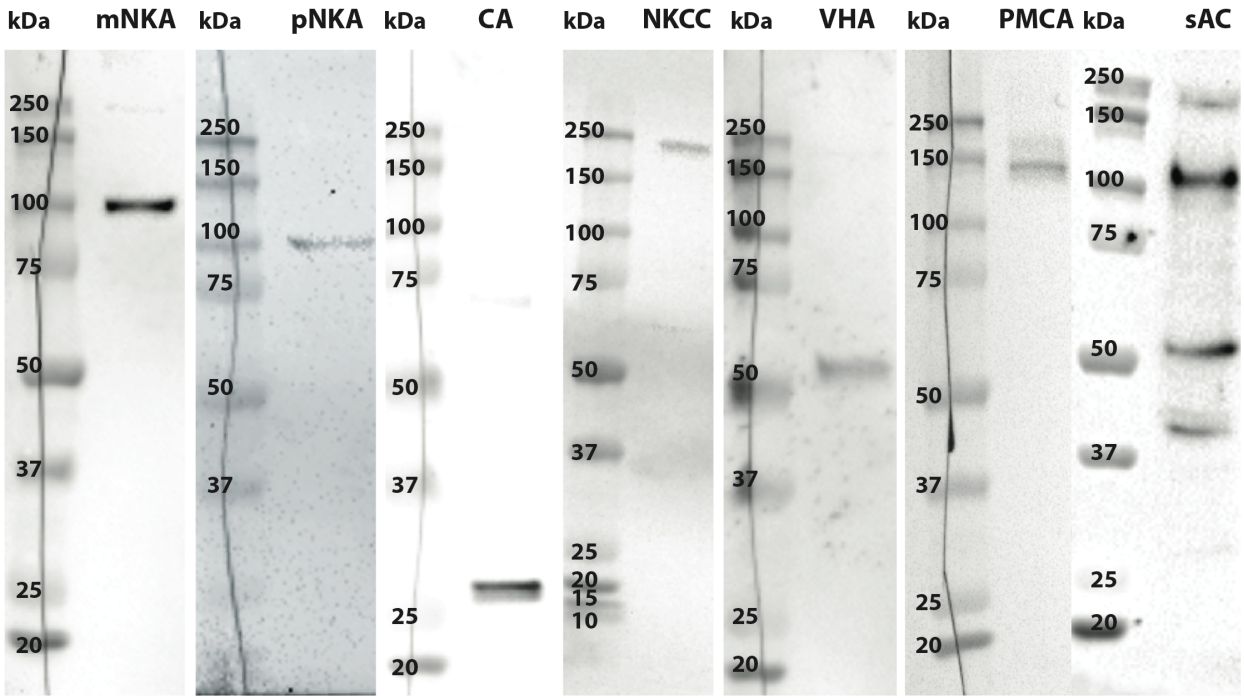

Figure 6.1: Western blot analysis of inner ear homogenates. Antibodies against monoclonal Na^+/K^+-ATPase (mNKA), polyclonal Na^+/K^+-ATPase (pNKA), carbonic anhydrase (CA), Na^+-K^+-Cl^--co-transporter (NKCC), V-type H^+ ATPase (VHA), plasma membrane calcium ATPase (PMCA), and soluble adenylyl cyclase (sAC) reveal bands matching the predicted size of respective proteins. Molecular marker is shown on the left of each respective blot.

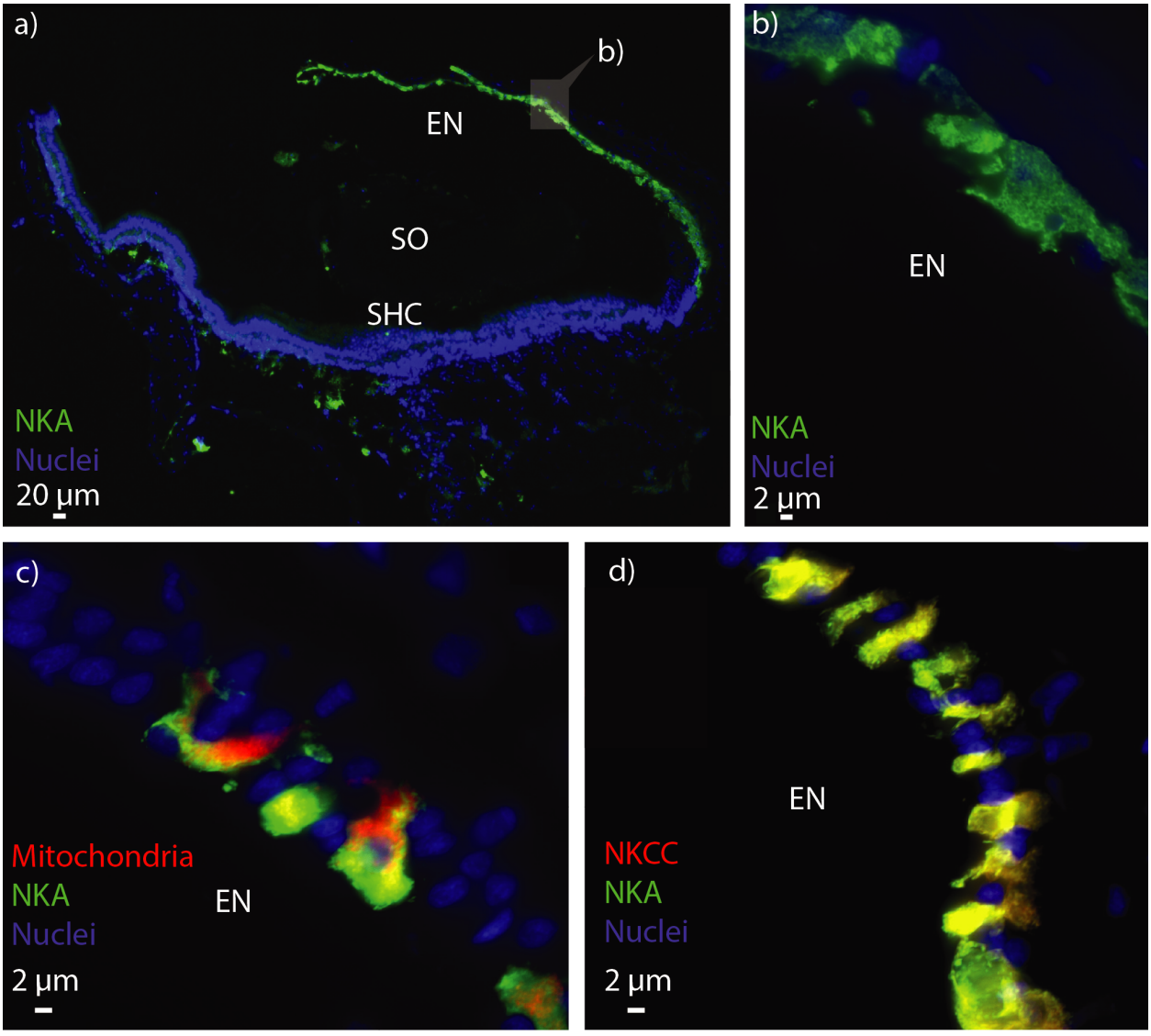

Figure 6.2: Characterization of Type-I ionocytes within the saccular epithelium. Histological saggital section immunostained with (**a**) Na^+/K^+-ATPase (NKA, green). (**b**) Magnified view of the NKA-rich ionocytes revealed abundant staining in a dense, speckled pattern resembling a developed basolateral infolding. Dual-immunostaining revealed the NKA-rich (green) ionocyte is also (**c**) mitochondrion-rich (red) and contain abundant (**d**) Na^+-K^+-$2Cl^-$-co-transporter (NKCC, red). Nuclei are stained blue. EN = endolymph. SO = sagittal otolith protein. SHC = sensory hair cell.

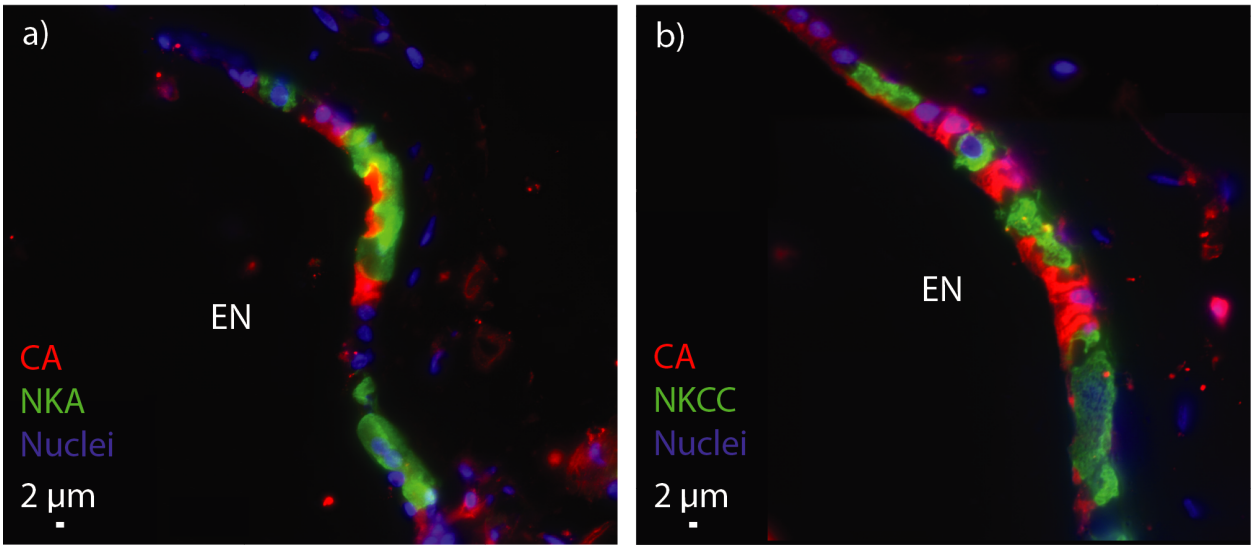

Figure 6.3: Evidence for two types of ionocytes within the saccular epithelium. Dual-immunostaining of ionocytes within the saccular epithelium revealed carbonic anhydrase (CA; red) is expressed in cells that are different from the (**a**) Na^+/K^+-ATPase (NKA; green) and (**b**) Na^+-K^+-$2Cl^-$-co-transporter (NKCC, green)-rich Type-I ionocyte. Nuclei are stained blue. EN = endolymph.

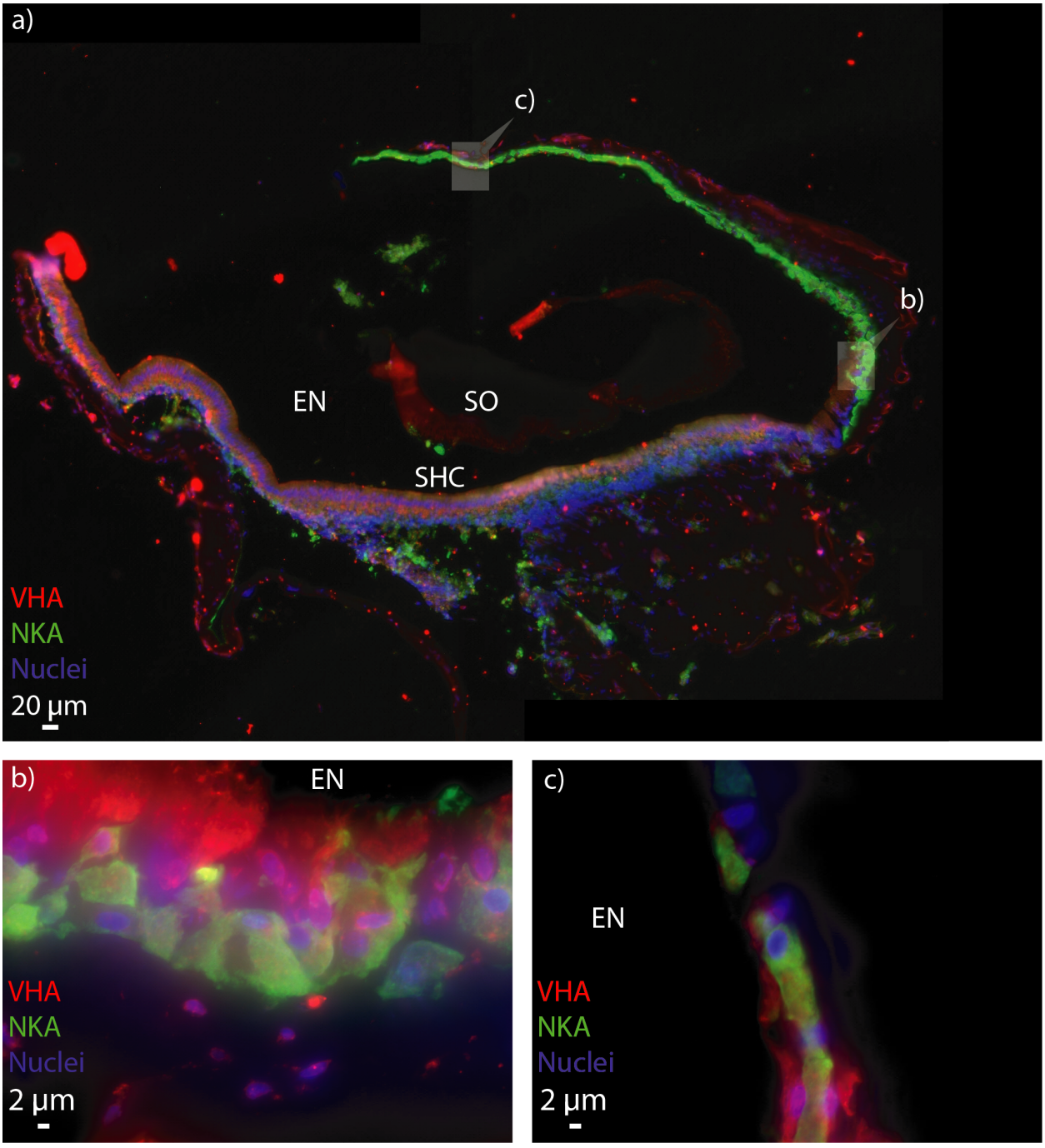

Figure 6.4: Characterization of Type-II ionocytes within the saccular epithelium. (**a**) Histological saggital section immunostained with Na^+/K^+-ATPase (NKA, green) and V-type H^+-ATPase (VHA, red). (**b**) Higher magnification image of saccular ionocytes of the larger meshwork ionocytes and (**c**) the smaller patches ionocytes indicate NKA-rich and VHA-rich cells are different cells. Nuclei are stained blue. EN = endolymph; SO = sagittal otolith protein. SHC = sensory hair cell.

PMCA was also abundantly expressed in saccular epithelial cells adjacent to the endolymph. The pattern observed following dual immunostaining with NKA indicates PMCA is present in Type-I and Type-II ionocytes (Figure 5a, b). Unlike NKA and NKCC1 (Figure 2d), NKA and PMCA immunofluorescent signals did not overlap significantly (Figure 5c), suggesting PMCA is predominantly present in cytoplasmic vesicles and not in the basolateral membrane.

Additionally, abundant sAC immunolabeling was detected throughout the saccular epithelium (Figure 5d). Dual immunostaining of sAC and NKA (Figure 5e, f) and sAC and PMCA (Figure 5g, h, i) revealed sAC was abundantly expressed in both Type-I and Type-II ionocytes.

Type-I and Type-II ionocytes in the meshwork area were larger than in the patches area (~40 µm vs. ~10 µm wide, respectively; Figure 4b, c). However, the protein expression profile in each ionocyte type was identical regardless of size. In addition to the previously reported presence of PMCA (Cruz et al., 2009) and VHA (Shiao et al., 2005), we detected NKA (Figure 2a) and sAC (Figure 5d) within the sensory hair cells. Unexpectedly, we also observed intense CA (Figure 6a, b), VHA (Figure 6c, d), and sAC (Figure 6e, f) immunoreactivity within the endothelial cells that form the abundant capillaries surrounding the meshwork area.

Figure 6.5: Presence of plasma membrane Ca^{2+} ATPase and soluble adenylyl cyclase in Type-I and Type-II ionocytes. (**a, b, c**) Dual immunostaining of plasma membrane Ca^{2+}-ATPase (PMCA, green) with Na^{+}/K^{+}-ATPase (NKA, red). Notice that PMCA is present in all NKA-rich cells (Type-I ionocyte), as well as in adjacent cells without NKA signal (Type-II ionocytes). (**d**) Histological saggital section immunostained with soluble adenylyl cyclase (sAC, red) and Na^{+}/K^{+}-ATPase (NKA, green). (**e,f**) higher magnification images reveal sAC is present in both the NKA-rich Type-I ionocytes (green) and Type-II ionocytes (indicated by ionocytes lacking NKA signal). (**g, h, i**) The presence of PMCA (green) and sAC (red) in both Type-I and Type-II ionocytes was further conformed by dual-staining. Nuclei are stained blue. EN = endolymph; SO = sagittal otolith protein. SHC = sensory hair cell.

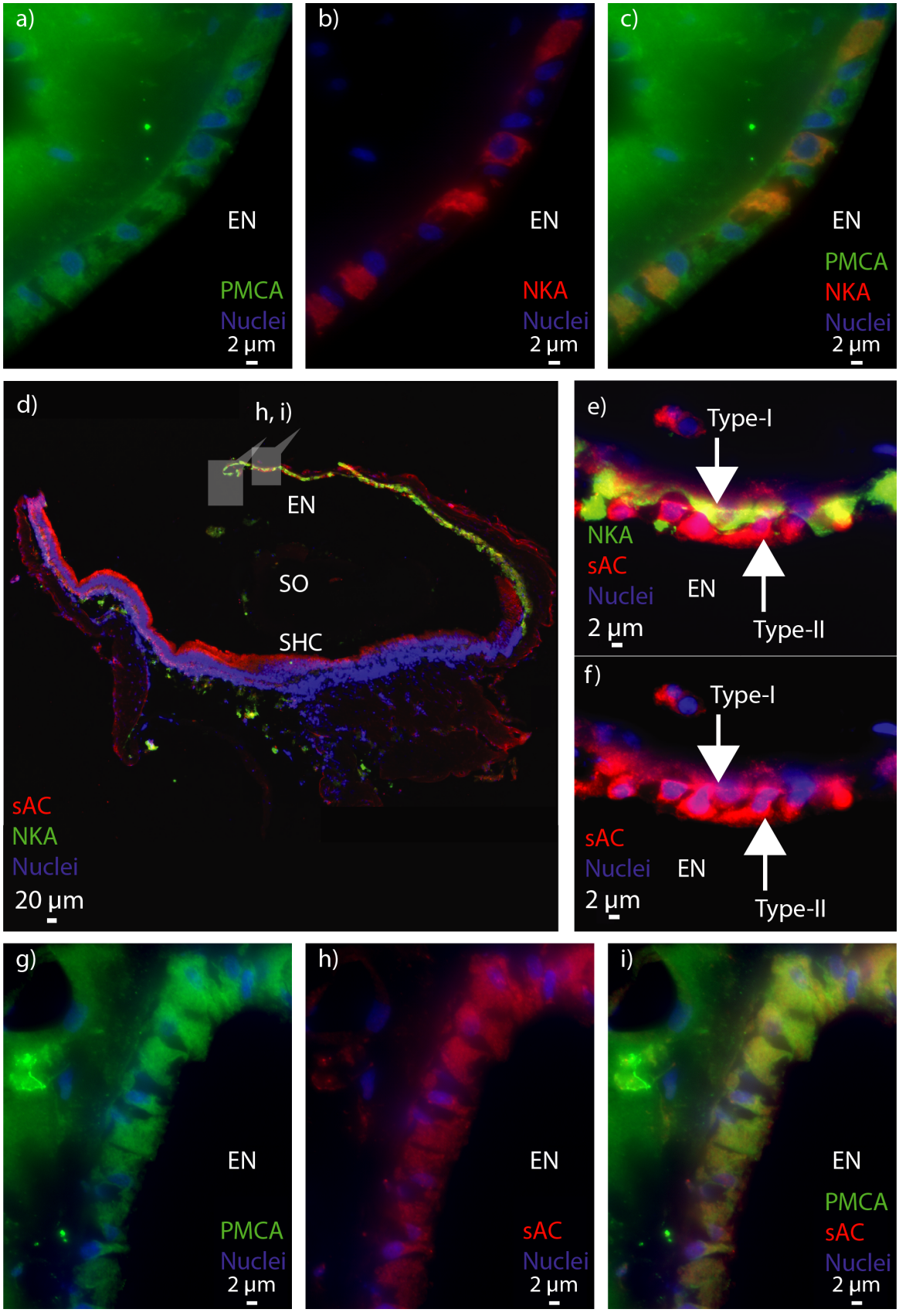
a)
EN
PMCA
Nuclei
2 µm
b)
EN
NKA
Nuclei
2 µm
c)
EN
PMCA
NKA
Nuclei
2 µm
d)
h, i)
EN
SO
SHC
sAC
NKA
Nuclei
20 µm
e)
Type-I
NKA
sAC
Nuclei
EN
2 µm
Type-II
f)
Type-I
sAC
Nuclei
EN
2 µm
Type-II
g)
EN
PMCA
Nuclei
2 µm
h)
EN
sAC
Nuclei
2 µm
i)
EN
PMCA
sAC
Nuclei
2 µm

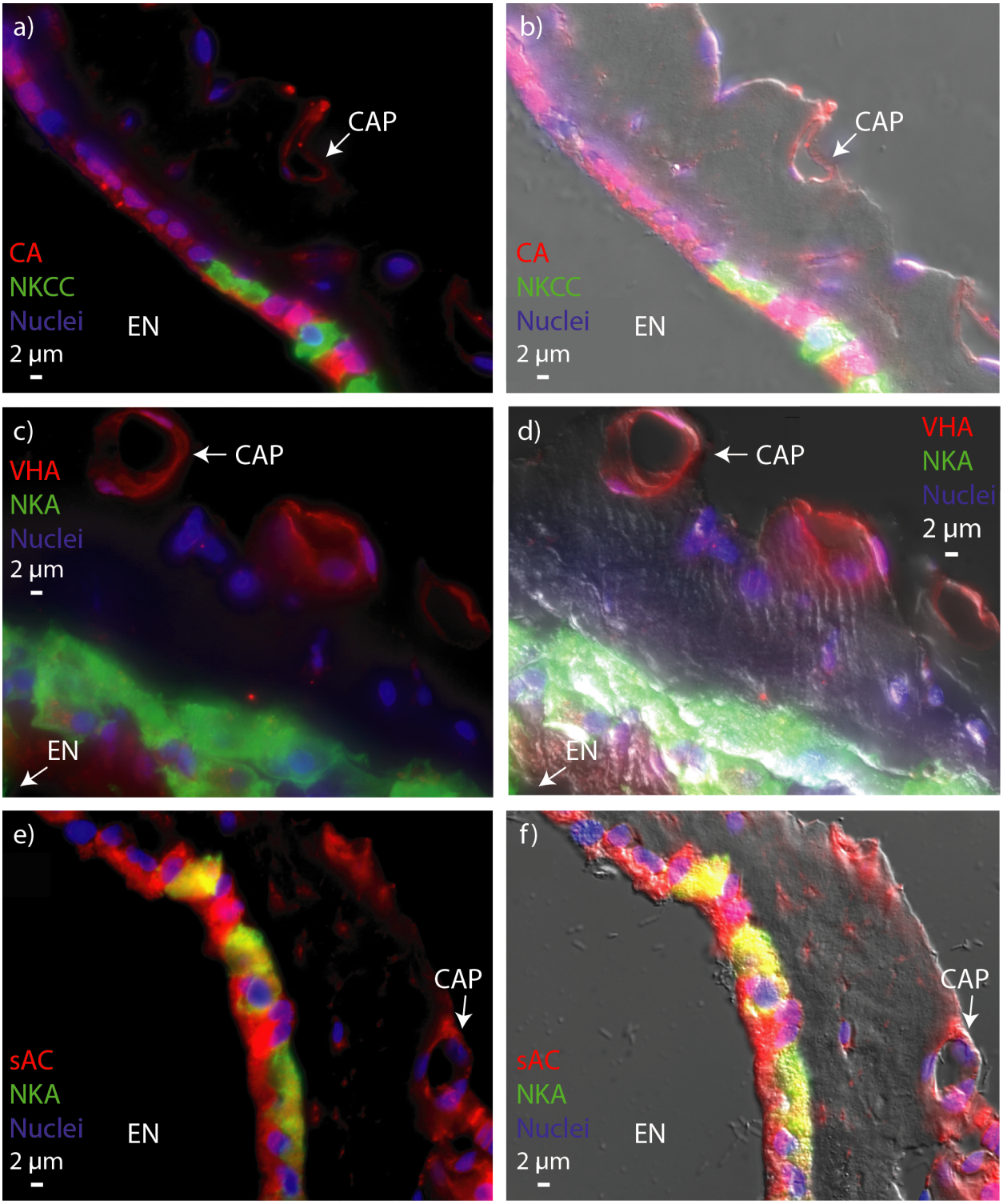

Figure 6.6: Inner ear saccular epithelium capillaries express CA, VHA, and sAC. Histological section dual-stained with (**a, b**) carbonic anhydrase (CA, red) and Na^+-K^+-$2Cl^-$-co-transporter (NKCC, green), (**c, d**) V-type H^+-ATPase-rich (VHA, green) and Na^+/K^+-ATPase (NKA, green), and (**e, f**) soluble adenylyl cyclase (sAC, red) and NKA (green). Nuclei are stained blue. EN = endolymph; CAP = capillary.

Discussion

Here, we characterized two types of ionocytes within the Pacific Chub Mackerel's saccular epithelium: Type-I ionocytes are MR and express abundant NKA, NKCC1, PMCA, and sAC whereas Type-II ionocytes express abundant CA, VHA, PMCA, and sAC (Figure 8). Ionocyte distribution and size patterns were similar to those reported in most previous studies (Mayer-Gostan et al., 1997; Pisam et al., 1998): larger ionocytes bordered the meshwork area while smaller ionocytes were found in the patches area. However, there were no differences in protein expression between the larger Type-I and Type-II meshwork ionocytes and the smaller Type-I and Type-II patches ionocytes, further supporting the idea that only two types of ionocytes exist within the saccular epithelium. This suggests that the differences in ionic composition between the proximal and distal endolymph are the result of different ion transporting rates in these two regions and not due to the presence of different ion transporting mechanisms. Additional factors that surely contribute to the heterogeneous endolymph ionic composition and otolith calcification rates include the activity of hair cells and the secretion of glycoproteins that promote carbonate precipitation, both taking place in the meshwork area and proximal endolymph (reviewed in Payan et al., 2004; Allemand et al., 2008).

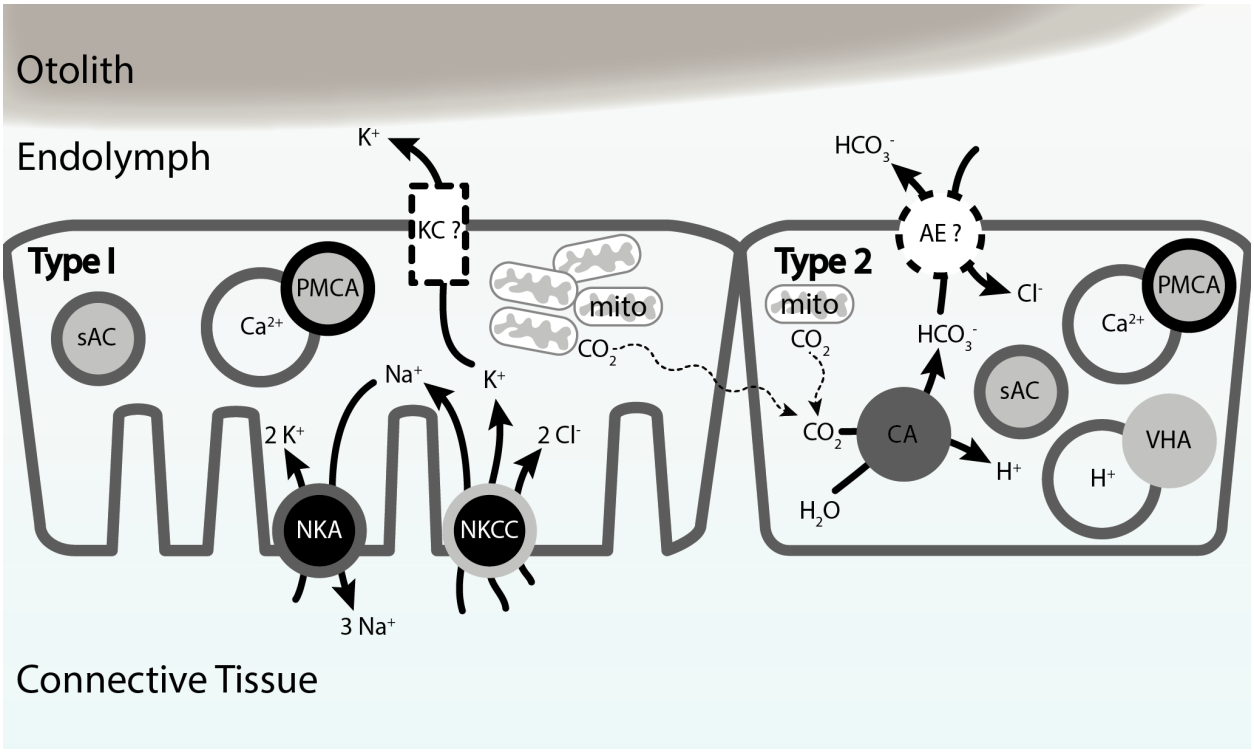

Figure 6.7: Proposed model for otolith calcification by the two types of ionocytes within the inner ear saccular epithelium. Abbreviations: Na^+/K^+-ATPase (NKA), Na^+-K^+-Cl^--co-transporter (NKCC), mitochondria (mito), carbonic anhydrase (CA), V-type H^+ ATPase (VHA), plasma membrane calcium ATPase (PMCA), soluble adenylyl cyclase (sAC), anion exchanger (AE), and K^+ channel (KC). Capillaries that supply O_2 (and potentially HCO_3^-) are not shown for simplicity, though they are especially important in the meshwork area. Ion transport is indicated by a solid line, and gas diffusion is indicated by a dashed, squiggly line.

Our results on the marine Pacific Chub Mackerel generally agree with the literature about ion transporting mechanisms in fish inner ear epithelia, which is largely based on research on freshwater fishes. The main differences were the localization of VHA and PMCA. The former was reported to be exclusively expressed in sensory hair cells in the inner ear of Zebrafish embryos (Shiao et al., 2005), and the latter was only studied at the mRNA level and predominantly found in hair cells as well (Cruz et al., 2009). Future experiments should confirm whether the differences between Pacific Chub Mackerel and Zebrafish are species or life stage-

specific, environmentally based (i.e. freshwater vs seawater), or due to different immunostaining techniques and antibodies.

Putative functions of fish inner ear epithelial ionocyte function.

Based on the presence of NKA and NKCC1, the Type-I ionocytes are likely responsible for secreting K^+ into the endolymph, where it can reach concentrations >40 higher than in blood plasma (Payan et al., 1997, 1999; Ghanem et al., 2008). Given that NKCC1 knockout results in inner ear collapses due to lack of fluid in Zebrafish larvae (Abbas and Whitfield, 2009), one of the roles of NKCC1-driven K^+ secretion is to osmotically drive fluid transport. Additionally, the K^+-rich endolymph is essential for mechanoreception by the sensory hair cells (Zdebik et al., 2009). This model would imply that Type-I ionocytes express K^+ channels in their apical membrane, and should be further investigated in future studies. The outwardly conducting KCNQ1/KCNE1 K^+ channels found on the apical membrane of the analogous "dark" cells of mammalian inner ear are promising candidates (Nicolas et al., 2001).

In contrast, the high abundance of CA and VHA in Type-II ionocytes suggests these cells are involved in promoting otolith calcification by secreting HCO_3^- into the endolymph and removing H^+. The CA-catalyzed hydration of CO_2 (for example from the abundant mitochondria from the adjacent Type-I ionocytes) would provide HCO_3^- to be secreted into the endolymph by yet unidentified apical anion exchangers. The H^+ that is simultaneously produced might be removed by VHA, either into intracellular vesicles as proposed by Mayer-Gostan *et al* (1997) or upon VHA insertion into the basolateral membrane as reported in the base-secreting cells of elasmobranch gills (Tresguerres et al., 2005; Roa and Tresguerres, 2016).

Both Type-I and Type-II ionocytes also expressed PMCA, which has been previously shown to be important for otolith calcification based on the effects of genetic knockdown (Cruz et al., 2009) and pharmacological inhibition of calmodulin-antagonist of PMCA activity (Mugiya and Yoshida, 1995). The presence of PMCA throughout the cytoplasm suggests Ca^{2+} sequestration in vesicles, which may be transported to the apical membrane and its contents exocytosed into the calcifying fluid as proposed in coral calcifying cells (Barott et al., 2015a; Barron et al., 2018). Other proposed transcellular pathways for Ca^{2+} transport include Ca^{2+} channels and Na^{+}/Ca^{2+} exchangers (Mugiya and Yoshida, 1995; Thomas et al., 2019), and the identification of their cellular and subcellular localizations would contribute greatly to the mechanistic model of otolith calcification.

A potential regulatory mechanism of otolith calcification.

Both Type-I and Type-II ionocytes contained sAC, an evolutionary conserved acid-base sensing enzyme that produces the messenger molecule cAMP (Chen et al., 2000; Tresguerres, 2014). The effects of plasma and endolymph acid-base status on otolith calcification are well established (Takagi, 2002; Payan et al., 2004; Allemand et al., 2008), and sAC may be one of the underlying signaling mechanisms that senses and regulates the activity of calcification-relevant ion transporting proteins. Supporting this possibility, some of the same ion-transporting proteins found in Type-I and Type-II ionocytes have been shown to be under sAC regulation in many other epithelia. In the intestine of marine teleosts, sAC senses elevations in $[HCO_3^-]$ and regulates NKA and NKCC activity to promote luminal carbonate precipitation and fluid transport (Tresguerres et al., 2010b; Carvalho et al., 2012). In marine elasmobranchs gills, sAC senses blood alkalosis and activates VHA -and possibly the apical anion exchanger pendrin- to mediate

compensatory HCO_3^- secretion and H^+ absorption (Tresguerres et al., 2010c; Roa et al., 2014; Roa and Tresguerres, 2016). In addition to being directly stimulated by HCO_3^-, sAC is stimulated by Ca^{2+}(Litvin et al., 2003), providing another potential regulatory mechanism for otolith calcification. Interestingly, sAC is also abundantly expressed in coral calcifying cells (Barott et al., 2017) and in oyster mantle (Barron et al., 2012), suggesting a conserved role in regulating transepithelial ion transport for calcification.

A novel regulatory role of capillaries in regulating otolith calcification?

The connective tissues surrounding the inner ear contain numerous capillaries, which are especially abundant near the meshwork area (Saitoh, 1990; Mayer-Gostan et al., 1997). Unexpectedly, we found the endothelial cells that form such capillaries to abundantly express CA, VHA, and sAC. This is consistent with previous reports of CA within the cytoplasm of capillaries in the analogous mammalian inner ear (Watanabe and Ogawa, 1984). We tentatively propose that the activities of these proteins are relevant for otolith calcification by mediating the transport of CO_2/HCO_3^- from the blood to the endolymph, and by facilitating the removal of excess H^+ generated as a result of $CaCO_3$ precipitation. In addition, the local acidification of the capillary lumen could trigger the Root effect in circulating red blood cells, thus promoting O_2 offloading to sustain aerobic metabolism of ionocytes and sensory hair cells within the saccular epithelium. Such a mechanism was originally described in fish swim bladder and eye (reviewed in Pelster, 2001), and more recently proposed to apply more broadly to other highly aerobic fish tissues including the eye (Fairbanks et al., 1969), muscle (Rummer et al., 2013), and intestine (Cooper et al., 2014).

Conclusions, future directions and significance.

Our proposed model is consistent with previous functional studies conducted on isolated fish inner ear organ that suggested the involvement of NKA, CA, and PMCA (as well as Na^+/Ca^{2+} exchanger, Ca^{2+} channels, and Na^+/H^+ exchanger) based on acid-base titration and $^{45}Ca^{2+}$ incorporation experiments in combination with pharmacological inhibitors (Mugiya and Yoshida, 1995; Payan et al., 1997). Furthermore, functional evidence for the roles of NKCC1 (Abbas and Whitfield, 2009) and PMCA (Cruz et al., 2009) is available through the genetic downregulation experiments on Zebrafish larvae mentioned above. More recently, the presence of many of those proteins as well as VHA has been confirmed through an extensive proteomic and transcriptomic survey (Thomas et al., 2019) (with the caveat that analyses were conducted on samples that contain both inner ear and brain tissue). Our results expand and complement those previous studies by establishing the transporter's cellular and subcellular localization, ultimately leading to the identification of two types of ionocytes. In addition, our results revealed sAC is present in both types of ionocytes, providing a potential mechanism that can regulate otolith calcification in response to acid-base variations. Ongoing efforts in our laboratory are attempting to functionally characterize the putative regulatory role of sAC on inner ear function; however, sAC's presence within both types of ionocytes, sensory hair cells, and capillaries is a significant hurdle for studies at the organ and whole organism level. For example, putative changes in protein or mRNA abundance in ionocytes in response to experimental manipulations would be confounded by the background provided by all the other cell types in the tissue, which are the majority. Thus, detailed functional studies on the underlying ion transport mechanism would require the development of ionocyte primary cultures. Similar considerations apply to

efforts to elucidating the functional roles of CA, VHA, and sAC in the capillaries near the meshwork area.

The inner ear organ allows fish to sense and respond to its environment and therefore is essential for survival. In addition, analyses on otolith rings provide valuable information regarding daily and seasonal growth bands, trace element signatures (Swearer et al., 1999), exposure to environmental salinity and temperature (Campana, 1999; Elsdon and Gillanders, 2002), and diet (Radtke et al., 1996; Nelson et al., 2011; von Biela et al., 2015). Thus, in addition to its intrinsic value from physiological and evolutionary perspectives, information about the cellular mechanisms underlying otolith calcification can improve current fisheries assessment tools and help predict the effects of environmental stressors, and in particular ocean acidification, on otolith growth and function from a mechanistic perspective.

Acknowledgements

GTK was supported by the National Science Foundation (NSF) Graduate Research Fellowship Program and the NSF Graduate Research Internship Program. This research was supported by grant NSF IOS #1754994 to M.T. We thank Jake Munich for his assistance in capturing Pacific Chub Mackerel.

Chapter VI, in part, has been submitted for publication of the material as it may appear in *Journal of Comparative Physiology – B*. Kwan, G.T., Smith, T.R., and Tresguerres, M. (*in review*). Immunological characterization of two ionocyte subtypes in the inner ear epithelium of Pacific Chub Mackerel (*Scomber japonicus*). The dissertation author was the primary investigator and author of this material.

References

Abbas, L., and Whitfield, T. T. (2009). Nkcc1 (Slc12a2) is required for the regulation of endolymph volume in the otic vesicle and swim bladder volume in the zebrafish larva. Development, 136: 2837–2848. doi:10.1242/dev.034215.

Allemand, D., Mayer-Gostan, N., De Pontual, H., Boeuf, G., and Payan, P. (2008). Fish otolith calcification in relation to endolymph chemistry. Handbook of Biomineralization: Biological Aspects and Structure Formation, 1: 291–308.

Allmon, E. B., and Esbaugh, A. J. (2017). Carbon dioxide induced plasticity of branchial acid-base pathways in an estuarine teleost. Scientific Reports, 7: 45680. Nature Publishing Group. doi:10.1038/srep45680.

Barott, K., Venn, A. A., Perez, S. O., Tambutté, S., and Tresguerres, M. (2015a). Coral host cells acidify symbiotic algal microenvironment to promote photosynthesis. Proceedings of the National Academy of Sciences of the United States of America, 112: 607–12. doi:10.1073/pnas.1413483112.

Barott, K. L., Perez, S. O., Linsmayer, L. B., and Tresguerres, M. (2015b). Differential localization of ion transporters suggests distinct cellular mechanisms for calcification and photosynthesis between two coral species. American Journal of Physiology - Regulatory, Integrative and Comparative Physiology, 309: R235–R246. doi:10.1152/ajpregu.00052.2015.

Barott, K. L., Barron, M. E., and Tresguerres, M. (2017). Identification of a molecular pH sensor in coral. Proceedings of the Royal Society B: Biological Sciences, 284: 20171769. doi:10.1098/rspb.2017.1769.

Barron, M. E., Roa, J. N. B. R., and Tresguerres, M. (2012). Pacific oyster mantle, gill and hemocytes express the bicarbonate-sensing enzyme soluble adenylyl cyclase. In FASEB journal : official publication of the Federation of American Societies for Experimental Biology.

Barron, M. E., Thies, A. B., Espinoza, J. A., Barott, K. L., Hamdoun, A., and Tresguerres, M. (2018). A vesicular Na+/Ca2+ exchanger in coral calcifying cells. Plos One, 13: e0205367. doi:10.1371/journal.pone.0205367.

Beier, M., Anken, R., and Hilbig, R. (2006). Sites of calcium uptake of fish otoliths correspond with macular regions rich of carbonic anhydrase. Advances in Space Research, 38: 1123–1127.

Bignami, S., Enochs, I. C., Manzello, D. P., Sponaugle, S., and Cowen, R. K. (2013). Ocean acidification alters the otoliths of a pantropical fish species with implications for sensory function. Proceedings of the National Academy of Sciences, 110: 7366–7370. doi:10.1073/pnas.1301365110.

Borelli, G., Guibbolini, M. E., Mayer-Gostan, N., Priouzeau, F., De Pontual, H., Allemand, D., Puverel, S., Tambutte, E., and Payan, P. (2003). Daily variations of endolymph composition: relationship with the otolith calcification process in trout. The Journal of experimental biology, 206: 2685–2692.

Bradford, M. M. (1976). A rapid and sensitive method for the quantitation of microgram quantities of protein utilizing the principle of protein-dye binding. Analytical Biochemistry, 72: 248–254. doi:10.1016/0003-2697(76)90527-3.

Campana, S. (1999). Chemistry and composition of fish otoliths: pathways, mechanisms and applications. Marine Ecology Progress Series, 188: 263–297. doi:10.3354/meps188263.

Campana, S. E., and Neilson, J. D. (1985). Microstructure of Fish Otoliths. Canadian Journal of Fisheries and Aquatic Sciences, 42: 1014–1032.

Carvalho, E. S. M., Gregório, S. F., Power, D. M., Canário, A. V. M., and Fuentes, J. (2012). Water absorption and bicarbonate secretion in the intestine of the sea bream are regulated by transmembrane and soluble adenylyl cyclase stimulation. Journal of Comparative Physiology B: Biochemical, Systemic, and Environmental Physiology, 182: 1069–1080.

Checkley, D. M., Dickson, A. G., Takahashi, M., Radich, J. A., Eisenkolb, N., and Asch, R. (2009). Elevated CO2 enhances otolith growth in young fish. Science (New York, N.Y.), 324: 1683.

Chen, Y., Cann, M. J., Litvin, T. N., Iourgenko, V., Sinclair, M. L., Levin, L. R., Buck, J., et al. (2000). Soluble adenylyl cyclase as an evolutionarily conserved bicarbonate sensor. Science (New York, N.Y.), 289: 625–8. doi:10.1126/science.289.5479.625.

Cooper, C. A., Regan, M. D., Brauner, C. J., De Bastos, E. S. R., and Wilson, R. W. (2014). Osmoregulatory bicarbonate secretion exploits H+-sensitive haemoglobins to autoregulate intestinal O2 delivery in euryhaline teleosts. Journal of Comparative Physiology B: Biochemical, Systemic, and Environmental Physiology, 184: 865–876.

Cruz, S., Shiao, J. C., Liao, B. K., Huang, C. J., and Hwang, P. P. (2009). Plasma membrane calcium ATPase required for semicircular canal formation and otolith growth in the zebrafish inner ear. Journal of Experimental Biology, 212: 639–647. doi:10.1242/jeb.022798.

Dijkgraaf, S. (1960). Hearing in Bony Fishes. Proceedings of the Royal Society B-Biological Sciences, 152: 51–54.

Elsdon, T. S., and Gillanders, B. M. (2002). Interactive effects of temperature and salinity on otolith chemistry: challenges for determining environmental histories of fish. Canadian Journal of Fisheries and Aquatic Sciences, 59: 1796–1808. doi:10.1139/f02-154.

Esbaugh, A. J., Heuer, R., and Grosell, M. (2012). Impacts of ocean acidification on respiratory gas exchange and acid-base balance in a marine teleost, *Opsanus beta*. Journal of

Comparative Physiology B: Biochemical, Systemic, and Environmental Physiology, 182: 921–934.

Esbaugh, A. J., Ern, R., Nordi, W. M., and Johnson, A. S. (2016). Respiratory plasticity is insufficient to alleviate blood acid–base disturbances after acclimation to ocean acidification in the estuarine red drum, *Sciaenops ocellatus*. Journal of Comparative Physiology B: Biochemical, Systemic, and Environmental Physiology, 186: 97–109. Springer Berlin Heidelberg.

Esbaugh, A. J., and Cutler, B. (2016). Intestinal Na+, K+, 2Cl-cotransporter 2 plays a crucial role in hyperosmotic transitions of a euryhaline teleost. Physiological Reports, 4: 1–12.

Fairbanks, M. B., Hoffert, J. R., and Fromm, P. O. (1969). The dependence of the oxygen-concentrating mechanism of the teleost eye (*Salmo gairdneri*) on the enzyme carbonic anhydrase. The Journal of general physiology, 54: 203–211.

Furukawa, T., and Ishii, Y. (1967). Neurophysiological studies on hearing in goldfish. Journal of Neurophysiology, 30: 1377–1403.

Georgalis, T., Gilmour, K. M., Yorston, J., and Perry, S. F. (2006). Roles of cytosolic and membrane-bound carbonic anhydrase in renal control of acid-base balance in rainbow trout, *Oncorhynchus mykiss*. American Journal of Physiology - Renal Physiology, 291: 407–421.

Ghanem, T. A., Breneman, K. D., Rabbitt, R. D., and Brown, H. M. (2008). Ionic composition of endolymph and perilymph in the inner ear of the oyster toadfish, *Opsanus tau*. Biological Bulletin, 214: 83–90.

Ibsch, M., Anken, R., Beier, M., and Rahmann, H. (2004). Endolymphatic calcium supply for fish otolith growth takes place via the proximal portion of the otocyst. Cell and Tissue Research, 317: 333–336.

Kwan, G. T., Wexler, J. B., Wegner, N. C., and Tresguerres, M. (2019). Ontogenetic changes in cutaneous and branchial ionocytes and morphology in yellowfin tuna (*Thunnus albacares*) larvae. Journal of Comparative Physiology B: Biochemical, Systemic, and Environmental Physiology, 189: 81–95. Springer Berlin Heidelberg. doi:10.1007/s00360-018-1187-9.

Ladich, F., and Schulz-Mirbach, T. (2016). Diversity in fish auditory systems: one of the riddles of sensory biology. Frontiers in Ecology and Evolution, 4: 1–26. doi:10.3389/fevo.2016.00028.

Lebovitz, R. M., Takeyasu, K., and Fambrough, D. M. (1989). Molecular characterization and expression of the (Na+ + K+)-ATPase alpha-subunit in *Drosophila melanogaster*. The EMBO Journal, 8: 193–202.

Litvin, T. N., Kamenetsky, M., Zarifyan, A., Buck, J., and Levin, L. R. (2003). Kinetic properties of 'soluble' adenylyl cyclase: Synergism between calcium and bicarbonate. Journal of Biological Chemistry, 278: 15922–15926.

Lytle, C., Xu, J. C., Biemesderfer, D., and Forbush, B. (1995). Distribution and diversity of Na-K-Cl cotransport proteins: a study with monoclonal antibodies. The American journal of physiology, 269: C1496–C1505.

Maneja, R. H., Frommel, a. Y., Geffen, a. J., Folkvord, a., Piatkowski, U., Chang, M. Y., and Clemmesen, C. (2013). Effects of ocean acidification on the calcification of otoliths of larval Atlantic cod *Gadus morhua*. Marine Ecology Progress Series, 477: 251–258.

Mayer-Gostan, N., Kossmann, H., Watrin, A., Payan, P., and Boeuf, G. (1997). Distribution of ionocytes in the saccular epithelium of the inner ear of two teleosts (*Oncorhynchus mykiss* and *Scophthalmus maximus*). Cell and Tissue Research, 289: 53–61.

Michael, K., Kreiss, C. M., Hu, M. Y., Koschnick, N., Bickmeyer, U., Dupont, S., Pörtner, H. O., and Lucassen, M. (2016). Adjustments of molecular key components of branchial ion and pH regulation in Atlantic cod (*Gadus morhua*) in response to ocean acidification and warming. Comparative Biochemistry and Physiology Part - B: Biochemistry and Molecular Biology, 193: 33–46. doi:10.1016/j.cbpb.2015.12.006.

Mugiya, Y., and Yoshida, M. (1995). Effects of Calcium Antagonists and Other Metabolic on in Vitro Calcium Deposition on Otoliths Rainbow Trout *Oncorhynchus mykiss*. Fisheries (Bethesda), 61: 1026–1030.

Munday, P. L., Hernaman, V., Dixson, D. L., and Thorrold, S. R. (2011). Effect of ocean acidification on otolith development in larvae of a tropical marine fish. Biogeosciences, 8: 1631–1641. doi:10.5194/bg-8-1631-2011.

Murayama, E., Takagi, Y., Ohira, T., Davis, J. G., Greene, M. I., and Nagasawa, H. (2002). Fish otolith contains a unique structural protein, otolin-1. European Journal of Biochemistry, 269: 688–696.

Nelson, J., Hanson, C. W., Koenig, C., and Chanton, J. (2011). Influence of diet on stable carbon isotope composition in otoliths of juvenile red drum *Sciaenops ocellatus*. Aquatic Biology, 13: 89–95.

Nicolas, M.-T., Demêmes, D., Martin, A., Kupershmidt, S., and Barhanin, J. (2001). KCNQ1/KCNE1 potassium channels in mammalian vestibular dark cells. Hearing Research, 153: 132–145. doi:10.1016/S0378-5955(00)00268-9.

Pannella, G. (1971). Fish Otoliths : Daily Growth Layers and Periodical Patterns. Science, 173: 1124–1127.

Payan, P., Kossmann, H., Watrin, a, Mayer-Gostan, N., and Boeuf, G. (1997). Ionic composition of endolymph in teleosts: origin and importance of endolymph alkalinity. The Journal of experimental biology, 200: 1905–1912.

Payan, P., Edeyer, A., de Pontual, H., Borelli, G., Boeuf, G., and Mayer-Gostan, N. (1999). Chemical composition of saccular endolymph and otolith in fish inner ear: lack of spatial uniformity. The American journal of physiology, 277: R123–R131.

Payan, P., Borelli, G., Priouzeau, F., De Pontual, H., Boeuf, G., and Mayer-Gostan, N. (2002). Otolith growth in trout *Oncorhynchus mykiss*: supply of Ca2+ and Sr2+ to the saccular endolymph. The Journal of experimental biology, 205: 2687–2695.

Payan, P., De Pontual, H., Bœuf, G., and Mayer-Gostan, N. (2004). Endolymph chemistry and otolith growth in fish. Comptes Rendus Palevol, 3: 535–547. doi:10.1016/j.crpv.2004.07.013.

Pelster, B. (2001). The Generation of Hyperbaric Oxygen Tensions in Fish. Physiology, 16: 287–291. doi:10.1152/physiologyonline.2001.16.6.287.

Pimentel, M. S., Faleiro, F., Dionisio, G., Repolho, T., Pousao-Ferreira, P., Machado, J., and Rosa, R. (2014). Defective skeletogenesis and oversized otoliths in fish early stages in a changing ocean. J Exp Biol, 217: 2062–2070. doi:10.1242/jeb.092635.

Pisam, M., Payan, P., LeMoal, C., Edeyer, A., Boeuf, G., and Mayer-Gostan, N. (1998). Ultrastructural study of the saccular epithelium of the inner ear of two teleosts, *Oncorhynchus mykiss* and *Psetta maxima*. Cell and Tissue Research, 294: 261–270.

Qin, Z., Lewis, J. E., and Perry, S. F. (2010). Zebrafish (*Danio rerio*) gill neuroepithelial cells are sensitive chemoreceptors for environmental CO2. Journal of Physiology, 588: 861–872.

Radtke, R. L., Lenz, P., Showers, W., and Moksness, E. (1996). Environmental information stored in otoliths: insights from stable isotopes. Marine Biology, 127: 161–170. doi:10.1007/BF00993656.

Roa, J. N., Munévar, C. L., and Tresguerres, M. (2014). Feeding induces translocation of vacuolar proton ATPase and pendrin to the membrane of leopard shark (*Triakis semifasciata*) mitochondrion-rich gill cells. Comparative Biochemistry and Physiology -Part A : Molecular and Integrative Physiology, 174: 29–37. Elsevier Inc. doi:10.1016/j.cbpa.2014.04.003.

Roa, J. N., and Tresguerres, M. (2016). Soluble adenylyl cyclase is an acid-base sensor in epithelial base-secreting cells. American Journal of Physiology - Cell Physiology, 311: C340–C349. doi:10.1152/ajpcell.00089.2016.

Roa, J. N., and Tresguerres, M. (2017). Bicarbonate-sensing soluble adenylyl cyclase is present in the cell cytoplasm and nucleus of multiple shark tissues. Physiological Reports, 5: e13090. doi:10.14814/phy2.13090.

Rummer, J. L., McKenzie, D. J., Innocenti, A., Supuran, C. T., and Brauner, C. J. (2013). Root Effect Hemoglobin May Have Evolved to Enhance General Tissue Oxygen Delivery. Science, 340: 1327–1329. doi:10.1126/science.1233692.

Saitoh, S. (1990). Localization and ultrastructure of mitochondria-rich cells in the inner ears of goldfish and tilapia. Journal of Icthyology, 37: 49–55.

Schade, F. M., Clemmesen, C., and Mathias Wegner, K. (2014). Within- and transgenerational effects of ocean acidification on life history of marine three-spined stickleback (*Gasterosteus aculeatus*). Marine Biology, 161: 1667–1676.

Shen, S. G., Chen, F., Schoppik, D. E., and Checkley, D. M. (2016). Otolith size and the vestibulo-ocular reflex of larvae of white seabass *Atractoscion nobilis* at high pCO2. Marine Ecology Progress Series, 553: 173–182.

Shiao, J. C., Lin, L. Y., Horng, J. L., Hwang, P. P., and Kaneko, T. (2005). How can teleostean inner ear hair cells maintain the proper association with the accreting otolith? Journal of Comparative Neurology, 488: 331–341.

Swearer, S. E., Caselle, J. E., Lea, D. W., and Warner, R. R. (1999). Larval retention and recruitment in an island population of a coral-reef fish. Nature, 402: 799–802.

Takagi, Y. (1997). Meshwork arrangement of mitochondria-rich, Na+,K+-ATPase-rich cells in the saccular epithelium of rainbow trout (*Oncorhynchus mykiss*) inner ear. Anatomical Record, 248: 483–489.

Takagi, Y. (2002). Otolith formation and endolymph chemistry: A strong correlation between the aragonite saturation state and pH in the endolymph of the trout otolith organ. Marine Ecology Progress Series, 231: 237–245.

Thomas, O. R. B., Swearer, S. E., Kapp, E. A., Peng, P., Tonkin-Hill, G. Q., Papenfuss, A., Roberts, A., Bernard, P., and Roberts, B. R. (2019). The inner ear proteome of fish. FEBS Journal, 286: 66–81.

Tohse, H., and Mugiya, Y. (2001). Effects of enzyme and anion transport inhibitor on in vitro incorporation of inorganic carbon and calcium into endolymph and otoliths in salmon *Oncorhynchus masou*. Comparative Biochemistry and Physiology - A Molecular and Integrative Physiology, 128: 177–184.

Tohse, H., Ando, H., and Mugiya, Y. (2004). Biochemical properties and immunohistochemical localization of carbonic anhydrase in the sacculus of the inner ear in the salmon *Oncorhynchus masou*. Comparative Biochemistry and Physiology - A Molecular and Integrative Physiology, 137: 87–94.

Tohse, H., Murayama, E., Ohira, T., Takagi, Y., and Nagasawa, H. (2006). Localization and diurnal variations of carbonic anhydrase mRNA expression in the inner ear of the rainbow

trout *Oncorhynchus mykiss*. Comparative biochemistry and physiology. Part B, Biochemistry & molecular biology, 145: 257–64. doi:10.1016/j.cbpb.2006.06.011.

Tohse, H., and Mugiya, Y. (2008). Sources of otolith carbonate: experimental determination of carbon incorporation rates from water and metabolic CO2, and their diel variations. Aquatic Biology, 1: 259–268. doi:10.3354/ab00029.

Tresguerres, M., Katoh, F., Fenton, H., Jasinska, E., and Goss, G. G. (2005). Regulation of branchial V-H(+)-ATPase, Na(+)/K(+)-ATPase and NHE2 in response to acid and base infusions in the Pacific spiny dogfish (*Squalus acanthias*). The Journal of Experimental Biology, 208: 345–54. doi:10.1242/jeb.01382.

Tresguerres, M., Buck, J., and Levin, L. R. (2010a). Physiological carbon dioxide, bicarbonate, and pH sensing. Pflugers Archiv European Journal of Physiology, 460: 953–964.

Tresguerres, M., Levin, L. R., Buck, J., and Grosell, M. (2010b). Modulation of NaCl absorption by [HCO3-] in the marine teleost intestine is mediated by soluble adenylyl cyclase. AJP: Regulatory, Integrative and Comparative Physiology, 299: R62–R71. doi:10.1152/ajpregu.00761.2009.

Tresguerres, M., Parks, S. K., Salazar, E., Levin, L. R., Goss, G. G., and Buck, J. (2010c). Bicarbonate-sensing soluble adenylyl cyclase is an essential sensor for acid/base homeostasis. Proceedings of the National Academy of Sciences of the United States of America, 107: 442–447.

Tresguerres, M. (2014). sAC from aquatic organisms as a model to study the evolution of acid/base sensing. Biochimica et Biophysica Acta - Molecular Basis of Disease, 1842: 2629–2635. Elsevier B.V. doi:10.1016/j.bbadis.2014.06.021.

von Biela, V., Newsome, S., and Zimmerman, C. (2015). Examining the utility of bulk otolith δ13C to describe diet in wild-caught black rockfish *Sebastes melanops*. Aquatic Biology, 23: 201–208. doi:10.3354/ab00621.

Watanabe, K., and Ogawa, A. (1984). Carbonic anhydrase activity in stria vascularis and dark cells in vestibular labyrinth. Annals of Otology, Rhinology & Laryngology, 93: 262–266.

Wilson, J. M., Randall, D. J., Donowitz, M., Vogl, A. W., and Ip, A. K. (2000). Immunolocalization of ion-transport proteins to branchial epithelium mitochondria-rich cells in the mudskipper (*Periophthalmodon schlosseri*). The Journal of Experimental Biology, 203: 2297–2310.

Wilson, J. M., Whiteley, N. M., and Randall, D. J. (2002). Ionoregulatory changes in the gill epithelia of coho salmon during seawater acclimation. Physiological and biochemical zoology : PBZ, 75: 237–49. doi:10.1086/341817.

Zdebik, A. A., Wangemann, P., and Jentsch, T. J. (2009). Potassium ion movement in the inner ear: Insights from genetic disease and mouse models. Physiology, 24: 307–316.

CHAPTER VII

Responses of Splitnose Rockfish (*Sebastes diploproa*) gill and inner ionocytes to hypercapnia

Introduction

The Splitnose Rockfish can be found along the eastern Pacific Ocean between the northern Gulf of Alaska to Baja California. Splitnose Rockfish mature between 6 - 9 years old, and the species is known to live up to 103 years old (Love et al., 2002; Cope, 2009). Year-of-the-young are often found hiding among kelp in the surface ocean, but eventually settle on the ocean bottom by the end of their first year (Love et al., 2002). Similar to other *Sebastes*, Splitnose Rockfish move to deeper water with increasing size and age. Adults are most commonly found between 215 to 350 meters, though they have been caught between 91 and 795 meters (Cope, 2009). Given its life history, the Splitnose Rockfish is sporadically exposed to upwelling as larvae and year-of-the-young – and chronically exposed to upwelling conditions as adults.

Upwelling is an oceanographic process that shoals the deeper high-CO_2 low pH, oxygen-poor, and colder water towards the surface (Rykaczewski and Checkley, 2008; Checkley and Barth, 2009). Upwelling events in the California Current System can last days to weeks at a time, and CO_2 and pH levels at 17 meters deep can sharply fall from 353 to 1016 μatm and 8.1 to 7.67, respectively (Hofmann et al., 2011; Frieder et al., 2012). As a result, coastal pelagic species such as the year-of-the-young Splitnose Rockfish often encounter acute high-CO_2 low pH stress. Furthermore, deeper seawater (~100 – 1,000 meters) along the Eastern Pacific also has a high-CO_2 low pH signature, with pH reaching as low as ~7.5 (Culberson and Pytkowicz, 1970; Levin, 2003; Nam et al., 2011). As a result, adult Splitnose Rockfish living at a depth below ~100 meters are chronically exposed to high-CO_2 low pH conditions (Nam et al., 2011). Given their life history, the Splitnose Rockfish is likely naturally adapted to high-CO_2 low pH conditions.

Over the past decade, there has been a spike in research on the effects of ocean acidification (OA) on marine organisms. OA is caused by the ocean's absorption of

anthropogenically generated CO_2 in the atmosphere. Projection of future surface ocean pH and pCO_2 predicts the average surface ocean pH will drop from ~8.0 (~400 μatm CO_2) to ~7.7 (~1,000 μatm CO_2) and ~7.4 (~2,000 μatm CO_2) by 2100 and 2300, respectively (Caldeira and Wickett, 2003, 2005). Exposure to such high-CO_2 conditions can induce acidosis in the internal fluids of marine organisms, potentially affecting multiple physiological functions and impairing fitness and survival. However, teleost fishes have a great capacity to regulate blood acid-base even when exposed to extremely high-CO_2 conditions (reviewed in Ishimatsu et al., 2008). For example, marine teleosts raised within recirculating aquaculture systems are sometimes chronically exposed to 30,000 μatm CO_2 (pH ~6.4) or even higher (Blancheton, 2000; Petochi et al., 2011; Fivelstad et al., 2015; reviewed in Ellis et al., 2016), and are still able to regulate blood pH (reviewed in Ishimatsu et al., 2008). This raises questions on whether OA poses a real threat to marine teleosts.

Does H^+ secretion increase energetic investment?

During high-CO_2 low pH exposure, marine teleosts must secrete H^+ into surrounding seawater to maintain internal blood pH homeostasis. However, H^+ secretion may be energetically costly since it is driven by ATPase enzymes, and because it may require the synthesis of new proteins. Furthermore, epithelial H^+ secretion typically takes place in concert with HCO_3^- accumulation in the plasma. This increased [HCO_3^-] within the plasma may induce downstream negative effects in its internal tissues throughout the body.

In marine teleosts, the Na^+/K^+-ATPases (NKA) rich gill ionocyte is proposed to be the site of H^+ secretion. Briefly, the abundant NKA enzyme located in the highly infolded basolateral membrane generates a low [Na^+] within the ionocyte, which drives H^+ secretion into

seawater in exchange for Na^+ via apical Na^+/H^+ exchangers (NHE) (reviewed in Hirose et al., 2003; Evans et al., 2005). To counteract blood acidosis, marine teleosts use this NKA-driven process to remove excess H^+ and accumulate HCO_3^- in the plasma (reviewed in Claiborne et al., 2002; Evans et al., 2005). Therefore, one frequent measurement of energy expenditure involved in H^+ secretion is estimated with relative NKA abundance in gill homogenate. In two previous studies on the Atlantic Cod (*Gadus morhua*), differences in relative NKA abundance was insignificant despite a 4-week exposure to 1,200 and 2,200 μatm (Michael et al., 2016), or a 4-month exposure to 3,000 μatm of CO_2 (Melzner et al., 2009a). However, relative NKA abundance was significantly higher in Atlantic Cod after a 12-month exposure to 6,000 μatm (Melzner et al., 2009a), and in Benthic Eelpout (*Zoarces viviparous*) after a 2-day exposure to 10,000 μatm of CO_2 (Deigweiher et al., 2008). These results suggest one of two possibilities: either marine teleosts are not stressed by lower CO_2 exposure (1,200 to 3,000 μatm of CO_2), or detecting a difference in energy expenditure within NKA-rich ionocytes may be more nuanced than previously anticipated.

One reason why NKA activity and abundance do not readily reflect increased acid-secretion may be because of the other role(s) the NKA-rich ionocyte performs. In addition to H^+ secretion, the marine teleost's NKA-rich gill ionocyte is known to consume a great deal of energy to secrete NaCl against the gradient (Keys, 1931; Keys and Willmer, 1932; reviewed in Evans et al., 2005). Briefly, the NKA-rich ionocyte works in concert with basolateral $Na^+/K^+/Cl^-$ co-transporters and apical Cl^- channels to secrete NaCl into surrounding seawater (reviewed in Hirose et al. 2003; Evans et al. 2005). Because both H^+ and NaCl secretion depend on the same electrochemical gradient, the energy necessary to maintain proper plasma osmolarity may mask any increase in H^+ secretion.

Another possibility is that H^+ secretion is upregulated within another type of ATPase such as the vacuolar-type H^+-ATPase (VHA). VHA has been shown to be co-localized within the NKA-rich ionocyte, and was previously proposed to translocate to the apical membrane to secrete H^+ (Allmon and Esbaugh, 2017). Yet despite an acute exposure to 30,000 μatm of CO_2, VHA remained within the cytoplasm (Allmon and Esbaugh, 2017). Other measurements of VHA responses were yielded conflicting results. Previous measurements detected significantly higher relative VHA abundance after exposure to 1,200 μatm, but not after exposure to 2,200 μatm of CO_2 (Michael et al., 2016). Furthermore, relative mRNA expression increased in most (but not all) higher CO_2 treatments (Michael et al., 2016; Allmon and Esbaugh, 2017). Altogether, while it may be possible that VHA contributes to H^+ secretion, its current role remains unknown.

Morphological changes in the apical opening may be another high-CO_2 low pH response that is independent of additional NKA synthesis. In response to ~30,000 μatm of CO_2 (pH 6.41), the apical opening of Japanese Flounder (*Paralichthys olivaceus*) gill ionocytes expressed numerous extended microvilli after a 24-hour exposure (Hayashi et al., 2013). This increase in apical surface area may be another method to facilitate H^+ secretion without increasing NKA investment. To date, no OA study has investigated the ionocyte's apical opening after exposure to near-future CO_2 levels.

Does the inner ear respond to the accumulated [HCO_3^-] in the blood plasma?

Another OA-relevant concern is the effects of increased [HCO_3^-] within the blood plasma on internally-facing organs such as the inner ear. Many previous studies have found significantly larger $CaCO_3$ otoliths under high-CO_2 low pH conditions, and have attributed the cause to the increased [HCO_3^-] within the blood plasma (reviewed in Heuer and Grosell, 2014). This was

concerning as an oversized otolith could impede proper sensing of balance and hearing (Heuer and Grosell, 2014).

However, otolith calcification occurs within the endolymph of the inner ear, an organ that has the capacity to regulate the fluids (and by extension, calcification). Furthermore, many OA studies have reported no significant differences in otolith size (Munday et al., 2011a; Simpson et al., 2011; Franke and Clemmesen, 2011; Frommel et al., 2013; Maneja et al., 2013; Schade et al., 2014; Perry et al., 2015; Sundin et al., 2019) – suggesting the inner ear may have some control over its otolith calcification process. In one such study, 7-day old larval Cod exposed to high-CO_2 low pH conditions (1,800 and 4,200 μatm) initially had significantly larger lapilli and sagittae otoliths compared to control (Maneja et al., 2013). But while the lapilli otolith remains significantly different after 46 days (albeit the magnitude is minuscule), the sagittae otolith within 46-day old larval cod was not significantly different despite roughly 5 and 11-fold difference in CO_2 exposure (Maneja et al., 2013). Therefore, given the importance of sensing balance and hearing, it is likely that the inner ear would protect itself against oversized otolith calcification. However, it is currently unknown how this response would be manifested.

In Chapter V of this dissertation, two types of inner ear ionocytes have been characterized (Kwan et al., *in review*). Briefly, the NKA-rich ionocyte contains abundant Na^+-K^+-Cl^--co-transporter, and is proposed to secrete K^+ into the endolymph for proper sensory function (Kwan et al., *in review*). On the other hand, the VHA-rich ionocyte contains abundant carbonic anhydrase, and may be transporting HCO_3^- into the endolymph (Kwan et al., *in review*). Because an oversized otolith could cause sensory problems, the inner ear ionocytes may respond by slowing calcification by limiting HCO_3^- transport. To the best of our knowledge, no study has yet quantified inner ear NKA or VHA in responses to hypercapnia.

Objective

The objective of this study was to examine whether both gill and inner ear ionocytes respond to high-CO_2 low pH condition in the Splitnose Rockfish. This was achieved by exposing adult Splitnose Rockfish to 3 days of hypercapnic conditions (pH ~7.5, ~1,600 μatm of CO_2) – which is equivalent to the surface ocean pH level predicted to occur before 2300 as well as the normal environment experienced by current adult Splitnose Rockfish. Subsequent western blotting, immunohistochemistry, and scanning electron microscopy of gill and inner ear tissue were used to quantify protein abundance, estimate intra-cellular protein translocation and ionocyte abundance, and assess apical morphology, respectively.

Methods

The following experiments were approved by the SIO-UCSD animal care committee under protocol no. S10320 in compliance with the IACUC guidelines for the care and use of experimental animals. All animals were collected under permit (#SCP13227) issued by the California Department of Fish and Wildlife.

Young-of-the-year Splitnose Rockfish were caught from drifting kelp paddies off the shores of La Jolla and raised in the Hubbs Experimental Aquarium (La Jolla, USA). The animals were fed frozen market squids and EWOS food pellet (Cargill Incorporated, Minneapolis, MN, USA), and raised in a flow-through system with seawater continuously pumped from the Scripps Coastal Reserve for >2 years. An additional adult Splitnose Rockfish was caught with bottom trawls at a depth of ~340 meters (May 2018; trawl in: 32º 40.88'N 117º 23.50'W, trawl out: 32º

43.27'N 117º 22.09'W) and examined with immunohistochemistry to compare with lab reared specimens.

The header tanks were also pumped with seawater from the Scripps Coastal Reserve, where the IKS Aquastar system (Karlsbad, Germany) monitored and continuously recorded the temperature and pH values. The control header tank was not manipulated, whereas the treatment header tank was bubbled with CO_2 to maintain a pH of 7.5. Each header tank supplied water to two 20-liter experimental tanks (0.3 liter min^{-1}) housing one individual. The experiment tanks were opaque, and the lids covered to limit atmospheric exposure and slow CO_2 degassing. Experimental tanks were randomly arranged and located on a shelf directly below the header tanks. Electrodes were calibrated at least once every 48 hours. Animals were not fed for at least 24 hours prior to experiment, nor were they fed during the experimental trial.

Splitnose Rockfish (total length: 11.88 ± 0.29 cm; weight: 42.86 ± 2.79; n=24) were given 12 hours of acclimation to the experimental chamber prior to exposure trials. There were no significant differences in length (p=0.7188) or weight (p=0.9202) between the two treatments. On the following morning, organisms were exposed to 72 hours of control or high-CO_2 low pH conditions. Seawater acid-base chemistry in the experiments was monitored using multiple methods: 1) pH in the header tanks and in the outflow of two fish tanks were recorded every 2 minutes using electrodes the IKS Aquastar System, 2) pH in the header tanks were measured once a day using a handheld pH meter (HACH HQ40D with PHC101) that was calibrated immediately prior to the measurements, and 4) discrete seawater samples from the header tanks were collected at the beginning and end of each experiment, and analyzed by the Dickson Lab (Scripps Institution of Oceanography) for pH, total alkalinity, and salinity (Table 7.1).

On sampling day, fish were anesthetized with tricaine mesylate (0.2 g/L) buffered with NaOH to match the seawater pH of the control or high CO_2 treatments. To minimize stress, this was performed by stopping the inflow of seawater, pouring an aliquot of concentrated anesthetic stock through an opening in the lid, and closing the outflow. The fish usually loses within 5 minutes, and blood was drawn with a heparinized syringe for pH and total CO_2 measurements to calculate [HCO_3^-]. Next, the fish was promptly euthanized by spinal pithing and gill and inner ear was sampled as follows: the first right gill arch was fixed for immunohistochemistry, the first left gill arch was fixed for scanning electron microscopy (SEM), and the second right and left gill arches were flash frozen in liquid nitrogen for Western blots. Because each fish has only two inner ear organs, samples were divided across the three analysis: flash frozen for western blot or fixed for immunohistochemistry or scanning electron microscopy.

Table 7.1: Water and blood chemistry during Splitnose Rockfish hypercapnic exposure experiments. *denotes significance at an α level set at $p<0.05$. Data presented as mean ± s.e.m.

	Control	**Hypercapnia**
pH	7.84 ± 0.03	7.49 ± 0.01 *
Alkalinity (μmol kgSW−1)	2216.78 ± 1.84	2216.70 ± 1.68
Salinity (ppt)	33.52 ± 0.02	33.36 ± 0.04
Temperature (°C)	18.77 ± 0.86	18.75 ± 0.85
pCO_2	663.84 ± 50.07	1591.56 ± 18.58 *
Blood pH	7.46 ± 0.05	7.36 ± 0.08
tCO2	5.84 ± 0.29	7.68 ± 0.57 *
[HCO_3^-]	4.28 ± 0.46	6.09 ± 1.16

Antibodies

Na^+/K^+-ATPase was immunodetected using a monoclonal α5 mouse antibody raised against the α-subunit of chicken NKA (a5, Developmental Studies Hybridoma Bank, Iowa City,

IA, USA; Lebovitz et al., 1989). This antibody specifically recognizes NKA α-subunits from multiple elasmobranch and teleost fishes including Leopard Shark (*Triakis semifasciata*; Roa et al 2014; Roa and Tresguerres 2017), Yellowfin Tuna (*Thunnus albacares*; Kwan et al., 2019), Coho Salmon (*Oncorhynchus kitsutch*; Wilson et al. 2002), Blue-Green Damselfish (*Chromis viridis*; Tang et al. 2014), Giant Mudskipper (*Periophthalmondon schlosseri*; Wilson et al. 2000), Pacific Chub Mackerel (*Scomber japonicus*; Kwan et al., *in review*), among others.

Vacuolar H^+-ATPase was immunodetected using a custom-made rabbit polyclonal antibody against the β-subunit conserved from cnidarians to mammals (epitope: AREEVPGRRGFPGY; GenScript, Piscataway, USA) that recognized VHA in multiple invertebrate (Tresguerres et al., 2013; Barott et al., 2015b; Hill et al., 2018) and vertebrate tissues (Roa et al., 2014; Roa and Tresguerres, 2017; Kwan et al., *in review*). Peptide preabsorption with excess peptide (1:5 antibody to peptide ratio on a molar basis; incubated overnight at 4°C on shaker) was performed to verify antibody specificity.

Mitochondria were immunolabeled using a mouse monoclonal antibody against cytochrome oxidase (complex V) (MTC02, catalog #: MA5-12017, Invitrogen, Grand Island, New York, USA); this antibody demonstrates specificity against a broad range of species including coral (Barott et al., 2015a), shark (Roa et al., 2014), and Pacific Chub Mackerel (Kwan et al., *in review*). The mouse monoclonal anti-NKCC antibody T4 (Lytle et al., 1995) was obtained from DSHB; and has been widely used to detect NKCC in fish tissues (Tresguerres et al., 2010b; Esbaugh and Cutler, 2016), including Zebrafish saccular epithelium (Abbas and Whitfield, 2009) and Pacific Chub Mackerel (Kwan et al., *in review*). Rabbit polyclonal antibodies against human CA II were purchased from Rockland Inc., Gilbertsville, USA (catalog #: 100-401-136); these antibodies are routinely used to immunodetect CA from teleost fishes

[e.g. (Georgalis *et al.*, 2006; Qin *et al.*, 2010], including in the saccular epithelium of Masu Salmon (*Oncorhynchus masou*) (Tohse et al., 2004) and Pacific Chub Mackerel (Kwan et al., *in review*).

The primary antibodies were detected using the following secondary antibodies: goat anti-mouse IgG-HRP or goat anti-rabbit IgG-HRP conjugate (Bio-Rad, Hercules, CA, USA) for western blot, and goat anti-mouse Alexa Fluor 546 and goat anti-rabbit Alexa Fluor 488 (Invitrogen, Grand Island, USA) for immunohistochemistry.

Western Blotting and Total Protein Analysis

Frozen tissue samples were immersed in liquid nitrogen, pulverized in a porcelain grinder, and submerged within an ice-cold, protease inhibiting buffer (250 mmol l^{-1} sucrose, 1 mmol l^{-1} EDTA, 30 mmol l^{-1} Tris, 10 mmol l^{-1} benzamidine hydrochloride hydrate, 200 mmol l^{-1} phenylmethanesulfonyl fluoride, 1 mol l^{-1} dithiothreitol, pH 7.5). Debris was removed from the samples at low speed centrifugation (3000xg, 10 minutes, 4°C), and the resulting supernatant was considered the crude homogenate. A subset of this crude homogenate was further subjected to a medium speed centrifugation (21130xg, 10 minutes, 4°C), and the supernatant and pellet were saved as cytoplasmic- and membrane-enriched fractions, respectively. If enough samples were available, total protein concentration was determined by the Bradford assay (Bradford, 1976). Samples were mixed with an equal volume of 90% 2x Laemmli buffer and 10% β-mercaptoethanol, and heated at 70°C for 5 minutes. Proteins (crude homogenate: 5 µg per lane; membrane: 2 µg per lane) were loaded onto a 7.5% polyacrylamide mini gel (Bio-Rad, Hercules, CA, USA) – alternating between control and high CO_2 treatments to avoid possible gel lane effects. The gel ran at 200 volts for 40 minutes, then transferred to a polyvinylidene difluoride

(PVDF) membrane using a wet transfer cell (Bio-Rad) at 100 mAmps at 4°C overnight. PVDF membranes were then incubated in tris-buffered saline with 1% tween (TBS-T) with milk powder (0.1 g/mL) at RT for 1 hour, then incubated with primary antibody (NKA: 10.5 ng/ml; VHA: 3 µg/ml) in blocking buffer at 4°C overnight. On the following day, PVDF membranes were washed in TBS-T (three times; 10 minutes each), incubated in blocking buffer with anti-rabbit secondary antibodies (1:10,000) at RT for 1 hour, and washed again in TBS-T (three times; 10 minutes each). Bands were made visible through addition of ECL Prime Western Blotting Detection Reagent (GE Healthcare, Waukesha, WI) and imaged and analyzed in a BioRad Universal III Hood using Image Lab software (version 6.0.1; BioRad). PVDF membranes were then Ponceau stained for 10 minutes, and re-imaged in the BioRad Universal III Hood, and analyzed with its Image Lab software.

In an effort to control for differences in protein loading, the same PVDF membrane was used for both VHA and NKA analysis, and their signal were normalized by their respective Ponceau signal. Existing antibody signal on the PVDF membrane was removed with stripping buffer (50 mM Tris, 1% SDS, 0.7% β-mercaptoethanol, pH 8), incubated for 10 minutes at 60°C, washed in DI water 15 minutes (three times; 15 minutes each) at RT, re-incubated in blocking at RT for 1 hour, and re-incubated in primary antibody at 4°C overnight. The next day, the membrane was washed in TBS-T (three times; 10 minutes each), incubated in blocking buffer with anti-mouse secondary antibodies (1:10,000) at RT for 1 hour, washed in TBS-T (three times; 10 minutes each), and imaged.

Immunohistochemistry and Gill Ionocyte Analysis

Splitnose Rockfish gill and inner ear tissues were fixed in 4% paraformaldehyde mixed in phosphate buffer saline (PBS) on a shaker at 4°C overnight. Samples were then dehydrated in 50% for 8 hours, then stored in 70% ethanol until processing. Fixed Splitnose Rockfish tissue were rinsed in PBS + 0.1% tween (PBS-T) at room temperature (RT) for 5 minutes, rinsed in ice-cold PBS with sodium borohydride (0.5 – 1.5 mg/mL; six times; 10 minutes each), incubated in blocking buffer (PBS-T, 0.02% normal goat serum, 0.0002% keyhole limpet hemocyanin) at RT for one hour, and with the primary antibodies (NKA: 40 ng/mL; VHA: 6 µg/mL) at RT overnight. On the following day, samples were washed in PBS-T (three times at RT; 10 minutes each), and incubated with fluorescent secondary antibodies (1:500) and counterstained with DAPI (1 µg/mL) at RT for 1 hour. Samples were washed in PBS-Tx (three times at RT; 10 minutes each), and imaged on an inverted confocal microscope (Zeiss LSM 800 with Zeiss ZEN 2.6 blue edition software; Cambridge, United Kingdom).

Following immunostaining and imaging, ionocyte distributions were estimated from the lamellae across three filament regions (lower, middle, and upper with respect to the branchial arch). Ionocytes were counted along the lamellar blood space. Additionally, the ionocyte size and the lamellar area were estimated using FIJI (Schindelin et al., 2012). In images where more than five lamellae were captured, we numbered individual lamella and used R (R Development Core Team, 2013) to randomly choose five lamellae to analyze. A total of 18 fish was analyzed, with five lamellae counted per region, three region per fish.

Scanning Electron Microscopy and Apical Morphology Analysis

Splitnose Rockfish gill and inner ear epithelium tissues were fixed in 3% paraformaldehyde and 0.35% glutaraldehyde in 0.1M cacodylate buffer overnight at 4°C. The samples were then dehydrated in 50% for 8 hours, then stored in 70% ethanol until processing. Samples were imaged using SEM following protocols described in Wegner et al. (2013) & Kwan et al. (2019). Briefly, fixed samples were dehydrated to 100% tert-butyl alcohol in 25% increments over 24 hours, frozen in 100% tert-butyl alcohol at 4°C, and freeze dried using a VirTis benchtop freeze dryer (SP Industries, Gardiner, New York). Samples were then sputter-coated with gold and viewed using a FEI Quanta 600 SEM (FEI, Hillsboro, USA) under high-vacuum mode.

The apical morphology of gill lamellar ionocytes was examined and imaged (5 lamellae per fish; n = 8 control; n = 9 high-CO_2). To ensure an unbiased analysis of apical morphology, the random assignment and apical morphology analysis were performed by different authors. The images taken by GK were sent to KJP to be recorded and renamed. Renamed images were then analyzed by MT, who determined whether the ionocytes had extended microvilli. This data was then re-organized by KJP, before statistical analysis by GK and MT.

Statistical Analysis

The Shapiro-Wilk normality test was used to assess normality. Outliers were identified using the robust regression followed by outlier identification (ROUT) method (Q = 10%), and removed from the analysis. In the Western blot analysis, ROUT detected one outlier (crude homogenate; 1 high CO_2) in the NKA immunoblot and three outliers (membrane fraction; 1

control; 2 high CO_2) in the VHA immunoblot. These outliers were removed from the statistical analysis. No outliers were detected in the inner ear immunoblots.

Additionally, apical morphology data was converted to a percentage via arcsine and square root transformation prior to analysis. If the assumptions of normality are met, then the unpaired t-test ($\alpha = 0.05$; two-tailed) or one-way ANOVA ($\alpha = 0.05$; two-tailed) was used to compare between the control and high CO_2 treatments. All values are expressed as means with standard error of the mean.

Results

Antibody Specificity

The specificity of the NKA and VHA antibodies in Splitnose Rockfish gill and inner ear tissues were verified with western blotting. Both NKA and VHA of rockfish gill and inner tissues yielded a single band at ~100 and ~53 kDA, respectively. For VHA, no signal was detected following peptide pre-absorption treatment (Supplementary Figure 7.1).

Gill NKA and VHA Protein Abundance

There were no differences in NKA abundance between treatments in the gill crude homogenate fractions (p=0.4778; Supplementary Figure 2A); however, NKA abundance in membrane-enriched fractions was ~50% significantly higher in the high-CO_2 treatment (n=9 control; n=8 low-pH; p=0.0215; Figure 7.1A). VHA abundance in the crude homogenate fraction was below the level of detection in both treatments. Although VHA was detectable in membrane enriched fractions, its abundance did not significantly vary between treatments (n=8 control; n=7 low-pH; p=0.1695; Figure 7.1B).

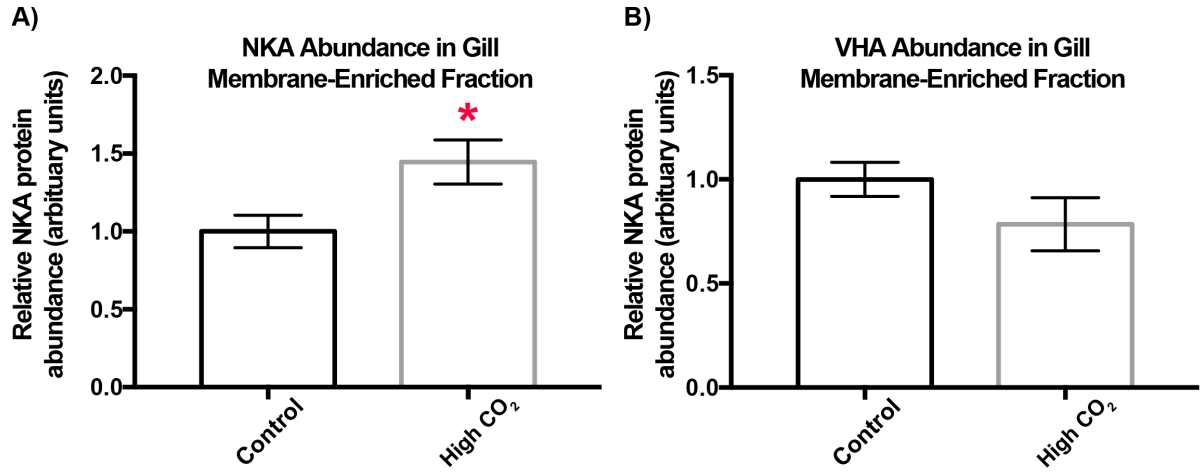

Figure 7.1: Relative Na^+/K^+-ATPase (NKA) and vacuolar-type H^+ ATPase (VHA) abundance in Splitnose Rockfish gill membrane fraction. Effects of high-CO_2 low pH conditions on the abundance of NKA and VHA in the gill membrane fraction. **A)** NKA abundance was significantly higher in high CO_2 exposed fish (n=9 control; n=8 low-pH; p=0.0215), whereas **B)** VHA abundance was not significantly different (n=8 control; n=7 low-pH; p=0.1695). *denotes significance at an α level set at $p<0.05$. Values are mean ± S.E.M.

Gill Ionocyte Characterization and Distribution

The gill of Splitnose Rockfish contains numerous NKA-rich ionocytes. Within the NKA-rich ionocyte, abundant NKA was detected in the highly infolded basolateral membrane, whereas VHA appears to be in cytoplasmic vesicles as its signal does not overlap with the basolateral NKA signal nor the apical membrane. No differences in VHA immunolocalization was detected between the control (Figure 7.2A, B, C) and high-CO_2 low pH treatment (Figure 7.2D, E, F). NKA-rich ionocytes were notably absent from the leading edge, but abundantly present along the trailing edge of the gill. While some NKA-rich ionocytes were detected on the gill filament, most of the NKA-rich ionocytes were present along the basal portion of the lamellae, and extending up to 20 – 50% of the lamellae (Figure 3A). A similar pattern was observed using SEM (Figure 7.3B, C). Furthermore, NKA-rich ionocytes within a wild-caught adult Splitnose Rockfish were

also limited to the trailing edge, and expressed similar patterns on the gill filament and lamellae (Supplementary Figure 7.3).

In addition to cytoplasmic VHA within the NKA-rich ionocytes (Figure 7.3D), VHA was also detected in the pavement cells (Figure 7.3E) and VHA-rich ionocytes (Figure 7.3F). Similar to the NKA-rich ionocyte (Figure 7.3G), VHA in the pavement cells appear cytoplasmic (Figure 7.3H). Additionally, VHA signal was more abundant within pavement cells without developed microridges (Figure 7.3H, Supplementary Figure 7.4B). In contrast to both the NKA-rich ionocyte, VHA within the VHA-rich ionocyte appears to line the basolateral membrane (Figure 7.3I) and does not appear to not be infolded (Supplementary Figure 7.4C). Furthermore, the VHA-rich ionocyte is not mitochondrion-rich and is distributed on both the gill filament and lamellae (Supplementary Figure 7.5). Finally, unlike the NKA-rich ionocyte, both VHA-immunostained pavement and VHA-rich ionocytes were present on both the leading and trailing edge of the gill.

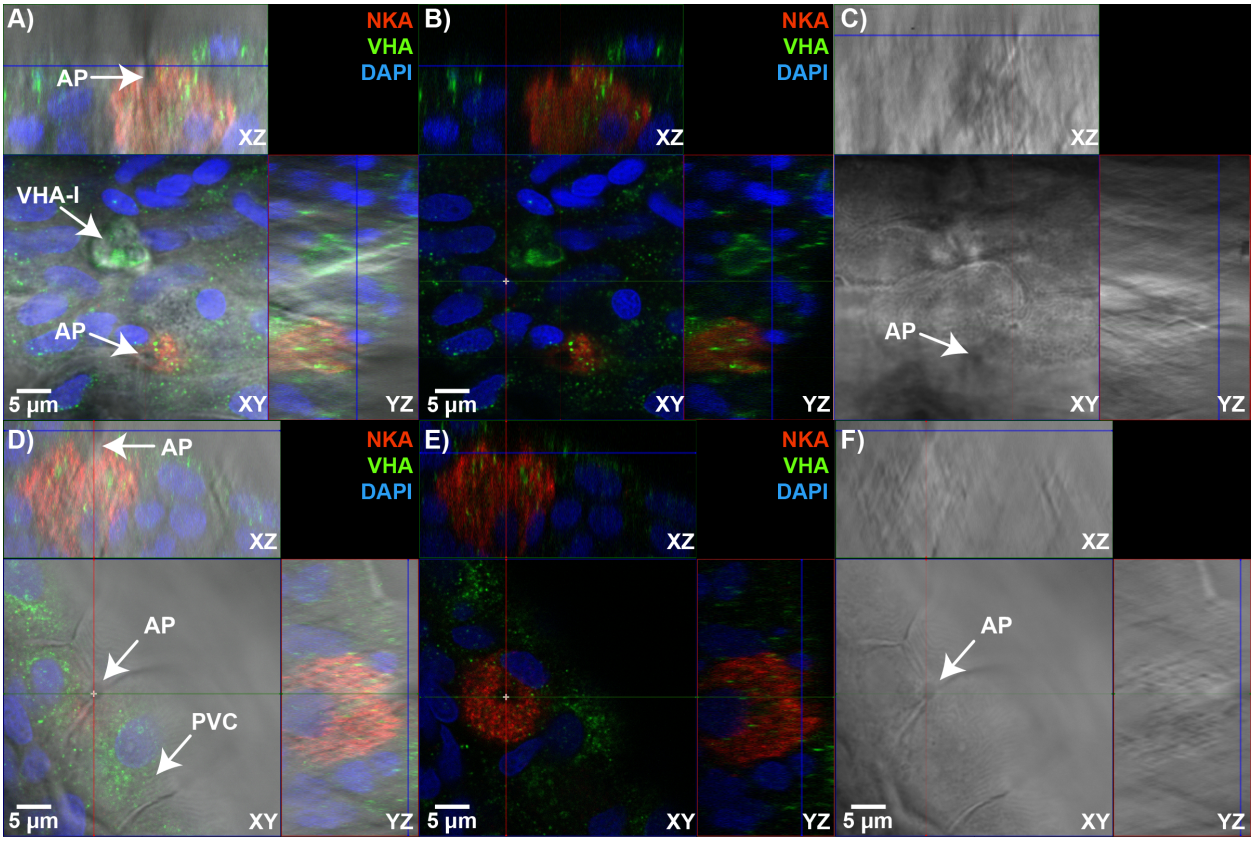

Figure 7.2: NKA-rich gill ionocytes in Splitnose Rockfish gills. Splitnose Rockfish gill ionocytes were immunostained and imaged in the XY, XZ, and YZ plane. No apparent difference in Na^+/K^+-ATPase (NKA, red) and vacuolar-type H^+ ATPase (VHA, green) localization was detected between the A, B, C) control and D, E, F) high CO_2 exposed Splitnose Rockfish. Cell nuclei were stained blue with DAPI. AP = apical pit. N = nuclei. PVC = pavement cell. VHA-I = VHA-rich ionocyte.

Figure 7.3: NKA and VHA immunostaining and scanning electron micrographs of Splitnose Rockfish gills. Immunostaining of Na^+/K^+-ATPase (NKA, red) and vacuolar-type H^+ ATPase (VHA, green) in the Splitnose Rockfish (*Sebastes diploproa*) gill in the XY, XZ, and YZ plane. **A)** NKA-rich ionocytes (NKA-I) were more abundantly present along the base of the lamellae than the filament. This was further verified by imaging of their apical openings using **B)** low magnification and **C)** high magnification scanning electron micrographs. Immunostaining of NKA and VHA in the XY, XZ, and YZ plane reveals VHA was is present within at least three cell types. These include **D)** NKA-I, **E)** pavement cell with (PVC w/ MR) and without microridge (PVC w/o MR), and **F)** VHA-rich ionocyte (VHA-I). **G, H, I)** Additional differential interference contrast was overlaid to image apical opening and cell morphology. Blank white arrows denote apical pit in SEM micrograph. Cell nuclei were stained blue with DAPI. AP = apical pit. N = nuclei. PVC w/ MR = pavement cell with microridge. PVC w/o MR = pavement cell without microridge. NKA-I = NKA-rich ionocyte. VHA-I = VHA-rich ionocyte.

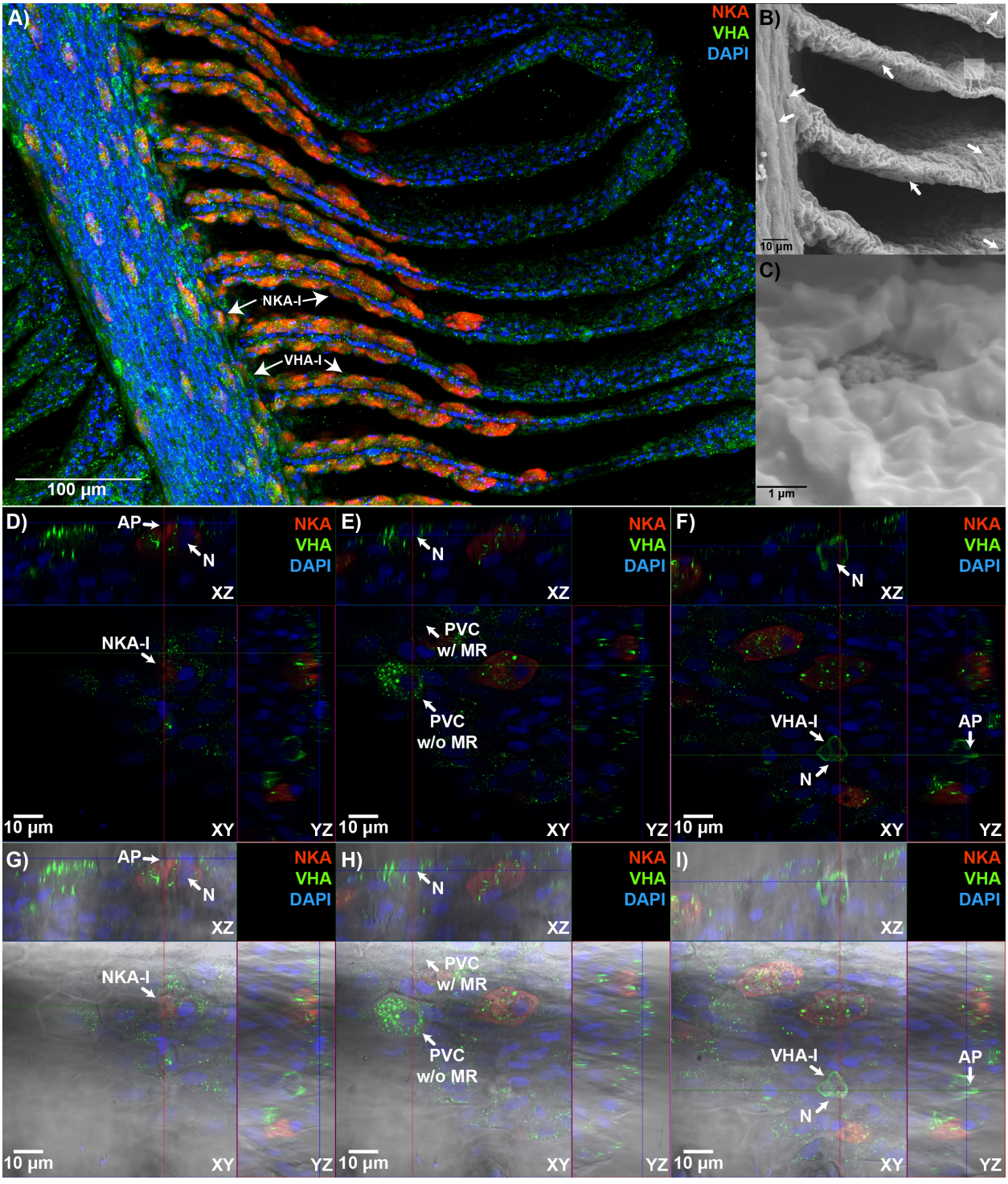
A)
NKA
VHA
DAPI
NKA-I
VHA-I
100 µm
B)
10 µm
C)
1 µm
D)
AP
N
XZ
NKA
VHA
DAPI
NKA-I
10 µm
XY
YZ
E)
N
XZ
NKA
VHA
DAPI
PVC
w/ MR
PVC
w/o MR
10 µm
XY
YZ
F)
N
XZ
NKA
VHA
DAPI
VHA-I
AP
N
10 µm
XY
YZ
G)
AP
N
XZ
NKA
VHA
DAPI
NKA-I
10 µm
XY
YZ
H)
N
XZ
NKA
VHA
DAPI
PVC
w/ MR
PVC
w/o MR
10 µm
XY
YZ
I)
XZ
NKA
VHA
DAPI
VHA-I
AP
N
10 µm
XY
YZ

Additionally, the distribution of NKA-rich ionocytes along the lamellae was compared between the control and hypercapnia treated fishes (Figure 7.4A, B). NKA-rich ionocyte abundance differed across gill filament regions: there were less ionocytes in the lamellae along the tip of the filament (5.41 ± 0.34) than at the middle (8.72 ± 0.37) and the base of the filament (8.01 ± 0.27; $p<0.001$; Figure 4C). Exposure to acute hypercapnic conditions did not change lamellar length across regions ($p=0.4428$). After normalizing by lamellar length, NKA-rich ionocyte density was not significantly different between treatments regardless of filament regions (n=9 per treatment; Tip: $p=0.2377$; Middle: $p=0.5475$; Base: $p=0.8442$; Figure 7.4D).

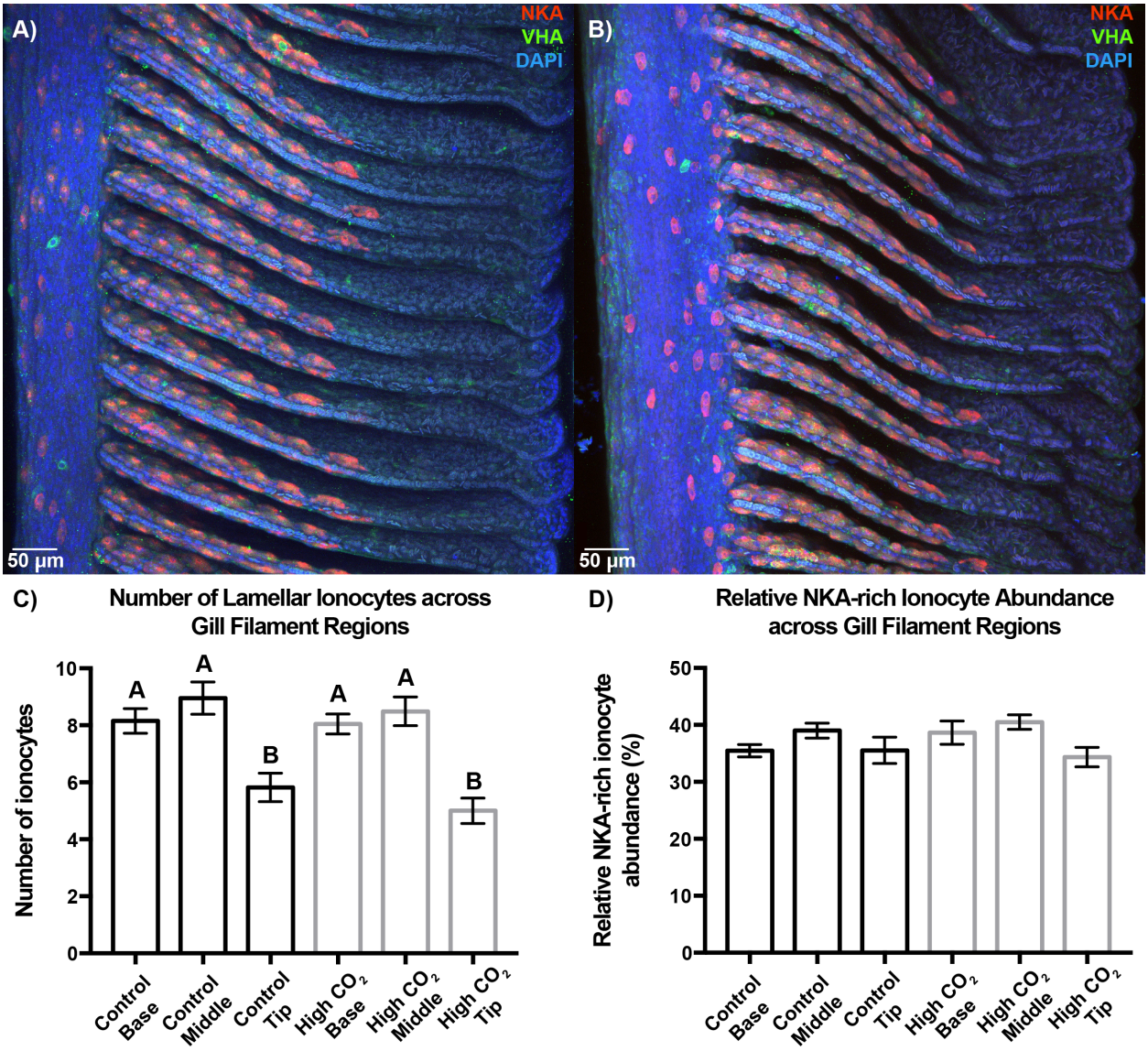

Figure 7.4: NKA-rich ionocyte density comparison. Relative ionocyte area of was estimated after Na^+/K^+-ATPase (NKA, red) and vacuolar-type H^+ ATPase (VHA, green) immunostaining of **A)** control and **B)** high CO_2 exposed Splitnose Rockfish. **C)** In both control and high CO_2 treated fish, the number of NKA-rich lamellar ionocytes at the base and middle of the gill filament was significantly higher than at the tip of the gill filament. **D)** After normalizing by gill lamellae distance, we found no differences in relative ionocyte area regardless of filament region or pH treatment. Cell nuclei were stained blue with DAPI. Alpha level set at $p<0.05$. Values are mean ± S.E.M.

Gill Ionocyte Apical Morphology

Consistent with our immunostaining and scanning electron micrographs, the NKA-rich ionocytes were more prominently present (and therefore easier to locate) along the basal portion of the lamellae than the gill filament. Therefore, our work focused on the ionocytes along the basal portion of the lamellae (Figure 7.4A, B). The NKA-rich ionocytes' apical morphology along the base of the lamellae ranges from apical opening without microvilli (Figure 7.5A) to apical opening with numerous protruding microvilli (Figure 7.5B). We found the apical openings of rockfishes exposed to high-CO_2 low pH conditions had significantly more opening with protruding microvilli (45.5%) than rockfishes in the control treatment (15%; p=0.0253; n=8 control, n=9 low-pH; Figure 7.5C).

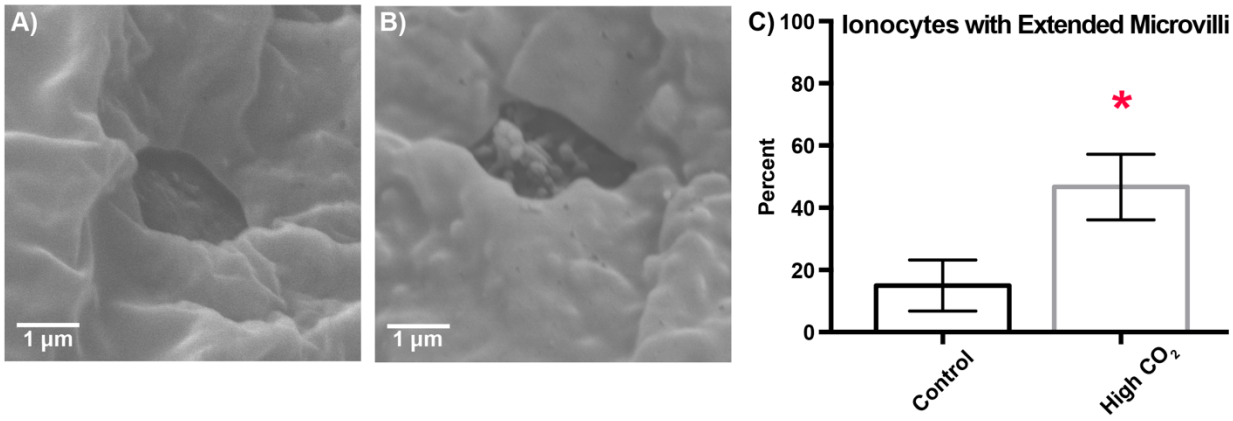

Figure 7.5: Apical morphological differences in Splitnose Rockfish gills. The apical surface morphology of gill ionocytes was compared after exposure to **A)** control or **B)** high CO_2 conditions. Splitnose Rockfish exposed to high CO_2 condition had significantly more ionocytes with extended microvilli than those in the control condition (n=8 control; n=9 high CO_2; p=0.0253). *denotes significance at an alpha level set at p<0.05. Values are mean ± S.E.M.

Inner Ear NKA and VHA Protein Abundance

In the crude homogenate fraction, there were no differences in NKA abundance between treatments (p=0.9104; Supplementary Figure 7.1B). VHA was also undetectable in the crude homogenate fraction (not shown). In the membrane-enriched fraction, we found no differences in inner ear NKA abundance between the control and low-pH treatments (p=0.2457; Figure 7.6A). In contrast, Splitnose Rockfish from the high-CO_2 treatment had significantly lower inner ear VHA abundance than fishes in the control treatment (p=0.0123; Figure 7.6B).

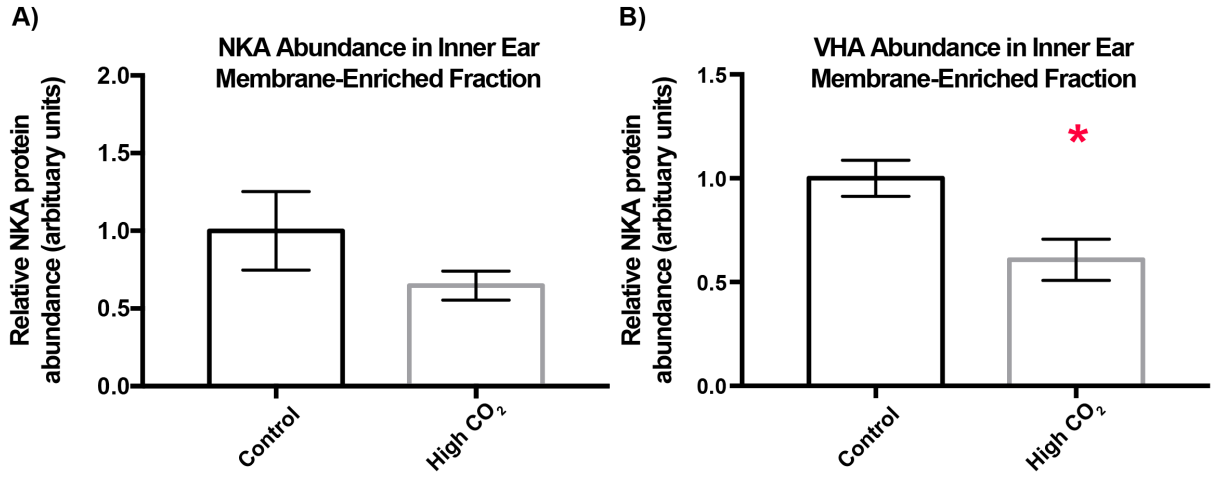

Figure 7.6: Relative Na^+/K^+-ATPase (NKA) and vacuolar-type H^+ ATPase (VHA)abundance in Splitnose Rockfish inner ear membrane fraction. NKA and VHA in the membrane fraction within the inner ear of control and high CO_2 exposed Splitnose Rockfish (*Sebastes diploproa*). A) NKA abundance was not significantly different (n=7 control; n=6 low-pH; p=0.2457), whereas B) VHA abundance was significantly different between the control and high CO_2 treatment (n=7 control; n=6 low-pH; p=0.0123). *denotes significance at an α level set at $p<0.05$. Values are mean ± S.E.M.

Inner Ear Ionocyte Characterization, Distribution, and Apical Morphology

Whole-mount immunostaining revealed two types of ionocytes (Fig 7.7A) within the inner ear of Splitnose Rockfish: the NKA-rich Type-I ionocyte (Fig 7.7B) and the VHA-rich Type-II ionocyte (Figure 7.7C). The Type-I ionocytes form a meshwork arrangement that frequently connects to adjacent Type-I ionocytes. Whereas, the Type-II ionocytes are distributed between the Type-I ionocytes and interspersed across the meshwork arrangement (Fig 7.7D). Immunostaining at higher magnification and across multiple focal planes reveals the NKA-rich Type-I ionocyte contains cytoplasmic and apical VHA, and the VHA-rich Type-II ionocyte contains a small amount of basolateral NKA (Figure 7.7E). The two types of inner ear ionocytes were further confirmed using Na^+-K^+-Cl^--co-transporter (abundantly present within Type-I ionocyte) and carbonic anhydrase (abundantly present within Type-II ionocyte) was performed with additional immunostaining (Kwan *et al.*, *in review*; Supplementary Figure 7.6).

Scanning electron micrographs further unveiled differences in apical morphology (Figure 7.7F). The first apical surface had dense, thick microvilli-like extensions, whereas the other apical surface had relatively barren apical surface with thinner cilia-like extensions (Figure 7.7G). Tracing of the area covered by the former apical morphological configuration reveals a pattern similar to the Type-I ionocyte (Figure 7.7H).

Intracellular VHA localization between the control and the high-CO_2 treatment was examined using immunohistochemistry. In both Type-I and Type-II ionocytes in the meshwork region, we found no apparent differences in intracellular VHA localization (Figure 7.8A, B). Similarly, no differences in apical morphology of inner ear ionocytes were detected between the two treatments (Figure 7.8C, D).

Figure 7.7: Immunostaining and scanning electron micrographs of Splitnose Rockfish inner ear. Immunostaining of Na^+/K^+-ATPase (NKA, red) and vacuolar-type H^+ ATPase (VHA, green) within the Splitnose Rockfish (*Sebastes diploproa*) inner ear meshwork region. **A)** NKA-rich ionocytes (Type-I) were abundantly present in a meshwork arrangement and interwoven between VHA-rich ionocytes (Type-II). **B, C)** Single channel exposure, **D)** higher magnification, and **E)** imaging in the XY, XZ, and YZ plane reveals the Type-I NKA-rich ionocytes contain apical VHA, and the Type-II ionocytes contain basolateral NKA. Additionally, **F)** low and **G)** high magnification scanning electron micrographs on the inner ear meshwork region reveal two different types of apical morphology. **H)** Tracing of the dense microvilli-like morphology (transparent red) reveals a distribution pattern similar to the meshwork arrangement of the NKA-rich ionocytes. Cell nuclei were stained blue with DAPI. BV = blood vessel.

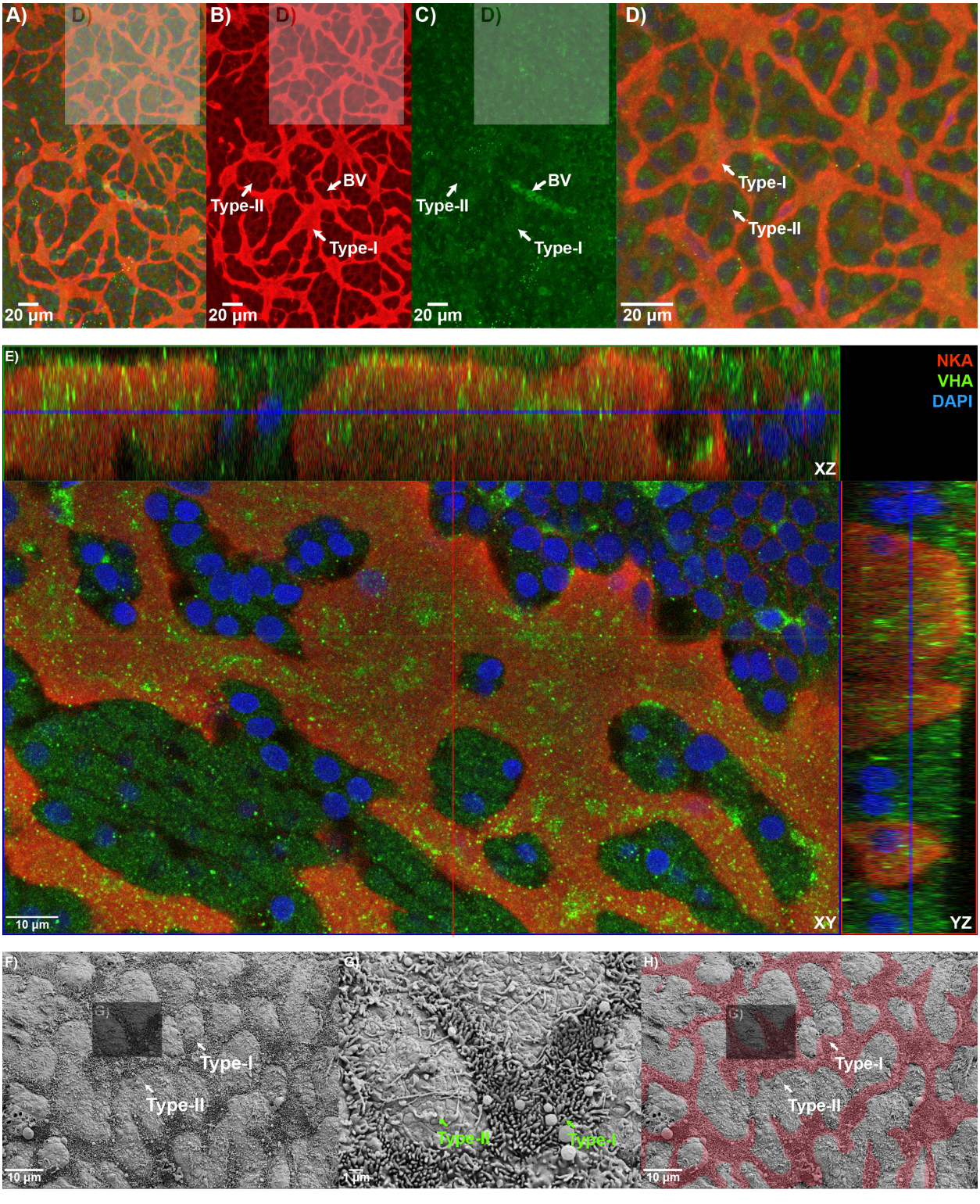
A)
D)
B)
D)
C)
D)
D)
Type-II
BV
Type-I
Type-II
BV
Type-I
Type-I
Type-II
20 µm
20 µm
20 µm
20 µm
E)
NKA
VHA
DAPI
XZ
10 µm
XY
YZ
F)
G)
H)
Type-I
Type-II
Type-II
Type-I
Type-I
Type-II
10 µm
10 µm
10 µm

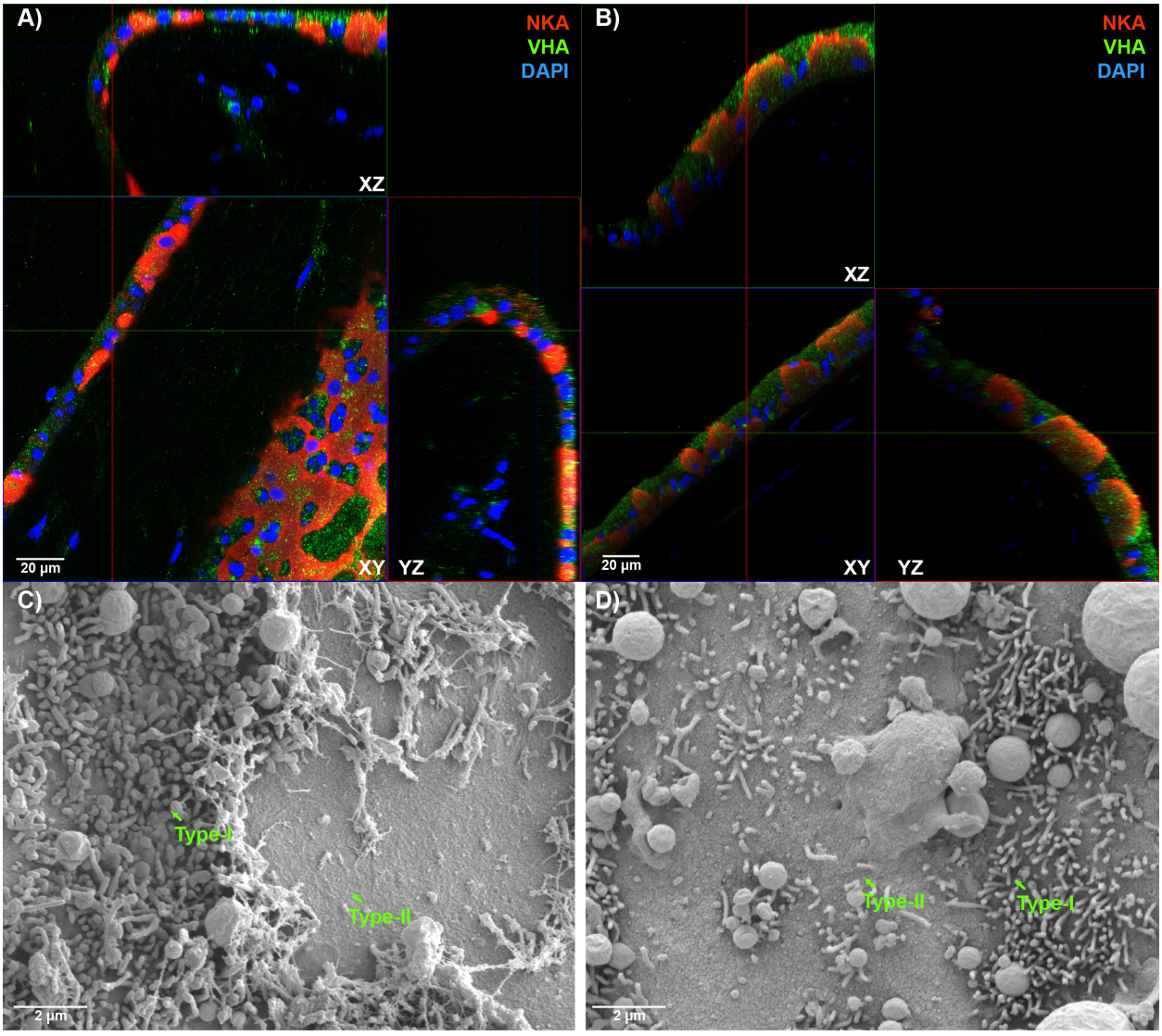

Figure 7.8: Immunostained inner ear from control and high CO_2 exposed Splitnose Rockfish. The inner ear of Splitnose Rockfish from **A)** control and **B)** high CO_2 treatment were immunostained with Na^+/K^+-ATPase (NKA, red) and vacuolar-type H^+ ATPase (VHA, green) and imaged from the XY, XZ, and YZ plane. Scanning electron micrographs of the inner ear ionocytes' Type-I and Type-II ionocytes from **C)** control and **D)** high-CO_2 treatment revealed no apparent differences in apical morphology. Cell nuclei were stained blue with DAPI.

Discussion

In response to 3 days of ~1,600 μatm of CO_2 exposure, the Splitnose Rockfish's gill ionocytes responded with significantly increased NKA abundance in the membrane fraction and greater extension of apical microvilli. Additionally, the Splitnose Rockfish's inner ear had significantly decreased VHA abundance in the membrane fraction in response to high-CO_2 low pH condition. Furthermore, we detected a VHA-rich ionocyte – a poorly characterized cell type that has only been previously reported once. Moreover, higher resolution confocal and SEM imaging allowed additional characterization of Type-I and Type-II inner ear ionocyte composition and apical morphology. To the best of our knowledge, this is the first study to document inner ear ionocyte response to hypercapnia, detect apical VHA and CA within Type-I inner ear ionocyte, localize basolateral NKA and NKCC within Type-II ionocyte, and determine the apical morphology of the two types of inner ear ionocytes. Altogether, these results highlight how gill ionocytes respond to high-CO_2 low pH conditions, and how inner ear ionocytes react to subsequent increase in [HCO_3^-].

Active and reserved NKA are distinguishable through centrifugation

This study suggests the Splitnose Rockfish's current acid-base machinery is sufficient to cope with the 3-day 1,600 μatm exposure using existing NKA-rich ionocytes with extended apical microvilli, and without additional synthesis of NKA-rich ionocytes. Importantly, our method allows the comparison of relative NKA abundance between the crude homogenate and the membrane fraction, which distinguishes between the enzymes held in reserve within the cytoplasm and those bound to the membrane and actively utilized. We found the membrane-enriched fraction of high-CO_2 exposed fishes was ~50% higher than the control, suggesting a

significant amount of NKA is likely held in reserve within the ionocyte. Thus, measurements using the crude homogenate fraction (which includes both active and reserved NKA) would likely mask measurements related to NKA utilization. Furthermore, any significant differences in relative NKA abundance when compared with the crude homogenate fraction may represent newly synthesized NKA (both within, or in a new ionocyte altogether) – which may be necessary during longer experimental durations and/or more severe high-CO_2 low pH treatments.

To our knowledge, all previous OA experiments have used crude homogenate fractions to measure relative NKA abundance. In two previous studies on the Atlantic Cod (*Gadus morhua*), differences in relative NKA abundance was insignificant despite a 4-week exposure to 1,200 and 2,200 μatm (Michael et al., 2016), or a 4-month exposure to 3,000 μatm of CO_2 (Melzner et al., 2009a). However, relative NKA abundance was significantly higher in Atlantic Cod after a 12-month exposure to 6,000 μatm (Melzner et al., 2009a), and in Benthic Eelpout (*Zoarces viviparous*) after a 2-day exposure to 10,000 μatm of CO_2 (Deigweiher et al., 2008). Taken together, this suggests NKA held in the ionocyte's reserve may already be capable of countering <3,000 μatm of CO_2. Moreover, this suggests the synthesis of additional NKA (within, or in a new ionocyte) was not necessary until exposure to >10,000 μatm of CO_2. Furthermore, this also explains why we did not observe additional NKA-rich ionocytes synthesized along the lamellae of our high-CO_2 exposed rockfish.

In the NKA-rich ionocyte's apical membrane, we also observed significantly more extended microvilli. This apical membrane likely contains NHE, which secretes H^+ into seawater using the driving force supplied by basolateral NKA. This expansion of apical surface area would likely increase NKA demand, which further supports our relative NKA abundance finding. Furthermore, our SEM observation is in agreement with a previous study, in which

visible microvilli extension were also detected in the gill ionocytes of Japanese Flounder (*Paralichthys olivaceus*) after a 24-hour exposure to pH 6.41 (~30,000 μatm of CO_2) (Hayashi et al., 2013). These results suggest the apical morphology of gill ionocytes can act as an acute response to mitigate acidotic stress. Future work should attempt to identify whether NKA translocation within marine teleost ionocytes occurs as shown in mammalian skeletal muscles (Pirkmajer and Chibalin, 2016). Further identification of the proteins located in the apical membrane would help verify the function of the microvilli. In summary, our relative NKA abundance, ionocyte density, and apical morphology results indicates increased energetic investment is necessary for H^+ secretion.

The role of VHA remains unknown

In Splitnose Rockfish gills, VHA was detected within three different cell types: the cytoplasm of NKA-rich ionocyte, the cytoplasm of pavement cell, and the basolateral membrane of VHA-rich ionocyte. Unlike NKA, VHA abundance in the gill membrane was not significantly different between the two treatments. This may be a result of VHA's presence in at least three different cell types, which would have diluted any potential treatment effects.

The colocalization of cytoplasmic VHA within NKA-rich ionocyte has been previously reported in the Longhorn Sculpin (*Myoxocephalus octodecemspinosus*) (Catches et al., 2006) and the Red Drum (Allmon and Esbaugh, 2017). Consistent with Allmon and Esbaugh (2017), we also did not find exposure to high-CO_2 low pH conditions to change VHA localization. Therefore, VHA's role in the H^+ secreting NKA-rich ionocyte remains unknown. One possible function of cytoplasmic VHA is to form of internal vesicles to concentrate H^+ away from vital cellular machinery. The use of transmission electron microscopy with immunogold will elucidate

whether VHA form vesicles within the NKA-rich ionocytes, and the combination of cell isolation with live imaging may be able to identify whether cytoplasmic VHA does indeed translocate within the cell under hypercapnic condition.

While the marine Splitnose Rockfish also have VHA in its gill pavement cells, we did not observe any apparent differences in VHA abundance or localization. Interestingly, we did observe greater VHA localization in pavement cells without their characteristic microridges – which is possibly a developing pavement cell. Future research on the role of VHA in pavement cell development should be performed on rapidly developing larval or juvenile fishes.

Finally, VHA-rich ionocytes have been previously reported in the Longhorn Sculpin (Catches et al., 2006). Given its basolateral expression, previous researchers have suggested this VHA-rich ionocyte likely contributes to HCO_3^- secretion. To perform this function, the VHA-rich ionocyte may also contain cytoplasmic carbonic anhydrase, apical HCO_3^-/Cl^- exchanger, and basolateral Na^+/H^+ exchanger. Future studies should attempt to immunostain these three proteins, and determine whether VHA translocation occurs during alkalosis.

Inner ear response to elevated CO_2 condition

During high-CO_2 low pH condition, the inner ear would be supplied with blood plasma with elevated HCO_3^- levels. Because cannulation of these small Splitnose Rockfish was not possible, proper blood pH measurements was not an option. Therefore, our blood parameters should be only examined in relative terms. In a study exposing the Gulf Toadfish (*Opsanus beta*) to a slightly higher CO_2 level (1,900 μatm), blood plasma [HCO_3^-] increased from 2.5 to 5 mM within 8 hours (Esbaugh et al., 2012). Assuming the rockfish's blood pH were within normal

range, then the calculated HCO_3^- level using our measured total CO_2 data would suggest [HCO_3^-] increased within the blood plasma of high-CO_2 treated fishes.

Elevated HCO_3^- level in the blood plasma is presumed to make its way into the endolymph via nearby blood vessels and ultimately increase otolith calcification (reviewed in Heuer and Grosell, 2014) – but this exact mechanism has not been shown. Furthermore, the endolymph in which the otolith calcifies is regulated by two types of inner ear ionocytes (Kwan et al., *in review*). To my knowledge, this is the first study that investigates the responses of inner ear ionocytes to the (presumably) higher [HCO_3^-] induced by high-CO_2 low pH condition.

The inner ear epithelium's NKA abundance in the membrane fraction was not significantly affected by the 3-day exposure to ~1,600 μatm of CO_2. This lack of difference in NKA abundance is not surprising given the Type-I ionocyte's crucial role in maintaining a K^+ rich environment for proper sensory hair cell function (Kwan et al., *in review*). Currently, the only OA study on inner ear function did not find differences in vestibulo-ocular reflex (Shen et al., 2016). Although this suggests the endolymph contains sufficient ions necessary for proper sensory hair cell function, the direct measurement of the endolymph's ion concentration (e.g. K^+, Ca^{2+}, total CO_2, pH) to verify this finding.

On the other hand, VHA abundance in the membrane fraction was nearly 50% lower after a 3-day exposure to ~1,600 μatm of CO_2. In my previous study on the Pacific Chub Mackerel, we proposed the Type-II ionocyte may be responsible for base-secretion. Given the Type-II ionocyte's co-localization with carbonic anhydrase and soluble adenylyl cyclase (sAC), the VHA-rich inner ear ionocyte is likely secreting HCO_3^- into the endolymph and H^+ into the interstitial space (*Kwan et al., in review*). Therefore, the decrease in relative VHA abundance may reflect VHA translocation from the basolateral membrane to the cytoplasm to slow HCO_3^-

transport. This is plausible as increased HCO_3^- accumulated in the blood plasma would require less energy (and thereby less membrane-bound VHA) to facilitate its transport into the endolymph and to slow down otolith calcification. However, VHA translocation may be occurring within any (or all) of these cells: inner ear ionocytes, sensory hair cells, surrounding arterioles, connective tissue, red blood cells. Because of the multiple types of tissue and the lack of crude homogenate data, we cannot discriminate amongst the cell types. Therefore, a more detailed analysis of specific cell type is necessary to determine where the reduction in membrane-bound VHA is occurring. Furthermore, this would be in direct contrast to the VHA-rich base-secreting ionocytes found within the elasmobranch gill (Tresguerres et al., 2007; Roa et al., 2014; Roa and Tresguerres, 2017). Previous research has demonstrated bicarbonate and subsequent sAC signaling is responsible for VHA translocation from the cytoplasm to the basolateral membrane (Tresguerres et al., 2007; Roa et al., 2014; Roa and Tresguerres, 2017). Future research investigating whether VHA translocates in response to HCO_3^- and/or sAC may help determine the mechanistic pathway regulating otolith calcification.

Unexpectedly, the combination of whole-mount immunostaining, confocal imaging, and scanning electron microscopy revealed new information on the inner ear ionocytes. The Type-I NKA-rich ionocyte have a dense microvilli bed along its apical membrane, yet only some of which appears to be apical VHA. To my knowledge, this is the first study to find cytoplasmic and apical VHA within the Type-I ionocyte. VHA's role in the Type-I ionocyte is unknown. But given its sparse distribution in the center of the dense microvilli bed, VHA may play a role in facilitating nearby ion-transport. The determination of the other proteins in the Type-I ionocyte's apical membrane may elucidate both VHA's and the Type-I ionocyte's role in otolith calcification.

In contrast, the Type-II VHA-rich ionocyte appears to have a relatively nude surface with numerous small pores along its apical membrane. Furthermore, confocal microscopy reveals the Type-II ionocyte contains a small amount of basolateral NKA and NKCC. To my knowledge, this is also the first study to find basolateral NKA and NKCC within the Type-II ionocyte. Given that the Type-II ionocyte is rich in CA and VHA, basolateral NKA and NKCC can help facilitate HCO_3^- transport via apical Na^+-HCO_3^- co-transporter and remove H^+ via basolateral NHE. Further determination of the Type-II ionocyte's membrane proteins would further develop the otolith calcification mechanism.

Acknowledgements

We are extremely grateful to Sabine Faulhaber for her technical expertise and generous assistance with the scanning electron microscope. We are also grateful to Ben Frable for collecting and preserving the wild-caught Splitnose Rockfish. The authors thank Angus Thies, Shane Finnerty, Till Harter, and Alex Clifford for assisting in specimen collection. We thank Phil Zerofski for maintaining the experimental aquarium. We also thank Taylor Smith, Shane Finnerty, and Gabriel Lopez for their help with animal husbandry. G.T.K. was supported by the National Science Foundation Graduate Research Fellowship Program and the Graduate Research Internship Program.

Chapter VII, in part is currently being prepared for submission for publication of the material. Kwan, G.T., Prime, K., Andrade, L.R., and Tresguerres, M. (*in prep*). Responses of Splitnose Rockfish (*Sebastes diploproa*) gill and inner ear ionocytes to hypercapnia. The dissertation author was the primary investigator and author of this material.

Appendix

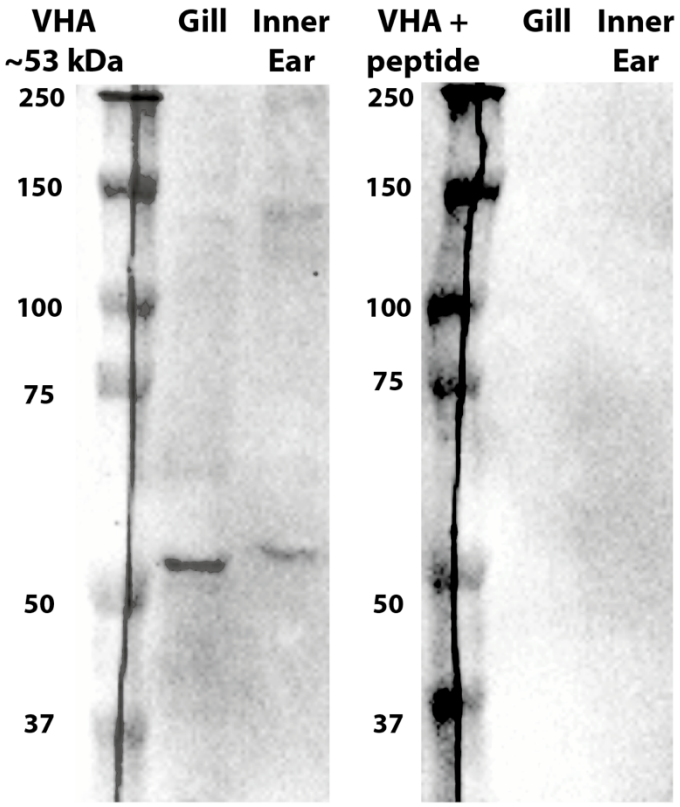

Supplementary Figure 7.1: Vacuolar-H^+ ATPase (VHA) peptide control. Splitnose Rockfish (*Sebastes diploproa*) gill and inner ear tissue were immunoblotted for VHA and revealed a single band at ~53 kDa. No signal was observed in the peptide preabsorption control.

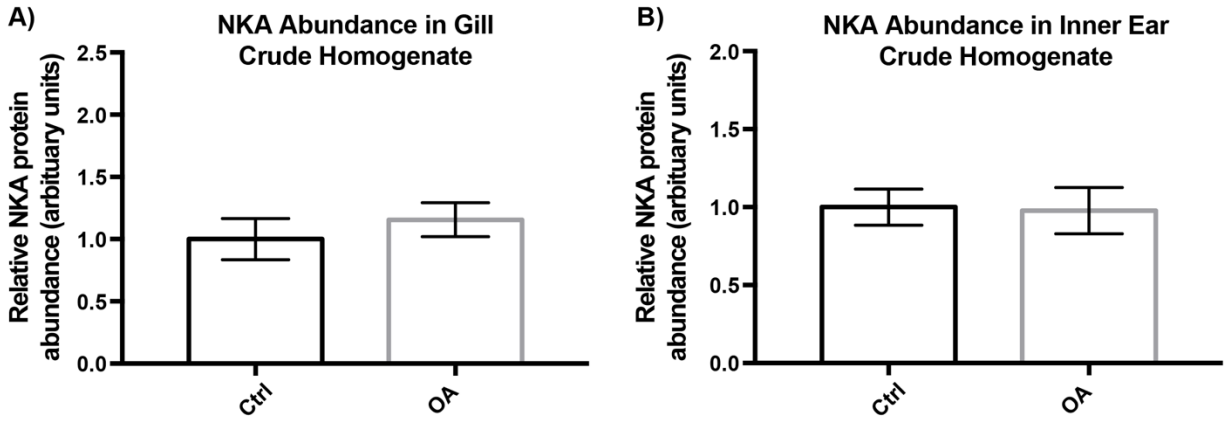

Supplementary Figure 7.2: Na^+/K^+-ATPase (NKA) in the crude homogenate fraction within the gill and inner ear of control and high CO_2 exposed Splitnose Rockfish (*Sebastes diploproa*). High CO_2 exposure did not significantly affect NKA abundance in the A) gill (n=9 control; n=9 low-pH; p=0.4778) or B) inner ear (n=8 control; n=9 low-pH; p=0.9104) of Splitnose Rockfish. *denotes significance at an α level set at $p<0.05$. Values are mean ± S.E.M.

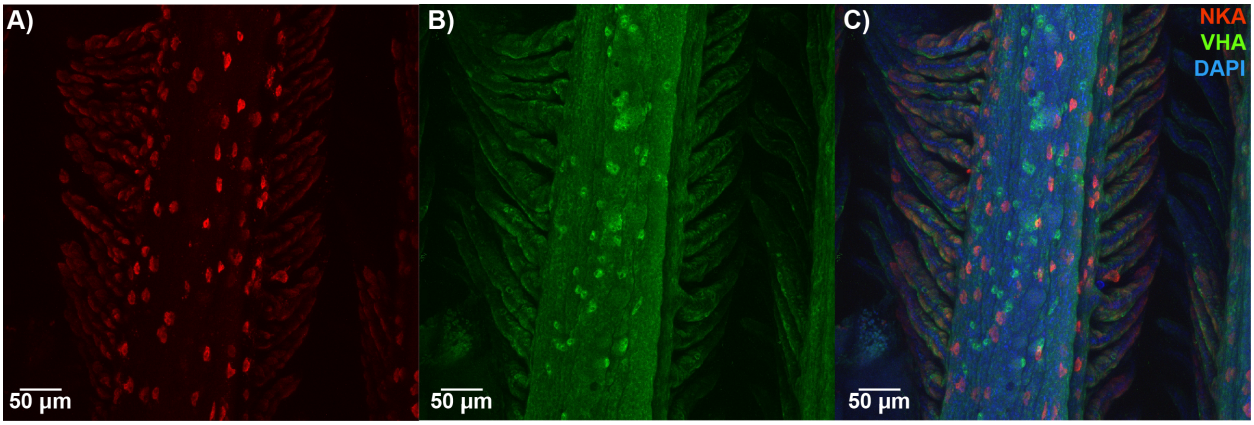

Supplementary Figure 7.3: Verification of gill ionocytes on a wild-caught adult Splitnose Rockfish. **A)** Na^+/K^+-ATPase (NKA, red) and **B)** vacuolar-type H^+ ATPase (VHA, green) are expressed together within some, **C)** but not all gill ionocytes. Cell nuclei were stained blue with DAPI.

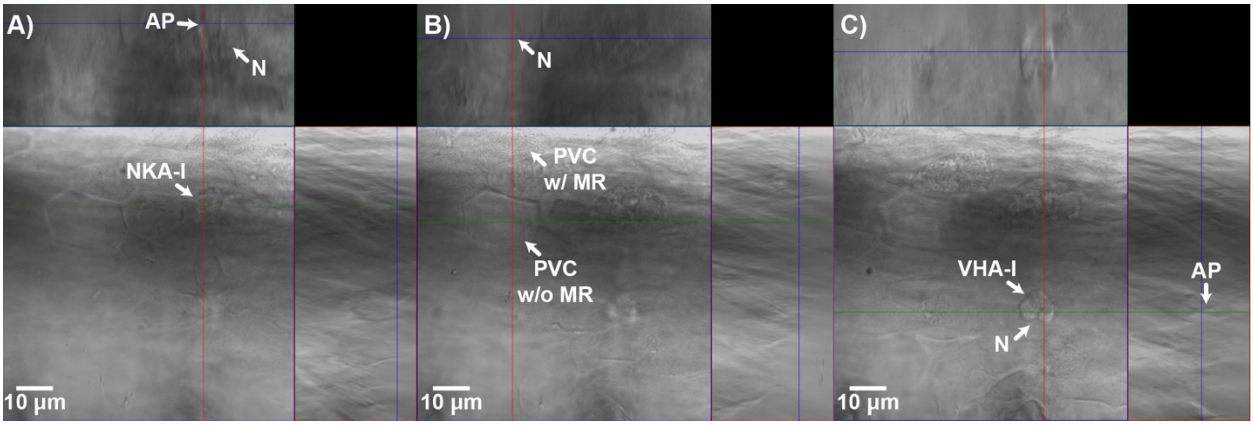

Supplementary Figure 7.4: Differential interference contrast of three cell types expressing vacuolar-type H^+ ATPase. Image depicts the cells in the XY, XZ, and YZ planes. Overlaying immunostaining shown in Figure 7.3. AP = apical pit. N = nuclei. PVC w/ MR = pavement cell with microridge. PVC w/o MR = pavement cell without microridge. NKA-I = NKA-rich ionocyte. VHA-I = VHA-rich ionocyte.

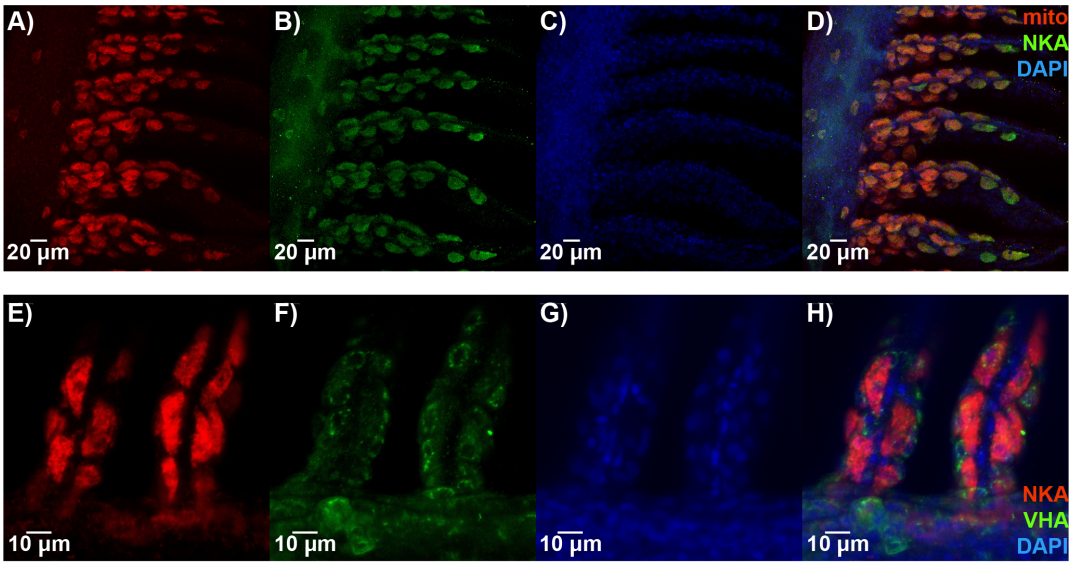

Supplementary Figure 7.5: Verification of the two types of gill ionocytes. **A)** Na^+/K^+-ATPase (NKA, green) are only expressed within mitochondrion-rich cells (mito, red). Whereas **B)** ionocytes containing abundant vacuolar-type H^+ ATPase (VHA, green) are not mitochondrion-rich (red). Cell nuclei were stained blue with DAPI.

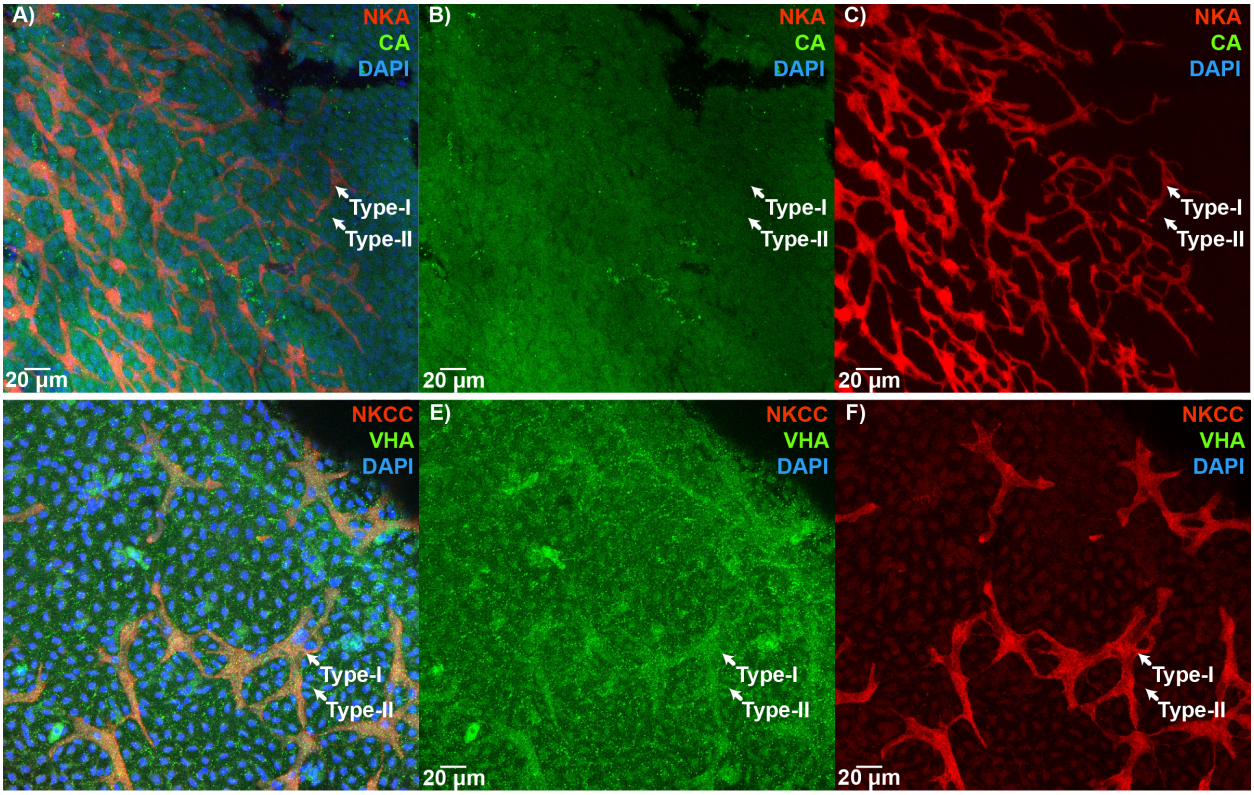

Supplementary Figure 7.6: Verification of the two types of inner ear ionocytes. **A, B, C)** Type-I ionocytes contain abundant Na^+/K^+-ATPase (NKA, red), but also a small amount of carbonic anhydrase (CA, green). **D, E, F)** Type-II ionocytes are abundant in vacuolar-type H^+ ATPase (VHA, green), but also contain a small amount of Na^+/K^+Cl^--co-transporter 1 (NKCC, red). Cell nuclei were stained blue with DAPI. BV=blood vessel.

References

Abbas, L., and Whitfield, T. T. (2009). Nkcc1 (Slc12a2) is required for the regulation of endolymph volume in the otic vesicle and swim bladder volume in the zebrafish larva. Development, 136: 2837–2848. doi:10.1242/dev.034215.

Allmon, E. B., and Esbaugh, A. J. (2017). Carbon dioxide induced plasticity of branchial acid-base pathways in an estuarine teleost. Scientific Reports, 7: 45680. Nature Publishing Group. doi:10.1038/srep45680.

Barott, K., Venn, A. A., Perez, S. O., Tambutté, S., and Tresguerres, M. (2015a). Coral host cells acidify symbiotic algal microenvironment to promote photosynthesis. Proceedings of the National Academy of Sciences of the United States of America, 112: 607–12. doi:10.1073/pnas.1413483112.

Barott, K. L., Perez, S. O., Linsmayer, L. B., and Tresguerres, M. (2015b). Differential localization of ion transporters suggests distinct cellular mechanisms for calcification and photosynthesis between two coral species. American Journal of Physiology - Regulatory, Integrative and Comparative Physiology, 309: R235–R246. doi:10.1152/ajpregu.00052.2015.

Blancheton, J. P. (2000). Developments in recirculation systems for Mediterranean fish species. Aquacultural Engineering, 22: 17–31.

Bradford, M. M. (1976). A rapid and sensitive method for the quantitation of microgram quantities of protein utilizing the principle of protein-dye binding. Analytical Biochemistry, 72: 248–254. doi:10.1016/0003-2697(76)90527-3.

Caldeira, K., and Wickett, M. E. (2003). Oceanography: anthropogenic carbon and ocean pH. Nature, 425: 365.

Caldeira, K., and Wickett, M. E. (2005). Ocean model predictions of chemistry changes from carbon dioxide emissions to the atmosphere and ocean. Journal of Geophysical Research-Part C-Oceans, 110: 12 pp.-12 pp.

Catches, J. S., Burns, J. M., Edwards, S. L., and Claiborne, J. B. (2006). Na+/H+ antiporter, V-H+-ATPase and Na+/K+-ATPase immunolocalization in a marine teleost (*Myoxocephalus octodecemspinosus*). Journal of Experimental Biology, 209: 3440–3447.

Checkley, D. M., and Barth, J. a. (2009). Patterns and processes in the California Current System. Progress in Oceanography, 83: 49–64. doi:10.1016/j.pocean.2009.07.028.

Claiborne, J. B., Edwards, S. L., and Morrison-Shetlar, A. I. (2002). Acid-base regulation in fishes: cellular and molecular mechanisms. Journal of Experimental Zoology, 293: 302–319. doi:10.1002/jez.10125.

Cope, J. M. (2009). Status of the U.S. splitnose rockfish (*Sebastes diploproa*) resource in 2009.

Culberson, C., and Pytkowicz, R. M. (1970). Oxygen-total carbon dioxide correlation in the Eastern Pacific Ocean. Journal of the Oceanographical Society of Japan, 26: 95–100.

Deigweiher, K., Koschnick, N., Portner, H.-O., and Lucassen, M. (2008). Acclimation of ion regulatory capacities in gills of marine fish under environmental hypercapnia. AJP: Regulatory, Integrative and Comparative Physiology, 295: R1660–R1670. doi:10.1152/ajpregu.90403.2008.

Ellis, R. P., Urbina, M. A., and Wilson, R. W. (2016). Lessons from two high CO2 worlds - future oceans and intensive aquaculture. Global Change Biology, 2100: 1–8. doi:10.1111/gcb.13515.

Esbaugh, A. J., Heuer, R., and Grosell, M. (2012). Impacts of ocean acidification on respiratory gas exchange and acid-base balance in a marine teleost, *Opsanus beta*. Journal of Comparative Physiology B: Biochemical, Systemic, and Environmental Physiology, 182: 921–934.

Esbaugh, A. J., and Cutler, B. (2016). Intestinal Na+, K+, 2Cl-cotransporter 2 plays a crucial role in hyperosmotic transitions of a euryhaline teleost. Physiological Reports, 4: 1–12.

Evans, D. H., Piermarini, P. M., and Choe, K. P. (2005). The Multifunctional Fish Gill: Dominant Site of Gas Exchange, Osmoregulation, Acid-Base Regulation, and Excretion of Nitrogenous Waste. Physiological Reviews, 85: 97–177. doi:10.1152/physrev.00050.2003.

Fivelstad, S., Kvamme, K., Handeland, S., Fivelstad, M., Olsen, A. B., and Hosfeld, C. D. (2015). Growth and physiological models for Atlantic salmon (*Salmo salar L.*) parr exposed to elevated carbon dioxide concentrations at high temperature. Aquaculture, 436: 90–94. Elsevier B.V. doi:10.1016/j.aquaculture.2014.11.002.

Franke, A., and Clemmesen, C. (2011). Effect of ocean acidification on early life stages of Atlantic herring (*Clupea harengus L.*). Biogeosciences, 8: 3697–3707. doi:10.5194/bg-8-3697-2011.

Frieder, C. A., Nam, S. H., Martz, T. R., and Levin, L. A. (2012). High temporal and spatial variability of dissolved oxygen and pH in a nearshore California kelp forest. Biogeosciences, 9: 3917–3930. doi:10.5194/bg-9-3917-2012.

Frommel, A. Y., Schubert, A., Piatkowski, U., and Clemmesen, C. (2013). Egg and early larval stages of Baltic cod, *Gadus morhua*, are robust to high levels of ocean acidification. Marine Biology, 160: 1825–1834.

Georgalis, T., Gilmour, K. M., Yorston, J., and Perry, S. F. (2006). Roles of cytosolic and membrane-bound carbonic anhydrase in renal control of acid-base balance in rainbow trout, *Oncorhynchus mykiss*. American Journal of Physiology - Renal Physiology, 291: 407–421.

Hayashi, M., Kikkawa, T., and Ishimatsu, A. (2013). Morphological changes in branchial mitochondria-rich cells of the teleost *Paralichthys olivaceus* as a potential indicator of CO2 impacts. Marine Pollution Bulletin, 73: 409–415. Elsevier Ltd. doi:10.1016/j.marpolbul.2013.06.034.

Heuer, R. M., and Grosell, M. (2014). Physiological impacts of elevated carbon dioxide and ocean acidification on fish. AJP: Regulatory, Integrative and Comparative Physiology, 307: R1061–R1084. doi:10.1152/ajpregu.00064.2014.

Hill, R. W., Armstrong, E. J., Inaba, K., Morita, M., Tresguerres, M., Stillman, J. H., Roa, J. N., and Kwan, G. T. (2018). Acid secretion by the boring organ of the burrowing giant clam, *Tridacna crocea*. Biology Letters, 14: 20180047. doi:10.1098/rsbl.2018.0047.

Hirose, S., Kaneko, T., Naito, N., and Takei, Y. (2003). Molecular biology of major components of chloride cells. Comparative Biochemistry and Physiology - B Biochemistry and Molecular Biology, 136: 593–620.

Hofmann, G. E., Smith, J. E., Johnson, K. S., Send, U., Levin, L. A., Micheli, F., Paytan, A., Price, N. N., Peterson, B., Takeshita, Y., Matson, P. G., Crook, E. D., Kroeker, K. J., Gambi, M. C., Rivest, E. B., Frieder, C. a., Yu, P. C., and Martz, T. R. (2011). High-frequency dynamics of ocean pH: a multi-ecosystem comparison. PLoS ONE, 6: e28983. doi:10.1371/journal.pone.0028983.

Ishimatsu, A., Hayashi, M., and Kikkawa, T. (2008). Fishes in high-CO2, acidified oceans. Marine Ecology Progress Series, 373: 295–302. doi:10.3354/meps07823.

Keys, A. B. (1931). Chloride and water secretion and absorption by the gills of the eel. Zeitschrift für vergleichende Physiologie, 15: 364–388. doi:10.1007/BF00339115.

Keys, A., and Willmer, E. N. (1932). 'Chloride secreting cells' in the gills of fishes, with special reference to the common eel. The Journal of Physiology, 76: 368–378. doi:10.1113/jphysiol.1932.sp002932.

Kwan, G. T., Wexler, J. B., Wegner, N. C., and Tresguerres, M. (2019). Ontogenetic changes in cutaneous and branchial ionocytes and morphology in yellowfin tuna (*Thunnus albacares*) larvae. Journal of Comparative Physiology B: Biochemical, Systemic, and Environmental Physiology, 189: 81–95. Springer Berlin Heidelberg. doi:10.1007/s00360-018-1187-9.

Kwan, G. T., Smith, T. R., and Tresguerres, M. (*in review*). Immunological characterization of two types of ionocytes in the inner ear epithelium of Pacific Chub Mackerel (*Scomber japonicus*). Journal of Comparative Physiology B - Biochemical Systemic and Environmental Physiology.

Lebovitz, R. M., Takeyasu, K., and Fambrough, D. M. (1989). Molecular characterization and expression of the (Na+ + K+)-ATPase alpha-subunit in *Drosophila melanogaster*. The EMBO Journal, 8: 193–202.

Levin, L. a. (2003). Oxygen minimum zone benthos: adaptation and community response to hypoxia. Oceanography and Marine Biology: an Annual Review, 41: 1–45.

Love, M., Yaklovich, M., and Thorsteinson, L. (2002). The Rockfishes of the Northeast Pacific. UC Press, Berkeley.

Lytle, C., Xu, J. C., Biemesderfer, D., and Forbush, B. (1995). Distribution and diversity of Na-K-Cl cotransport proteins: a study with monoclonal antibodies. The American journal of physiology, 269: C1496–C1505.

Maneja, R. H., Frommel, a. Y., Geffen, a. J., Folkvord, a., Piatkowski, U., Chang, M. Y., and Clemmesen, C. (2013). Effects of ocean acidification on the calcification of otoliths of larval Atlantic cod *Gadus morhua*. Marine Ecology Progress Series, 477: 251–258.

Melzner, F., Göbel, S., Langenbuch, M., Gutowska, M. A., P??rtner, H. O., and Lucassen, M. (2009). Swimming performance in Atlantic Cod (*Gadus morhua*) following long-term (4-12 months) acclimation to elevated seawater PC O2. Aquatic Toxicology, 92: 30–37.

Michael, K., Kreiss, C. M., Hu, M. Y., Koschnick, N., Bickmeyer, U., Dupont, S., Pörtner, H. O., and Lucassen, M. (2016). Adjustments of molecular key components of branchial ion and pH regulation in Atlantic cod (*Gadus morhua*) in response to ocean acidification and warming. Comparative Biochemistry and Physiology Part - B: Biochemistry and Molecular Biology, 193: 33–46. The Authors. doi:10.1016/j.cbpb.2015.12.006.

Munday, P. L., Gagliano, M., Donelson, J. M., Dixson, D. L., and Thorrold, S. R. (2011). Ocean acidification does not affect the early life history development of a tropical marine fish. Marine Ecology Progress Series, 423: 211–221.

Nam, S., Kim, H. J., and Send, U. (2011). Amplification of hypoxic and acidic events by la Nia conditions on the continental shelf off California. Geophysical Research Letters, 38: 1–5.

Perry, D. M., Redman, D. H., Widman, J. C., Meseck, S., King, A., and Pereira, J. J. (2015). Effect of ocean acidification on growth and otolith condition of juvenile scup, *Stenotomus chrysops*. Ecology and Evolution, 5: 4187–4196.

Petochi, T., Di Marco, P., Priori, A., Finoia, M. G., Mercatali, I., and Marino, G. (2011). Coping strategy and stress response of European sea bass *Dicentrarchus labrax* to acute and chronic environmental hypercapnia under hyperoxic conditions. Aquaculture, 315: 312–320. Elsevier B.V. doi:10.1016/j.aquaculture.2011.02.028.

Pirkmajer, S., and Chibalin, A. V. (2016). Na,K-ATPase regulation in skeletal muscle. American Journal of Physiology - Endocrinology and Metabolism, 311: E1–E31.

Qin, Z., Lewis, J. E., and Perry, S. F. (2010). Zebrafish (*Danio rerio*) gill neuroepithelial cells are sensitive chemoreceptors for environmental CO2. Journal of Physiology, 588: 861–872.

R Development Core Team. (2013). R: A language and environment for statistical computing. R foundation for statistical computing. Vienna, Austria.

Roa, J. N., Munévar, C. L., and Tresguerres, M. (2014). Feeding induces translocation of vacuolar proton ATPase and pendrin to the membrane of leopard shark (*Triakis semifasciata*) mitochondrion-rich gill cells. Comparative Biochemistry and Physiology -Part A : Molecular and Integrative Physiology, 174: 29–37. Elsevier Inc. doi:10.1016/j.cbpa.2014.04.003.

Roa, J. N., and Tresguerres, M. (2017). Bicarbonate-sensing soluble adenylyl cyclase is present in the cell cytoplasm and nucleus of multiple shark tissues. Physiological Reports, 5: e13090. doi:10.14814/phy2.13090.

Rykaczewski, R. R., and Checkley, D. M. (2008). Influence of ocean winds on the pelagic ecosystem in upwelling regions. Proceedings of the National Academy of Sciences, 105: 1965–1970. doi:10.1073/pnas.0711777105.

Schade, F. M., Clemmesen, C., and Mathias Wegner, K. (2014). Within- and transgenerational effects of ocean acidification on life history of marine three-spined stickleback (*Gasterosteus aculeatus*). Marine Biology, 161: 1667–1676.

Schindelin, J., Arganda-Carreras, I., Frise, E., Kaynig, V., Longair, M., Pietzsch, T., Preibisch, S., Rueden, C., Saalfeld, S., Schmid, B., Tinevez, J., White, D. J., Hartenstein, V., Eliceiri, K., Tomancak, P., and Cardona, A. (2012). Fiji: an open-source platform for biological-image analysis. Nature Methods, 9: 676–682. doi:10.1038/nmeth.2019.

Shen, S. G., Chen, F., Schoppik, D. E., and Checkley, D. M. (2016). Otolith size and the vestibulo-ocular reflex of larvae of white seabass *Atractoscion nobilis* at high pCO2. Marine Ecology Progress Series, 553: 173–182.

Simpson, S. D., Munday, P. L., Wittenrich, M. L., Manassa, R., Dixson, D. L., Gagliano, M., and Yan, H. Y. (2011). Ocean acidification erodes crucial auditory behaviour in a marine fish. Biology Letters, 7: 917–920.

Sundin, J., Amcoff, M., Mateos-González, F., Raby, G. D., and Clark, T. D. (2019). Long-term acclimation to near-future ocean acidification has negligible effects on energetic attributes in a juvenile coral reef fish. Oecologia. Springer Berlin Heidelberg. doi:10.1007/s00442-019-04430-z.

Tang, C. H., Leu, M. Y., Yang, W. K., and Tsai, S. C. (2014). Exploration of the mechanisms of protein quality control and osmoregulation in gills of *Chromis viridis* in response to reduced salinity. Fish Physiology and Biochemistry, 40: 1533–1546.

Tohse, H., Ando, H., and Mugiya, Y. (2004). Biochemical properties and immunohistochemical localization of carbonic anhydrase in the sacculus of the inner ear in the salmon *Oncorhynchus masou*. Comparative Biochemistry and Physiology - A Molecular and Integrative Physiology, 137: 87–94.

Tresguerres, M., Parks, S. K., Wood, C. M., and Goss, G. G. (2007). V-H+-ATPase translocation during blood alkalosis in dogfish gills: interaction with carbonic anhydrase and involvement in the postfeeding alkaline tide. AJP: Regulatory, Integrative and Comparative Physiology, 292: R2012–R2019. doi:10.1152/ajpregu.00814.2006.

Tresguerres, M., Levin, L. R., Buck, J., and Grosell, M. (2010). Modulation of NaCl absorption by [HCO3-] in the marine teleost intestine is mediated by soluble adenylyl cyclase. AJP: Regulatory, Integrative and Comparative Physiology, 299: R62–R71. doi:10.1152/ajpregu.00761.2009.

Tresguerres, M., Katz, S., and Rouse, G. W. (2013). How to get into bones : proton pump and carbonic anhydrase in Osedax boneworms How to get into bones : proton pump and carbonic anhydrase in Osedax boneworms. Proceedings of the Royal Society.

Wegner, N. C., Sepulveda, C. A., Aalbers, S. A., and Graham, J. B. (2013). Structural adaptations for ram ventilation: Gill fusions in scombrids and billfishes. Journal of Morphology, 274: 108–120.

Wilson, J. M., Randall, D. J., Donowitz, M., Vogl, A. W., and Ip, A. K. (2000). Immunolocalization of ion-transport proteins to branchial epithelium mitochondria-rich cells in the mudskipper (*Periophthalmodon schlosseri*). The Journal of Experimental Biology, 203: 2297–2310.

Wilson, J. M., Whiteley, N. M., and Randall, D. J. (2002). Ionoregulatory changes in the gill epithelia of coho salmon during seawater acclimation. Physiological and biochemical zoology : PBZ, 75: 237–49. doi:10.1086/341817.

Chapter VIII

General Discussion

Synopsis. The focus of my dissertation was to characterize different ionocytes involved in maintaining blood acid-base balance, and of inner ear ionocytes responsible for generating the endolymph conducive to otolith calcification. This information could be used to assess the physiological responses of fishes to high-CO_2 low pH conditions (hypercapnia) such as those experienced during ocean acidification (OA) and aquaculture, something I was able to do in the later chapters of my dissertation.

All animals must regulate their internal acid-base levels to maintain homeostasis. To do so, organisms utilize ionocytes to actively transport ions across an epithelium to regulate ionic, osmotic, and A/B levels. Changes in CO_2/pH levels naturally occur due to external changes in the environment or as a result of the fish's metabolism. Recently, concerns about future OA have called for further investigation about acid-base regulating mechanisms. Any significant increase in seawater pCO_2 and the subsequent drop in pH have the potential to increase the energetic cost of H^+ secretion. Furthermore, predicted future OA conditions will reduce $[CO_3^{2-}]$ in seawater. Although this was originally predicted to impair the biomineralization of aragonite structures including fish otoliths, subsequent studies reported increased (rather than decreased) otolith sizes in response to OA (Checkley et al., 2009; Munday et al., 2011; Schade et al., 2014; Shen et al., 2016; reviewed in Grosell et al., 2019). In retrospect, this is not surprising because the otoliths are not in direct contact with seawater. Instead, otoliths are calcified within the endolymph, a fluid that is encased inside the inner ear epithelium and which has a unique chemical composition that is controlled by specialized ionocytes. In turn, the inner ear epithelium is in contact with blood capillaries, and the ionic and acid-base composition of the blood is regulated by other ionocyte types present in the skin of larval fishes, and in the gills of juveniles and

adults. Therefore, I pursued the combined characterization of gill, skin, and inner ear ionocytes, and their responses to hypercapnia.

My dissertation reflects the need to first build adequate techniques and skills to subsequently study a given scientific question. In Chapter II, I described that Blacksmith (*Chromis punctipinnis*) anxiety and shoaling behaviour was not affected by predicted OA conditions, though their behavior was affected by changes in temperature. In Chapter III, I detailed a novel technique for quantifying larval skin ionocytes in an accurate and reproducible manner that was subsequently used in Chapter IV and Chapter V. Through those experiments, I also became proficient in immunohistochemistry, a technique I used in every subsequent chapter of my dissertation. In Chapter IV, I characterized skin and gill ionocytes in Yellowfin Tuna (*Thunnus albacares*) reared in an aquaculture facility in Panama, and provided baseline information about their localization, distribution, and morphology throughout larval, transformation, and adult life stages. In addition, I discovered the presence of ionocytes along the gill interlamellar fusion and filament fusion, specialized gill structures found within ram-ventilating fishes. In Chapter V, I examined the responses of larval White Seabass (*Atractoscion nobilis*) to OA-like conditions, specifically NKA abundance, relative skin ionocyte area, and oxygen consumption rate. Despite a three-fold difference in pCO_2 between control and OA-exposed fish (~550 and ~1,800 μatm of CO_2), there were no differences in any parameter – suggesting larval fishes are more resilient to hypercapnia than previously thought. However, during this research I additionally identified that the "control" larvae developed from parents that have been kept in high pCO_2 levels comparable to my experimental treatment, and that the eggs had been spawned and fertilized in that same water. Since extreme hypercapnia is routinely found in recirculating aquaculture systems (RAS), my findings opened new questions about

potential fish transgenerational adaptation to OA. In Chapter VI, I characterized two types of ionocytes within the inner ear saccular epithelium of Pacific Chub Mackerel's (*Scomber japonicus*). This is one of the most detailed studies about the cellular mechanisms involved in sustaining teleost inner ear function and otolith calcification, and it gains additional significance because most previous studies had been conducted on freshwater fish species. In Chapter VII, I was finally able to use the information I generated about basic fish physiology to investigate responses to OA-like conditions. Here, I examined Splitnose Rockfish (*Sebastes diploproa*) responses of gill and inner ear ionocytes to a 3-day hypercapnic exposure (~660 and ~1,600 μatm of CO_2 in control and experimental treatment, respectively). Although exposure to elevated pCO_2 did not induce an increase in the number of gill ionocytes or total gill NKA abundance, it did increase relative NKA abundance in gill cell membranes, and resulted in more extended ionocyte microvilli. These regulatory mechanisms presumably allow rockfish to maintain blood acid-base homeostasis without significantly increasing energy expenditure. Furthermore, I also detected decreased VHA abundance in inner ear cellular membranes. This is the first evidence of a proteomic change in fish inner ear in response to OA; however, further studies must establish the physiological relevance of this finding. Overall, this work provides an in-depth multi-layer analysis of acid/base regulation within marine fishes within gill, skin, and inner ear ionocytes, and is a testament to the intrinsic complexity within biological processes.

The importance of basic science in OA research. While OA is a disturbance to seawater chemistry, the vast majority of the potential effects of OA on fish are due to putative disturbances of acid-base homeostasis of internal fluids including blood plasma, inner ear endolymph, and cerebral spinal fluid. Importantly, fish routinely experience acid-base stress as a

result of their normal metabolic activity and during exposure to normal environmental variability. Furthermore, some of the routine challenges to acid-base homeostasis are often more abrupt than those predicted to be induced by OA. Indeed, in an effort to maximize and identify biological responses, the majority of the previous studies have exposed fish to unrealistically high CO_2 levels. While informative for aquaculture scenarios, this approach could hide important details about fishes' natural responses to hypercapnia, and potentially overestimate the effects of OA. I chose to adopt an alternative approach consisting in first characterizing the ionocytes responsible for maintaining acid-base homeostasis in specialized epithelia (e.g. gill, skin, inner ear, and choroid plexus), and then examining their responses to high-CO_2 low pH conditions. In this way, I was able to generate information that is relevant for marine fishes in both current and future hypercapnic conditions.

As discussed in Chapter VI, adult Splitnose Rockfish did not need to synthesize additional ionocytes to manage a 3-day exposure to 1,600 μatm of CO_2. However, their gill ionocyte's apical surface had more extended microvilli, and their total NKA within the cellular membrane fraction increased under high CO_2 condition. This suggests the Splitnose Rockfish has the capacity to respond to rapid environmental CO_2 increase (such as upwelling) using existing NKA-rich ionocytes, and to upregulate H^+ secretion by inserting a subset of NKA enzymes from cytoplasmic vesicles into the basolateral membrane. Future studies quantifying the energetics necessary to extend microvilli, translocate existing NKA, and synthesize additional NKA or new NKA-rich ionocytes can help determine whether future teleosts will need to consume more energy to survive in a higher-CO_2 environment.

In addition, longer or more intense hypercapnia may require additional responses. For example, total NKA abundance in Benthic Eelpout (*Zoarces viviparus*) gills increased in

response to more extreme CO_2 levels (10,000 μatm for 2 days; Deigweiher *et al.*, 2008) and/or in Cod (*Gadus morhua*) gills after longer duration (6,000 μatm for 12 months; Melzner *et al.*, 2009). But while at first sight those results seem to indicate a fairly severe effect of OA on fish physiology, those CO_2 levels are beyond the most extreme predicted future scenarios – casting doubts about their relevance for fish conservation.

The results shown in Chapter IV further suggest parental acclimation to high CO2 conditions may increase the resilience of larval offspring. Despite a 5-day exposure to ~1,800 μatm of CO_2, larval White Seabass did not need to increase relative ionocyte area, total NKA abundance, or oxygen consumption rate. Furthermore, fish exposed to these elevated CO_2 levels experienced similar mortality and growth rates compared to control fish. Interestingly, these larvae were spawned from parents that have been living in a recirculating aquaculture system for >5 years and experiencing pCO_2 between 200 and 3,000 μatm, with an average of ~1,200 μatm. Also, eggs and sperm were spawned into the same tank, and fertilization and the first stages of embryo development took place in the same tank as well. This entails two possibilities, which are not mutually exclusive. First, selection to elevated CO_2 might have taken place at the egg, sperm, and embryo stages. Second, the parents might have experienced DNA methylation or histone modifications in their germline resulting in epigenetic changes that somehow confer resilience to OA. Future investigation of promoters and methylation of acid-base relevant genes could reveal whether differences exist between larval White Seabass spawned in aquaculture systems and those spawned from wild-caught parents. Alternatively, larval fish responses to future OA conditions may be energetically negligible. Consistent with our study, a previous study on larval Cod from wild-caught parents also found no differences in relative ionocyte area (over the yolk sac only) and oxygen consumption rate after exposure to ~1,100 μatm of CO_2

from fertilization to hatching (Dahlke *et al.*, 2017). Though much more work is necessary to confirm or refute this hypothesis, A/B regulation could simply incur such a low energetic cost that it is undetectable. If that was the case, it could imply that fishes (at least in the early larval stages) may be, or can become resilient to future CO_2 stress.

Future directions. Many questions remain unanswered and in need of further investigations. Here, I will briefly highlight three future avenues of research: characterizing the VHA-rich gill ionocytes, identifying the site of glycoprotein production within the inner ear, and the comparison of inner ear sensory system and potential multigenerational larval adaptation from wild-caught or aquaculture-raised teleosts.

The VHA-rich ionocyte was not only detected in the Splitnose Rockfish gill, but also larval White Seabass skin, adult Treefish (*Sebastes serriceps*) gill, and adult White Seabass gill. Our preliminary work reveals VHA is localized along the basolateral membrane (Chapter VII) along with basolateral H^+/K^+-ATPase and Na^+/H^+-exchanger 2 (see Appendix I). All three of these proteins suggest the secretion of H^+ into the blood plasma, which is indicative of a HCO_3^- secreting cell. To function as a base-secreting ionocyte, this ionocyte is likely to also contain cytoplasmic carbonic anhydrase, apical HCO_3^-/Cl^- exchanger, and/or apical Na^+/HCO_3^- co-transporter. Inducing an alkalosis through feeding or injection of HCO_3^- via a cannula could also help determine the VHA-rich ionocyte's potential role in HCO_3^- secretion across the skin and gill epithelia.

The inner ear ionocytes is responsible for secreting the endolymph responsible for otolith calcification. Besides HCO_3^- and Ca^{2+} ions, otolith calcification requires the synthesis of glycoproteins such as otolith matrix protein-1 (OMP-1). The exact cell responsible for

glycoprotein synthesis remains unspecified, but previous immunostaining of OMP-1 have localized its presence within the meshwork and patches epithelium (Murayama et al., 2004). Immunostaining of OMP-1 and NKA or VHA could determine whether glycoprotein synthesis occurs within Type-I and/or Type-II ionocytes. Furthermore, the transport of glycoprotein, Ca^{2+}, and HCO_3^- within intracellular vesicles have been previously proposed (Dunkelberger et al., 1980; Gauldie and Nelson, 1988; Zhang, 1992). Further investigation exploring the sub-cellular localization of these different proteins using transmission electron microscopy and immunogold could further unravel another essential mechanism responsible for otolith calcification.

Under normal conditions, the sagittae otolith is composed of aragonite. However, animals within RAS and/or aquaculture farms typically experience elevated CO_2 (5,000 μatm to 30,000 μatm) much higher than those used within predicted OA scenarios (1,000 μatm to 3,000 μatm). One previous study has reported otoliths from aquaculture-raised (unknown CO_2) Atlantic Salmon (*Salmo salar*) were composed of vaterite (Reimer et al., 2016). Comparison of inner ear sensory systems (e.g. hearing sensitivity) between aquaculture-raised and wild-caught teleosts would reveal whether hypercapnia could affect otolith function. Additionally, some aquaculture facilities also maintain a broodstock to spawn additional fish stocks. This provides a unique opportunity to analyze multigenerational teleost adaptation to chronic hypercapnia, and subsequent transcriptomic, proteomic, and physiological comparisons of larval fishes born from parents within RAS and wild-caught parents may identify potential resilience to hypercapnic conditions.

References

Checkley, D. M., Dickson, A. G., Takahashi, M., Radich, J. A., Eisenkolb, N., and Asch, R. (2009). Elevated CO2 Enhances Otolith Growth in Young Fish. Science, 324: 1683–1683. doi:10.1126/science.1169806.

Dunkelberger, D. G., Dean, J. M., and Watabe, N. (1980). The ultrastructure of the otolithic membrane and otolith in the juvenile mummichog, *Fundulus heteroclitus*. Journal of Morphology, 163: 367–377.

Gauldie, R. W., and Nelson, D. G. A. (1988). Aragonite twinning and neuroprotein secretion are the cause of daily growth rings in fish otoliths. Comparative Biochemistry and Physiology -- Part A: Physiology, 90: 501–509.

Grosell, M., Munday, P. L., Farrell, A. P., and Brauner, C. J. (2019). Carbon Dioxide. In Fish Physiology, pp. 1–410. Ed. by A. P. Farrell and C. J. Brauner. Academic Press, Cambridge.

Munday, P. L., Gagliano, M., Donelson, J. M., Dixson, D. L., and Thorrold, S. R. (2011). Ocean acidification does not affect the early life history development of a tropical marine fish. Marine Ecology Progress Series, 423: 211–221.

Murayama, E., Takagi, Y., and Nagasawa, H. (2004). Immunohistochemical localization of two otolith matrix proteins in the otolith and inner ear of the rainbow trout, *Oncorhynchus mykiss*: Comparative aspects between the adult inner ear and embryonic otocysts. Histochemistry and Cell Biology, 121: 155–166.

Reimer, T., Dempster, T., Warren-Myers, F., Jensen, A. J., and Swearer, S. E. (2016). High prevalence of vaterite in sagittal otoliths causes hearing impairment in farmed fish. Scientific Reports, 6: 25249. Nature Publishing Group. doi:10.1038/srep25249.

Schade, F. M., Clemmesen, C., and Mathias Wegner, K. (2014). Within- and transgenerational effects of ocean acidification on life history of marine three-spined stickleback (*Gasterosteus aculeatus*). Marine Biology, 161: 1667–1676.

Shen, S. G., Chen, F., Schoppik, D. E., and Checkley, D. M. (2016). Otolith size and the vestibulo-ocular reflex of larvae of white seabass *Atractoscion nobilis* at high pCO2. Marine Ecology Progress Series, 553: 173–182.

Zhang, Z. (1992). Relationship of saccular ultrastructure to otolith growth in the teleost *Oreochromis niloticus*. Journal of Morphology, 212: 99–107.

APPENDIX I

VHA-rich Ionocyte: Characterizing a Second Type of Gill Ionocyte within Marine Teleost

Marine teleosts regulate the Acid/Base (A/B) status of their internal fluids by excreting excess H^+ and HCO_3^- using specialized ionocytes. As shown in Chapter V, the ionocytes are exclusively found in the skin of larval fish, and later appear in the gills as these develop. In adult fish, ionocytes are predominantly found in the gills. In Chapter VI, I detected two types of gill ionocytes: the NKA-rich ionocyte with cytoplasmic VHA as well as the VHA-rich ionocyte. My observations were similar to those on another marine Longhorn Sculpin (*Myoxocephalus octodecemspinosus*), which proposed these VHA-rich ionocytes are likely HCO_3^- secreting cells (Catches et al., 2006).

In addition to the Splitnose Rockfish gills, I have also observed VHA-rich ionocyte within adult Treefish (*Sebastes serriceps*) gill ionocytes (Figure 10.1), adult White Seabass (*Atractoscion nobilis*) gill ionocytes (not shown), and larval White Seabass skin ionocytes (Figure 9.2A). Unlike the NKA-rich ionocyte's highly infolded basolateral membrane, the VHA-rich ionocyte contains a large cytoplasmic space (Figure 9.2 B, C). In contrast to NKCC's co-localization with NKA (Figure 9.2 D, E), basolateral HKA appears to co-localize with VHA-rich cells (Fig 9.2 F, G). Additionally, both larval White Seabass skin ionocytes (Figure 9.3A) and adult White Seabass gill ionocytes (Figure 9.3B, 9.4) expressed NHE2 in the basolateral membrane of VHA-rich ionocytes as well as in the apical membrane of NKA-rich ionocytes. Altogether, basolateral VHA, HKA, and NHE2 can all transport H^+ across the basolateral epithelium, which agrees with the ionocyte's proposed role of HCO_3^- secretion. Further localization of cytoplasmic carbonic anhydrase, apical HCO_3^-/Cl^- exchanger, and/or apical Na^+/HCO_3^- co-transporter will help characterize this VHA-rich ionocyte. Further functional studies are necessary to determine the VHA-rich ionocyte's function. The combined use of cell

isolation, live imaging, pH dye, exposure to high [HCO_3^-], and pharmacological inhibitors may further demonstrate the VHA-rich ionocyte's function.

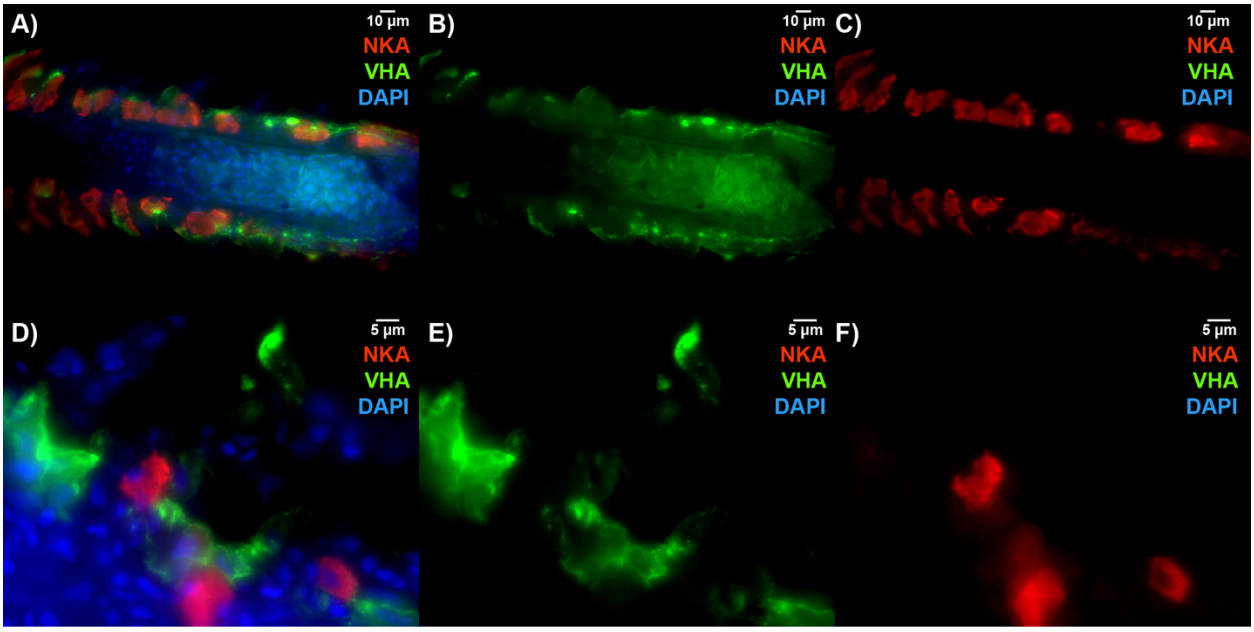

Figure 9.1: Adult Treefish gills express two types of gill ionocytes. **A, B, C)** Low and **D, E, F)** high magnification immunostaining of NKA (red) and VHA (green) reveals two types of ionocytes exist within the gills of adult Treefish. Abbreviations: NKA = vesicular-like bodies, VHA = vacuolar-type H^+ ATPase.

Figure 9.2: Characterizing the VHA-rich ionocytes on larval White Seabass. **A)** NKA-rich (green) and VHA-rich ionocytes (red) can be found throughout the larval skin surface. **B, C)** The NKA-rich ionocytes have basolateral infolded membranes, whereas the VHA-rich ionocytes do not. **D)** Abundant NKCC (green) can be found within the NKA-rich ionocytes (red), whereas **E)** HKA (green) is expressed within both NKA-rich ionocytes as well as another cell type (white arrow). **F, G)** Dual immunostaining of NKCC (red) and HKA (green) is expressed in the basolateral membrane of cells resembling VHA-rich ionocytes. Abbreviations: NKA = vesicular-like bodies, VHA = vacuolar-type H^+ ATPase, NKCC = Na^+-K^+-Cl^--co-transporter, HKA = H^+/K^+-ATPase.

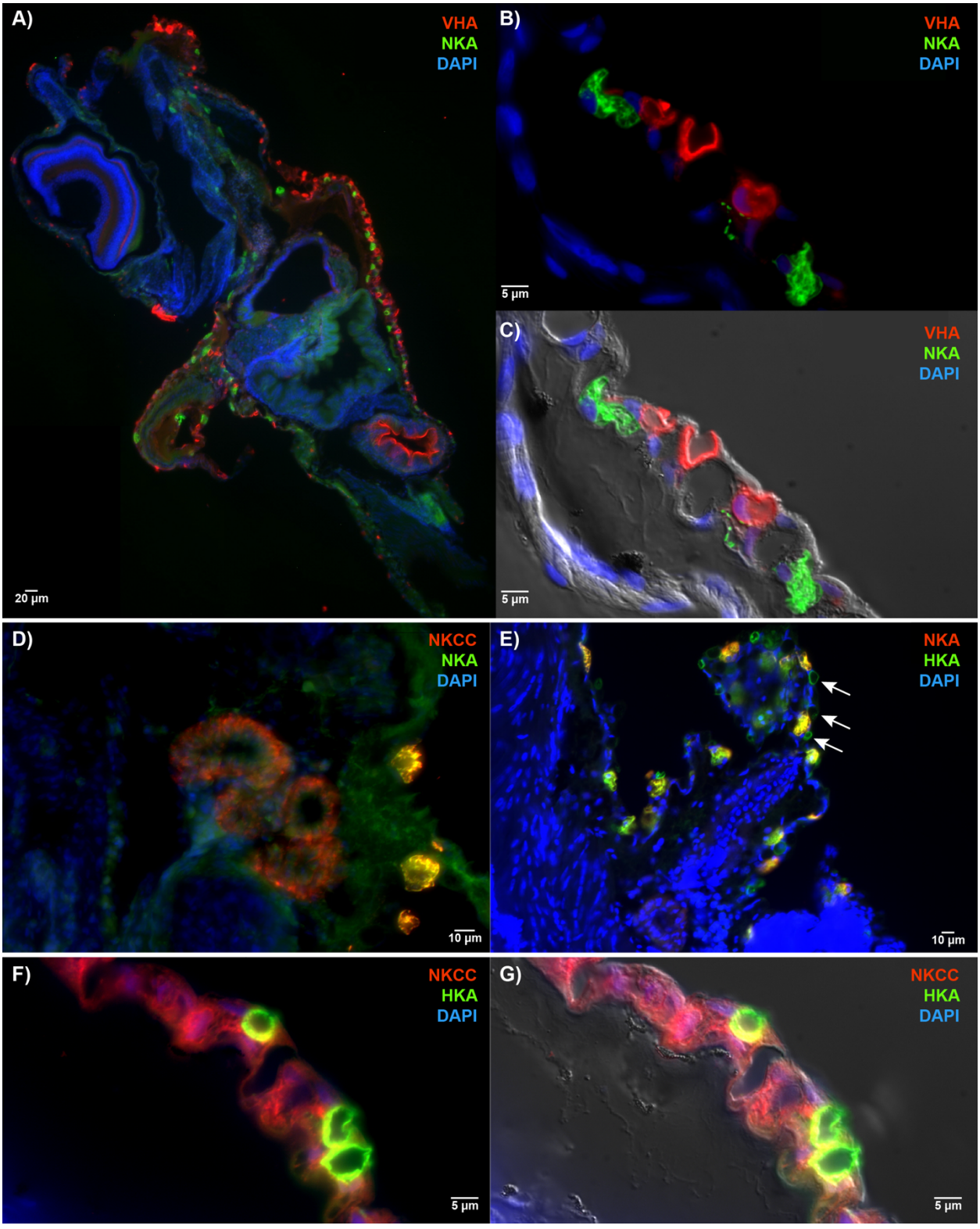
A)
VHA
NKA
DAPI
20 µm
B)
VHA
NKA
DAPI
5 µm
C)
VHA
NKA
DAPI
5 µm
D)
NKCC
NKA
DAPI
10 µm
E)
NKA
HKA
DAPI
10 µm
F)
NKCC
HKA
DAPI
5 µm
G)
NKCC
HKA
DAPI
5 µm

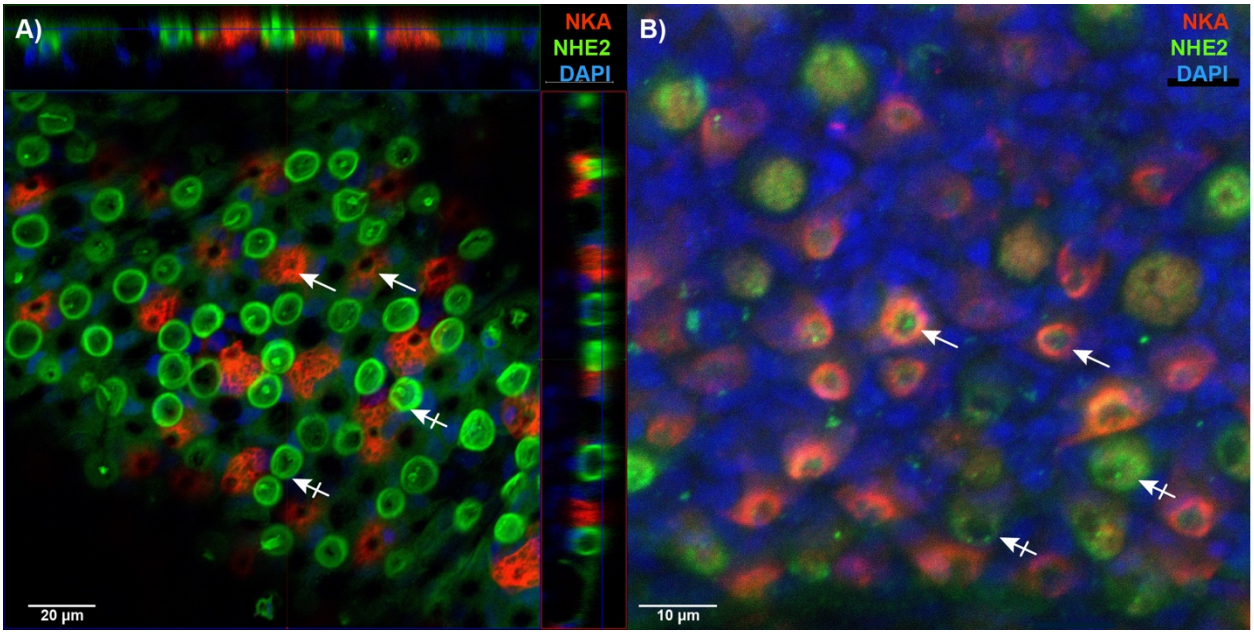

Figure 9.3: NHE2 expression in both NKA-rich and VHA-rich ionocytes. In both **A)** larval White Seabass skin ionocytes and **B)** adult White Seabass gill ionocytes, NHE2 (green) is expressed on the apical membrane of NKA-rich ionocytes (red; white arrow) and basolateral membrane of VHA-rich ionocytes (white arrow with perpendicular line). Abbreviations: NKA = vesicular-like bodies, VHA = vacuolar-type H^+ ATPase, NHE2 = Na^+/H^+ exchanger-2.

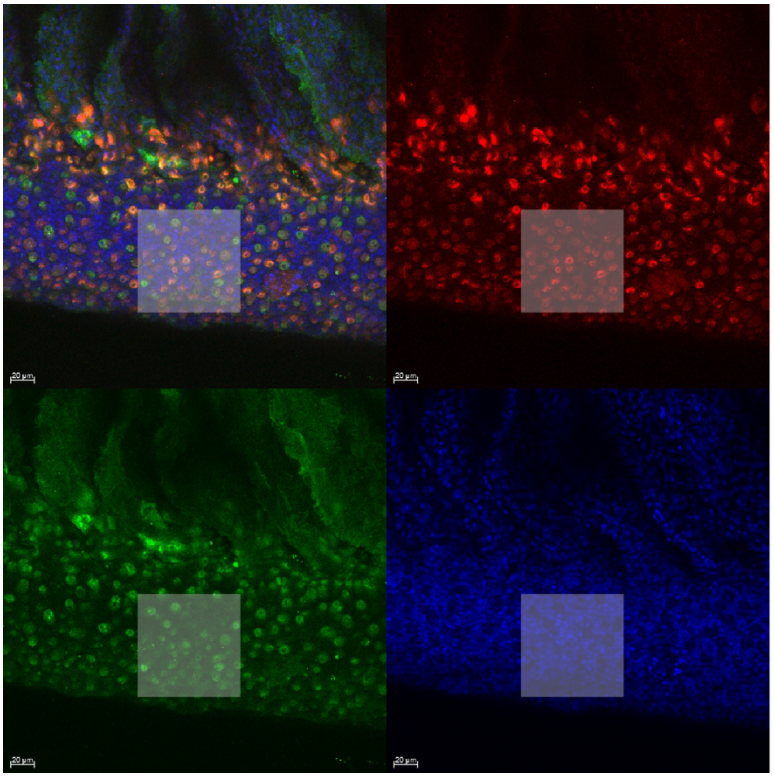

Figure 9.4: Adult White Seabass gills express two types of gill ionocytes. **A, B, C, D)** Low magnification immunostaining of NKA (red) and NHE2 (green) reveals two types of ionocytes exist within the gills of adult White Seabass. The area within the white square is magnified in Figure 8.3A. Abbreviations: NKA = vesicular-like bodies, NHE2 = Na^+/H^+ exchanger-2.

Reference

Catches, J. S., Burns, J. M., Edwards, S. L., and Claiborne, J. B. (2006). Na+/H+ antiporter, V-H+-ATPase and Na+/K+-ATPase immunolocalization in a marine teleost (*Myoxocephalus octodecemspinosus*). Journal of Experimental Biology, 209: 3440–3447.

APPENDIX II

Vesicular-Like Bodies within the Inner Ear: Are they Artifact or Natural?

In the Splitnose Rockfish inner ear, we found vesicle-like bodies (VB) ranging from 0.5 to 3 μm in diameter (Fig 10.1A). Furthermore, several of which appear to be embedded within the tubular network of Type-I ionocytes (Fig 10.1B) as well as within the gel matrix surrounding the sensory hair cells (Figure 10.1C). Finally, high magnification of the surface of the VB reveals a consistent pattern (Fig 10.1D). While this suggests VB are biological in nature, Ibsch *et al.* (2001) postulates these are merely artifacts from sub-optimal fixation of lipids within the ionocytes. During standard SEM fixation, protein fixation is prioritized using aldehydes, then followed by lipid fixation using osmium tetroxide. During the period of protein fixation, VB may blister out of surrounding cells during fixation, and fixed a short while during osmium tetroxide post-fixation. Evidently, much of the VB was reduced when inner ear epithelium was fixed with the combined incubation of traditional fixatives and osmium tetroxide (Ibsch et al., 2001). While this suggests better SEM fixation could greatly reduce VB, it remains possible that VB are naturally produced within inner ear ionocytes. VB's have been proposed to accumulate Ca^{2+}, HCO_3^-, and glycoproteins, which are then expelled into the endolymph within a VHA membrane where it continues alkalinizing the vesicle to promote $CaCO_3$ nucleation (Dunkelberger et al., 1980; Gauldie and Nelson, 1988; Zhang, 1992). Further examination using SEM and TEM following freeze-fracturing may help identify whether VB naturally occurs. Furthermore, transmission electron microscopy can help determine whether VB expresses VHA (or any other proteins), and whether they are a natural part of the otolith calcification process.

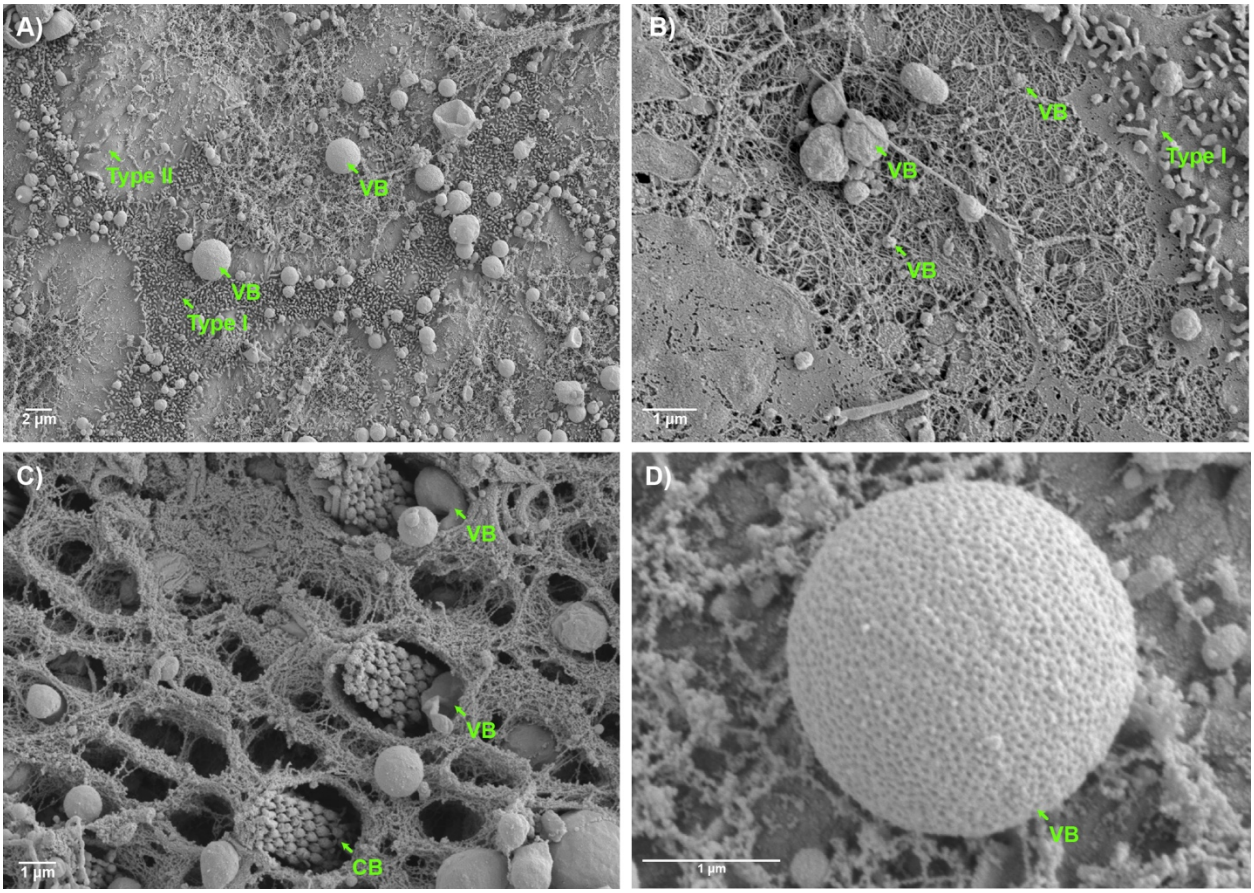

Figure 10.1: Vesicular-like bodies within the inner ear epithelium. **A)** Vesicular-like bodies (VB) are present on the Type-I and Type-II ionocytes. Additionally, VB can be found **B)** within Type-I ionocytes as well as **C)** within the otolith gel matrix surrounding the ciliary bundle of sensory hair cells. Finally, a high magnification of the VB reveals a consistent pattern on its surface. Abbreviations: VB = vesicular-like bodies, CB = ciliary bundle of sensory hair cells.

References

Dunkelberger, D. G., Dean, J. M., and Watabe, N. (1980). The ultrastructure of the otolithic membrane and otolith in the juvenile mummichog, *Fundulus heteroclitus*. Journal of Morphology, 163: 367–377.

Gauldie, R. W., and Nelson, D. G. A. (1988). Aragonite twinning and neuroprotein secretion are the cause of daily growth rings in fish otoliths. Comparative Biochemistry and Physiology -- Part A: Physiology, 90: 501–509.

Ibsch, M., Anken, R. H., Vöhringer, P., and Rahmann, H. (2001). Vesicular bodies in fish maculae are artifacts not contributing to otolith growth. Hearing Research, 153: 80–90.

Zhang, Z. (1992). Relationship of saccular ultrastructure to otolith growth in the teleost *Oreochromis niloticus*. Journal of Morphology, 212: 99–107.